EQUILIBRIUM AND STABILITY IN VORTEX AND WAVE FLOWS

A Dissertation

Presented to the Faculty of the Graduate School

of Cornell University

in Partial Fulfillment of the Requirements for the Degree of

Doctor of Philosophy

by

Paolo Luzzatto-Fegiz

January 2011

EQUILIBRIUM AND STABILITY IN VORTEX AND WAVE FLOWS

Paolo Luzzatto-Fegiz, Ph.D.

Cornell University 2011

This dissertation focuses on the development of theoretical and numerical methodologies to study equilibrium and stability in conservative fluid flows. These techniques include: a bifurcation-diagram approach to obtain the stability properties of families of steady flows; a theory of Hamiltonian resonance for vortex arrays; an efficient numerical method for computing vortices with arbitrary symmetry; and a variational principle for compressible, barotropic or baroclinic flows. We employ these theoretical and numerical approaches to obtain new results regarding the structure and stability of several fundamental vortex and wave flows. The applications that we examine involve simple representations of fundamental fluid problems, which may be regarded as prototypical of flows associated with transport and mixing in the ocean and in the atmosphere, with aquatic animal propulsion, and with the dynamics of vortices in quantum condensates.

We address two issues affecting the use of a variational argument to determine stability of families of steady flows. By building on ideas from bifurcation theory, we link turning points in a velocity-impulse diagram to gains or losses of stability. We introduce concepts from imperfection theory into these problems, enabling us to reveal hidden solution branches. The resulting methodology detects exchanges of stability through an “imperfect velocity-impulse” (IVI) diagram. We apply the IVI diagram approach to wide variety of vortex and wave flows. These examples include elliptical vortices, translating and ro-

tating vortex pairs, single and double vortex rows, distributed vortices, as well as steep gravity waves. For a few of the flows considered, our work yields the first available stability boundaries. In addition, the IVI diagram methodology leads us to the discovery of several new families of steady flows, which exhibit lower symmetry.

We next examine conditions for the development of an oscillatory instability in two-dimensional vortex arrays. By building on the theory of Krein signatures for Hamiltonian systems, we show that a resonant instability cannot occur for one or two vortices. To predict the onset of resonance for three or more vortices, we develop a simple approximate technique, which compares favorably with full analyses. In addition, we propose a simple technique to immediately check the accuracy of a detailed linear stability analysis.

All of the uniform-vorticity equilibria analyzed in this dissertation were computed using a newly developed numerical approach. This methodology, which is based on Newton iteration, employs a new discretization to radically increases the efficiency of the calculation. In addition, we introduce a procedure to remove the degeneracies in the steady vorticity equation, thus ensuring convergence for general vortex configurations. Our method enables the computation, for the first time, of steady vortices that do not exhibit any geometric symmetry, in an unbounded flow.

Finally, we re-examine the variational principle that underpins the IVI diagram stability approach. We show that this principle may be obtained, in a conceptually straightforward manner, by first considering the classical principle of virtual work. This link enables us to readily formulate generalizations to compressible, barotropic and baroclinic flows.

BIOGRAPHICAL SKETCH

Paolo Luzzatto-Fegiz was born in Milan, Italy, on August 16, 1981. He grew up in Milan, and completed high school by graduating from the Liceo Scientifico Leonardo da Vinci in 2000. He moved to the United Kingdom for his university studies, graduating with a Bachelor degree in Aerospace Engineering from the University of Southampton in 2003, and with a Master of Science in Applied Mathematics from Imperial College London in 2004. He subsequently moved to the United States, where he obtained a Master of Science in Aerospace Engineering from Cornell University in 2007.

To Julie.

ACKNOWLEDGEMENTS

First and foremost, I would like to thank my advisor, Professor Charles H. K. Williamson, for his guidance and advice. I am especially grateful for his strong support for these theoretical projects, which perhaps represented a somewhat unconventional pursuit within the context of an experimental research group.

I would like to thank Professor Lance Collins and Professor Sidney Leibovich for agreeing to serve on my special committee. I am particularly thankful for several exciting conversations with Professor Leibovich, whose course on fluid stability triggered early work on determining the stability properties of a specific family of vortex configurations. Special thanks are also due to Professor Paul Steen, as well as to his research group, for interesting discussions on topics in bifurcation and imperfection theory.

During my time at Cornell, I have also had the opportunity to benefit from interactions with other members of the Fluid Dynamics Research Laboratories; in particular, I would like to thank Matthew Horowitz, Timothy Morse, Andrew Mackowski, and Matthew Scase.

Finally, I would like to gratefully acknowledge financial support from a Cornell University Graduate Fellowship.

TABLE OF CONTENTS

LIST OF FIGURES

CHAPTER 1

INTRODUCTION

Problems involving the evolution of coherent fluid structures commonly arise within a wide range of physical situations. Classic examples include the motion of large-scale vortical and wave structures in planetary flows (McDonald, 1999), the evolution of fluid turbulence (Dritschel *et al.*, 2008), aquatic animal propulsion (Dabiri, 2009), the dynamics of confined plasmas (Kiwamoto *et al.*, 2007), as well as organized structures in quantum condensates (Keeling & Berloff, 2008). In all of these fields, the interaction of vortices and waves is fundamental to the underlying dynamics.

For such systems, steady fluid solutions can play a special role in characterizing the dynamics: stable flows might be realized in practice, while unstable ones may act as attractors in the unsteady evolution (see e.g. Moffatt, 1985; Dritschel, 1995). According to this point of view, it is important to be able to calculate possible steady states for a given flow, as well as to reliably determine their stability properties.

Once a family of steady solutions has been determined, their stability is traditionally ascertained through either a time-dependent simulation, or by means of a study of the eigenmodes of the linearized equations. Unfortunately, determining stability by either of these approaches is often a process substantially more laborious than computing the steady vortex flows. This is epitomized by the fact that the stability properties of several comparatively simple flows have been the subject of protracted debates. Prominent examples include steep gravity waves (Stokes, 1879; Longuet-Higgins, 1978*a*; Tanaka, 1983; Longuet-Higgins, 1984*b*; Tanaka, 1985; Longuet-Higgins, 1985; Saffman, 1985),

co-rotating vortex pairs (Saffman & Szeto, 1980; Dritschel, 1985; Kamm, 1987; Saffman, 1988; Dritschel, 1995), as well as Kármán streets of finite-area vortices (Saffman & Schatzman, 1982*a*; Kida, 1982; Meiron *et al.*, 1984; Jiménez, 1987). More recently, similar debates have developed for ellipsoidal vortices in quasi-geostrophic flows (see Meacham, 1992; Miyazaki *et al.*, 1999; Dritschel *et al.*, 2005).

For this reason, the development of a simple stability approach (circumventing the need for a complete linear analysis) would represent a particularly useful tool. Such an approach could be used in its own right to obtain basic stability information and immediately discover new solutions, or it could be employed in conjunction with more complex stability methods to provide a quick check of accuracy.

A separate issue, which further complicates the problem of determining equilibrium and stability, stems from the fact that a number of technical challenges still remain, when computing equilibrium flows. As a matter of fact, computing steady solutions of the Euler equations can often prove far more technically involved than performing time-dependent simulations. This difficulty follows from the existence of an infinite number of conservation laws associated with Euler's equations, which give rise to a set of degeneracies in the steady equation (see Saffman, 1992; Crowdy, 2002; Elcrat *et al.*, 2005, for a recent discussion and examples). Such degeneracies typically prevent convergence for numerical methods that seek general steady solutions.

With these challenges in mind, the problems treated in this dissertation are organized around the search for theoretical and numerical approaches capable of addressing these fundamental problems regarding equilibrium and stability

in conservative fluid flows. Each chapter in this dissertation corresponds to a self-contained paper, which has either been published, or is currently under review. Each chapter also includes the Introduction and Conclusion sections specific to the paper. The publications that make up this thesis are listed below, in the order in which they appear in the dissertation:

LUZZATTO-FEGIZ, P. & WILLIAMSON, C.H.K. 2010 Stability of conservative flows and new steady-fluid solutions from bifurcation diagrams exploiting a variational argument. *Physical Review Letters,* **104**, 044504.

LUZZATTO-FEGIZ, P. & WILLIAMSON, C.H.K. Stability of steady flows and new fluid equilibria from Imperfect Velocity-Impulse diagrams. Submitted to *Journal of Fluid Mechanics.*

LUZZATTO-FEGIZ, P. & WILLIAMSON, C.H.K. 2010 Stability of elliptical vortices from Imperfect Velocity-Impulse diagrams. *Theoretical and Computational Fluid Dynamics* **24**, 181188.

LUZZATTO-FEGIZ, P. & WILLIAMSON, C.H.K. 2010 Resonant instability in two-dimensional vortex arrays. *Proceedings of the Royal Society A*. In press.

LUZZATTO-FEGIZ, P. & WILLIAMSON, C.H.K. An accurate and efficient method for computing uniform vortices. Submitted to *Journal of Computational Physics.*

LUZZATTO-FEGIZ, P. & WILLIAMSON, C.H.K. A derivation of Kelvin's argument, leading to extensions for compressible, barotropic and baroclinic flows. Submitted to *Journal of Fluid Mechanics.*

In addition, the following papers derive from other work completed within the duration of this doctoral work, and are currently in preparation:

LUZZATTO-FEGIZ, P. & WILLIAMSON, C.H.K. The structure and stability of uniform and distributed opposite-signed vortex pairs. To be submitted to *Journal of Fluid Mechanics.*

LUZZATTO-FEGIZ, P. & WILLIAMSON, C.H.K. Stability and evolution of uniform vortices related to vortex merger. To be submitted to *Journal of Fluid Mechanics.*

LUZZATTO-FEGIZ, P. & WILLIAMSON, C.H.K. Structure and stability of the finite-area Kármán vortex street. To be submitted to *Physics of Fluids.*

A complete list of papers and conference presentations associated with this thesis is found in Appendix A. The content of each chapter in the thesis is outlined below.

In chapter 2, we build on ideas from bifurcation theory to show that, for suitably constructed families of steady flows, exchanges of stability are linked to turning points in impulse. In addition, we find that the *direction* of the change of stability (loss or gain) can be inferred from the shape of a velocity-impulse diagram for the solution family. In order to detect previously undiscovered bifurcations, we introduce to these vortex flows the idea of computing "imperfect" steady solutions. By applying an appropriate imperfection, one obtains a qualitative change in the bifurcation structure at the joint between solution branches, immediately revealing the bifurcation and the associated exchange of stability. Therefore all exchanges of stability are apparent in an "imperfect velocity-impulse" diagram. Chapter 2 outlines the key elements of this methodology, and illustrates the technique with a few preliminary results. Readers who are not already familiar with these topics in vortex dynamics are encouraged to initially skip the reading of this chapter, and to proceed directly to chapter 3,

which includes a more accessible introduction to these problems.

In chapter 3, we discuss in detail the concepts underlying the IVI diagram approach. In particular, we define precisely how one-parameter families of solutions must be constructed, in order to ensure that turning points in impulse correspond to exchanges of stability. We also apply the IVI diagram approach to wide variety of vortex and wave flows. These examples include elliptical vortices, translating and rotating vortex pairs, single and double vortex rows, distributed vortices, as well as steep gravity waves. Where previous results from linear stability analysis exist, the stability data from our IVI diagrams agree precisely with results in the literature. For a few of the flows considered, our work yields the first available stability boundaries. In addition, for several of the flows that we examine, the IVI diagram methodology leads us to the discovery of new families of steady flows, which exhibit lower symmetry.

In order to provide a more detailed example involving the construction of an IVI diagram, we examine in further detail the case of an isolated elliptical vortex in chapter 4. By considering this classical flow, we discuss different types of possible imperfections for vortex equilibria, and we present detailed results regarding the first three bifurcations (associated with azimuthal wavenumbers $m = 3, 4, 5$). We obtain the first stability results for these solution branches, and explore the $m = 3, 5$ bifurcated families in their entirety for the first time.

In chapter 5, we take a step back, and examine the two main routes to instability in a conservative flow: *exchange of stability*, and *resonant instability*. By building on the concept of Krein resonance in a Hamiltonian system, we show that, when considering one vortex, or two vortices, instability takes place through an exchange of stability; this implies that, for these flows, an IVI dia-

gram can be used to capture all changes of stability. To predict the onset of resonance for three or more vortices, we develop a simple approximate technique, which compares favorably with full analyses. Preliminary work indicates that this analysis can be generalized to more realistic models of geophysical flows (such as, for example, the quasigeostrophic equations).

In chapter 6, we turn to the problem of computing steady solutions of the Euler equations. We employ kinematic and dynamic constraints to construct what are, in essence, a *modified* set of steady Euler equations; these can be reliably solved (through a standard Newton iteration procedure) to give general vortex or wave equilibria. For flows that can be well-approximated by a collection of uniform vortices, we introduce a new discretization scheme, which can yield an improvement in accuracy of several orders of magnitude over previous techniques. This numerical technique was used to compute all of the steady flows results presented in this dissertation.

Finally, in chapter 7, we generalize the IVI diagram stability approach to compressible, barotropic or baroclinic flows. In order to achieve this, the key step involves finding an appropriate variational principle associated with steady flows of these types. There currently exists a vast body of work concerning variational principles for fluid flow (see e.g. the classic paper of Holm *et al.*, 1985). However, to the best of our knowledge, all analyses developed so far have made use of a potential vorticity or quasigeostrophic approximation, and therefore do not account for baroclinic vorticity generation (as may occur, for example, at the boundary of a vortex ring that is lighter or heavier than surrounding fluid). By considering ideas from classical mechanics, we develop a conceptually simple analysis of this problem, which nevertheless produces

what is, to the best of our knowledge, the first variational principle for steady flows involving baroclinic vorticity production. This principle enables one to apply the IVI diagram stability approach to baroclinic flows.

In the remainder of this chapter, we provide a very brief overview of the fundamental concepts underlying equilibrium and dynamics in vortical fluid flows, with the aim of providing a minimal amount of general background for readers that may not already be familiar with topics in vortex dynamics. Each of these subjects is treated in greater detail in the introduction section of each chapter, where relevant references are also discussed.

1.1 Fundamentals

In this section, we provide a basic introduction to the topics treated in this dissertation. Some of these fundamentals can of course also be accessed, in significantly greater detail, in dedicated monographs, including for example the book by Saffman (1992).

1.1.1 Inviscid vorticity dynamics

When investigating the evolution of vortex or wave configurations, the focus is often placed on inertial instabilities (as discussed, for example, in Eloy & Le Dizès, 2001). In the absence of solid boundaries or critical layers, it may therefore be possible to neglect viscous effects, such that the dynamics are well

approximated by the Euler equation:

$$\frac{\partial \boldsymbol{u}}{\partial t} + \boldsymbol{u} \cdot \nabla \boldsymbol{u} = -\frac{\nabla p}{\rho}, \tag{1.1}$$

where $\boldsymbol{u}$ is the velocity field, p is the pressure, and ρ is the density. As for a viscous fluid, the kinematics are described by the continuity equation:

$$\frac{\partial \rho}{\partial t} + \nabla \cdot (\rho \boldsymbol{u}) = 0 \tag{1.2}$$

If the fluid is barotropic, taking the curl of (1.1) causes the pressure term on the right-hand side to vanish identically. This enables a substantial simplification in the representation of the flow, since p does not appear any longer in the governing equations. Defining the vorticity $\boldsymbol{\omega} = \nabla \times \boldsymbol{u}$, and assuming, for the purposes of this introduction, constant-density flow, the curl of Euler's equation yields, after some manipulation of the nonlinear term:

$$\frac{\partial \boldsymbol{\omega}}{\partial t} + \boldsymbol{u} \cdot \nabla \boldsymbol{\omega} = \boldsymbol{\omega} \cdot \nabla \boldsymbol{u}. \tag{1.3}$$

This equation has many remarkable properties. For example, equation (1.3) for $\boldsymbol{\omega}$ is identical to the equation governing the motion and stretching of a line element of fluid in a general background flow. This observation corresponds to the fact that *vortex lines move with the fluid*, as was indeed already realized by Helmoltz (1858) in the seminal paper that is generally considered as the starting point of the subject of vortex dynamics.

If the fluid is incompressible, one can also introduce a vector potential $\boldsymbol{A}$, such that $\boldsymbol{u} = \nabla \times \boldsymbol{A}$. It can then be shown (for example, using tensor notation) that $\boldsymbol{A}$ and $\boldsymbol{\omega}$ are related through a Poisson-type equation:

$$\nabla^2 \boldsymbol{A} = -\boldsymbol{\omega} \tag{1.4}$$

(In two dimensions, $\boldsymbol{A} = \mathbf{e}_z \psi$, and (1.4) becomes $\nabla^2 \psi = -\omega$.) Equation (1.4) may be readily inverted by the Green function approach, such that $\boldsymbol{A}$ (and therefore

$\boldsymbol{u}$) can be written as a Biot-Savart integral over the vorticity distribution. Therefore, given a specific vorticity distribution, one can directly compute the associated velocity field. In addition, since the vorticity moves with the local fluid velocity, one may compute the evolution of the flow by simply using $\boldsymbol{u}$ to advect the vorticity to its new location. This idea constitutes the essence of vortex-based methods for flow simulation (see e.g. Cottet & Koumoutsakos, 2000), and is at the core of any investigation in the equilibrium and stability of a vortex flow.

1.1.2 Steady vortex flows

A particularly important class of problems involves flows that are steady, in the sense that at each point in space all fluid properties are constant. A special case is given by flows that are steady in a *moving* reference frame (which may be translating or rotating.) Typical examples include the translating vortex pairs known as "modons" in geophysics (Kizner & Khvoles, 2004), rotating arrays observed in Bose-Einstein condensates (Keeling & Berloff, 2008), as well as periodic or solitary gravity waves. If dissipation is negligible, one can compute steady flows without the need to introduce any external forcing. For example, for two-dimensional, constant-density flows in a moving reference frame, the steady vorticity equation can be written as:

$$\boldsymbol{u}_{\mathrm{mov}} \cdot \nabla\omega = 0, \tag{1.5}$$

where $\boldsymbol{u}_{\mathrm{mov}} = \boldsymbol{u} - \boldsymbol{U}$ is the fluid velocity in a reference frame moving with velocity $\boldsymbol{U}$. Equation (1.5) states that the velocity field needs to be everywhere parallel to contours of constant vorticity. (Another way of stating this requirement is

that streamlines and contours of constant vorticity must coincide, in the moving reference frame.) Physically, this ensures that a vortex configuration does not deform, while it travels in space.

From a numerical standpoint, (1.5) can be solved by assuming an initial structure for the vorticity distribution, computing the associated fluid velocity, and progressively adjusting $\omega(\boldsymbol{x})$ until (1.5) is satisfied. A detailed discussion of this problem is presented in chapter 6.

1.1.3 Stability by conservation laws

Once steady states are found, stability properties may be determined in a number of ways. Two classic approaches involve performing a linear stability analysis (which can be used to yields growth rates and frequencies for various perturbation modes), as well as simulation (which delivers the flow's long-term evolution, from a specific initial condition).

A distinct, additional stability approach relies on the fact that Euler's equations exhibit several conserved quantities (including, for example, energy and impulse). These conservation laws (which are implicit in the dynamical equations) can severely constrain the dynamics, and may in principle be employed to gain stability information. For example, we may define a "space" given by several possible perturbations that can be applied to the flow, and consider the changes in a particular quantity (such as the energy) due to each perturbation. Let us further suppose that we may be able to show that, for a specific fluid flow, any perturbation is associated with a decrease in energy. This implies that any changes from the equilibrium state would require a change of energy, which is

impossible; therefore the flow must be stable. This fact (which was already realized by Lord Kelvin in 1875) constitutes an extremely powerful idea, which forms the underlying foundation of several stability approaches (see e.g. Holm *et al.*, 1985).

In practice, however, the application of these conservation-law stability methodologies can be technically challenging, since one needs to characterize the shape of the energy surface for *any* small perturbations from the equilibrium state. Typically, for this calculation to be feasible, one must know the fluid flow analytically, so that an energy functional may be constructed and differentiated a sufficient number of times. For flows that are known only numerically (as is more often the case, in modern studies) this approach can be prohibitively difficult to implement.

For this reason, it is valuable to approach this stability problem by trying to infer the properties of the energy surface through some other, *indirect* diagnostic. One possible strategy involves organizing the steady fluid solutions into *families*, which may depend on one or more parameters. Then one may attempt to formulate a link between changes in the curvature of the energy surface, and other, easily measurable properties of the fluid flow, as the family of solutions is traversed.

This idea, when placed in a more general context, is at the core of much work in bifurcation theory and dynamical systems theory, originating with the classic work of Poincaré (1885). While there exists, of course, a large body of work on this general topic (see e.g. Guckenheimer & Holmes, 1985), a number of outstanding issues have so far prevented the development of bifurcation approaches for vortex and wave flows. For example, since a fluid constitutes an

infinite-dimensional system, there are infinitely many ways in which solutions may be assembled into one-parameter families. This and other issues have so far prevented the development of a general bifurcation approach for vortex and wave flows (see Saffman, 1992; Dritschel, 1995, and references therein).

Chapter 2 comprises a contribution to *Physical Review Letters*, and therefore provides a very concise overview of how we address these outstanding issues. The chapter demonstrates an approach that delivers stability properties from a new type of bifurcation diagram, which involves the velocity and impulse of the steady flows. Chapter 3, which comprises a contribution to *Journal of Fluid Mechanics*, includes a presentation of these theoretical developments in a significantly more comprehensive form, which may perhaps be more accessible to the reader. This paper, while appearing later chronologically, may be more palatable to read first as an introduction to the topic. In addition, chapter 3 also articulates the theory in significantly greater detail, making use of examples involving several fundamental vortex and wave flows.

CHAPTER 2

STABILITY OF CONSERVATIVE FLOWS AND NEW STEADY FLUID SOLUTIONS FROM BIFURCATION DIAGRAMS EXPLOITING A VARIATIONAL ARGUMENT

Published as

LUZZATTO-FEGIZ, P. & WILLIAMSON, C. H. K. (2010)

Physical Review Letters **104**, 044504.

There has been extensive debate on issues affecting the use of a variational argument to determine stability, in conservative fluid systems. In this Letter, we address these issues, and introduce a practical and general stability approach, involving bifurcation diagrams. We build on ideas from bifurcation theory, and thereby for families of steady flows we are able to link turning points in a velocity-impulse diagram to gains or losses of stability. We further introduce concepts from imperfection theory into these fluid flow problems, enabling us to reveal otherwise hidden solution branches. Our approach applies to a wide range of flows. As a brief illustration involving a well-defined and practically important problem, we study a pair of counter-rotating vortices. The approach results in stability boundaries in precise agreement with linear analysis, yet further enables us to discover a new family of steady vortices, which surprisingly do not exhibit any symmetry. All applications of our approach so far lead us to the discovery of lower-symmetry solutions.

Problems involving equilibrium and stability of flows with negligible dissipation commonly arise within a wide range of disciplines. Examples of par-

ticularly active areas of work, in this sense, include the dynamics of confined plasmas (Kiwamoto *et al.*, 2007), vortical and wave structures in planetary flows (McDonald, 1999), as well as organized structures in quantum condensates (Keeling & Berloff, 2008). In all of these fields, the interaction of coherent vortices is fundamental to understanding the underlying dynamics.

For such systems, a particularly important question concerns the existence and stability of any steady states. While stable solutions are likely to be realized in practice, unstable states may act as attractors for the unsteady dynamics (Moffatt, 1986). Unfortunately, establishing stability properties is usually a process far more laborious than finding the steady solutions. The wide variety of fluid stability methods include perturbation methods (linear or non-linear; see Drazin & Reid, 1981), control-inspired approaches based on recent major advances on the theory of non-normal modes (Bagheri *et al.*, 2009), time-dependent simulations (Duraisamy & Lele, 2008), or Lyapunov arguments to establish that a perturbation is bounded in time (Moffatt, 1986).

A subset of the latter set of approaches involves finding a conserved quantity, say, C (such as the energy), whose first variation δC (taken with respect to fluid perturbations) vanishes for the steady flow of interest. Showing that the second variation $\delta^2 C$ is positive or negative-definite for all perturbations is then sufficient to establish stability, since a growing perturbation would violate conservation of C. This idea is at the core of the Arnol'd theorems, and, more generally, of the method of Casimirs, which has been used to study magnetohydrodynamic, plasma and geophysical flows (Arnol'd, 1965; Holm *et al.*, 1985).

However, an outstanding problem prevents the application of these varia-

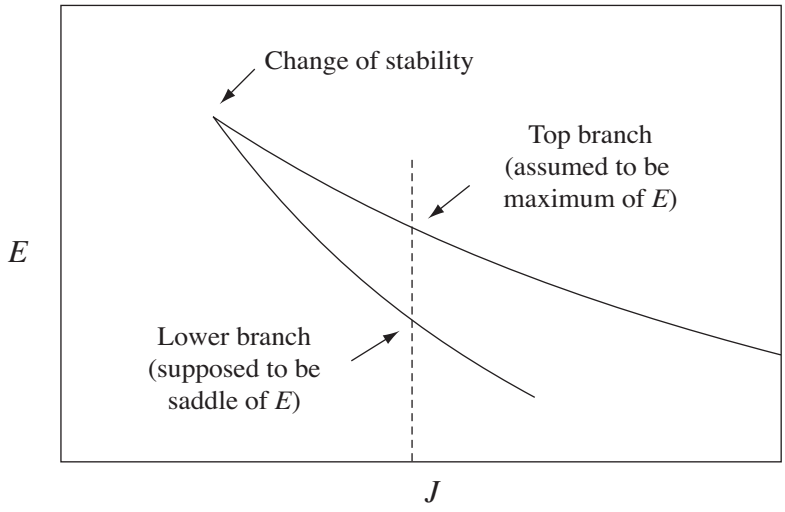

Figure 2.1: Sketch of impulse and excess energy for a family of steady flows involving a co-rotating vortex pair, illustrating the argument of Saffman (Saffman & Szeto, 1980; Saffman, 1992).

tional ideas to a wide range of flows of practical interest. If a flow is known only numerically (as is often the case), calculating $\delta^2 C$ for *all* possible perturbations represents a severe challenge, as fluid systems are typically infinite-dimensional (Dritschel, 1985).

An important and general class of fluid solutions is given by flows that appear steady when observed in a moving frame. Examples include the translating vortex pairs known as 'modons' in geophysics (Kizner & Khvoles, 2004), the rotating arrays observed in Bose-Einstein condensates (Keeling & Berloff, 2008), as well as waves in fluid media. For these flows, the quantity C could in principle be found through an argument stated by Lord Kelvin (Thomson, 1875) and formalized analytically by Benjamin (1976). Benjamin's analysis may be summarized, for example, for a vortex array rotating at rate Ω, having excess kinetic energy E and angular impulse J:

$$E = \frac{1}{2}\iint \omega\psi \,\mathrm{d}x\,\mathrm{d}y, \quad J = -\frac{1}{2}\iint \omega|\boldsymbol{x}|^2 \,\mathrm{d}x\,\mathrm{d}y, \tag{2.1}$$

where ω and ψ are the vorticity and streamfunction satisfying $\nabla^2\psi = -\omega$, and E and J are the finite parts of the kinetic energy and angular momentum, for an unbounded flow (Saffman, 1992). After defining a constrained energy functional $H = E - \Omega J$, Benjamin showed that a stationary point of H with respect to vorticity-preserving perturbations corresponds to a steady flow in the rotating frame (Benjamin, 1976; Saffman, 1992). (A similar analysis holds for translating flows.) Recently Fukumoto & Moffatt (2008) have extended Benjamin's work to three-dimensional flows.

Since H is conserved, stability can be studied by evaluating the second variation $\delta^2 H$ at the equilibrium; a maximum or minimum of H must be stable, while a saddle of H is typically unstable. However, as discussed earlier, computing $\delta^2 H$ is often not feasible. The practical implementation of Kelvin's argument to rigorously detect stability has therefore been the subject of extended debate.

Saffman & Szeto (1980) attempted to circumvent the computation of $\delta^2 H$ as follows. For the family of flows they studied, for fixed impulse J, they found two solution branches, joined at a fold point in a plot of E versus J (see figure 2.1). The branch with the highest E was assumed to be a (stable) energy maximum (implying negative-definite $\delta^2 H$), while the lower branch was speculated to be a saddle (and therefore unstable).

Two fundamental issues associated with this approach were however raised by Dritschel (1985), who pointed out the lack of a firm link between a (J, E) plot (which is two-dimensional) and the properties of the H surface (which exists in an infinite-dimensional space). Furthermore, Dritschel (1985) observed that, even if such a link could be found, changes of stability could also occur at bifurcations, which would remain undetected. This would render the method

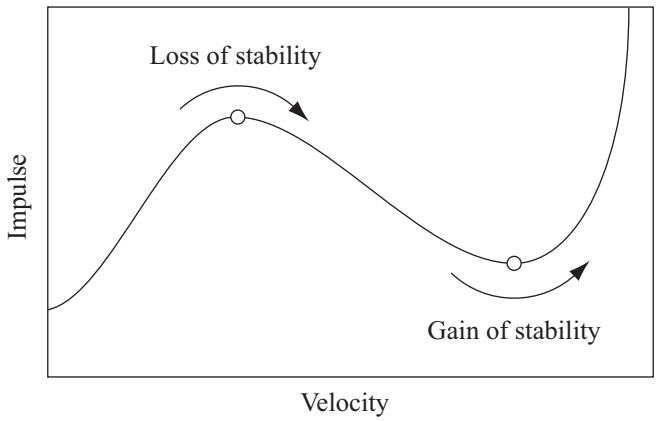

Figure 2.2: Schematic velocity-impulse diagram. A minimum or maximum of the impulse is associated with a loss or gain of stability, respectively, as the curve is traversed from right to left.

unreliable. Subsequently, Dritschel (1995) gave examples for which a (J, E) plot fails to predict the onset of instability. This proved that such an implementation of Kelvin's ideas does not always work.

In this Letter, we resolve both of these issues by introducing a novel approach to the problem. We bring across ideas from dynamical systems theory (Poincaré, 1885; Katz, 1978; Thompson, 1979; Maddocks, 1987), and introduce them to the study of conservative fluid flows. We build on these concepts to rigorously link extrema, that may be found in a velocity-impulse bifurcation diagram, to changes of stability. The use of a velocity-impulse diagram resolves the first issue raised by Dritschel, concerning the use of impulse-energy plots.

In addition, we introduce concepts from imperfection theory (Golubitsky & Schaeffer, 1985; Thompson, 1975; Chen & Steen, 1996) to these fluid flow problems; these ideas enable us to detect any hidden bifurcations in the velocity-impulse diagrams. By employing imperfection theory, we are therefore able to address the second issue pointed out by Dritschel.

At this point, we provide a brief overview of our approach. If one first computes solution families for steady flows, then our method can detect losses or gains of stability. These correspond to the creation or destruction of saddles of the energy functional H. Given the fact that families of steady flows usually contain at least one member whose stability properties can be found easily from standard methods, we can thereafter establish stability properties for all the equilibria.

We shall first show that extrema in impulse are linked to changes of stability. We start with the equation $\delta H = 0$, and differentiate it along the solution family to investigate changes in $\delta^2 H$. We formalize the constrained extremization problem associated with steady flows by first writing, for an inviscid fluid in three dimensions:

$$H(\boldsymbol{\ell}, \Omega, J_0) = E(\boldsymbol{\ell}) - \Omega\,[J(\boldsymbol{\ell}) - J_0], \tag{2.2}$$

where $\boldsymbol{\ell}$ is the position of each fluid particle, such that $\delta\boldsymbol{\ell}$ is the incompressible and irrotational displacement field used for the variation giving $\delta H = 0$ (see Fukumoto & Moffatt, 2008); J_0 is the prescribed value of the impulse, while Ω acts as a Lagrange multiplier. We may parametrize solutions by either Ω or J_0 (Benjamin, 1976). While the velocity Ω of the rotating frame is easily set for equilibrium calculations (Deem & Zabusky, 1978), specifying J_0 is more computationally intensive, as the impulse is given by the integral in Eq. (2.1). However, since J is conserved (Saffman, 1992), J_0 must be considered fixed when studying stability.

In contrast to previous studies, where typically Ω is employed to characterize the solutions, we choose J_0 as the control parameter, and define the solution vector $q \equiv (\boldsymbol{\ell}^{\mathrm{T}}, \Omega)^{\mathrm{T}}$. Writing H as the volume integral $\int h\,\mathrm{d}V$, a stationary point

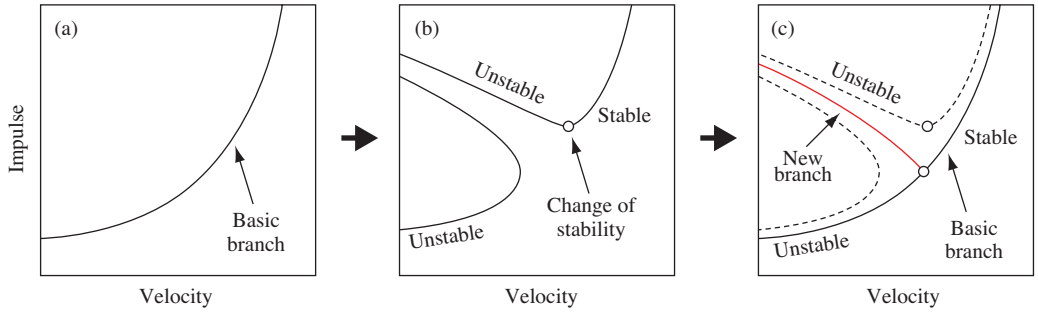

Figure 2.3: Typical construction of an imperfect-velocity-impulse diagram. (a) shows a velocity-impulse diagram for a basic branch of steady solutions. Introducing an imperfection and re-computing the steady states breaks the basic branch into two distinct branches (shown in b), revealing a change of stability. In (c), by bringing the imperfection to zero, we recover the underlying new solution branch.

of H (which is associated with a steady flow) is given by:

$$\delta H(q, J_0) = \int \sum_{i=1}^{4} \delta q_i \frac{\partial h}{\partial q_i} \, \mathrm{d}V \equiv \langle \delta q, H' \rangle = 0, \tag{2.3}$$

where H' denotes the functional derivative of H.

To be able to deal with any turning points in J_0, we introduce the arc length s along the solution curve to parametrize the equilibria, and write $[q_e(s), J_0(s)]$, where q_e represents an equilibrium solution, for given J_0. The vector tangent to the solution curve is then $\mathrm{d}q_e/\mathrm{d}s \equiv \dot{q}_e$. If the first variation $\langle \dot{q}_e, H' \rangle$ vanishes, the corresponding second variation can be used to detect a change of stability that is not associated with a bifurcation. This will be true if $\dot{q}_e$ represents an incompressible rearrangement of the flow's vorticity, as required for Eq. (2.3) to hold. Since $\dot{q}_e$ is tangent to the solution path, it follows that the family of solutions must be constructed through incompressible rearrangements of a given vorticity distribution. This provides a simple criterion to organize steady flows into well-defined families.

To derive an expression for the second variation of H with respect to $\dot{q}_e$, we

first introduce the notation $\kappa = \langle \dot{q}_e, H'' \dot{q}_e \rangle$, which is effectively the change of H associated with a perturbation along the family. We then differentiate Eq. (2.3) along the solution family to obtain:

$$\langle \delta q, H'' \dot{q}_e \rangle + \langle \delta q, \frac{\partial H'}{\partial J_0} \rangle \dot{J}_0 = 0, \tag{2.4}$$

where we have, once again, denoted differentiation with respect to s by means of a dot. Substituting $\delta q = \dot{q}_e$ then turns the first term into κ. We re-write the second term by noting that $\partial H / \partial J_0 = \Omega$, yielding $\langle \dot{q}_e, \frac{\partial H'}{\partial J_0} \rangle = \dot{\Omega}$. Hence we obtain:

$$\kappa = -\dot{\Omega}\, \dot{J}_0, \tag{2.5}$$

such that $\kappa = 0$ for $\dot{\Omega} = 0$ or $\dot{J}_0 = 0$. However, we note that, in order for $\dot{q}_e$ to enable an instability, $\dot{q}_e$ must also leave the impulse unchanged, beside yielding $\kappa = 0$. To linear order, this gives the additional requirement $\langle \dot{q}_e, J' \rangle = \dot{J}_0 = 0$. Hence the only case of interest is $\dot{J}_0 = 0$. In other words, *extrema in impulse are associated with changes of stability*.

In order to assess whether an extremum in impulse corresponds to a loss or a gain of stability, we need to find the direction of the change of sign of κ, as the $\kappa = 0$ case is traversed. For example, for an initially stable flow starting at a maximum of H (as is usually the case for unbounded flows; see Moffatt, 1986), a switch from $\kappa < 0$ to $\kappa > 0$ will be linked to loss of stability. We differentiate κ with respect to s to obtain:

$$\dot{\kappa} = -\dot{\Omega}\, \ddot{J}_0 \quad \text{at} \quad \dot{J}_0 = 0. \tag{2.6}$$

Notice that the sign of $\dot{\kappa}$ depends only on the signs of $\dot{\Omega}$ and $\ddot{J}_0$. Remarkably, both of these can be immediately detected from a velocity-impulse diagram (Ω, J), as shown in figure 2.2.

To summarize, we find that a local extremum in impulse is associated with a change of stability, as shown earlier. Secondly, we obtain that *a velocity-impulse diagram instantly reveals whether the extremum yields a gain or loss of stability*. Our analysis therefore solves the first issue raised by Dritschel, namely the absence of a rigorous connection between an impulse-energy diagram and a change of stability.

We now address the second issue pointed out by Dritschel, since bifurcations to new solution families would remain undetected using solely the analysis we have presented so far. To resolve this, we exploit ideas from the study of imperfect dynamical systems. For inviscid flows, we introduce an imperfection through a simple physical idea.

Given a numerically found solution branch (sketched in figure 2.3a), we construct an imperfection by introducing a flow element that breaks any geometric symmetry in the fluid, and re-compute the solutions. (We find that the specific choice of imperfection is unimportant, provided the symmetry of the original flow is broken.) If a bifurcation exists, we find that the result consists of two distinct branches (figure 2.3b). Taking the imperfection's magnitude to zero then reveals a new family of solutions, as shown in figure 2.3c. (A similar behavior holds for both pitchfork and transcritical bifurcations.) The extrema in impulse for the imperfect branches yield the stability properties for both the original and the new family of equilibrium flows. Therefore, we find that any hidden bifurcations are uncovered, ensuring that all changes of stability are detected through an "imperfect-velocity-impulse" diagram.

Finally, to illustrate how one may straightforwardly obtain stability boundaries and discover new solution branches using imperfect-velocity-impulse dia-

grams, we select a well-defined example flow. We examine the opposite-signed, unequal-circulation vortex pairs previously studied by Dritschel (1995). (We should clarify that this is but one example in a wide range of flows where this method might be applied.) For the flow of interest, since the total circulation is different from zero, this configuration rotates about a fixed point. For large separation distances, one recovers two point vortices, which can easily be shown to be stable (Saffman, 1992). Model flows of this form have been used in geophysical applications (Kizner & Khvoles, 2004). We represent the vortices as two patches of uniform vorticity with magnitude ω_0, and compute equilibrium states numerically. Requiring that the family must be obtained through incompressible rearrangements of the vorticity then implies that the area of each vortex must be held fixed along the family.

We first constructed the velocity-impulse diagram for the basic family with area ratio $A_1/A_2 = 0.3$, as shown in figure 2.4a. A loss of stability can be immediately detected at the minimum in J in the figure. To search for undiscovered branches, we introduced a point vortex (of strength, relative to the largest vortex, $\Gamma_{PV}/\Gamma_1 = 10^{-4}$) at one of the stagnation points of the co-rotating flow (marked by the bull's eye in figure 2.4d), thus ensuring that the symmetry exhibited by the flow is broken. Re-computing the equilibria, we find that the solution curve is split into distinct branches (dashed lines in figure 2.4c), revealing an additional loss of stability at a minimum in J. Finally, by bringing the imperfection to zero, we discover a new family of solutions (red line in figure 2.4b,c), which terminates with the vortex configuration shown in figure 2.4b. The new vortices do not exhibit any symmetry, which is particularly surprising given the simplicity of the flow. The discovery of the existence and stability of these nonsymmetric flows has been made evident by the approach in this Letter.

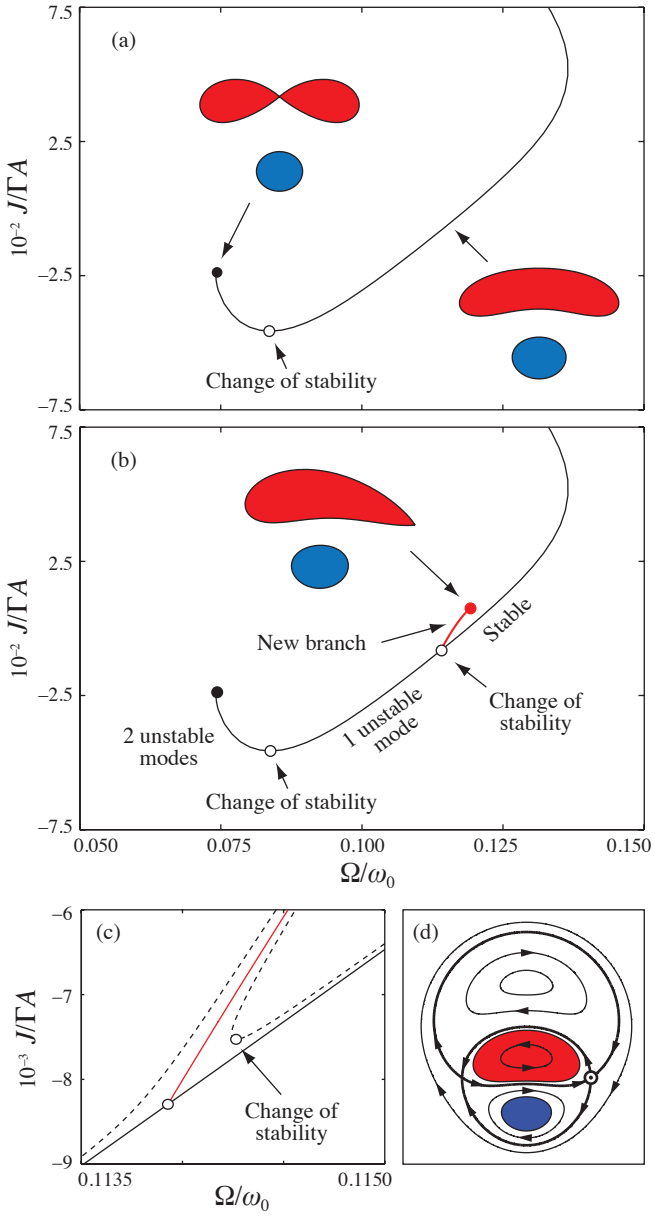

Figure 2.4: Stability of the opposite-signed pair with vorticity magnitude ω_0, area ratio $A_1/A_2 = 0.3$, total area A and total circulation Γ. (a) shows the basic family. (d) displays the streamlines in a frame moving with the vortices. The imperfection is constructed by introducing a weak point vortex at the saddle point marked by a bull's eye (⊙). Re-computing the solutions (dashed lines in c) yields the stability properties for the family, while revealing a new branch of solutions, which do not exhibit any symmetry (red line in b, c). Filled and empty circles denote limiting shapes and changes of stability.

In conclusion, we have developed an approach yielding stability boundaries directly from families of steady flows. Obviously, the approach employed in this Letter is not intended to be a substitute for more powerful or detailed stability analyses. However, this method, which rigorously uses velocity-impulse diagrams, enables one to detect bifurcations and determine in a straightforward manner stability boundaries for fluid flow. Clearly this technique can also be used in correspondence with more complicated approaches. Further to this, the discovery of lower symmetry solutions using our approach appears to be a general feature of all flows so far studied. In our ongoing work, we have applied our stability approach to a wide range of vortical and wave flows (Luzzatto-Fegiz & Williamson, 2011*b*). Our methodology should prove useful across a broad range of topics of current interest, including for example geophysical flows (see the recent review of van Heijst & Clercx, 2008), Bose-Einstein condensates (see e.g. the recent letter by Keeling & Berloff, 2008), and aquatic biolocomotion (where optimal vortex formation plays an important role, as highlighted, for example, by current work at Caltech; see Dabiri, 2009). We have also been able to generalize our stability approach to stratified and compressible flows.

CHAPTER 3

DETERMINING THE STABILITY OF VORTEX FLOWS THROUGH IMPERFECT VELOCITY-IMPULSE DIAGRAMS

Submitted to *Journal of Fluid Mechanics*.

In 1875, Lord Kelvin stated an energy-based variational argument for equilibrium and stability in conservative flows. The possibility of building a rigorous implementation of Kelvin's argument, based on the construction of a simple bifurcation diagram, has been the subject of debate in the past. In this paper, we build on ideas from dynamical systems theory, and construct a link between turning points in fluid impulse and exchanges of stability. We show that the shape of a velocity-impulse diagram, for a family of equilibrium solutions, immediately determines whether stability is lost or gained at the exchange of stability. Further to this, we are able to detect bifurcations to new families of steady flows by calculating steady solutions which have been made "imperfect" through the deliberate introduction of asymmetries in the vorticity distribution. The resulting stability approach, which employs "imperfect velocity-impulse" (IVI) diagrams, can be used to determine the number of unstable modes for each equilibrium flow belonging to a family of steady states. We show that, in order to ensure that an IVI diagram correctly defines exchanges of stability, each solution in the family must have the same Casimir invariants. Several well-known analytical families of solutions (for example, Stuart vortices) do not meet this requirement; therefore their stability cannot be inferred from turning points in a simple bifurcation diagram. In addition, we clarify the general relationship between energy, impulse, and phase velocity, for families of conservative flows. As an illustration of our stability approach, we construct IVI diagrams for sev-

eral classical flows, including the Kirchhoff elliptical vortices, opposite-signed vortex pairs (of both rotating and translating type), infinite single and double-rows of vortices, as well as steep gravity waves. By considering an example involving the Chaplygin-Lamb dipole, we also illustrate how the stability of a specific flow may be determined, by embedding it within a properly constructed series of solutions. Where previous results from linear stability analysis exist, the stability data from our IVI diagrams agree precisely with results in the literature. To the best of our knowledge, for a few of the flows considered here (including the discretized Chaplygin-Lamb dipole, and the finite-area Kármán street subject to superharmonic perturbations), our work yields the first available stability boundaries. For several of the flows that we examine, the IVI diagram methodology leads us to the discovery of new families of steady flows, which exhibit lower symmetry.

3.1 Introduction

Over a century ago, Sir William Thomson (1876) (now more widely known as Lord Kelvin) proposed an energy argument for determining equilibrium and stability in an inviscid, homogeneous flow. Thomson stated his argument without proof; the first analytical confirmation of his ideas is traditionally attributed to Arnol'd (1966) or Brooke Benjamin (1976).

Thomson considered flows that are steady when observed in a reference frame that is translating or rotating with constant velocity. In this context, steadiness does not necessarily imply a flow that is quiescent, but rather that

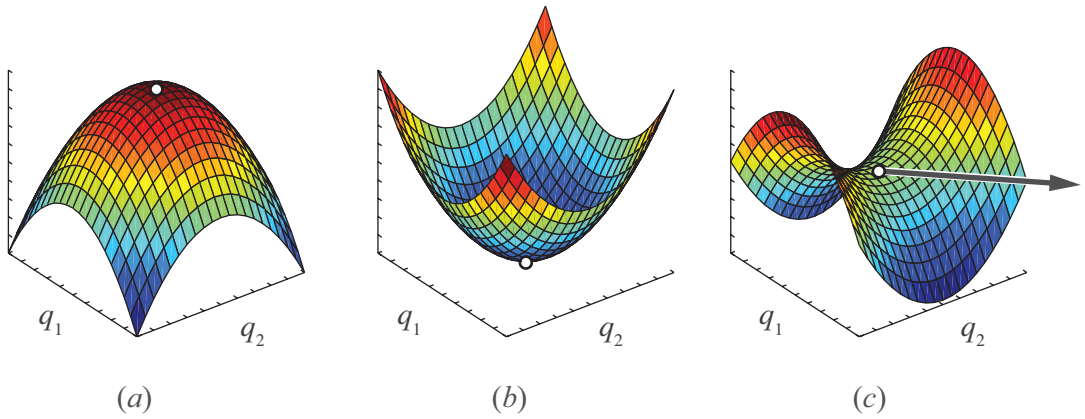

Figure 3.1: Schematic illustrating the relation between the second variation of H and the stability of an equilibrium, shown here for a solution space $\boldsymbol{q} = (q_1, q_2)^{\mathrm{T}}$. If the equilibrium represents a maximum (*a*) or a minimum (*b*) of the energy, moving away from the equilibrium point would require a change of energy, which is impossible. Hence equilibria (*a*) and (*b*) must be stable. On the other hand, if the solution is associated with a saddle of the energy (as shown in *c*), instability is possible.

a specified set of flow properties (such as velocity and pressure) is constant in time, for any given point space, in the moving reference frame. Classic examples of steady flows include the elliptical vortices discovered by Kirchhoff (1876), the vortex pair solutions of Chaplygin and Lamb (see Meleshko & van Heijst, 1994), as well as the vortex ring solutions of Hill and Norbury (1973).

According to Kelvin's argument, any flow that meets this definition of steadiness corresponds to a stationary value of the energy, under perturbations that preserve the flow's vorticity and impulse. As already noted by Thomson (1876), for flows that conserve energy, the link between stationary points of the energy and steady flows has important consequences for stability. If the steady flow corresponds to a (possibly local) maximum or minimum of the energy, a displacement of the system away from the equilibrium point would require a change of energy, which is impossible. Hence the equilibrium flow must be stable. By the same reasoning, a necessary condition for instability is that the flow

must correspond to a saddle of the energy, as illustrated in figure 3.1. This idea is at the core of the well-known stability theorems of Arnol'd (1965, 1966), and forms the basis of several stability methodologies (see, for example, Holm *et al.*, 1985).

However, the application of these energy-based ideas to determine stability is often limited by practical considerations. As a matter of fact, to use these methodologies one has to evaluate the second-order change in energy (that is, the second variation) under all admissible perturbations. This may be possible for certain flows that admit explicit analytical solution. On the other hand, computing the second variation of the energy for a *numerically* obtained flow is prohibitively difficult, as one has to consider a second-order expansion involving an infinite number of possible perturbations (Dritschel, 1985). This issue places a severe limitation on the practical implementation of Kelvin's argument.

Motivated by the need to circumvent this difficulty, Saffman & Szeto (1980, 1981) proposed a different implementation of Kelvin's argument. We summarize here the exposition in their 1980 paper. In their work, Saffman & Szeto computed numerically a family of steady, corotating vortex pairs, having equal area and uniform vorticity. (These solutions can be parametrized, for example, by the separation distance between the vortices.) Having obtained the steady states, Saffman & Szeto (1980) calculated also their energy E and angular impulse J. In an attempt to intuitively deduce which solutions represented maxima of the energy, for a given impulse, they constructed a plot of E versus J; for their family of solutions, they found that the plot displayed a simultaneous turning point in E and J (as schematically shown in figure 3.2). Saffman & Szeto (1980) then proposed that the "highest" curve in the plot would be a maximum

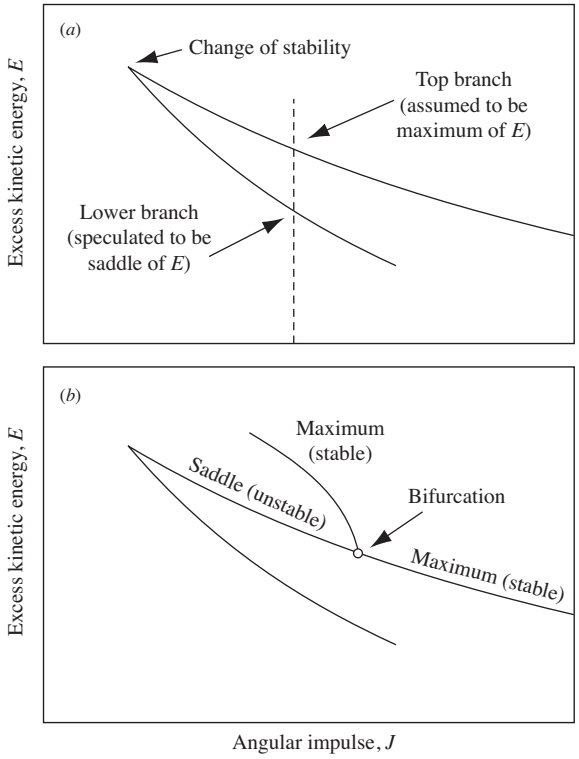

Figure 3.2: Sketch of impulse and excess energy for a co-rotating vortex pair, illustrating the approach of Saffman. For the flow considered by Saffman & Szeto (1980), there exist two branches of energy E, for a given impulse J. The top branch was assumed to be a (stable) maximum, while the lower one was speculated to be a saddle (and thus unstable).

in E (for a given impulse J), while the lower branch would likely be a saddle of E. Hence the top branch would be stable, the lower branch would likely be unstable, and the connection between the two branches would correspond to a change of stability. For this flow, Kamm (1987) and Dritschel (1995) found that the stability boundary obtained from a (J, E) plot was later agreed with detailed linear stability calculations.

However, the approach proposed by Saffman & Szeto (1980) is affected by two fundamental issues, which were pointed out by Dritschel (1985, 1995). In a seminal paper on the stability properties of rotating vortex arrays, Dritschel

(1985) pointed out the absence of a rigorous link between the properties of the energy surface (which exists in the infinite-dimensional space of possible vorticity rearrangements) and the shape of an energy-impulse plot, (which is two-dimensional). Furthermore, Dritschel (1985, 1995) observed that, even if such a link could be firmly established, *additional* changes of stability could also occur away from extrema in E and J, by means of bifurcations to (hitherto undiscovered) families of solutions. This point was corroborated by the findings reported in Dritschel (1995). This paper studied (using a linear stability analysis) several families of steady flows for which a loss of stability occurred at a location along the solution curve *before* the extremum in energy and impulse. These results led Dritschel (1995) to conclude, regarding Saffman's interpretation of Kelvin's ideas, that "the argument, based on Kelvin's variational principle ... that the margin of stability can be decided from the $E(J)$ curve alone ... does not always work." As a consequence of these two issues, the stability method proposed by Saffman & Szeto (1980) has since been considered unreliable (D. Crowdy, 2008, private communication); indeed, to the best of our knowledge, energy-impulse plots have not been employed in any other vortex dynamics studies to date.

In addition to the conceptual issues highlighted above, there is a simple practical problem that can arise in attempting to employ an energy-impulse diagram to diagnose stability boundaries, since the "upper" and "lower" energy branches may be found to essentially overlap. An example of this behaviour was encountered by Kamm (1987), who studied the fist three bifurcations from the family of elliptical vortices. Kamm's data for the first bifurcation (which was computed accurately to four significant figures) is reproduced in figure 3.3(a). This issue is compounded by the fact that, for a flow in N space-dimensions, the energy must be computed through a $2N$-dimensional integral (since one needs

to first integrate over the vorticity field to obtain the fluid velocity, which is, in turn, integrated to find the kinetic energy). Achieving a sufficient accuracy in E to enable distinction of the two branches can be numerically expensive.

On the other hand, it should be noted that, for the elliptical vortices studied by Kamm (1987), the original and bifurcated solution branches do not actually coincide in *all* variables. This can be made clear, for example, by plotting the impulse J versus the angular velocity Ω of the vortex shapes, as shown in figure 3.3*b*; the bifurcated branch then becomes immediately apparent. This suggests that, even in the case that the energy-impulse approach could be salvaged from a conceptual standpoint, it would be desirable to instead develop a methodology involving a different set of parameters.

We were motivated to re-examine this problem by the fact that a simple stability approach, based on the construction of a suitable bifurcation diagram, could be valuable in a wide range of applications. For example, we note here that several debates (each spanning at least a decade) have existed over the stability of comparatively simple flows. Examples include co-rotating vortex pairs (Saffman & Szeto, 1980; Dritschel, 1985; Kamm, 1987; Saffman, 1992; Dritschel, 1995), as well as ellipsoidal vortices in quasigeostrophic flows (Meacham, 1992; Miyazaki *et al.*, 1999; Dritschel *et al.*, 2005). It is conceivable that a simple stability approach, beside proving valuable in its own right, could also be used to quickly confirm correct results from linear analysis, and question possibly spurious ones. A bifurcation-diagram stability methodology could therefore complement more involved stability approaches, such as linear analysis or time-dependent simulations, which would yield additional information about growth rates and long-term evolution of the flow.

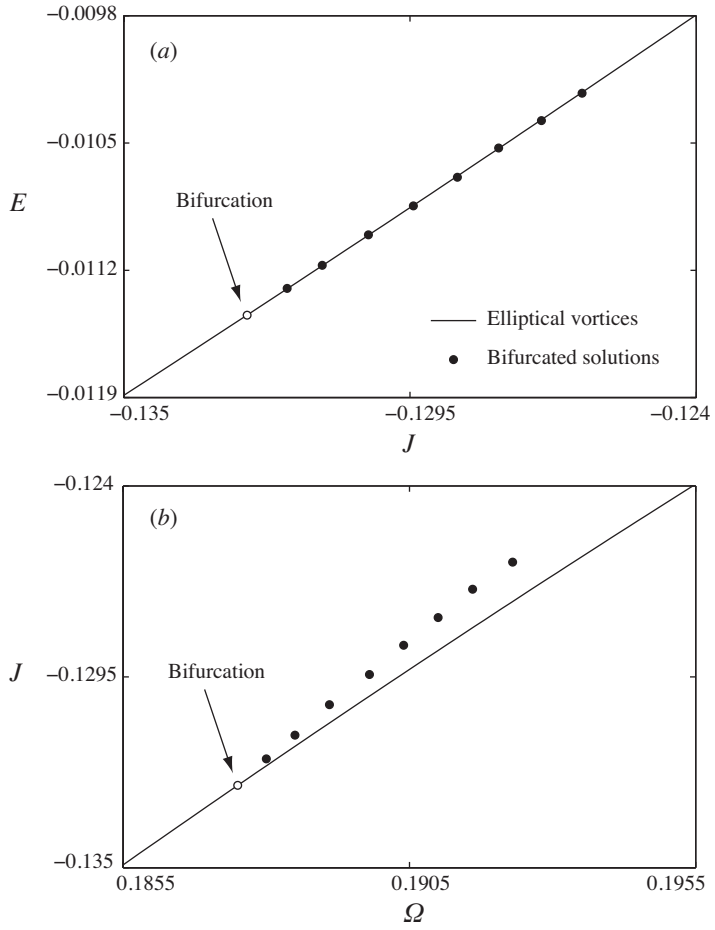

Figure 3.3: Neighbourhood of the first bifurcation from the family of Kirchhoff elliptical vortices, as computed by Kamm (1987). As pointed out by Kamm, for each bifurcated solution that he obtained numerically, there exists a corresponding elliptical vortex having the same energy and impulse (to at least four significant figures). Extracting stability properties from an impulse-energy diagram (shown in *a*) is therefore not feasible. On the other hand, Kamm remarked that vortices that had the same (E, J) did not also have the same angular velocity Ω. Hence the two families appear as distinct curves in a velocity-impulse diagram (as plotted in *b*).

It should be noted that the study of the stability of families of solutions for conservative fluid systems extends well beyond the context of vortex dynamics. A classic example involves the study of the stability of gravity waves of fixed wavelength L. This particular problem has seen extensive debate regarding the location, along the solution family, of the onset of instability (Longuet-Higgins, 1978*a*, 1984*b*; Tanaka, 1985; Saffman, 1985). Similar problems abound in a range of other settings. As a further example, we mention here the study of Jones & Roberts (1982), who considered a family of steadily translating, isentropic perturbations in a model of a quantum condensate. Remarkably, they found that their family of solutions exhibited a simultaneous extremum in energy E and linear pseudomomentum p, yielding a curve similar to the one sketched in figure 3.2. This led them to also formulate a heuristic argument linking an extremum in a plot of (E, p) to a change of stability (Jones *et al.*, 1986); they supported their argument by evaluating the energy change associated with a particular possible perturbation, exploiting a technique introduced by Derrick (1964). For this problem, the linear stability analysis carried out recently by Berloff & Roberts (2004) indicates that the stability predictions in Jones *et al.* (1986) are correct. However, the argument of Jones *et al.* (1986) remains vulnerable to the same issues pointed out by Dritschel (1985, 1995). It remains unknown whether bifurcations to lower-symmetry states may exist. A rigorous turning-point stability approach could therefore have applications outside the realm of classical fluid mechanics.

This paper is structured as follows. We begin, in § 3.2.1, by briefly reviewing the analytical basis for Kelvin's argument. In § 3.3.2, we develop ideas from bifurcation theory for conservative fluid flow problems, and show that extrema in a velocity-impulse diagram (instead of energy-impulse) are actually associated

with exchanges of stability, thereby addressing the first issue raised by Dritschel (1985, 1995). The second issue raised by Dritschel, namely, the possibility that exchanges of stability associated with bifurcations may be overlooked, is addressed in § 3.4, through the introduction of ideas from the study of imperfect dynamical systems. Therefore, for a family of steady flows, we are able to detect all exchanges of stability through the use of an "imperfect velocity-impulse" (IVI) diagram. A preliminary account of the IVI diagram methodology has recently appeared in a Letter by Luzzatto-Fegiz & Williamson (2010*b*), which outlines some elements of the analysis presented in § 3.3.2 and 3.4. In this paper, section 3.5 considers several examples involving vortical flows, where the IVI diagram approach is successfully employed to determine stability; furthermore, the approach automatically yields bifurcations to new families of solutions, which exhibit lower symmetry. As an example involving a different type of flow, in § 3.6 we look at steep gravity waves. Finally, in § 3.8, we discuss possible future applications of the stability method, as well its applicability in conjunction with other, more complex approaches.

3.2 Kelvin's argument for equilibrium and stability

3.2.1 The analytical basis for Kelvin's variational argument

In this section, we summarize the mathematical framework underlying Kelvin's argument; we pay particular attention to the nature of the variation employed, as this is essential to establishing a precise link between extrema in a velocity-impulse diagram and changes of stability (as discussed in § 3.3.2), and aim

to provide sufficient background for readers who may not be acquainted with these variational ideas.

While Kelvin's statement of his energy argument dates back to 1876, the development of a mathematical framework had to wait almost a century, starting with the pioneering work of Arnol'd (1966). The first analytical confirmation of Kelvin's argument (for a two-dimensional flow, in a moving reference frame) is traditionally attributed to Brooke Benjamin (1976); Kelvin's argument was subsequently generalized to three-dimensional flows (Fukumoto & Moffatt, 2008).

In order to carefully define the variation we begin by stipulating the conditions that a realistic flow perturbation must satisfy. Let us consider a homogeneous fluid of unit density, and suppose that the perturbation is enacted through a displacement field, say, $\delta\boldsymbol{\ell}(\boldsymbol{x})$, such that a fluid particle originally at $\boldsymbol{x}$ is moved to $\boldsymbol{x} + \delta\boldsymbol{\ell}(\boldsymbol{x})$. The first condition on the perturbation follows from the fact that, since the fluid is incompressible, we must have $\nabla \cdot \delta\boldsymbol{\ell} = 0$. As an additional condition, we suppose that the perturbation respects Kelvin's circulation theorem; that is, we must have, through the variation:

$$\oint_C \boldsymbol{u} \cdot \mathrm{d}\boldsymbol{x} = \text{constant}, \tag{3.1}$$

which must hold for any contour C that is advected by $\delta\boldsymbol{\ell}(\boldsymbol{x})$. As first shown by Arnol'd (1966), this is equivalent to requiring that the vorticity in the flow is advected by $\delta\boldsymbol{\ell}$, and that vorticity production (or destruction) only occurs through vortex stretching (see also Lynden-Bell & Katz, 1981; Moffatt, 1985). This requirement is traditionally named the *isovortical condition* (Arnol'd, 1966), and is formalized mathematically as:

$$\delta\boldsymbol{\omega} = \nabla \times (\delta\boldsymbol{\ell} \times \boldsymbol{\omega}). \tag{3.2}$$

It might appear, at first glance, that considering only isovortical perturbations is overly restrictive, and that this, in turn, may lead to stability predictions of limited use. However, we must stress that, for an inviscid flow, the isovortical condition is actually *necessary* to ensure that the stability results are accurate. As a matter of fact, for a conservative fluid, there is no process that can introduce or remove vorticity within the flow. From an intuitive standpoint, we may suppose that perturbations could be associated, for example, with vortices or solid bodies that are introduced or displaced at large distances from the fluid configuration of interest. Since the far-field of the flow associated with a compact vortex or with a moving body is irrotational, the resulting perturbation on the original flow must be isovortical. We will be making use of the incompressible and isovortical conditions in the rest of this section.

Before focusing on the variational principle, let us briefly consider, for completeness, the expressions for the total energy and linear and angular momenta of the flow ($T, \boldsymbol{L}, \boldsymbol{M}$), together with their connection to the excess kinetic energy and linear and angular fluid impulses ($E, \boldsymbol{I}, \boldsymbol{J}$). Through integration by parts, and using, for example, tensor notation, one may show (Saffman, 1992)):

$$\begin{aligned} T &= \frac{1}{2}\int |\boldsymbol{u}|^2 \,\mathrm{d}V \\ &= \frac{1}{2}\int \boldsymbol{A}\cdot(\boldsymbol{n}\times\boldsymbol{u})\,\mathrm{d}S + \frac{1}{2}\int \boldsymbol{\omega}\cdot\boldsymbol{A}\,\mathrm{d}V \qquad (3.3) \\ \boldsymbol{L} &= \int \boldsymbol{u}\,\mathrm{d}V \\ &= \frac{1}{(D-1)}\int [\boldsymbol{u}(\boldsymbol{n}\cdot\boldsymbol{x}) - \boldsymbol{n}(\boldsymbol{u}\cdot\boldsymbol{x})]\,\mathrm{d}S + \frac{1}{(D-1)}\int \boldsymbol{x}\times\boldsymbol{\omega}\,\mathrm{d}V \qquad (3.4) \\ \boldsymbol{M} &= \int \boldsymbol{x}\times\boldsymbol{u}\,\mathrm{d}V \\ &= \frac{1}{2}\int \boldsymbol{n}\times\boldsymbol{u}|\boldsymbol{x}|^2\,\mathrm{d}S - \frac{1}{2}\int \boldsymbol{\omega}|\boldsymbol{x}|^2\,\mathrm{d}V, \qquad (3.5) \end{aligned}$$

where $\boldsymbol{A}$ is the vector potential (defined such that $\boldsymbol{u} = \nabla\times\boldsymbol{A}$), while D is the

number of space dimensions in which the flow takes place (typically two or three). Therefore, each of $(T, \boldsymbol{L}, \boldsymbol{M})$ can be expressed as the sum of a surface and a volume integral. While the latter is typically well-defined, the surface integrals above are either divergent or depend on the shape of the surface of integration. However, since these surface integrals involve the velocity $\boldsymbol{u}$ on a surface in the far field, they depend, to leading order, on the total circulation in the flow. Therefore, we can point out that these integrals are unchanged by an isovortical perturbation. Hence, provided we compare only flows with the same circulation, we can meaningfully employ the volume integrals appearing in the right-hand sides of (3.3)-(3.5) as substitutes for the energy and momenta. These volume integrals yield the definitions for the excess kinetic energy E and the linear and angular impulses $\boldsymbol{I}$, $\boldsymbol{J}$, respectively.

When considering steady flows in a moving reference frame, it is often natural to treat the velocity of the moving frame as a control parameter (see, for example, Deem & Zabusky, 1978; Burbea & Landau, 1982). However, we prefer to select a control parameter that is conserved by the dynamics; for this reason, we employ a prescribed value of the impulse (denoted as $\boldsymbol{I}_0$ or $\boldsymbol{J}_0$) as the control parameter (this point is further discussed in § 3.3.2).

We should also point out that, for flows with nonvanishing total circulation, the impulse $\boldsymbol{I} = (D-1)^{-1} \int \boldsymbol{x} \times \boldsymbol{\omega} \, \mathrm{d}V$ may always be made zero by placing the coordinate origin at the centroid of vorticity of the configuration. Similarly, for flows with zero total circulation, one can choose the origin of the coordinate system to give vanishing angular impulse $\boldsymbol{J} = -\frac{1}{2} \int \boldsymbol{\omega} |\boldsymbol{x}|^2 \, \mathrm{d}V$. Therefore, if we consider solution families with prescribed circulation, it is sufficient to employ only one of the two impulses to parametrize the steady states. In the rest of this

section, we review the analysis for a rotating reference frame. Similar arguments hold for a translating reference frame.

Let us now consider the details of the variational principle. Kelvin proposed that, with vorticity and impulse given, a steady flow corresponds to a stationary point of the energy. This statement can be formalized mathematically by making use of the theory of Lagrange multipliers (e.g. Lanczos, 1986), such that equilibrium flows would be expected to correspond to stationary points of the functional:

$$H = E - \mathbf{\Omega} \cdot (\boldsymbol{J} - \boldsymbol{J}_0), \tag{3.6}$$

where $\mathbf{\Omega}$ takes the role of a Lagrange multiplier. When considering changes about a flow with a specified vorticity distribution, $E, \boldsymbol{J}$ may be considered as functionals of the position of each fluid particle, $\boldsymbol{\ell}(\boldsymbol{x})$ such that we may write $E[\boldsymbol{\ell}], \boldsymbol{J}[\boldsymbol{\ell}]$. Furthermore, we note that, since we introduced $\boldsymbol{J}_0$ as a control parameter, $\mathbf{\Omega}$ constitutes a variable that must be found as part of the solution. We can therefore define a solution vector $q = (\boldsymbol{\ell}, \mathbf{\Omega})$ and require the variation to vanish:

$$\delta H[q; \delta q] = \delta E[\boldsymbol{\ell}; \delta \boldsymbol{\ell}] - \mathbf{\Omega} \cdot \delta \boldsymbol{J}[\boldsymbol{\ell}; \delta \boldsymbol{\ell}] - \delta \mathbf{\Omega} \cdot (\boldsymbol{J}[\boldsymbol{\ell}] - \boldsymbol{J}_0) = 0, \tag{3.7}$$

where the notation, say, $\delta H[a; \delta b]$ represents the variation of H, with respect to b, evaluated at a. Note that $\boldsymbol{\ell}$ and $\mathbf{\Omega}$ are independent of each other. Therefore, for $\delta H[q; \delta q]$ to always vanish under independent variations $\delta \boldsymbol{\ell}, \delta \mathbf{\Omega}$, we must have:

$$\delta H[q; \delta \boldsymbol{\ell}] = \delta E[\boldsymbol{\ell}; \delta \boldsymbol{\ell}] - \mathbf{\Omega} \cdot \delta \boldsymbol{J}[\boldsymbol{\ell}; \delta \boldsymbol{\ell}] = 0 \tag{3.8}$$

$$\delta H[q; \delta \mathbf{\Omega}] = \boldsymbol{J} - \boldsymbol{J}_0 = 0 \tag{3.9}$$

Equation (3.9) simply requires that the flow impulse matches the prescribed value $\boldsymbol{J}_0$; for the rest of this section, we focus on (3.8). Taking the variation, one

obtains, for the excess kinetic energy:

$$\delta E[\boldsymbol{\ell};\delta\boldsymbol{\ell}] = \frac{1}{2}\int \left(\delta\boldsymbol{A}\cdot\boldsymbol{\omega} + \boldsymbol{A}\cdot\delta\boldsymbol{\omega}\right)\mathrm{d}V \tag{3.10}$$

$$= \frac{1}{2}\int (\boldsymbol{A}\cdot\frac{\partial(\delta\boldsymbol{A})}{\partial n} - \delta\boldsymbol{A}\cdot\frac{\partial\boldsymbol{A}}{\partial n})\,\mathrm{d}S + \int \boldsymbol{A}\cdot\delta\boldsymbol{\omega}\,\mathrm{d}V, \tag{3.11}$$

where we have integrated twice by parts, and made use of the fact that $\nabla^2\delta\boldsymbol{A} = -\delta\boldsymbol{\omega}$. (The dependence of $\delta\boldsymbol{\omega}$ on $\delta\boldsymbol{\ell}$ will be introduced below.) The surface term is zero, provided $\delta\boldsymbol{\omega}$ decays sufficiently rapidly in the far field. Therefore (3.8) becomes:

$$\delta H[q;\delta\boldsymbol{\ell}] = \int (\boldsymbol{A} - \frac{\boldsymbol{\Omega}}{2}|\boldsymbol{x}|^2)\cdot\delta\boldsymbol{\omega}\,\mathrm{d}V \equiv \int \overline{\boldsymbol{A}}\cdot\delta\boldsymbol{\omega}\,\mathrm{d}V, \tag{3.12}$$

where $\overline{\boldsymbol{A}}$ is the vector potential in the moving reference frame.

Let us now employ the isovortical condition, and substitute (3.2) into the above. After integration by parts, one obtains:

$$\delta H[q;\delta\boldsymbol{\ell}] = \int \overline{\boldsymbol{A}}\cdot[\boldsymbol{n}\times(\delta\boldsymbol{\ell}\times\boldsymbol{\omega})]\,\mathrm{d}S - \int \delta\boldsymbol{\ell}\cdot(\overline{\boldsymbol{u}}\times\boldsymbol{\omega})\,\mathrm{d}V, \tag{3.13}$$

where, once again, the surface integral vanishes, provided $\delta\boldsymbol{\ell}$ decays sufficiently rapidly with distance from the origin. Finally, one must note that, since $\delta\boldsymbol{\ell}$ must be incompressible, its components are not independent. However, we may write $\delta\boldsymbol{\ell} = \nabla\times\delta\boldsymbol{a}$, where $\delta\boldsymbol{a}(\boldsymbol{x})$ is an arbitrary vector field. Integrating by parts one more time, and assuming that surface terms vanish, we finally obtain:

$$\delta H[q;\delta\boldsymbol{\ell}] = -\int \delta\boldsymbol{a}\cdot[\nabla\times(\overline{\boldsymbol{u}}\times\boldsymbol{\omega})]\,\mathrm{d}V, \tag{3.14}$$

such that $\delta H[q;\delta\boldsymbol{\ell}] = 0$, with arbitrary $\delta\boldsymbol{a}$, requires:

$$\nabla\times(\overline{\boldsymbol{u}}\times\boldsymbol{\omega}) = \boldsymbol{0}, \tag{3.15}$$

which can be recognized as the steady vorticity equation, in the moving reference frame. Hence a stationary point of the energy, with given impulse, corresponds to a steady flow in the moving reference frame. A similar analysis may

of course be performed for translating systems, with ($\boldsymbol{U}$, $\boldsymbol{I}$) replacing ($\boldsymbol{\Omega}$, $\boldsymbol{J}$) (see e.g. Fukumoto & Moffatt, 2008).

3.3 Linking velocity-impulse diagrams and exchanges of stability

From a historical standpoint, the notion that a bifurcation diagram could be used to detect changes of stability dates back at least to the work of Poincaré (1885) on self-gravitating fluid figures of equilibrium (see the monograph of Chandrasekhar, 1969, for a historical perspective). However, examining the history of the subject quickly reveals that the practical use of stability approaches based on bifurcation diagrams is fraught with subtle issues, which can often give rise to incorrect stability predictions. A classical example is given by the self-gravitating figures of equilibrium given by the series of Maclaurin spheroids (which start with a spherical, uniformly rotating liquid mass). At ellipticity 0.8127, these are connected to the tri-axial Jacobi ellipsoids by a steady-state bifurcation (see Lyttleton, 1953; Chandrasekhar, 1969). However, contrary to what may be expected from a naive application of bifurcation theory, the Maclaurin spheroids retain their stability after this bifurcation. The explanation for this fact is that the ellipsoids have equatorial circulation that is different from that of the Maclaurin spheroids; by Kelvin's circulation theorem, this implies that an inviscid transition between the two families of solutions is impossible (Lynden-Bell, 1965). (Another view, proposed here in § 3.3.3, would be that the ellipsoids and the spheroids cannot in fact be joined into a "proper" family of solutions.)

Other misleading predictions due to subtle conceptual issues abound; another example is found in a letter between Sir George Gabriel Stokes (1879) and Lord Kelvin, where Stokes suggested that water waves might undergo a change of stability at a turning point in wave velocity. A similar expectation was expressed, approximately a century afterwards, by Longuet-Higgins (1978*a*). This prediction was however contradicted by the numerical results of Tanaka (1983), who showed that instability develops well *after* the turning point in phase velocity. Tanaka's stability boundary was later confirmed by further numerical studies (Tanaka, 1985), and the structure of the change of stability was the subject of extensive additional work (Longuet-Higgins, 1984*b*, 1985; Saffman, 1985). As we argue below, here the issue lies with the fact that the wave velocity is *not* a meaningful control parameter for the purpose of determining stability, and a different parameter should be used.

To summarize, the studies mentioned above raise two important points. Firstly, one must carefully define how steady flows should be grouped into solution families. Secondly, the choice of the correct control parameter may not be obvious. We address both of these issues below.

3.3.1 The nature of changes of stability in conservative fluid flows

Let us begin by discussing the possible instability mechanisms for a generic conservative fluid system, and discuss the link between the eigenvalues that one obtains from a linear stability analysis and the shape of the energy landscape in the neighbourhood of a steady state.

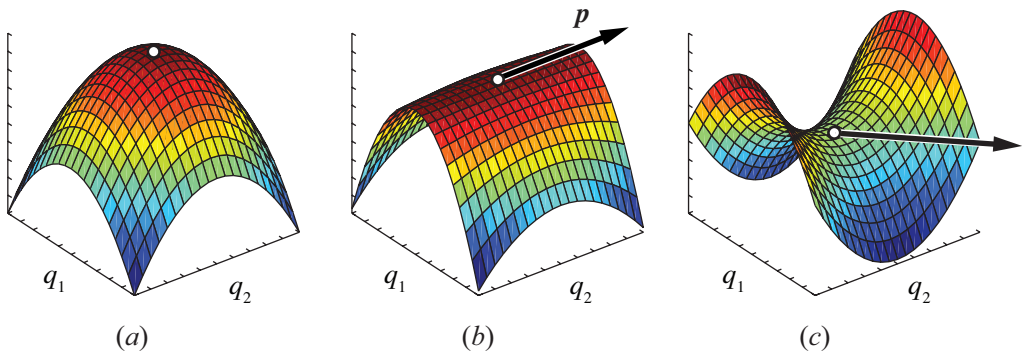

Figure 3.4: Diagram illustrating the development of a saddle of the energy, sketched here for a solution space with coordinates $\boldsymbol{q} = (q_1, q_2)$. Supposing that the family of solutions begins with an equilibrium corresponding to a maximum in energy (as shown in *a*), we first encounter a marginal state (sketched in *b*), for which there exists a perturbation (associated with the vector $\boldsymbol{p}$ in the figure) that keeps the energy constant. All other perturbations are still associated with a decrease in energy. In (*c*), a saddle has formed; it is then possible to perturb the system so as to increase, decrease, or maintain constant energy. The latter possibility (marked by an arrow) enables an instability to develop.

Firstly, we must point out that the Euler equations are unchanged by the time-reversal transformation $(\boldsymbol{u}, t) \to -(\boldsymbol{u}, t)$. This symmetry implies that, if σ is an eigenvalue of the linearized problem, so must be $-\sigma$. Since complex eigenvalues must always appear as complex conjugate pairs $\sigma = \sigma_{\mathrm{R}} \pm \mathrm{i}\sigma_{\mathrm{I}}$, the eigenvalues of a reversible system must occur in complex quartets $\pm(\sigma_{\mathrm{R}} \pm \mathrm{i}\sigma_{\mathrm{I}})$; the only exceptions are given by purely real or purely imaginary eigenvalues, which may occur in pairs, or by a single zero eigenvalue (Lamb & Roberts, 1998).

Next, in order to distinguish between different instability mechanisms, let us begin by considering a steady flow that, for some suitable values of the control parameter λ, can be easily shown to correspond to a local maximum of the energy. By Kelvin's argument, this flow is stable; the associated energy landscape is represented schematically in figure 3.4(*a*). The fact that the flow constitutes a maximum of the energy is equivalent to stating that the imposition of *any* eigen-

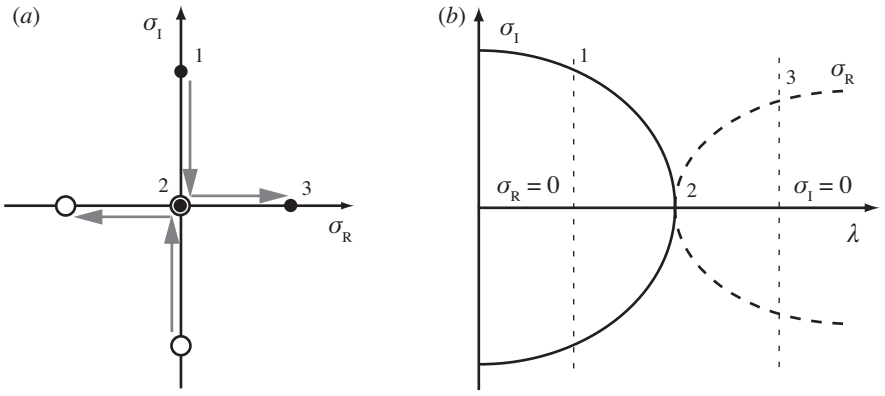

Figure 3.5: Eigenvalue behaviour, as a function of a control parameter λ, in the neighbourhood of an exchange of stability, showing (*a*) evolution in the complex plane, and (*b*) a plot of both the real and imaginary parts of the eigenvalue as a function of λ.

mode must yield a negative change of energy (in the dynamical systems literature, such modes are said to have negative *signature*; see Arnol'd & Avez, 1968; Lamb & Roberts, 1998). For any linear eigenmode, the corresponding eigenvalues must be purely imaginary, as the occurrence of a real part would give rise to instability. The eigenvalue structure is represented schematically by case 1 in figure 3.5.

Let us now suppose that, as the control parameter reaches some critical value, say $\lambda = \lambda_c$, the flow becomes unstable. For this to be possible, we must have that the energy landscape switches to a saddle (as illustrated in figure 3.4*b*, *c*). In the complex plane, the symmetry due to time-reversibility implies that the the change of stability must correspond to the coalescence of an eigenvalue pair at the origin (case 2 in figure 3.5), after which the eigenvalues move onto the real axis, implying instability (shown by case 3 in figure 3.5). (In the dynamical systems literature, this eigenvalue behaviour is known as an *exchange of stability*.) When the eigenvalue pair vanishes at λ_c, the associated eigen-

mode yields a perturbation that, when imposed on the base flow, does not grow or decay, and therefore also represents a steady state. This steady state may be a new one, which is not included in the previously known family of equilibrium flows, but which instead constitutes the beginning of another series of solutions, connected to the original family of steady flows at a bifurcation. The study of this particular case, where the exchange of stability is associated with a bifurcation, is deferred to § 3.4 in this paper.

On the other hand, an exchange of stability may instead turn out to *not* correspond to a bifurcation (incidentally, when first observed for gravity waves, this point proved contentious; see Tanaka, 1985; Saffman, 1985). When this happens, the eigenmode does not yield a new equilibrium flow, and instead produces a steady state that belongs to the original family. In other words, in the absence of a bifurcation, the eigenmode associated with a change of stability must revert to a trivial mode of the system at $\lambda = \lambda_c$. This type of instability is the focus of the next section.

Finally, we mention a third type of instability that may occur in a conservative system. In certain circumstances, a steady flow corresponding to an energy saddle may nevertheless be stable. When this occurs, all eigenvalues are of course imaginary; however, while there are still modes with negative signature, there will now be one or more eigenmodes with positive energy signature (corresponding to the "upward" direction of the saddle). As we progress along the family of solutions, if two eigenmodes with opposite signature happen to eventually have the same (imaginary) eigenvalues, they may cooperate and coalesce into a *single* eigenmode, yielding zero overall energy change and therefore enabling instability. In the complex plane, this corresponds to the collision

of two pairs of eigenvalues along the imaginary axis (away from the origin), after which the eigenvalues move along the direction of the real axis, giving rise to a complex quartet. An instability of this type constitutes a resonance phenomenon, and yields a perturbation whose amplitude grows while also undergoing oscillation. More complex resonance behaviours are also possible (Lamb & Roberts, 1998).

This latter type of instability is not addressed in this paper; however, in a separate contribution, we present arguments indicating that an oscillatory instability is impossible for two-dimensional flows involving fewer than three vortices (Luzzatto-Fegiz & Williamson, 2010*a*). This finding is corroborated by the fact that oscillatory instabilities have indeed never been reported for two-dimensional flows involving one or two vortices (see e.g. Thomson, 1880*b*; Love, 1893; Dritschel, 1985; Kamm, 1987; Dritschel, 1995; Ehrenstein & Rossi, 1999; Meunier *et al.*, 2002).

3.3.2 Linking extrema in impulse to changes of stability

In this section, we focus on detecting exchanges of stability that are *not* associated with a bifurcation. According to the discussion in the previous section, this involves examining perturbations that, once applied to a given equilibrium, yield a steady flow that still belongs to the original family of solutions. In other words, we must consider perturbations that take an equilibrium flow and transform it into a *neighbouring* steady flow on the solution series. To detect instabilities, we seek conditions for which the energy signature associated with such a perturbation changes sign, as this will represent the creation (or destruction) of

an energy saddle, as sketched in figure 3.4.

Firstly, let us return to the fact that, in § 3.2.1, we chose the fluid impulse (either $\boldsymbol{I}_0$ or $\boldsymbol{J}_0$) as the control parameter for families of steady flows. This decision may seem impractical, since the velocity may be treated simply as an independent variable, while the fluid impulse must be obtained as an integral over the vorticity field. However, our choice may be explained as follows. For a conservative flow, we propose a definition of a "true" control parameter as a quantity that, once specified, is conserved by the dynamics. Of course, the frame velocity $\boldsymbol{\Omega}$ is not conserved by the dynamics, and is in fact not even defined for an unsteady flow. On the other hand, the impulse $\boldsymbol{J}$ is indeed conserved in an inviscid flow, and is therefore maintained constant if the flow departs from equilibrium.

We should also note that the solutions found for a steady flow are of course the same, regardless of the choice of parametrization. On the other hand, the *stability properties* will depend on the parameter used. For example, if we employ $\boldsymbol{\Omega}$ as the fixed parameter, we will obtain different stability boundaries than if we were to choose $\boldsymbol{J}_0$ (this is also true, for example, for a linear stability analysis; see Lyttleton, 1953, for a discussion relevant to self-gravitating fluid masses). The upshot is that, when only computing *equilibria*, one may use any convenient control parameter; on the other hand, when trying to evaluate stability (through a linear analysis, a bifurcation diagram, or other means) a physically meaningful choice of control parameter is crucial to obtaining correct stability results.

Let us start the derivation by writing the stationary condition ($\delta H[q;\delta q] = 0$) from Kelvin's argument using notation from functional analysis. Consider, for example, flow that is steady in a rotating frame, and choose axes such that

$\boldsymbol{\Omega} \cdot \boldsymbol{J} = (0, 0, \Omega J)$ (without loss of generality). The steady flow then corresponds to:

$$\delta H[q; \delta q] = \int \sum_{i=1}^{4} \frac{\partial h}{\partial q_i} \delta q_i \mathrm{d}V \equiv \langle H', \delta q \rangle, \tag{3.16}$$

where h is, in essence, an energy density per unit volume, and a prime denotes the functional (Fréchet) derivative with respect to q. We allow for the possible existence of turning points in the control parameter J_0 by introducing an auxiliary parameter s, which increases monotonically along the solution family (s may be thought of, for example, as a suitably defined arclength in the solution space). Then steady solutions can be described as $[q_0(s), J_0(s)]$, where q_0 denotes the equilibrium state corresponding to a given J_0.

Following the discussion in the previous section, in order to find exchanges of stability that do not correspond to bifurcations, we must focus on perturbations that, when applied to a member of the solution family, simply yield a neighbouring solution. In the notation introduced above, such a perturbation must be proportional to the vector $\dot{q}_0$, where a dot denotes differentiation with respect to s. This may of course be verified by noting that, given a steady state $q_0(s)$, another solution a distance δs away from $q_0(s)$ is given by $q_0 + \dot{q}_0\, \delta s + O(\delta s^2)$.

In order to detect the formation (or the destruction) of an energy saddle we examine the change in H associated with $\dot{q}_0$. By employing (3.16) with $\delta q = \dot{q}_0$, we find that the first-order variation in H with respect to $\dot{q}_0$ is zero, that is,

$$\delta H[q_0; \dot{q}_0] = 0. \tag{3.17}$$

We next consider the second variation, given by:

$$\delta^2 H[q_0; \dot{q}_0] = \langle \dot{q}_0 H'', \dot{q}_0 \rangle. \tag{3.18}$$

We now need to find a simple expression for $\delta^2 H[q_0, \dot{q}_0]$. To do so, let us return to the stationary condition $\delta H[q, \delta q] = 0$; since this holds for any location along the solution branch, we have that $\mathrm{d}(\delta H)/\mathrm{d}s = 0$ anywhere along the solution family. Noting that, along the solution family, H depends on q and J_0, the chain rule of differentiation gives:

$$\langle \dot{q}_0 H'', \delta q \rangle + \langle \frac{\partial H'}{\partial J_0}, \delta q \rangle \dot{J}_0 = 0. \tag{3.19}$$

If we specialize (3.19) to the case $\delta q = \dot{q}_0$, the first term becomes $\delta^2 H[q_0, \dot{q}_0]$, as needed. To simplify the second term in (3.19), note that $\partial H/\partial J_0 = \Omega$, such that $\langle \partial(H')/\partial J_0, \dot{q}_0 \rangle = \dot{\Omega}_0$. This leads to the following remarkably compact expression:

$$\delta^2 H[q_0, \dot{q}_0] = -\dot{\Omega}_0 \dot{J}_0. \tag{3.20}$$

We therefore expect the formation (or destruction) of a saddle of H to occur for either $\dot{\Omega}_0 = 0$ or $\dot{J}_0 = 0$. However, the case $\dot{\Omega}_0 = 0$ may be discarded on simple physical grounds. As a matter of fact, for the perturbation $\dot{q}_0$ to be physically realizable, it must leave the impulse unchanged, such that $\langle J', \dot{q}_0 \rangle = 0$. However, along the solution family, we may write

$$\langle J', \dot{q}_0 \rangle = \dot{J} = \dot{J}_0. \tag{3.21}$$

Hence, for q_0 to be physically admissible, we must have $\dot{J}_0 = 0$; in other words, we have to be at a turning point of J_0. Therefore whether $\dot{\Omega}_0$ vanishes or not is irrelevant, and we find that *turning points in impulse are associated with changes of stability*.

If the solutions were initially at a maximum in H, the turning point in J_0 must correspond to the formation of a saddle, and therefore to a loss of stability. However, if the solution series is already unstable to, say, n modes of perturbation, the turning point may yield either a loss or a gain of stability. We now wish

to distinguish between these two cases; to do so, we need to establish whether a saddle is created or destroyed. We start by determining whether $\delta^2 H[q_0, \dot{q}_0]$ is switching from positive to negative (or vice-versa). In order to do so, we differentiate (3.20) with respect to s:

$$\frac{\mathrm{d}}{\mathrm{d}s}\left(\delta^2 H[q_0, \dot{q}_0]\right) = -\dot{\Omega}_0 \ddot{J}_0 \qquad \text{for} \qquad \dot{J}_0 = 0. \tag{3.22}$$

We note that the sign of both quantities on the right hand side can be instantly read from the the shape of a plot of Ω_0 and J_0. Hence *the shape of a velocity-impulse diagram can be used to find whether stability is lost or gained at a turning point in impulse.*

As an example, let us consider a family of solutions, in an unbounded fluid, beginning with a stable state. In the absence of solid boundaries, the energy may always be decreased by "spreading out" the vorticity (for example, one can impose some waviness along the circumference of the vortex). Hence a minimum of the energy cannot be reached in an unbounded flow, and a stable flow will instead typically correspond to an energy maximum (a fact that was already realized by Thomson, 1880*a*), such that $\delta^2 H < 0$ for any perturbation. Therefore, for instability to occur, we need $\delta^2 H[q_0, \dot{q}_0]$ to switch from negative to positive. This, in turn, implies $-\dot{\Omega}_0 \ddot{J}_0 > 0$. Therefore, when traversing a velocity-impulse plot from left to right, stability is lost at a maximum in impulse, as illustrated in figure 3.6(*a*). By the same argument, we can also infer that a local minimum of the impulse is linked to a gain of stability, as the diagram is traversed from left to right (as shown in figure 3.6*b*). An important consequence of this result is that it is possible to keep count of the number of unstable modes for each portion of the solution branch. For example, in the case sketched in figure 3.6(*c*), we can deduce that the flow *returns to stability* after the second turning point, while in the scenario depicted in (*d*) the flow becomes unstable with respect to *additional*

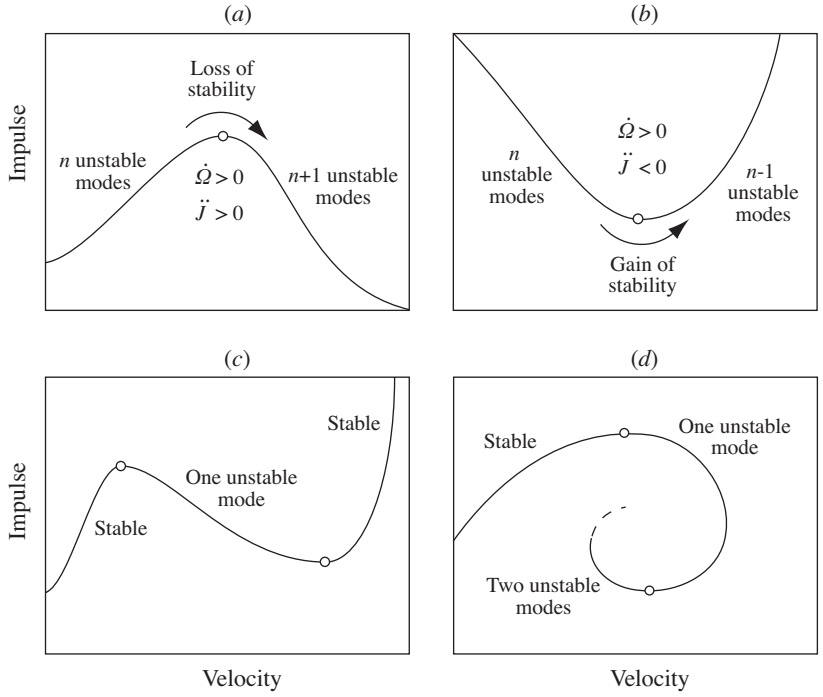

Figure 3.6: Schematic velocity-impulse diagrams. A maximum or minimum of the impulse is associated with a gain or loss of stability, respectively, as the curve is traversed from right to left.

modes as we wind around a spiral in a velocity-impulse diagram.

Of course, the analysis presented here can also be applied to flows that are steady in a translating (instead of rotating) frame, provided (Ω, J) in the above are replaced with (U, I). Furthermore, while most families of flows of practical interest will typically start at a maximum of energy, it is possible to construct bounded inviscid flows corresponding to minima of the energy (this is the case, for example, for flow in a circular container where vorticity is arranged in a layer neighbouring the wall; see Thomson, 1880*a*). For such problems, the direction of the changes of stability marked in figure 3.6 is simply reversed.

In summary, we have shown that turning points in impulse are linked to exchanges of stability. Further to this, the analysis presented above allows us

to distinguish between a gain and a loss of stability directly from a velocity-impulse diagram.

3.3.3 Building solution families through kinematically possible, irrotational perturbations

In the previous section, we derived a turning-point stability approach for families of steady conservative flows. In this section, we address the somewhat subtle issue of what constitutes a well-defined family of solutions.

The essence of this problem may be introduced by drawing a comparison between a simple vortical flow and an example involving the stability of solid structures, for which well-established turning-point theorems are also available (Thompson, 1979; Thompson & Hunt, 1973). Consider a cantilevered beam, clamped at one end, with a point load P applied at the free end, resulting in a displacement ϵ. As we change the load P, we naturally obtain a family of steady states, which we may represent through a load-displacement diagram (P, ϵ). We contrast this with the problem of developing a family of steady states for a fluid flow, starting, for example, with a circular, uniform vortex. Among the possible options, we may make the vortex elliptical, change the vorticity distribution while keeping the vortex axisymmetric, or split the vortex into two or more distinct parts; are all of these valid possibilities?

In order to resolve this question, we return to the analysis presented in the previous section, and recall that, at the change of stability, the mode enabling instability is $\dot{q}_0 = (\dot{\boldsymbol{\ell}}_0, \dot{\Omega}_0)$. Further to this, recall that, for $\dot{q}_0$ to represent a realistic

flow perturbation, $\boldsymbol{\ell}_0$ must be a kinematically possible displacement field, as required in the analysis of Kelvin's argument discussed § 3.2.1. However, as noted earlier, $\dot{q}_0$ also represents the connection between two neighboring steady states on a solution branch. This implies that it must be possible to move between neighboring solutions through a kinematically possible displacement field. In other words, *new solutions must be found by applying kinematically possible perturbations to a given steady flow.* If we return to the example in the previous paragraph, the only option that satisfies this criterion involves deforming the vortex outline into an elliptical (or, possibly, more complex) shape, while maintaining the area and vorticity constant.

In practice, if one is computing steady flows numerically, the process of imposing a tentative kinematic displacement field while searching for new solutions may be difficult to implement. For this reason, it is convenient to consider a different viewpoint to enforce this condition. Conservative flows admit a set of conserved quantities (beside energy and impulse), known as *Casimirs* in the Hamiltonian mechanics literature (Holm *et al.*, 1985; Shepherd, 1990; Morrison, 1998). For certain flows, the requirement that two equilibria are related by a series of kinematically possible displacements is equivalent to requiring that they have the same set of Casimirs.

For example, for a two-dimensional, homogeneous flow, any area-integral of a function of the vorticity (say, $\int f(\omega)\,\mathrm{d}A$) can be shown to be a Casimir (Saffman, 1992). Provided f is a smooth function, enforcing an arbitrary set of Casimirs is equivalent to prescribing the values of the area-integrals of any integer power of the vorticity, $C_n = \int \omega^n\,\mathrm{d}A$, with $n = 1, 2, 3....$ This can be advantageous, since for a given vorticity field $\omega(\boldsymbol{x})$, the C_n's can easily be computed numerically.

Furthermore, this simple rule to build solution families can be used to check whether the stability of a previously obtained solution series can be inferred from a bifurcation diagram. In fact, it seems that many solution sets in the literature do not actually satisfy this condition. Examples of *analytical* flows whose Casimirs change along the solution series include the nonsymmetric, opposite-signed vortex pairs discovered by Chaplygin (1903) (these are described in detail in Meleshko & van Heijst, 1994), as well as the solutions of Stuart (1967), which range from a row of point vortices to a shear layer. This implies that, differently from suggestions to the contrary (see p. 191 in the monograph by Saffman, 1992), the stability of the Stuart vortices cannot be directly analysed through a turning-point argument.

We should also note here that numerical methods for computing steady flows often assume a specified vorticity distribution (Ehrenstein & Rossi, 1999; Meunier *et al.*, 2002), or select a particular functional relationship between the vorticity ω and the streamfunction ψ inside each vortex (Eydeland & Turkington, 1988; van de Fliert, 1995; Chavanis & Sommeria, 1996, 1998). While they are practically advantageous from a numerical standpoint, these assumptions often lead to solution series whose stability may not be determined from a turning point approach.

To conclude this section, we note that, when computing vortices numerically, there are several methods that one may employ to prescribe the values of the Casimirs throughout the solution procedure. If choosing to discretize vortices through patches of uniform vorticity, it is sufficient to ensure that each vortex region maintains the same area A and edge vorticity jump $\Delta\omega$, as we traverse the solution family. For smooth vorticity distributions, a Casimir-preserving

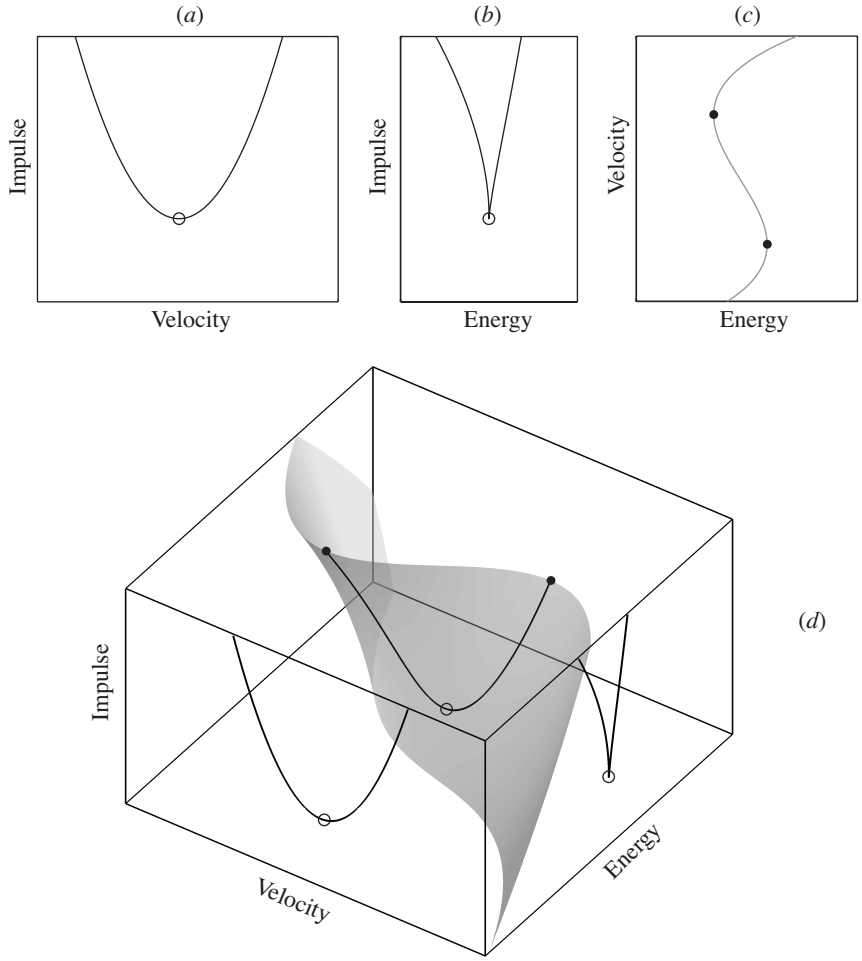

Figure 3.7: Sketch of the relationship between energy, impulse, and velocity, in the neighbourhood of an exchange of stability that is not associated with a bifurcation.

scheme was proposed by Vallis *et al.* (1989), who constructed a relaxation approach for finding maximum-energy (and thus stable) steady flows in a fixed reference frame. A theoretical generalization of their work was proposed by Shepherd (1990) for moving reference frames; however, to the best of our knowledge, Shepherd's theory has not yet been successfully implemented in a numerical technique (as pointed out recently by Morrison & Flierl, 2009)). Remarkably, it seems that the general problem of computing *unstable* steady flows with prescribed Casimirs has not been addressed before.

3.3.4 The relationship between extrema in impulse and extrema in energy

Past studies of steady uniform vortices have observed that turning points of energy were found to coincide with extrema in impulse, to the accuracy of the numerical calculations performed (Saffman & Szeto, 1980; Dritschel, 1985; Kamm, 1987; Dritschel, 1995). In fact, there is a simple analysis that can be used to show that $\dot{E} = 0$ and $\dot{J} = 0$ must occur simultaneously, as we explain below.

Let us consider a family of solutions with prescribed Casimir invariants, and write the stationary condition $\delta H = 0$ as:

$$\langle E', \delta q \rangle = \langle (\Omega J)', \delta q \rangle \tag{3.23}$$

such that, choosing $\delta q = \dot{q}_0$, and noting $\langle E', \dot{q}_0 \rangle = \dot{E}, \langle (\Omega J)', \dot{q}_0 \rangle = \Omega \dot{J}$, we have:

$$\dot{E} = \Omega \dot{J}. \tag{3.24}$$

Therefore, provided $\Omega \neq 0$, an extremum in impulse must also correspond to an extremum in energy. In an impulse-energy plot, this gives rise to a cusp for any family of solutions constructed through kinematically possible, irrotational perturbations, as sketched in figure 3.7(a, b).

Let us visualize this result in the three-dimensional space described by velocity, impulse, and energy. The family of steady solutions will correspond to a (one-dimensional) curve in this space, which may be reconstructed from the two-dimensional views of figure 3.7(a) and (b). The result is shown figure 3.7(a) and (b); for clarity, the curve is embedded onto a two-dimensional surface (shown in grey in the figure).

From a broader viewpoint, turning points of this type are, in fact, a manifestation of the cusp catastrophe, which was first treated in the context of singularity theory by Whitney (1955) (see also Thom, 1972; Arnol'd, 1984). A remarkable feature of cusp catastrophes is that they are structurally stable, since a small deformation of the two-dimensional surface sketched in figure 3.7*c* will still yield the same qualitative features in the projected views. This inherent robustness allows cusps catastrophes to arise in a wide variety of contexts in science and engineering; examples include self-gravitating masses in astrophysics (Katz, 1978; Chavanis, 2002), thin shell structures in engineering (Thompson, 1975, 1979) and chemical reactors (Maddocks, 1987).

Returning to the problem of diagnosing stability of steady flows, we conclude that, at least in principle, it is indeed possible to link a cusp in an impulse-energy diagram to a change of stability, as was suggested on a heuristic basis by Saffman & Szeto (1980). However, doing so requires one to first address a number of complications. Firstly, one needs to compute numerically E for each steady state; as explained in § 3.1, this is significantly more computationally expensive that evaluating the impulse. Secondly, obtaining the direction of the change of stability requires reading the second derivative in energy (that is, $\ddot{E}$) along the family of solutions. This, in turn, implies that one must be able to distinguish between a "top" and a "bottom" branch in a (J, E) plot. As discussed in § 3.1, there are several known flows where this is not feasible (Kamm, 1987). For these reasons, the use of an impulse-energy plot for determining stability, while possible in principle, does not seem to offer any immediate practical advantages over a velocity-impulse diagram.

3.3.5 Alternative parametrizations: flows that are periodic in space

We briefly consider here the special case of flows that are periodic in one space direction (say, x), such that for any flow property ϕ we can write $\phi(x, y, z) = \phi(x + L, y, z)$, where L is the width of the periodic strip. It can be shown that the mathematical formulation of Kelvin's argument discussed in § 3.2.1 also holds for space-periodic flows, provided the displacement field employed to take the variation is also periodic. Furthermore, simple physical arguments dictate that steady flows in a periodic strip must either translate or be stationary (Meiron *et al.*, 1984). The absence of any rotating equilibria implies that (Ω, J) are irrelevant, and any steady state is associated with

$$\delta H = \delta[E - U(I - I_0)] = 0. \tag{3.25}$$

For these flows, we may apply the velocity-impulse approach introduced earlier in § 3.3.2, by simply considering families of solutions with given Casimirs and L = constant. However, for any flow with non-zero overall circulation over one cell of width L (such as, for example, a row of identical vortices), the linear impulse can always be made to vanish by placing the coordinate origin at the vorticity centroid (Saffman, 1992). Therefore, for a wide class of flows, one cannot use turning points in I_0 for stability purposes. Furthermore, even for flows with non-zero impulse (such as a Kármán vortex street) it may be advantageous to be able to parametrize the solution family by L, instead of I_0. We therefore show here how to recast the argument of § 3.3.2 in terms of this parametrization.

Consider families of solutions for which I_0 takes a single prescribed value, such that the dependence on the fluid impulse vanishes along the solution se-

ries. Let us suppose that L may be considered as a control parameter. This implies that the flow remains space-periodic at all times, which in turn requires that any perturbation must have the same periodicity as the original flow. Then, by following steps similar to those in (3.16)-(3.20), we first find:

$$\delta^2 H[q_0, \dot{q}_0] = \langle \frac{\partial H'}{\partial L}, \dot{q}_0 \rangle \dot{L}. \tag{3.26}$$

Let us now focus on finding a simple expression for the right-hand side in (3.26). Since the impulse is required to be constant along the family of solutions, and U does not depend explicitly on L, we have that $\partial H/\partial L = \partial E/\partial L$. We therefore can write:

$$\delta^2 H[q_0, \dot{q}_0] = \frac{\mathrm{d}}{\mathrm{d}s}\Big(\frac{\partial E}{\partial L}\Big)\dot{L}, \tag{3.27}$$

and, taking the total derivative with respect to s:

$$\frac{\mathrm{d}}{\mathrm{d}s}\Big(\delta^2 H[q_0, \dot{q}_0]\Big) = \frac{\mathrm{d}}{\mathrm{d}s}\Big(\frac{\partial E}{\partial L}\Big)\ddot{L} \quad \text{at} \quad \dot{L} = 0, \tag{3.28}$$

which is essentially the same result as in § 3.3.2, with (Ω, J) replaced by $(\partial E/\partial L, -L)$. Therefore, a turning point in L corresponds to a change of stability for a superharmonic mode, and whether the change corresponds to a loss or gain of stability follows from the shape of a plot of L and $\partial E/\partial L$.

To conclude this section, we consider the practical problem of computing $\partial E/\partial L$ in a numerical setting. Once the series of steady flows has been obtained, we may find $\partial E/\partial L$ by calculating the energy $E(q, L)$, as well as $E(q, L + \Delta L)$ for each equilibrium, and using the finite-difference approximation $\partial E/\partial L \approx [E(q, L + \Delta L) - E(q, L)]/\Delta L$. However, this requires that we calculate the energy twice for each steady state. This may be avoided if we instead consider the *total* derivative $\mathrm{d}E/\mathrm{d}L$, defined as the change of E, with respect to L, taken *along* the

family of solutions. By the chain rule, this can be written as:

$$\begin{aligned} \frac{\mathrm{d}E}{\mathrm{d}L} &= \langle E', \dot{q}_0 \rangle \left(\frac{\partial L}{\partial s} \right)^{-1} + \frac{\partial E}{\partial L} \\ &= \frac{\partial E}{\partial L}, \end{aligned} \tag{3.29}$$

since $\langle E', \dot{q}_0 \rangle = 0$ along the solution family. Therefore we may obtain $\partial E/\partial L$ by simply computing E for each steady state, evaluating the energy difference ΔE between two equilibria whose L differs by a small amount ΔL, and using the approximation $\partial E/\partial L = \mathrm{d}E/\mathrm{d}L \approx \Delta E/\Delta L$. Hence it is sufficient to evaluate E once for each equilibrium flow to obtain an approximation for $\partial E/\partial L$.

3.4 Introducing imperfections to reveal bifurcations in steady flows

Let us now return to the problem of detecting an exchange of stability that *is* associated with a bifurcation to a new family of steady solutions. The velocity-impulse diagram introduced in § 3.3.2 is, by itself, insufficient to find these changes of stability, as they are not associated with turning points in a control parameter. This is, in essence, the second objection raised by Dritschel (1985), which applies to any stability approach based exclusively on the use of turning points.

In order to make this problem somewhat more concrete, let us consider a simple analytical example, of a type common in singularity theory, by examining the steady solutions of the problem $\mathrm{d}q/\mathrm{d}t = q^3/2 - \lambda q$, where λ is the control parameter. The equation $\mathrm{d}q/\mathrm{d}t = 0$ has solution $q = 0$ for any λ, and $q = \pm\sqrt{2\lambda}$

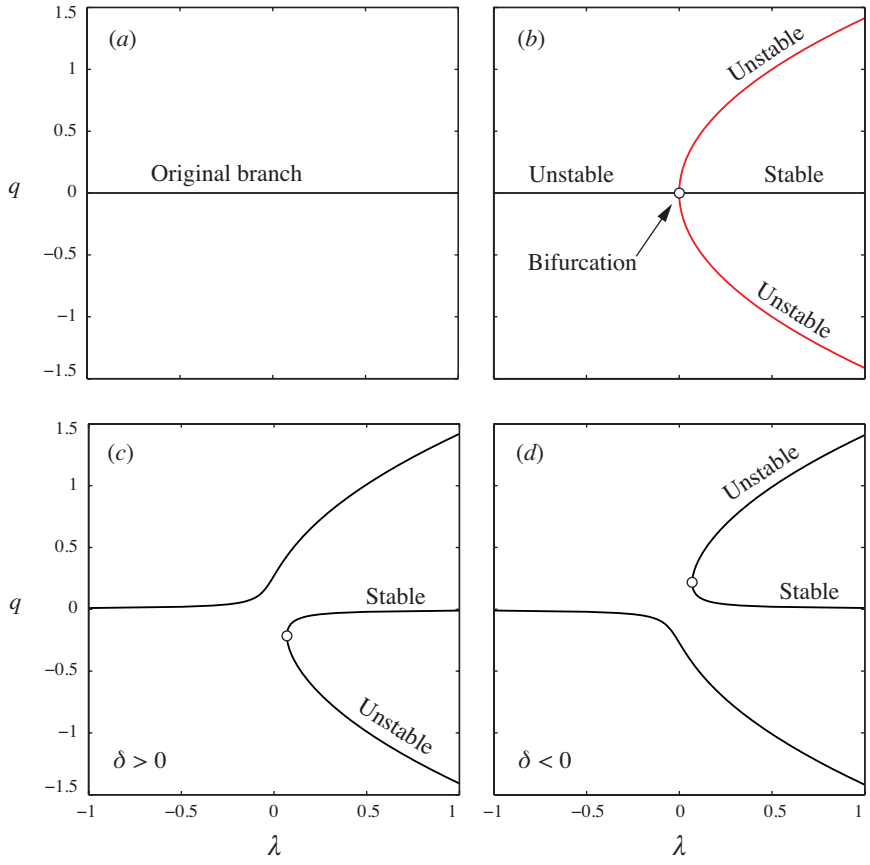

Figure 3.8: Illustration of the effect of introducing an imperfection, with reference to solutions of the example equation $q^3/2 - \lambda q = 0$. Suppose we are seeking solutions numerically; we may obtain the branch $q = 0$ (shown in *a*), but would likely miss the existence of a bifurcation at the intersection with another solution branch (*b*). The associated change of stability would then go undetected without a linear stability analysis. However, since the bifurcation point is structurally unstable, modifying the equilibrium equation to $q^3/2 - \lambda q + \delta = 0$ (with $\delta = \pm 0.01$) breaks the diagram into distinct branches (*c*,*d*), uncovering the bifurcation.

for $\lambda > 0$, such that the intersection of the two series of steady states gives rise to a bifurcation.

However, let us suppose here that we are computing solutions numerically, say, starting from an arbitrary location along the $q = 0$ branch (as sketched in figure 3.8*a*). We would then be likely to continue marching along the same trivial solution branch, unaware of the bifurcation at $\lambda = 0$ (which is shown in

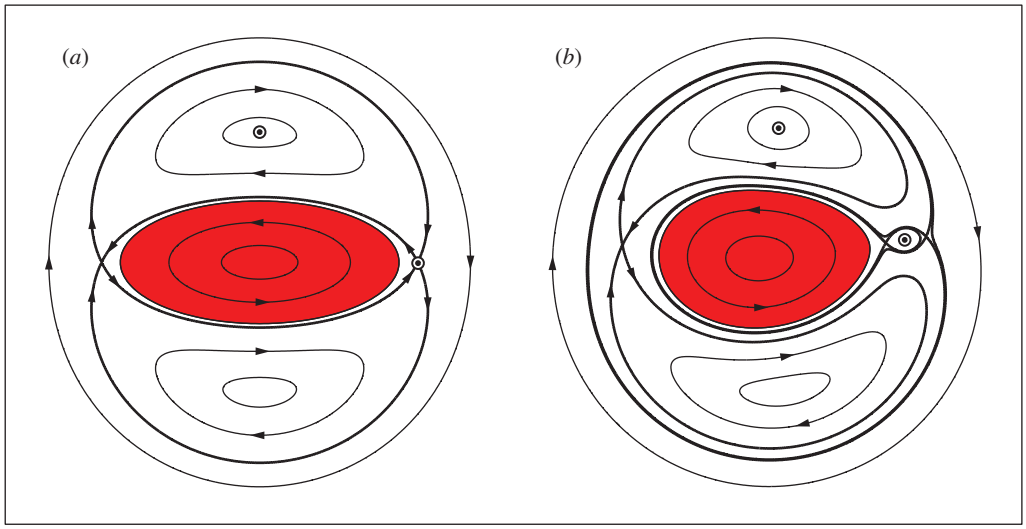

Figure 3.9: Illustration of the effect of introducing a symmetry-breaking imperfection, for a vortical flow. (*a*) shows the streamlines of the flow field in the reference frame that is co-rotating with the elliptical vortex shape. In order to break the geometric symmetry in the flow, we introduce point vortices at certain stagnation points (marked by the bull's eyes in *b*), and seek the vortex shape and point vortex positions yielding a steady flow. For the purposes of preparing this illustration, a comparatively strong pair of point vortices was used; in practice, very weak point vortices are effective in detecting bifurcations.

figure 3.8*b*), thus failing to detect the associated change of stability.

However, a basic result from singularity theory is that bifurcations connecting different families of steady solutions are not robust under small changes in the governing equations, and will instead break into distinct branches, ultimately giving rise to turning points (Poston & Stewart, 1978; Golubitsky & Schaeffer, 1985). The effects of this structural instability have been observed across a wide range of areas of work, ranging from structural mechanics (Thompson, 1975) to the growth of viscous fingers at the interface between two fluids (Casademunt & Jasnow, 1991), to capillary bridges (Chen & Steen, 1996). To the best of our knowledge, this use of imperfections has never been explored before in the study of vortex dynamics.

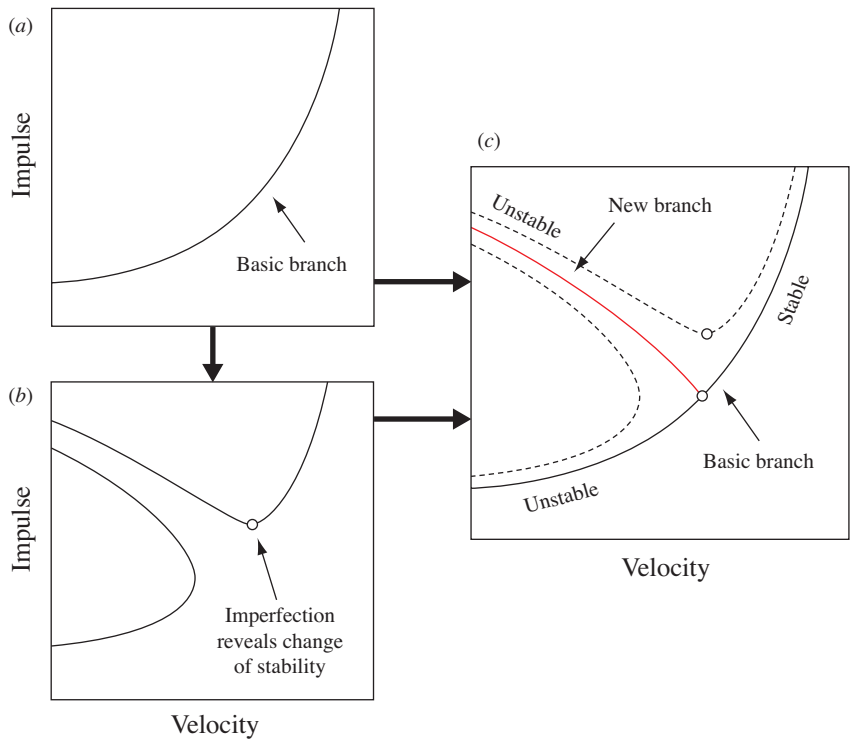

Figure 3.10: Construction of an imperfect velocity-impulse (IVI) diagram. (*a*) shows a velocity-impulse diagram for a basic branch of steady solutions. Introducing a small imperfection and re-computing the steady states breaks the basic branch into two distinct branches (shown in *b*), revealing a change of stability. In (*c*), by bringing the imperfection to zero, and re-computing the steady states, we recover the underlying new solution branch (shown in red).

For the example in question, we may introduce a small change in the governing equations by writing $\mathrm{d}q/\mathrm{d}t = q^3/2 - \lambda q + \delta$, where δ is a parameter governing the strength of the imperfection. The "imperfect" steady solutions are shown in figure 3.8(c, d), for $\delta > 0$ and $\delta < 0$ respectively. In either case, we can compute the families of solutions numerically, and immediately discover the bifurcated branch. Furthermore, if λ can be considered constant through the dynamics, a turning point approach can be applied to the imperfect branches shown in the figure, leading to stability predictions for the original solutions, *as well as* for the bifurcated branches.

For vortex flows, we propose an imperfection approach by focusing on the problem of breaking any geometric symmetry exhibited by the steady flow. As an example, we consider here the steady elliptical vortices first found by Kirchhoff (1876); the associated streamlines, as seen in a frame of reference that is rotating with the vortex shape, are shown in figure 3.9*a*. We choose to introduce a point vortex at each of the two stagnation points marked by a bull's eye in the figure, thus breaking all the geometric symmetries in the vorticity distribution. *We then proceed to re-compute the steady states.* Note that this involves solving also for the locations of the stagnation points at which the point vortices are located. Figure 3.9*b* shows a case where a very strong imperfection has been employed, leading to a flowfield that, while steady, clearly lacks any symmetry.

We must stress here that the *imperfection* involves the construction of a new, slightly asymmetric steady flow, which is closely related to a previously known, more symmetric equilibrium flow. In other words, this essentially involves the solution of a modified *equilibrium* problem. This is not to be confused with the introduction of a symmetry-breaking *perturbation*, which may lead to a *dynamical* behavior that also exhibits similar symmetry breaking.

We can now formulate a further development for a velocity-impulse diagram. Suppose we have computed a family of steady solutions numerically (as shown schematically in figure 3.10*a*), and wish to verify whether any bifurcations exist. We then introduce a symmetry-breaking imperfection, in the manner explained above; if a hidden branch exists, we find that the basic family is broken into two imperfect branches (figure 3.10*b*). By taking the strength of the point vortices back to zero, we recover the underlying bifurcated branch (shown in figure 3.10*c*). The turning points in the imperfect branches (which are

now shown as dashed lines in figure 3.10*c*) can be used to diagnose stability for both the basic and the bifurcated branch. Therefore *all exchanges of stability are apparent in an "imperfect velocity-impulse" diagram.*

3.5 Stability of vortical flows from IVI diagrams

We consider here several examples of the application of the imperfect velocity-impulse (IVI) diagram stability technique. In this section, we focus on the steady vortical flows depicted in figure 3.11(*a*)-(*f*); an example involving gravity waves (see figure 3.11*g*) is discussed further below, in § 3.6.

In all of the vortical examples below, velocity and impulse are normalized as:

$$\Omega^* = \Omega\,\tilde{\omega}^{-1}, \qquad U^* = U(\tilde{\Gamma}\tilde{\omega})^{-1},$$
$$J^* = J\,\tilde{\omega}\Gamma^{-2}, \qquad I^* = I\,\tilde{\Gamma}^{-3/2}\tilde{\omega}^{-1/2}, \tag{3.30}$$

where Γ is the total circulation of the flow, $\tilde{\Gamma} = \int |\omega|\,\mathrm{d}A$ and $\tilde{\omega} = \max|\omega|$. For space-periodic solutions of energy E, in a periodic cell of width L, we also employ:

$$E^* = E\,\tilde{\Gamma}^{-2}, \qquad L^* = L\,\tilde{\Gamma}^{-1/2}\tilde{\omega}^{1/2}. \tag{3.31}$$

Since our main focus here is on the stability methodology, we represent each flow through a collection of uniform-vorticity regions. The constraint that families of solutions must be constructed through kinematically possible displacements is therefore satisfied by fixing the area and the vorticity inside each patch (as explained in § 3.3.3).

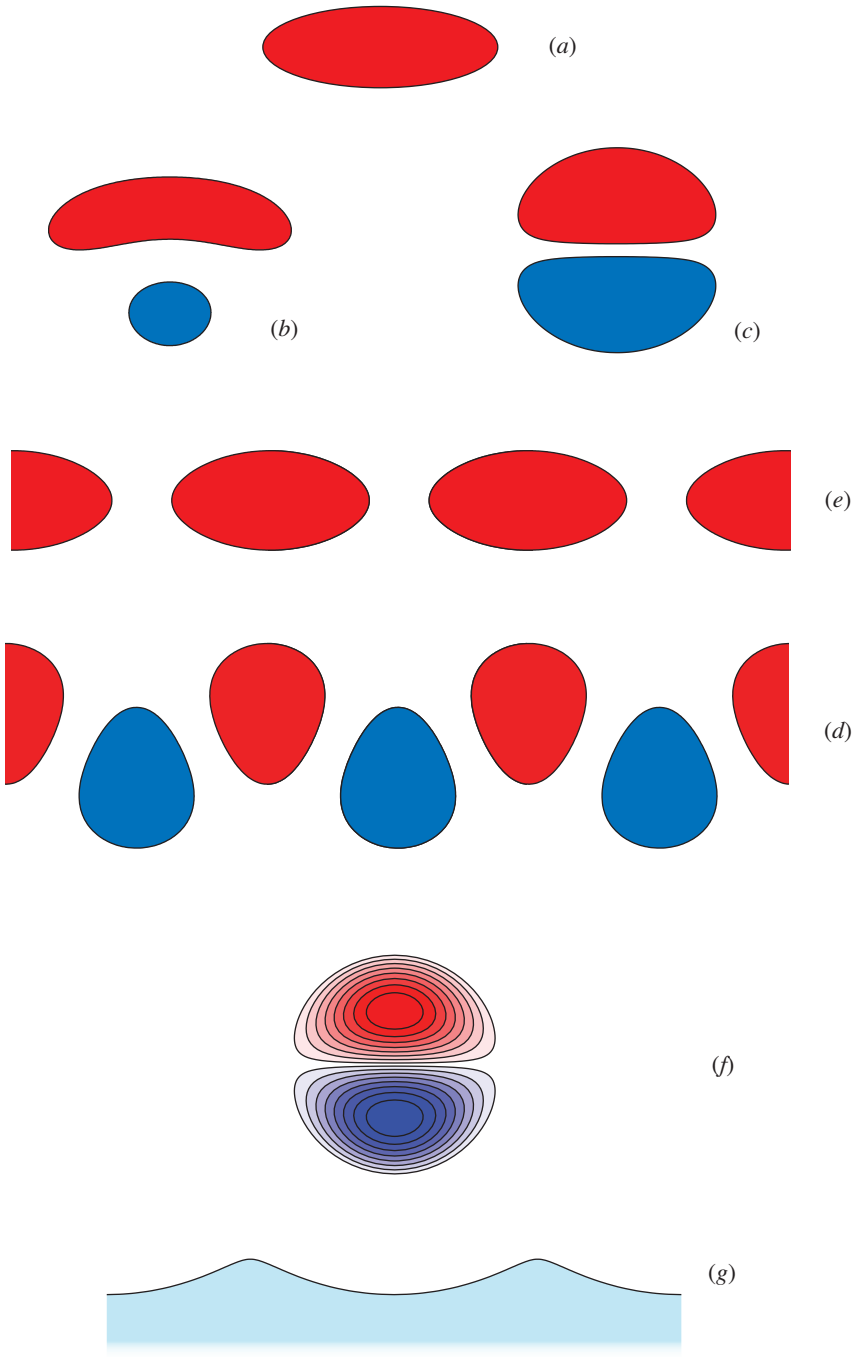

Figure 3.11: Flows whose stability we investigate through the IVI-diagram approach. Kirchhoff elliptical vortices (*a*), rotating opposite-signed vortex pairs (*b*), translating vortex pairs (*c*), vortex row (*d*), finite-area von Kármán vortex street (*e*), discretized Chaplygin-Lamb dipole (*f*), and steep gravity waves (*g*).

In order to find a steady flow in a moving reference frame, we must iteratively adjust the shape of each vortex until the boundary is a streamline of the flow, in the moving reference frame. In other words, we need to solve $\overline{\boldsymbol{u}} \cdot \boldsymbol{n} = 0$ along each contour, where $\overline{\boldsymbol{u}}$ is the velocity of the flow in the co-moving frame, and $\boldsymbol{n}$ is the unit normal to the boundary (Deem & Zabusky, 1978; Pullin, 1992). As noted in § 3.4, we expect that any bifurcated branches that we may encounter will exhibit fewer symmetries than the original solutions. In order to ensure that all bifurcations are correctly captured, we therefore need to employ a numerical approach capable of resolving vortices with arbitrary shapes. In addition, previous studies have shown that families of uniform vortices may terminate with a vortex configuration exhibiting one or more corners (Saffman & Tanveer, 1982; Wu *et al.*, 1984; Overman, 1986). Hence we must also be able to efficiently resolve small-scale features in the flow.

For these reasons, we developed a novel numerical approach that can efficiently compute uniform vortices of arbitrary shapes. In essence, the method involves a new discretization of the vortex boundary, which enables us to resolve small-scale features in the vortices by means of relatively few degrees of freedom. The discretized set of equations is then small enough to be solved quickly by Newton iteration. This, in turn, ensures convergence even for lower-symmetry vortices. More information on the numerical method is available in Luzzatto-Fegiz & Williamson (2010*c*); we intend to present a detailed description in a future contribution. For selected equilibria, we verified the precision of the solution by varying the number of degrees of freedom in the discretization; these checks indicate that the data reported here was computed accurately to at least seven significant figures.

3.5.1 The Kirchhoff elliptical vortices

We start our collection of examples with the elliptical vortices discovered by Kirchhoff (1876). These vortices constitute a family of solutions that begins with the circular vortex, and terminates into a vortex sheet as the axis ratio b/a approaches zero (Saffman, 1992). These steady states can be characterized analytically; it can be shown that their impulse and velocity are related by $J^* = (2\Omega^* - 1)(8\pi\Omega^*)^{-1}$, where the angular velocity is related to the axis ratio $\lambda = b/a$ by $\Omega^* = \lambda(\lambda + 1)^{-2}$. Since $J^* = (4\pi)^{-1}$ for the circular vortex, while $J^* \to -\infty$ as the vortex sheet solution is approached, we choose to plot $-(4\pi J^*)^{-1}$ instead of J^* (as shown in figure 3.12*a*; note that the value of Ω^* for any extrema in impulse would be unchanged). According to the discussion presented in § 3.3.2, since $J^*(\Omega^*)$ is monotonic, any exchanges of stability have to occur through bifurcations. (We should note that, in general, the bifurcated branches will *not* admit an analytic representation.)

In order to search for bifurcations, we initialize our numerical approach by introducing an imperfection in a near-circular vortex, through the placement of two point vortices at certain stagnation points of the co-rotating flow, thus breaking all geometric symmetries in the vorticity distribution, as shown in figure 3.12(*d*). The circulation in each point vortex is taken to be $\Gamma_{PV}/\Gamma = 10^{-4}$. The initial configuration corresponding to a circular vortex can be argued to be stable, as discussed in § 3.3.2. (Incidentally, the circular vortex can also be shown to be linearly and nonlinearly stable; see Thomson, 1880*b*; Dritschel, 1988*b*). We then seek the first loss of stability by computing imperfect steady flows with progressively lower velocity and impulse. At $(\Omega^*, J^*) \doteq (0.18815, -0.13183)$, we encounter a turning point in impulse, after which J^* begins to increase, thus

revealing a loss of stability (this imperfect branch is shown by the right-hand dashed line in figure 3.12*c*).

We continue to seek bifurcations from the basic solution family by considering an elliptical vortex located shortly after the turning point described above, and introducing the same imperfection again. This enables us to map the second imperfect branch, for both increasing and decreasing J^* (a portion of this branch is shown by the dashed line on the left-hand of figure 3.12*c*). By repeating this process, we detect the first three bifurcations, all of which turn out to correspond to losses of stability, as marked in figure 3.12(*b*).

By taking the strength of the point vortices to zero, we are able to recover the underlying bifurcated branches (shown by red lines in the figure), which are found to terminate with the limiting shapes shown in figure 3.12(*b*). The intersection between the bifurcated and original solution series yields the locations of the changes of stability.

To conclude this section, we note that the locations of changes of stability presented here, obtained from an IVI diagram, match precisely the results from the linear stability analysis of Love (1893). Love's analysis formed the basis of part of the work of Kamm (1987), who computed the beginning of the bifurcated branches presented here; the second bifurcated branch (shown in red in figure 3.12*b*) was later explored in its entirety (Cerretelli & Williamson, 2003*a*). More detailed information about the IVI diagram for the elliptical vortices can be found in Luzzatto-Fegiz & Williamson (2010*c*). We should also note here that, in a separate work, the authors study the stability of the second branch through a linear stability analysis and nonlinear simulations, finding precise agreement with the information presented here (Luzzatto-Fegiz & Williamson, 2011*c*).

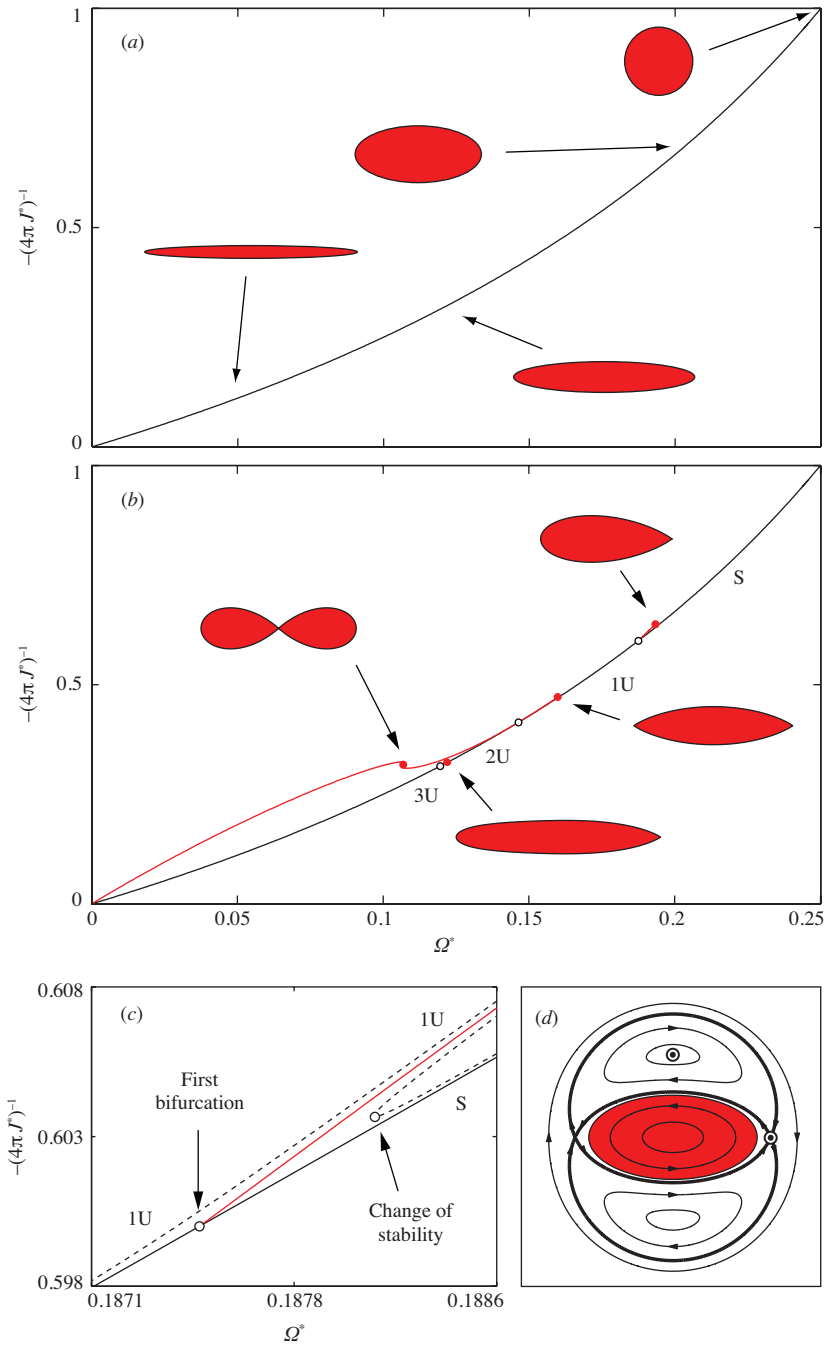

Figure 3.12: (*a*) shows the velocity-impulse plot for the Kirchhoff ellipses. Since no extrema in impulse are immediately apparent, any exchanges of stability have to develop through bifurcations. We break the flow's symmetry by introducing weak point vortices at certain stagnation points of the rotating flow (marked by bull's eyes ⊙ in *d*). The first three bifurcated branches, found using the IVI diagram approach, are depicted in (*b*). A close-up of the structure of the first bifurcation is shown in (*c*). Filled and empty circles denote limiting shapes and changes of stability, respectively.

3.5.2 The unequal-circulation pair

We examine equilibrium flows given by a pair of opposite-signed vortices, having equal vorticity magnitude but unequal circulation. Flows of this type were first computed by Dritschel (1995). We consider here the family of solutions obtained for circulation ratio given by $\Gamma_2/\Gamma_1 = -0.3$.

In order to establish the stability properties at the beginning of the family of solutions, we first note that a configuration involving vortices whose separation distance is much larger than the typical core size is susceptible to two types of perturbation modes (Dritschel, 1985). The first type involves core deformations, which must be stable if the vortex is near-circular (as noted in the previous section). The second type of perturbation involves a displacement of each vortex core (without deformation), and can thus be analyzed by examining the stability of an array of point vortices. It is easy to show that two point vortices must always be stable, regardless of their relative strength; therefore a pair of well-separated vortices must be stable.

We begin by computing the basic family of steady states, which is shown in figure 3.13(*a*). We can immediately point out a loss of stability at a turning point in J^*. In order to find out whether any undiscovered bifurcations exist, we break the left-right symmetry in the vorticity distribution shown in figure 3.13(*d*) by a placing point vortex at one of the saddle-type stagnation points of the co-rotating flow. The point vortex has strength, relative to the largest vortex, $\Gamma_{PV}/\Gamma_1 = 10^{-4}$. As we proceed to compute steady imperfect flows with progressively lower J^*, we discover a turning point in impulse at $(\Omega^*, J^*) \doteq (0.11426, -0.00405)$, which corresponds to an additional loss of stability (as shown by the close-up in figure 3.13*c*). Following a procedure similar

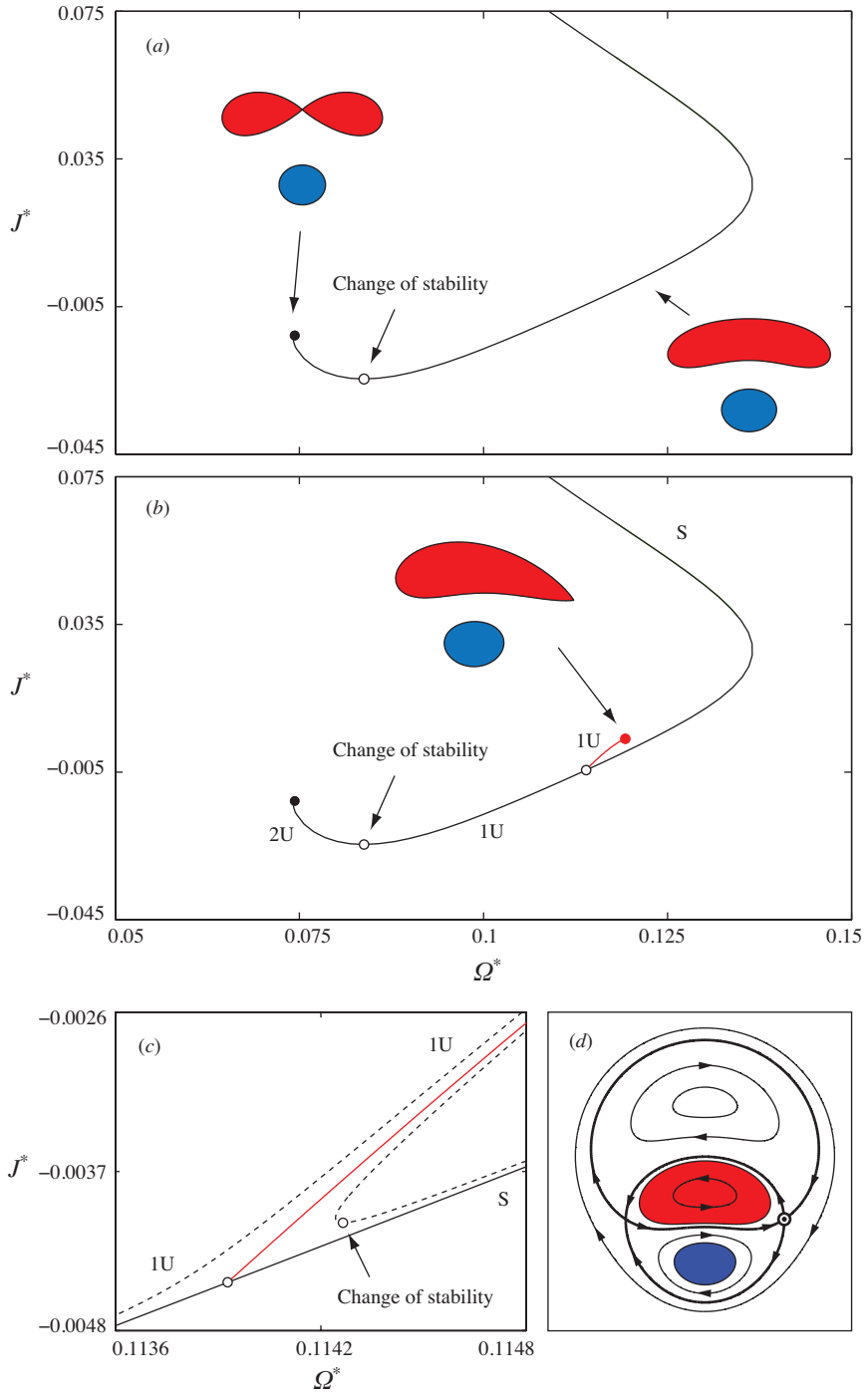

Figure 3.13: (*a*) is the velocity-impulse diagram for the opposite-signed, uniform vortex pair with area ratio $A_1/A_2 = 0.3$. The imperfection is constructed by introducing a point vortex at the stagnation point marked by a bull's eye (⊙) in (*d*). The IVI-diagram approach leads us to discover of new family of vortices (shown in *b*), which do not exhibit any symmetry. A close-up of the associated bifurcation is shown in (*c*).

to the one employed for the elliptical vortices, computed the next imperfect branch, and sought additional bifurcations from the original family; however, we found none.

For this flow, the bifurcated branch (shown in red in figure 3.13*b*, *c*) corresponds to a new family of vortices, whose shapes do not exhibit any symmetry. This family of solutions terminates with the limiting shape shown in figure 3.13*b*.

Finally, we note that the stability boundaries found from the IVI diagram in figure 3.13 match precisely results from the linear stability analysis of Dritschel (1995). Further to this, the IVI diagram delivers a new family of nonsymmetric steady vortices, together with their stability properties.

3.5.3 The equal-circulation pair

This section focuses on the opposite-signed vortex pair with equal vorticity *and* circulation magnitude. (This may be considered a special case of the unequal-area pair of § 3.5.2, with $\Gamma_2/\Gamma_1 = -1$.) The basic family of solutions (shown in figure 3.14*a*) was first obtained by Pierrehumbert (1980). It should be noted that the limiting shape (first accurately computed in Saffman & Tanveer, 1982) has a "rugby-ball" appearance, which is drastically different from the limiting shapes that one obtains for unequal-strength vortices (see figure 3.13*a* and 3.14*a*). This discrepancy persists as Γ_2/Γ_1 takes values close to -1. As noted by Dritschel (1995), reconciling these two solution series represents an outstanding question.

For this flow, we break all geometric symmetries by letting the two vortices

have slightly different areas (such that $\Gamma_2/\Gamma_1 = -0.995$), while also introducing a point vortex at one of the saddle-type stagnation points marked by a bull's eye in figure 3.14(*d*). The strength of the point vortex is fixed by the requirement that the configuration must still translate along a straight line, which in turn implies that the overall circulation must be zero (that is, $\Gamma_1 + \Gamma_2 + \Gamma_{PV} = 0$).

As for the unequal-strength pair, the equal-circulation pair can also easily be shown to be stable when the vortices are well-separated. By following the imperfect branch to lower values of impulse, we discover a turning point for $(U^*, I^*) \doteq (0.10820, 0.27531)$, corresponding to a loss of stability (shown in detail in figure 3.14*c*). Continuing the search for new solution branches, we find a rich bifurcation structure. These further bifurcations are not reported here; we hope to give a detailed account of these results in a separate contribution. The first bifurcation described above leads to a new family of steady vortices, shown in red in figure 3.14(*b*, *c*). We should stress that, in spite of their lower symmetry, these vortices translate along a straight line.

The location of the first loss of stability matches precisely the stability boundary calculated by Dritschel (1995) through a linear analysis. The IVI diagram approach also leads us to the discovery of a new family of lower-symmetry vortices. Furthermore, we may recognize the limiting shape shown on the left of figure 3.14*b* as the *equal-area version* of the limiting state for the unequal-area vortices, seen in figure 3.13*a*. We may therefore interpret the unequal-area vortices of § 3.5.2 as *the first imperfect branch* of the equal-area family, for which the imperfection (in this case, the circulation difference between the vortices) has been brought to large values. Therefore the use of imperfection theory proposed here naturally reconciles the two families of solutions.

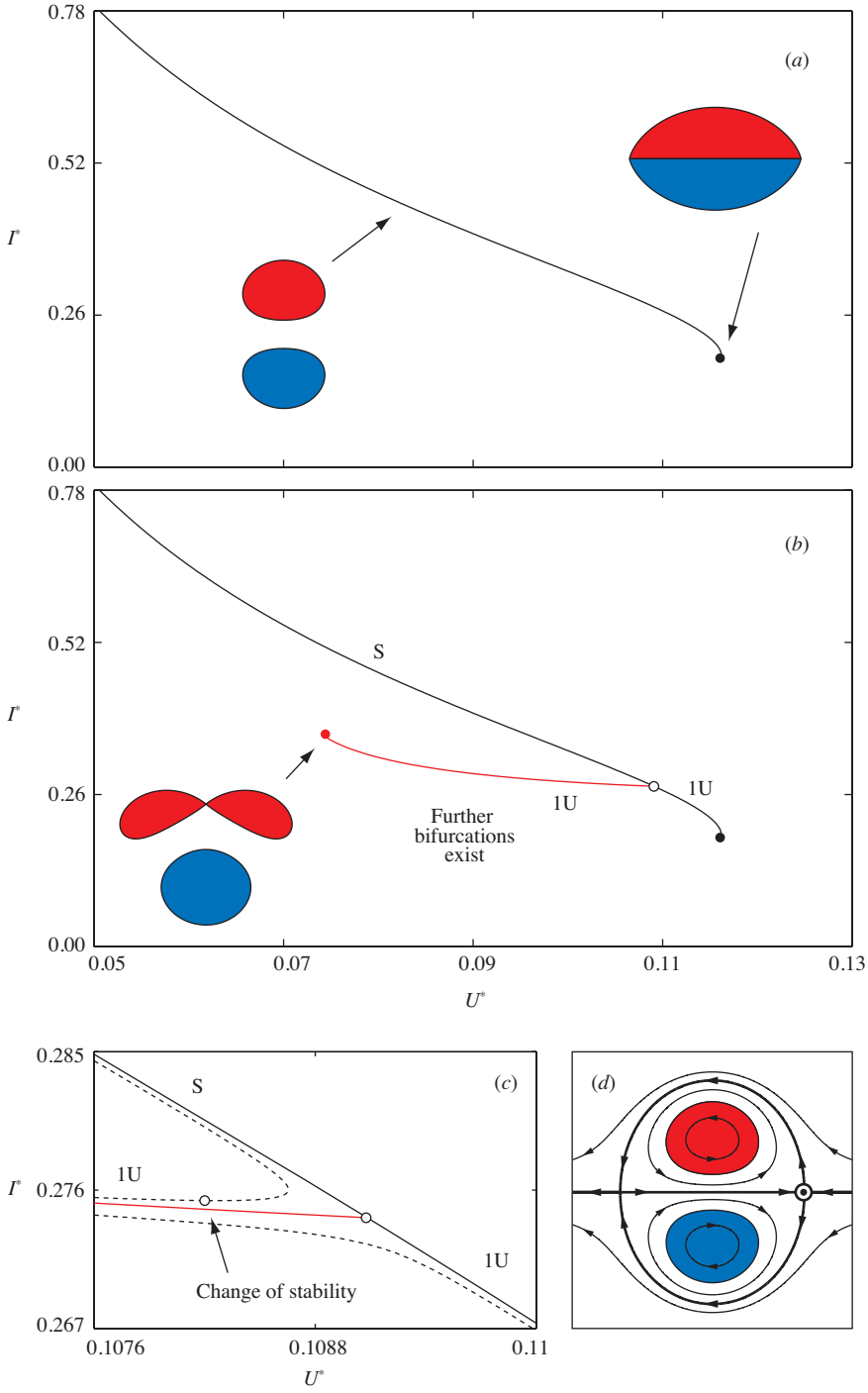

Figure 3.14: (*a*) is the velocity-impulse plot for the equal-area, translating vortex pair. The symmetry of the flow is broken by decreasing (by a small amount) the area of one of the two vortices, while introducing a point vortex (marked by ⊙ in *d*), whose strength is chosen so as to ensure that the overall circulation remains zero. The imperfect velocity-impulse diagram in (*b*) shows the first bifurcation uncovered through this approach. A close-up of the first bifurcation is in (*c*).

3.5.4 The single vortex row

We next examine a row of identical uniform vortices, whose centroids are separated by a non-dimensional distance L^*. Solutions of this type were first computed numerically by Pierrehumbert & Widnall (1981) and Saffman & Szeto (1981). Since these vortices do not translate, in order to detect exchanges of stability we must construct the vortex spacing-energy plot $(L^*, \partial E^*/\partial L^*)$, as explained in § 3.3.5. In the case of well-separated vortices (that is, $L^* \gg 1$), the superharmonic point-vortex behaviour must correspond simply to a pure shift of the whole configuration (Saffman, 1992). Hence the family of solutions starts by being stable to superharmonic perturbations. By building the plot shown in figure 3.15(*a*) for the basic family, we immediately detect a loss of stability at a turning point in L^*.

To introduce an imperfection in this periodic flow, we employ a two-step process, as shown in figure 3.15(*b*), (*c*) and (*d*). Firstly, we introduce a point vortex at the saddle-type stagnation point between the vortices (highlighted by a grey box in figure 3.15*b*). This changes the local flow field, turning each original *saddle* into a *center*, and creating two new saddle-type stagnation points in its neighbourhood, as exemplified in figure 3.15(*c*). Depending on the sign of the point vortex, the new stagnation points are along a line that is either parallel to the vortex row (for $\Gamma_{PV}/\Gamma > 0$, shown in *c*), or orthogonal to it (for $\Gamma_{PV}/\Gamma < 0$; this is not shown here). Therefore, by introducing an additional point vortex at one of these new stagnation points, we can break either the left-right or top-bottom symmetry in the figure, respectively.

We found that these imperfections do *not* lead to new bifurcated branches. These stability results match data from the linear analysis of Kamm (1987).

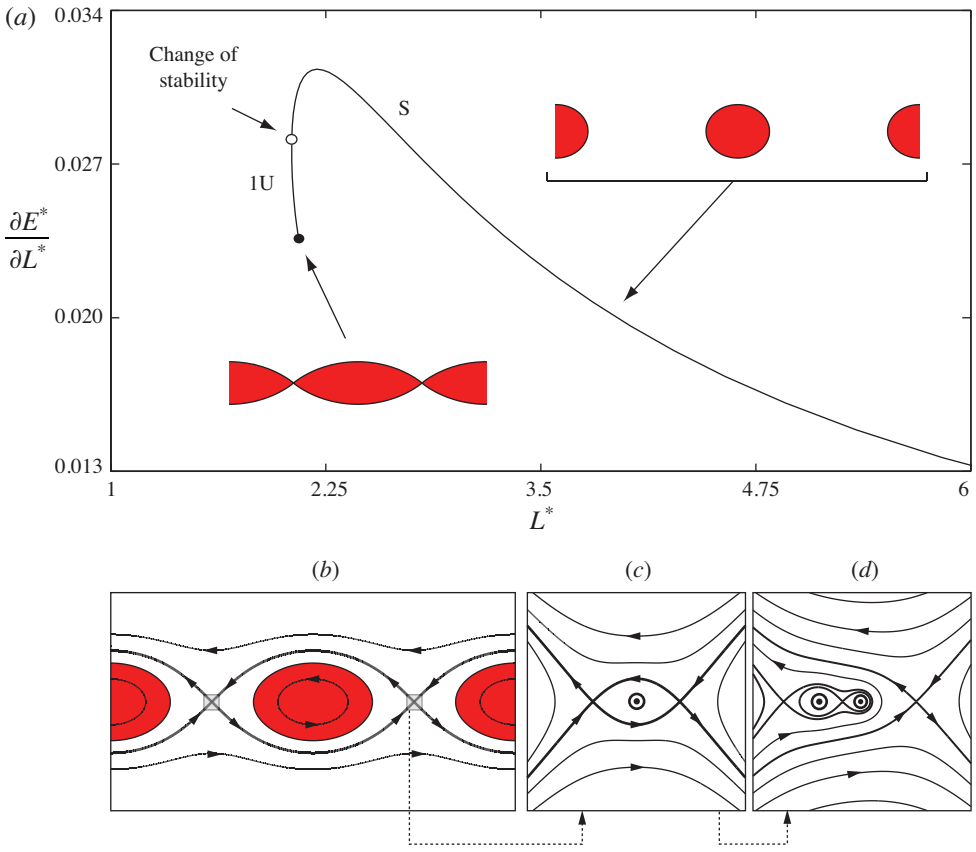

Figure 3.15: Stability of the linear vortex array, for superharmonic perturbations. For space-periodic flows, the velocity-impulse plot (U^*, I^*) is replaced by a diagram of $(L^*, \partial E^*/\partial L^*)$, where changes of stability occur at turning points in L^*, as marked in (a). The flow in one periodic strip (of width L^*) is made nonsymmetric through a two-step process, as shown in (b, c, d). The neighbourhood of a stagnation point (highlighted by a gray box in b) is first altered by introducing a point vortex of strength Γ_{PV} (marked by the larger bull's eye in c), which changes the local flow topology. This creates two new stagnation points near the original one. Introducing a further point vortex at one of these locations (marked by the left-hand bull's eye in d) breaks the left/right symmetry. No bifurcations were found, in accordance with classic stability results.

3.5.5 The finite-area von Kármán vortex street

In this section, we consider the stability of a vortex street, which may be obtained by replacing the point vortices in the classic configuration studied by von Kármán (1912) with finite-area, uniform vortices. This configuration was studied in Saffman & Schatzman (1981, 1982*b*) and Meiron *et al.* (1984). It should be noted that these studies focused on changes in the *subharmonic* response due to the introduction of finite areas. In their calculations, closely-spaced vortices were not computed, as resolving accurately the vortex boundaries proved prohibitively expensive.

The classic point-vortex stability analysis of von Kármán (1912) indicates that, for $L^* \gg 1$, the configuration is stable to superharmonic perturbations (see Saffman, 1992, for a modern treatment). In order to determine stability properties for the finite-area solutions, we begin by choosing a specific value of the impulse I^*, which is subsequently held fixed though the calculations. We then compute steady flows as L^* is varied. For the example shown here, we took $I^* = 2^{-3/2}$. The basic family of solutions is shown in figure 3.16(*a*); this immediately reveals a loss of stability at a turning point in L^*. Incidentally, we note that the numerical procedure employed here allows us to accurately resolve, for the first time, all solutions up to the limiting shape, which is shown in figure 3.16(*a*).

The imperfection is constructed following essentially the procedure employed for a single row of vortices (which is described in the previous section). It can be shown that, for vortices in a periodic strip that translate along a straight path, the total circulation must be zero (Meiron *et al.*, 1984). Therefore, the size of the vortex in the top row was reduced to ensure that the total circulation in

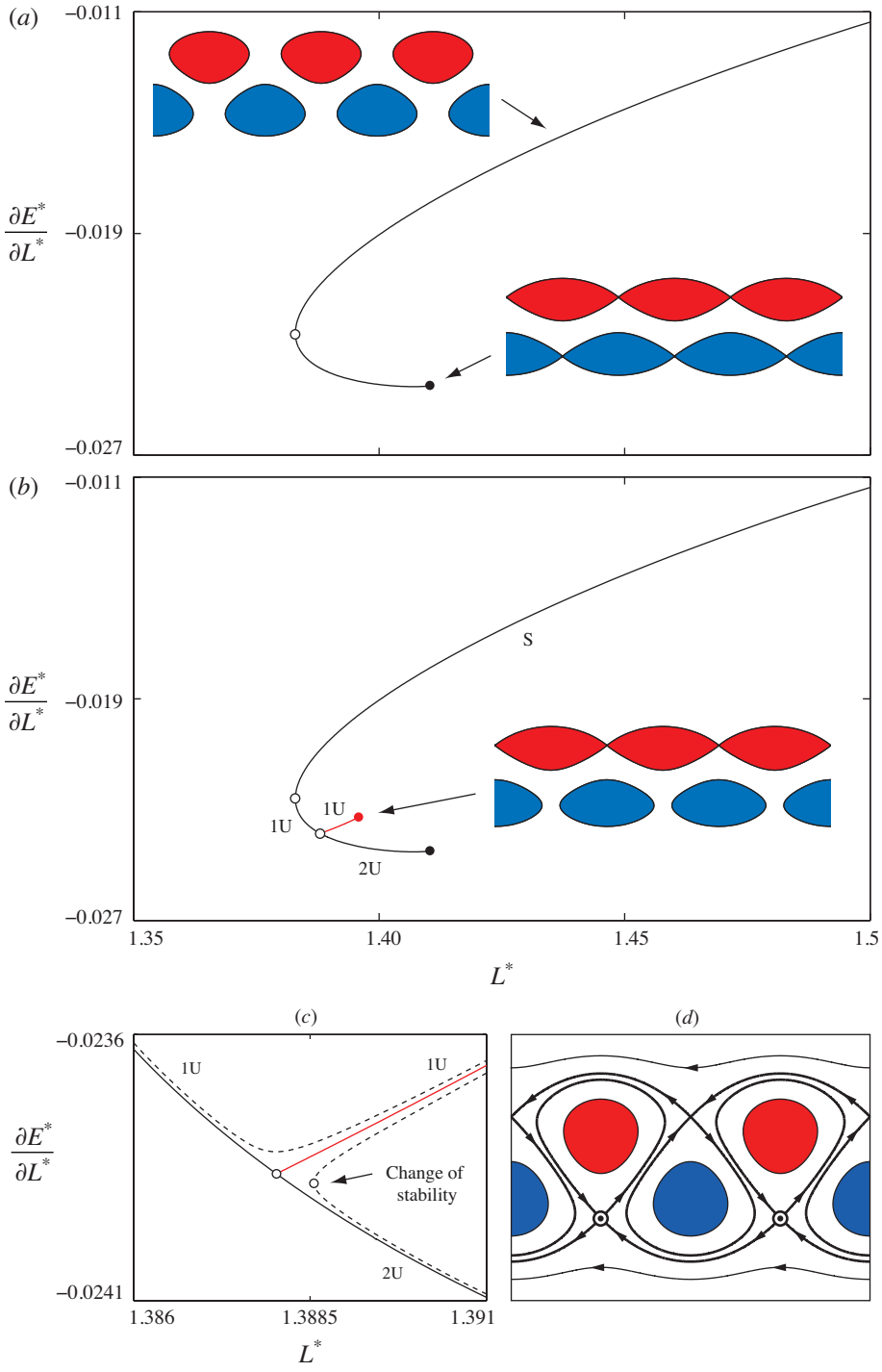

Figure 3.16: Stability diagram for the Kármán street, for varying L^*, and fixed impulse. The imperfection is constructed by introducing a weak point vortex at one of the stagnation points marked by a bull's eye in (*d*). Re-computing the steady states, we find that the solution family is broken into two distinct branches (shown by the dashed lines in *c*), revealing an additional loss of stability (marked in *c*).

the periodic strip vanished.

Breaking the flow's symmetry allows us to find a second loss of stability, occurring after the turning point in L^* described above; this is shown in figure 3.16(c). We should note that, in fact, the turning point in the imperfect branch shown in figure 3.16(c) persists even if a single point vortex is employed; in this figure, a single point vortex with strength $\Gamma_{PV}/\Gamma_1 = 10^{-4}$ was used.

As mentioned above, past studies of the stability of the finite-area Karman street have focused on the behaviour of subharmonic modes for well-separated vortices. To the best of our knowledge, the stability results that we report in this section are new. It would be interesting to investigate how the stability properties of the street change, as one examines streets with different impulse I^*.

3.5.6 Distributed vortices: the Chaplygin-Lamb dipole

While our examples so far have focused on uniform vortices, we examine here the properties of a more realistic representation of a vortex pair. Our starting point is the symmetric, translating pair solution that was described independently by Chaplygin (1903) and Lamb (1932), which involves an analytic representation of a steady, smooth vorticity distribution extending over a finite region (see also Meleshko & van Heijst, 1994). In order to construct an IVI diagram for this flow, we must *embed* the Chaplygin-Lamb dipole into a family of solutions with fixed Casimirs. This family of solutions would connect the Chaplygin-Lamb solution with a steady flow given by two well-separated, distributed vortices, which can be argued to be stable by the simple arguments described in

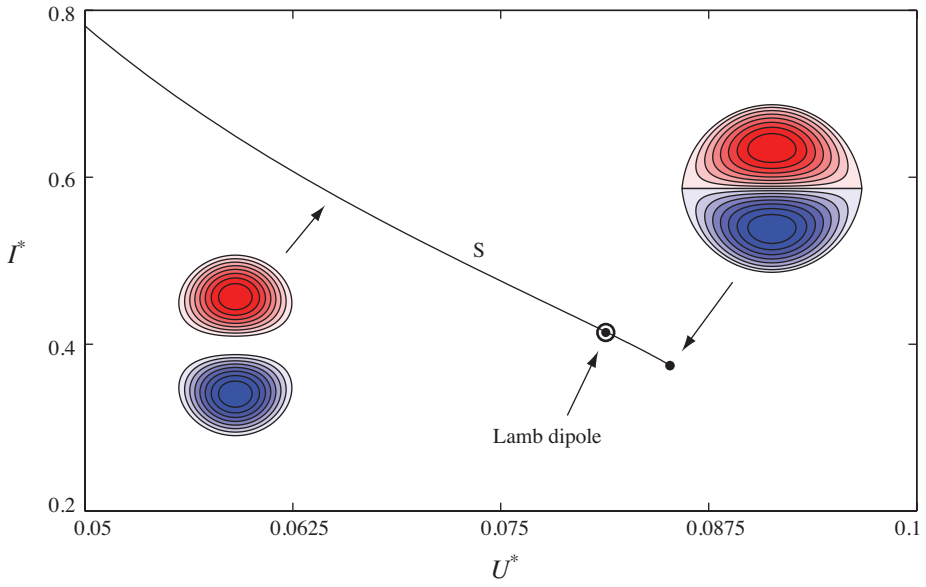

Figure 3.17: Velocity-impulse diagram for the family of distributed vortices based on the Chaplygin-Lamb dipole. The vorticity distribution is approximated using a collection of nested uniform vortices. By introducing an imperfection using an approach similar to the one used for the uniform vortex pair (see figure 3.14), we reveal the absence of any bifurcations (at least up to $U^* \approx 0.083$). The original Chaplygin-Lamb dipole is marked by a bull's eye.

§ 3.5.3.

We choose to approximate each vortex by a set of nested, uniform-vorticity regions. The discretization is constructed using the procedure described by Legras & Dritschel (1993), who showed that using eight contours for a vortex with compact support yields an excellent approximation for the dynamics of the flow. Once all of the areas A_i and vorticity jumps $\Delta\omega_i$ are computed (with $i = 1, 2, ..., 8$), keeping all $A_i, \Delta\omega_i$ constant along the family is sufficient to ensure all solutions have the same Casimirs, as explained in § 3.3.3.

We first compute the basic family of steady flows, and obtain the velocity-impulse diagram shown in figure 3.17. For reference, the same figure also displays (with a bull's eye) the impulse and velocity for the Chaplygin-Lamb

dipole. Note that the original solution is remarkably close to the approximate family (for the same velocity U^*, the impulse difference is $I^* - I^*_{\text{Lamb}} = 7.7 \times 10^{-4}$, or about 0.2%), which suggests that the integral properties of the configuration are represented very accurately. The imperfection is constructed as in § 3.5.3, through the combined introduction of a point vortex at one of the saddle-type stagnation points, and the shrinking of the area of one of the outermost vortex patches. While we computed imperfect branches with a variety of point vortex strengths (in the range $\Gamma_{\text{PV}}/\Gamma_1 = 10^{-4}$ to 10^{-2}), we did not find any bifurcation, at least up to $U^* \approx 0.083$ (past the Chaplygin-Lamb approximation), after which the numerical procedure for the imperfect system converged very slowly to a steady solution.

Since there are no turning points in I^* or bifurcations before the bull's eye in figure 3.17 is reached, the discretized version of the Chaplygin-Lamb dipole must be stable. This suggests that the original, smooth solution should also be stable, at last in a global sense. Of course, one may expect that the lowest vorticity levels (not represented in our discretization) may be rapidly stripped from the configuration through the neighbourhood of the rear stagnation point.

We should note here that there is evidence from *viscous* numerical simulations that certain flows with non-zero linear impulse may spontaneously evolve towards a state close to the Chaplygin-Lamb dipole, which would suggest that this solution is at least robust under viscous evolution (J. H. G. M. van Geffen, 1998; Nielsen & Rasmussen, 1997; Sipp *et al.*, 2000; Satijn *et al.*, 2004; Delbende & Rossi, 2009). However, to the best of our knowledge, no linear stability analysis has been performed on this flow before (as noted, for example, by Meleshko & van Heijst, 1994; Kizner & Khvoles, 2004; Waite & Smolarkiewicz, 2008). Sur-

prisingly, the analysis presented here appears to be the first formal stability result for a discretized Chaplygin-Lamb dipole.

3.6 Stability of steep gravity waves from velocity-impulse diagrams

To highlight the fact that the IVI diagram technique can be applied to other conservative systems for which steady states are associated with a variational principle, we briefly consider here steep gravity waves on the surface of a homogeneous, irrotational fluid of infinite depth. For this flow, a variational principle follows directly from the Hamiltonian formulation of Zakharov (1968). For fixed wave period L, waves that steadily translate with velocity c correspond to a stationary point of the Hamiltonian H, defined such that

$$\delta H = \delta(T + V) - c\,\delta P \tag{3.32}$$

where T and V are are the kinetic and potential energy, respectively, and P is the wave impulse per unit wavelength, given by $P = L^{-1}\int u\,\mathrm{d}A$ (for a fluid of unit density). Since there is a clear analogy between $(T + V, c, P)$ above and (E, U, I) from § 3.3.2, the results (3.20)-(3.22) can be immediately applied. Therefore, for gravity waves, turning points in wave impulse P are associated with exchanges of stability.

In order to find the shape $\eta(x)$ for the steady waves, we solve numerically the classic problem involving the steady Bernoulli equation $1/2|\boldsymbol{u}|^2 + gy - cu = \text{const.}$ and the kinematic condition $\overline{\boldsymbol{u}} \cdot \boldsymbol{n} = 0$ at the interface. As discussed in § 3.5, the numerical method needs to be able to resolve lower-symmetry flows and

fine-scale features in the interface; the discretization procedure used is therefore similar to the one employed for the steady vortices, and will also be described in detail in a future contribution. As is customary in the study of gravity waves, we normalize P and c by the wavelength L and by the gravitational acceleration g, such that $P^* = Pg^{-1/2}L^{-3/2}$, $c^* = c(gL)^{-1/2}$.

3.6.1 Superharmonic instabilities of gravity waves

We first compute the basic family of steady solutions, which originates with a state corresponding to a quiescent surface, and terminates with waves exhibiting a 120° corner (see Longuet-Higgins & Fox, 1978, and references therein). The resulting family of solutions is shown in figure 3.18(*a*). For gravity waves, an imperfection was constructed as follows. It is well known that a stagnation point exists above each wave crest, if the flow is observed in a frame of reference moving with the waveform (Grant, 1973). We can therefore introduce an imperfection in a manner essentially similar to the single vortex row (as illustrated later in figure 3.18*d*). No bifurcated branches were found. Therefore, for superharmonic instabilities, figure 3.18(*a*) shows the complete IVI diagram. We can immediately note that there is a loss of stability at the turning point in impulse in the figure.

The location of this instability, found from an IVI diagram, agrees with predictions from linear analysis, as may be expected (Tanaka, 1983, 1985; Longuet-Higgins, 1986). We must point out that Longuet-Higgins & Fox (1978) showed, using asymptotic techniques, that as the limiting wave is approached, the family of solution meets a countable infinity of turning points in c and P, effectively

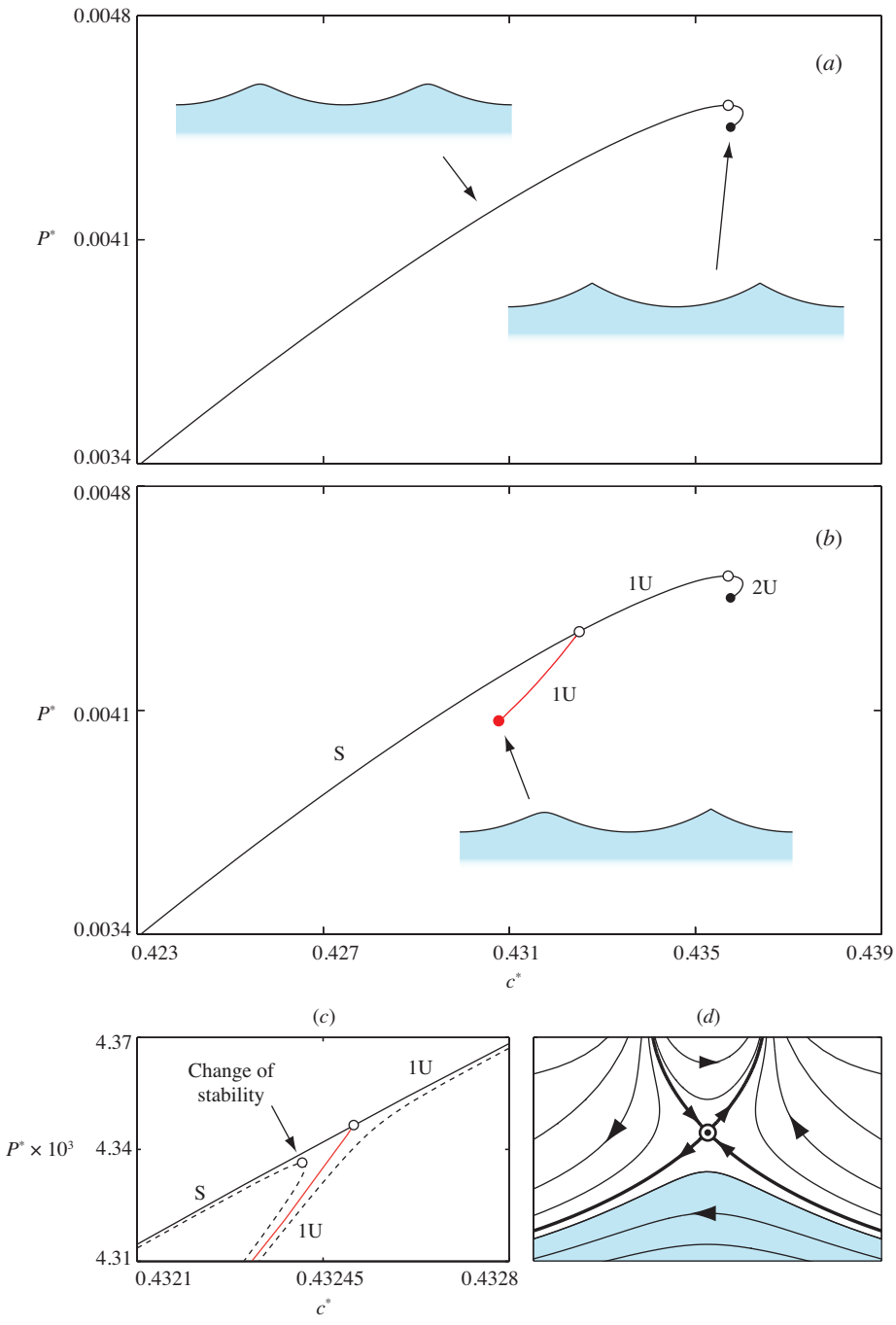

Figure 3.18: IVI diagram for steep gravity waves with phase velocity c^* and impulse P^*. The waves are periodic ver a distance $L = 2L_0$, where L_0 is the period of the original family of solutions shown in (*a*).

giving rise to a spiral in the velocity-impulse diagram. Our results link each of these turning points to a loss of stability.

We should also note that, for the specific problem of water waves, Longuet-Higgins (1984*a*) showed that turning points in energy coincide with turning points in impulse. In addition, while focusing on gravity waves on deep water, Saffman (1985) used the Hamiltonian formulation of Zakharov (1968) to prove that water waves undergo an exchange of stability at any turning point in energy. In fact, the work presented in this paper shows that the link between extrema in impulse / energy and exchanges of stability holds for any conservative system whose steady states are associated with a variational principle. Furthermore, we have shown that the shape of a velocity-impulse diagram delivers the direction of the change of stability.

3.6.2 Instabilities for waves with period $L = 2L_0$

Since no bifurcations were found when considering superharmonic instabilities, we now consider subharmonic modes with period $L = 2L_0$, where L_0 is the wavelength of the original wave family. We proceed by including two wave crests in our computational domain, and we seek solutions with periodicity $\eta(x) = \eta(x + 2L_0)$, which may arise as bifurcations from the original family given by $\eta(x) = \eta(x + L_0)$.

The imperfection is now constructed by introducing point vortices (of strength $\Gamma = 10^{-4}(L^{3/2}g^{1/2})$) at every other stagnation point above the wave crests. Computing the imperfect solutions reveals a turning point in P, indicating a loss of stability to a subharmonic perturbation (as shown in figure 3.18*b*, *c*). Taking

the strength of the point vortices to zero, we recover the bifurcated solution family shown in red in the figure, which corresponds to a family of solutions of lower symmetry.

Finally, we note that, as may be expected, the location of this change of stability, found through the IVI diagram approach, matches the linear stability results of Longuet-Higgins (1978*b*). Subharmonic bifurcations were also previously studied by Chen & Saffman (1980), who computed a substantial portion of this lower-symmetry family of solutions. It appears that the algorithm used by Chen & Saffman was unable to efficiently resolve the lower-symmetry limiting state, which is obtained here for the first time.

3.7 Discussion

A point that deserves to be highlighted concerns the nature of the variation used to construct the argument underlying the stability analysis, as this choice directly affects the meaning of any stability results. The class of perturbations used to calculate the variation is ultimately the same as the one with respect to which stability (or instability) is established through the IVI diagrams. Furthermore, the perturbation that transforms one steady flow into a neighboring one, in an IVI diagram, must *also* belong to this class. Therefore, for an IVI diagram based on Kelvin's argument, families of solutions must be built trough the imposition of an irrotational *and* kinematically possible displacement field; the resulting rearrangement of fluid particles may, in fact, produce or destroy vorticity through vortex stretching (although three-dimensional flows were not explored here). The requirement that the displacement field must be irrotational

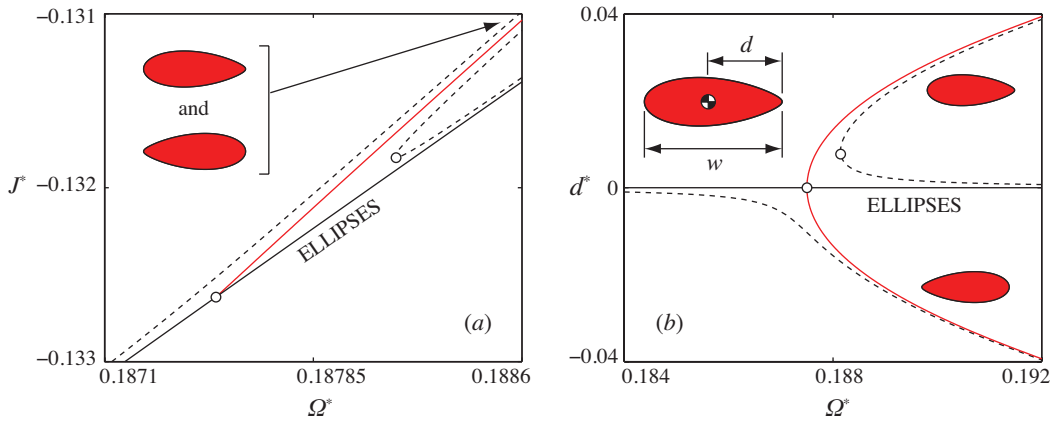

Figure 3.19: Diagram clarifying the nature of some of the bifurcations reported. (*a*) shows the first symmetry-breaking bifurcation from the family of elliptical vortices, in an IVI diagram. The imperfection used is described in § 3.5.1. (*b*) shows a plot of $d^* = d/w - 1/2$ versus Ω^*; the bifurcation can be immediately recognized as a pitchfork.

is by no means unrealistic and is, in fact, necessary to ensure that the evolution of the flow respects Kelvin's circulation theorem. For example, we may suppose that the perturbation results from the influence of a distant vorticity distribution, or from the motion of a solid body in the far field.

From a practical standpoint, one is of course not tied to having to use a variational approach to find the steady states; instead, one may compute the steady solution by any suitable numerical approach, and then exploit the resulting IVI diagram to obtain stability properties. This is indeed the procedure used in this paper. For simplicity, our example flows were discretized through collections of uniform vortices; however, we must emphasize that the stability approach applies equally to smooth vorticity distributions.

We should also comment here on the specific choice of imperfection employed to promote symmetry-breaking. In all of the examples presented here, we make use of weak point vortices, which are introduced at stagnation points

of the co-moving flow. We can report that we have also tested several different types of imperfections, including sources and sinks, weak background flows involving simple shear, as well as strain fields of different order (an example of the effect of different background fields on the form of a steady state may be found in Ehrenstein & Le Dizès, 2005). In all of the examples we considered, we found that all bifurcations are detected, provided that all geometric symmetries of the flow are broken. The algorithm used to compute the steady states adjusts automatically the step along the solution family between neighbouring steady states (say, Δs), so as to retain a prescribed accuracy in the results; all bifurcations shown were discovered without the need to manually adjust Δs. Once a bifurcation was found, we computed a few additional solutions (with Δs reduced by a factor of about 5) near the turning points, so as to obtain the smooth curves displayed in the insets of figures (3.12)-(3.18).

It may be helpful to show explicitly the correspondence between the patterns arising in an IVI diagram, and those associated with typical bifurcation plots that may be familiar from dynamical systems theory. The IVI diagram in figure 3.19(*a*) shows a close-up of the first bifurcation encountered for the elliptical vortices. By contrast, figure 3.19(*b*) shows data for the same steady flows in a different plot, where the impulse J^* has been replaced by d^*, a quantitative measure of the asymmetry in the larger vortex (this parameter is defined in the figure). The point being made here is that, by plotting the same data in a different manner, we can immediately see that this bifurcation is of pitchfork-type. The two sides of the fork correspond to vortices that are *mirror* images of one another; these branches are collapsed into a single one in an IVI diagram, as they have the same impulse. Of course, turning points in the plot in figure 3.19(*b*) do not, in general, yield the stability information that is otherwise retrieved from

an IVI diagram.

Another somewhat subtle point, which is worth mentioning here, regards the precise definitions of stability underlying an IVI diagram. For a generic system, linear stability is typically studied by examining the spectrum of an operator (say, **A**), which represents the linearized dynamics. However, if **A** has non-normal eigenmodes, the linearized system may actually exhibit different stability from what the spectrum of **A** might suggest; this requires one to distinguish between *spectral* and *linear* stability, and to introduce more advanced theoretical techniques (Holm *et al.*, 1985; Schmid & Henningson, 2001). The IVI diagram procedure sidesteps these issues, since stability is found from the spectrum of the operator H'', which is self-adjoint and therefore must have normal eigenmodes. On the other hand, we must be careful to point out that the creation of a saddle (as detected by an IVI diagram) is, strictly speaking, only necessary for instability; this indicates that an IVI diagram may overestimate the number of unstable modes for an equilibrium. However, we should emphasize that, for all examples considered in this paper, the number of unstable modes from the IVI diagrams always matches available results from a linear stability analysis.

3.8 Concluding remarks

In this paper, we take as a starting point a variational argument that has its roots in the work of Lord Kelvin, and build on ideas from dynamical systems theory and imperfection theory to show that exchanges of stability can be detected directly from families of equilibrium solutions.

We address the first issue raised by Dritschel (1985) with respect to the pos-

sible use of bifurcation diagram namely, that a rigorous link between turning points and exchanges of stability has not previously been established. In this paper, we develop a turning point approach, which links folds in impulse to exchanges of stability. In addition, we demonstrate that one can use the shape of a velocity-impulse diagram to infer whether stability is lost or gained at the turning point. The analysis presented here shows that turning points (which arise commonly in conservative fluid flows) are in fact a manifestation of a cusp catastrophe,which is a recurrent feature for bifurcation diagrams across a wide variety of physical systems. For flows in a periodic strip, the same results hold, but one can replace the velocity and impulse (U, I) with the energy and strip-width parameters $(\partial E/\partial L, L)$.

Dritschel (1985) also brought attention to the fact that, in the presence of undiscovered bifurcations, a simple turning point approach would fail to capture all exchanges of stability. We address this second issue by introducing symmetry-breaking imperfections in these conservative fluid problems, and also by computing families of imperfect steady states. This methodology enables us to immediately detect bifurcations to new families of steady solutions, therefore uncovering the associated changes of stability.

A separate issue concerns the definition of a "proper" family of fluid solutions. This difficulty can be exemplified by drawing a comparison with problems in solid mechanics, where one can simply vary the applied load or displacement to obtain a family of solutions. By contrast, in a fluid flow, one may change the vorticity distribution in an infinite number of ways, each yielding a different solution family. We address this issue by showing that one must keep a particular set of quantities (known as Casimirs) constant along the solution fam-

ily. It is important to note that several existing families of analytical solutions (such as the one found by Stuart, 1967) do not satisfy this requirement. Therefore their stability may not be determined by simply seeking turning points in some control parameter for the analytical family (as has been previously suggested; see Saffman, 1992). Instead, in order to determine stability, one must embed an equilibrium flow into a family of solutions with the same Casimirs.

We apply the imperfect velocity-impulse (IVI) diagram stability methodology to a wide range of classical flows. Where linear stability results are available, the stability boundaries and number of unstable modes delivered by the IVI diagrams agree precisely with data in the literature. In addition, we consider several flows for which a corresponding linear analysis has not yet been performed; for these problems, we obtain what are, to the best of our knowledge, the first available stability results. These new findings include the stability boundaries and bifurcated branches for a Kármán street subject to superharmonic perturbations, as well as the first formal proof of stability for a discretized version of the Chaplygin-Lamb dipole.

For most of the flows examined, the introduction of imperfections leads us to the discovery of new families of steady solutions, which exhibit lower symmetry. The stability of these new equilibrium flows also follows from the application of the IVI diagram technique. Among the new flows presented here, we discover steady vortices that do not exhibit *any* geometric symmetry, and find *nonsymmetric*, equal-area vortex pairs that translate along a straight path. These results also enable us to resolve an outstanding question on the structure of families of vortex pairs. Previous work had revealed a qualitative difference between the limiting solutions for equal-area vortex pairs, and those for vortex

pairs of unequal area, even as the area ratio approaches unity (Dritschel, 1995). In this paper, we resolve this issue by showing that the unequal-area vortices correspond, in fact, to the newly discovered lower-symmetry, equal-area vortex pairs.

Finally, we note that the IVI-diagram technique is comparatively simple to implement, provided one can rely on an efficient numerical procedure to compute the steady states. By comparison, to compute a bifurcated solution branch by a traditional approach, one needs to first perform a linear stability analysis to find the equilibrium solution for which the exchange of stability occurs. One then must calculate the corresponding eigenmode and superpose it onto the equilibrium solution, using the result as an initial guess for starting to compute the new branch. It is easy to see that, for a wide range of flows, it is significantly easier to instead insert one or more symmetry-breaking flow elements, and compute the imperfect steady states.

Nevertheless, we should emphasize that the IVI diagram methodology is obviously not meant to replace other stability approaches, such as linear analysis or simulation, which can be used to yield, for example, growth rates and long-term evolution. Of course, the methodology presented here may be employed in combination with other, possibly more involved, stability approaches.

CHAPTER 4

STABILITY OF ELLIPTICAL VORTICES FROM "IMPERFECT-VELOCITY-IMPULSE" DIAGRAMS

Published as

LUZZATTO-FEGIZ, P. & WILLIAMSON, C. H. K. (2010)

Theoretical and Computational Fluid Dynamics **24**, 181–188.

In 1875, Lord Kelvin proposed an energy-based argument for determining the stability of vortical flows. While the ideas underlying Kelvin's argument are well established, their practical use has been the subject of extensive debate. In a forthcoming paper, the authors present a methodology, based on the construction of "Imperfect-Velocity-Impulse" (IVI) diagrams, which represents a rigorous and practical implementation of Kelvin's argument for determining the stability of inviscid flows.

In this work, we describe in detail the use of the theory by considering an example involving a well-studied classical flow, namely the family of elliptical vortices discovered by Kirchhoff. By constructing the IVI diagram for this family of vortices, we detect the first three bifurcations (which are found to be associated with perturbations of azimuthal wavenumber $m = 3, 4$ and 5). Examination of the IVI diagram indicates that each of these bifurcations contributes an additional unstable mode to the original family; the stability properties of the bifurcated branches are also determined. By using a novel numerical approach, we proceed to explore each of the bifurcated branches in its entirety.

While the locations of the changes of stability obtained from the IVI diagram approach turn out to match precisely classical results from linear analysis, the

stability properties of the bifurcated branches are presented here for the first time. In addition, it appears that the $m = 3, 5$ branches had not been computed in their entirety before.

In summary, the work presented here outlines a new approach representing a rigorous implementation of Kelvin's argument. With reference to the Kirchhoff elliptical vortices, this method is shown to be effective and reliable.

4.1 Introduction

More than a century ago, Lord Kelvin proposed that a steady vortical flow realizes an extremum of the kinetic energy, for a given impulse (Thomson, 1876). It appears that Kelvin regarded this proposition as being self-evident, as he provided no proof for it; the first analytical confirmation is instead due to Benjamin (1976). The argument can be illustrated as follows, with reference to a vortex configuration rotating at a rate Ω. Under vorticity-preserving perturbations, a steady two-dimensional flow is associated with a stationary point of the functional H:

$$H = E - \Omega J, \tag{4.1}$$

where E and J are the excess kinetic energy and angular impulse, respectively, given by:

$$E = -\frac{1}{4\pi} \iiiint \omega(\mathbf{x})\, \omega(\mathbf{x}') \log|\mathbf{x} - \mathbf{x}'| \, \mathrm{d}x \, \mathrm{d}y \, \mathrm{d}x' \, \mathrm{d}y' \tag{4.2}$$

$$J = -\frac{1}{2} \iint \omega(\mathbf{x}) \, |\mathbf{x}|^2 \, \mathrm{d}x \, \mathrm{d}y. \tag{4.3}$$

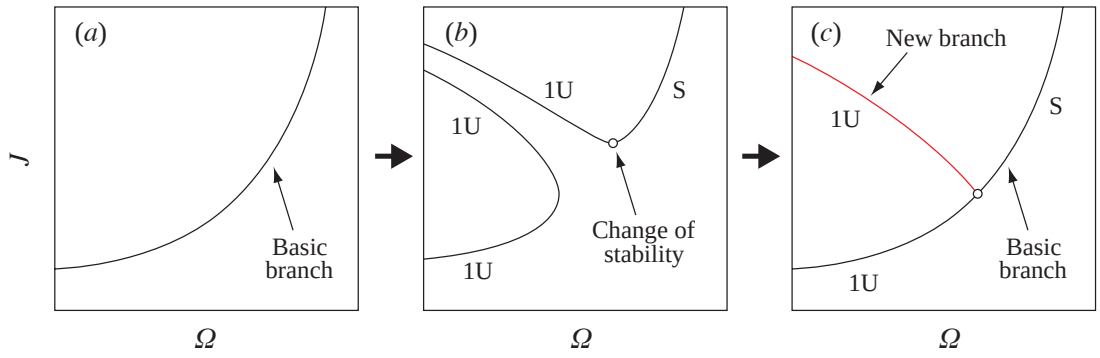

Figure 4.1: Typical construction of an Imperfect-Velocity-Impulse (IVI) diagram. (*a*) shows a velocity-impulse diagram for a basic branch of steady solutions. Introducing a small perturbation and re-computing the steady states breaks the basic branch into two distinct branches (shown in *b*), revealing a change of stability. In (*c*), by bringing the perturbation to zero, we recover the underlying new solution branch (shown in red).

In the above, ω is the vorticity, while the integrals are taken over all space. Since E and J are conserved in an inviscid fluid, while Ω is treated as a fixed parameter, H is also a conserved quantity. If the stationary point is a maximum or a minimum in the solution space (implying that the second variation $\delta^2 H$ is positive or negative definite), then a displacement away from the solution would lead to a change in H, which is impossible; hence the solution must be stable to isovortical perturbations, thus yielding a sufficient condition for stability. Similarly, a necessary condition of instability is that the stationary point is a saddle (Thomson, 1876). The second variation $\delta^2 H$ can therefore be used, in principle, to assess stability; unfortunately, computing $\delta^2 H$ is often unfeasible, since solutions of practical interest are usually known only numerically. The implementation of Kelvin's argument has thus been the subject of extensive debate.

Saffman & Szeto (1980), having numerically found steady solutions for two co-rotating vortices, circumvented this difficulty as follows. Equation 4.1 can be interpreted as establishing extrema of E under the constraint that J = const.,

with Ω taking the role of a Lagrange multiplier. A plot of E versus J for their flow then shows that, for a given J, there exist two E branches, joined at a fold point. The top branch was interpreted as a maximum (and hence stable), while the lower branch was speculated to be a saddle (possibly unstable).

However, Dritschel (1985) later pointed out that there seems to be no necessary link between the shape of a plot of E versus J and the curvature of the H surface. Furthermore, he stated that even if such correspondence could be established, additional changes of stability could occur away from folds in E and J, by means of bifurcations to new families of solutions. As a consequence of these arguments, the method proposed by Saffman & Szeto has been considered unreliable.

In a forthcoming paper, we address both of these issues by proposing a new approach to this problem (Luzzatto-Fegiz & Williamson, 2010*b*). By building on ideas from dynamical systems theory, we show that changes of stability are associated with extrema in a velocity-impulse diagram (instead of an impulse-energy diagram). We deal with the second issue raised by Dritschel (1985) by exploiting the fact that bifurcations are not structurally stable (Poston & Stewart, 1978); hence by introducing a small imperfection and re-computing the steady states, we obtain distinct solution branches, thus uncovering any bifurcations. All changes of stability are therefore apparent in an "Imperfect-Velocity-Impulse" (IVI) diagram.

Let us consider, as a schematic example of a typical construction of an IVI diagram, a possible scenario involving the detection of a subcritical bifurcation for a family of equilibrium solutions of the Euler equations (see figure 4.1). Firstly, the steady base flows are computed, and the associated velocity-impulse dia-

gram is plotted (figure 4.1*a*). Introducing a small imperfection in the governing equations, and re-computing the steady states, breaks the original curve into two distinct branches, revealing an extremum in J (figure 4.1*b*). Since the extremum consists of a local minimum, it can be shown that stability is lost as the curve is traversed from right to left (Luzzatto-Fegiz & Williamson, 2010*b*, 2011*b*). Therefore, if we suppose, for example, that the right-most portion of the branch is stable (marked by 'S' in the figure), the portion of the branch to the left of the minimum in J will have one unstable mode (denoted by '1U'). Finally, by taking the strength of the imperfection to zero, we recover the underlying bifurcated solution branch (shown in red in figure 4.1*c*).

As an example of the practical use of the IVI diagram approach, we consider the stability of the family of elliptical vortices discovered by Kirchhoff (1876). While the elliptical family can be characterized analytically, detecting bifurcations through an IVI diagram requires finding equilibrium vortices numerically; the computational procedure is outlined in § 4.2. In § 4.3.1, we describe the unfolding of the IVI diagrams for the elliptical vortices. A large body of work exists regarding the stability of the Kirchhoff ellipses (see for example Love, 1893; Moore & Saffman, 1971); in § 4.3.2, these results are employed to verify the efficacy of the IVI diagram approach.

4.2 Computational method

In order to ensure that all solutions are captured, we must employ a numerical method that is capable of resolving arbitrary vortex shapes; this is particularly important in the light of the fact that bifurcations commonly lead to new fam-

ilies of solutions having fewer (if any) symmetries relative to the original solution. Furthermore, it is known that families of uniform vortices usually terminate with limiting vortex states, whose boundaries exhibit one or more corners (Wu *et al.*, 1984; Overman, 1986); computing such shapes calls for a particularly efficient numerical approach. We intend to submit the full details of the method for publication shortly (Luzzatto-Fegiz & Williamson, 2011*a*); in what follows, we briefly outline the approach.

A patch of uniform vorticity corresponds to a steady state if, as the vortex translates or rotates, its boundary does not deform. This implies that, in a frame of reference moving with the vortex, the component of the velocity field normal to the boundary must vanish. For a rotating configuration, we can therefore write:

$$\mathbf{u}_c \cdot \mathbf{n} = 0 \tag{4.4}$$

on the vortex boundary, where $\mathbf{u}_c = (u_c, v_c) = (u, v) + \Omega(y, -x)$ is the velocity in the co-rotating frame, and $\mathbf{n}$ is the unit-normal vector to the boundary. For a given vorticity distribution, the velocity field $\mathbf{u}$ is obtained by inverting the Poisson equation $\nabla^2\psi = -\omega$ by means of the appropriate Green function (see e.g. Saffman, 1992). The vorticity field can then be iteratively adjusted until Eq. 4.4 is satisfied.

Since Deem & Zabusky (1978) first employed the method of contour dynamics to solve Eq. 4.4, a large variety of approaches has been developed to find equilibrium uniform vortices. These techniques make use of either Newton iteration (e.g. Elcrat *et al.*, 2005) or of a relaxation approach to obtain new solutions (e.g. Pierrehumbert, 1980). Unfortunately, each approach is limited in the possible range of vortex shapes it can resolve. While Newton iteration guarantees

convergence and can therefore, in principle, capture arbitrary shapes, it may become prohibitively expensive for vortices exhibiting fine-scale features. On the other hand, relaxation methods are much less computationally intensive, and can thus affordably resolve details such as corners; however, as convergence is not assured, they usually fail to compute shapes having fewer than two planes of symmetry (Dritschel, 1985, e.g.).

We address these issues by introducing a methodology that overcomes the large computational expenses associated with Newton iteration. Given a guess for a new solution, we compute the correction normal to the vortex shape (say, $\gamma(s)$) as a function of arc-length along the boundary s. We then expand γ in a Fourier series in terms of a modified arclength parameter $\tilde{s}$, constructed according to local curvature, in order to ensure fast convergence in the series. This allows us to affordably and reliably compute vortices of arbitrary shape. We choose Ω as the control parameter, and employ generalized continuation to ensure that we can negotiate any turning points; new solutions are obtained by employing an Euler predictor and a Newton corrector. The vortex is taken to have unit vorticity and area.

The accuracy in the solution typically depends on the number of modes M used in the Fourier expansion and on the size of the step $\delta\ell$ taken in the solution space; the algorithm uses a fixed value of M and adjusts $\delta\ell$ to ensure that the highest-order terms in the Fourier series are negligibly small. The method was initially tested against the exact elliptical solutions, while selected bifurcated branches were checked by changing M and $\delta\ell$; for all of the results presented here, the shapes were verified to be accurate to at least seven significant figures. All calculations were performed on a laptop computer with a 1.83 GHz pro-

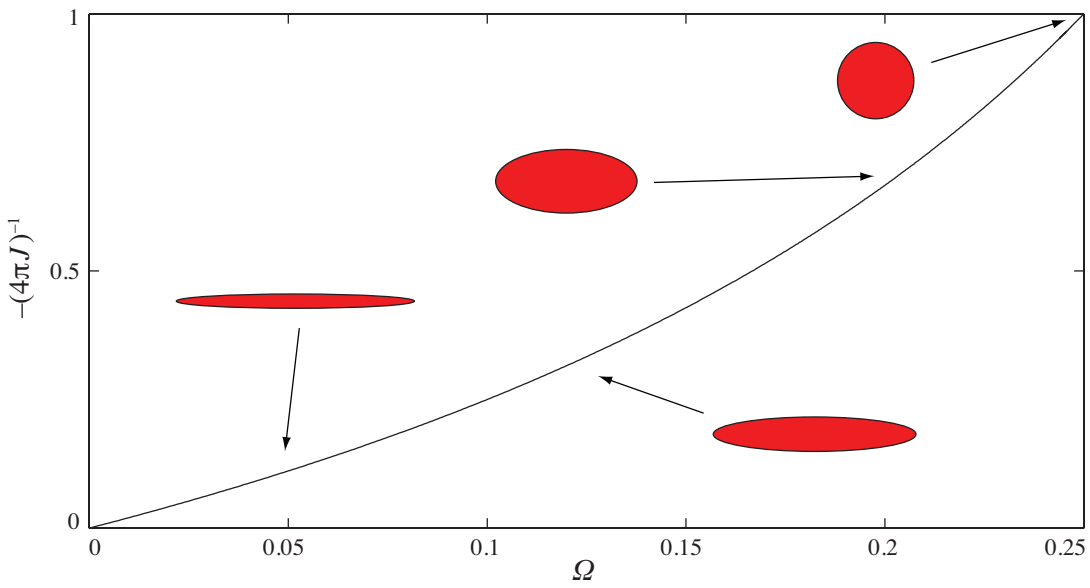

Figure 4.2: Velocity-impulse plot for the Kirchhoff ellipses. Since no extrema are immediately apparent, any exchanges of stability have to develop through bifurcations.

cessor, which is an indication of the modest computational power required to implement the approach.

4.3 Stability of elliptical vortices

4.3.1 Number of unstable modes and bifurcated branches from IVI diagrams

The Kirchhoff vortices represent a rare case of a vortical solution of the Euler equation that can be represented analytically (see Kirchhoff, 1876; Lamb, 1932; Saffman, 1992). Once again considering, without loss of generality, patches with

unit vorticity and area, it can be show that the impulse is given by:

$$J(\Omega) = \frac{2\Omega - 1}{8\pi\Omega}, \tag{4.5}$$

where Ω is related to the axis ratio $\lambda = b/a$ by $\Omega = \lambda(\lambda+1)^{-2}$. Since J is singular as $\lambda \to 0$, and $J = -(4\pi)^{-1}$ at $\lambda = 1$, we choose to plot $-(4\pi J)^{-1}$ instead of J (see figure 4.2; notice that the value of Ω for any extrema would be unchanged). Since $J(\Omega)$ is monotonic, any changes of stability have to occur through bifurcations.

The family of solutions begins with a circular vortex (top-right-hand corner in figure 4.2) and terminates into a vortex sheet (located at the origin in the figure). The circular vortex can be argued to be stable, since any deformation of the boundary would tend to 'spread out' its vorticity. This, in turn, would lead to a decrease in the flow's kinetic energy, which is not possible in an inviscid flow; thus the circular vortex must be stable (as already noted by Thomson, 1880*a*). Alternatively, a straightforward linear stability analysis (see Thomson, 1880*c*; Saffman, 1992) can be used to obtain the same conclusion. (Incidentally, the circular vortex has also been shown to be nonlinearly stable by Dritschel, 1988*c*). By starting with a near-circular vortex and using an IVI diagram to detect the introduction of unstable modes along the family, we can therefore determine the stability properties of the elliptical vortices.

The imperfection is constructed as follows. Examining the flow field in the co-rotating frame (for which streamlines are shown in figure 4.3), one can find four stagnation points, two residing in the recirculation regions above and below the vortex in the figure (marked by a cross, $\times$), and two taking the form of saddle points (denoted by the bull's eyes, $\odot$). We either introduce a weak point vortex in each of the recirculation regions, or place a point source and a sink at each of the saddle nodes. In the results presented here, we switch between these

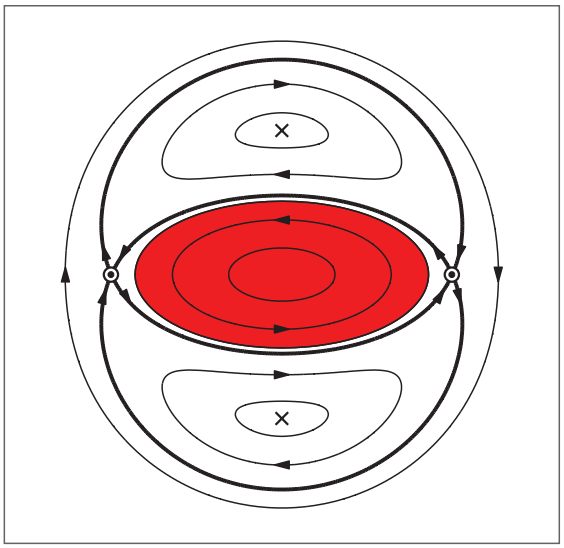

Figure 4.3: Streamlines in a frame of reference rotating with the elliptical vortex. The shaded region is occupied by uniform vorticity. The imperfection can be constructed by either placing a point vortex at each of the stagnation points marked by a cross (×), or by introducing a source and a sink of equal strengths at the stagnation points denoted by a bull's eye (⊙).

two imperfections depending on which construction yields the clearest example of bifurcation breaking, as we shall explain in further detail below. The addition of these flow elements is accommodated by a small modification to the code outlined in § 4.2; this involves counting the contribution to **u** from the flow elements, while solving for the position of the stagnation points in the co-rotating flow. The strength of each imperfection is treated as a fixed parameter.

We begin to develop the IVI diagram for the elliptical vortices by considering a near-circular vortex, introducing a source-sink combination, and recomputing the steady states. As a fraction of the circulation of the elliptical vortex, each source / sink is chosen to have strength $m/\Gamma = \pm 10^{-4}$. We gradually reduce Ω and seek new steady states. A local minimum in impulse J is reached at $\Omega \doteq 0.1877405$, indicating that stability is lost at this location (as shown in the left-hand diagram in figure 4.4*a*), while revealing the presence of a bifurca-

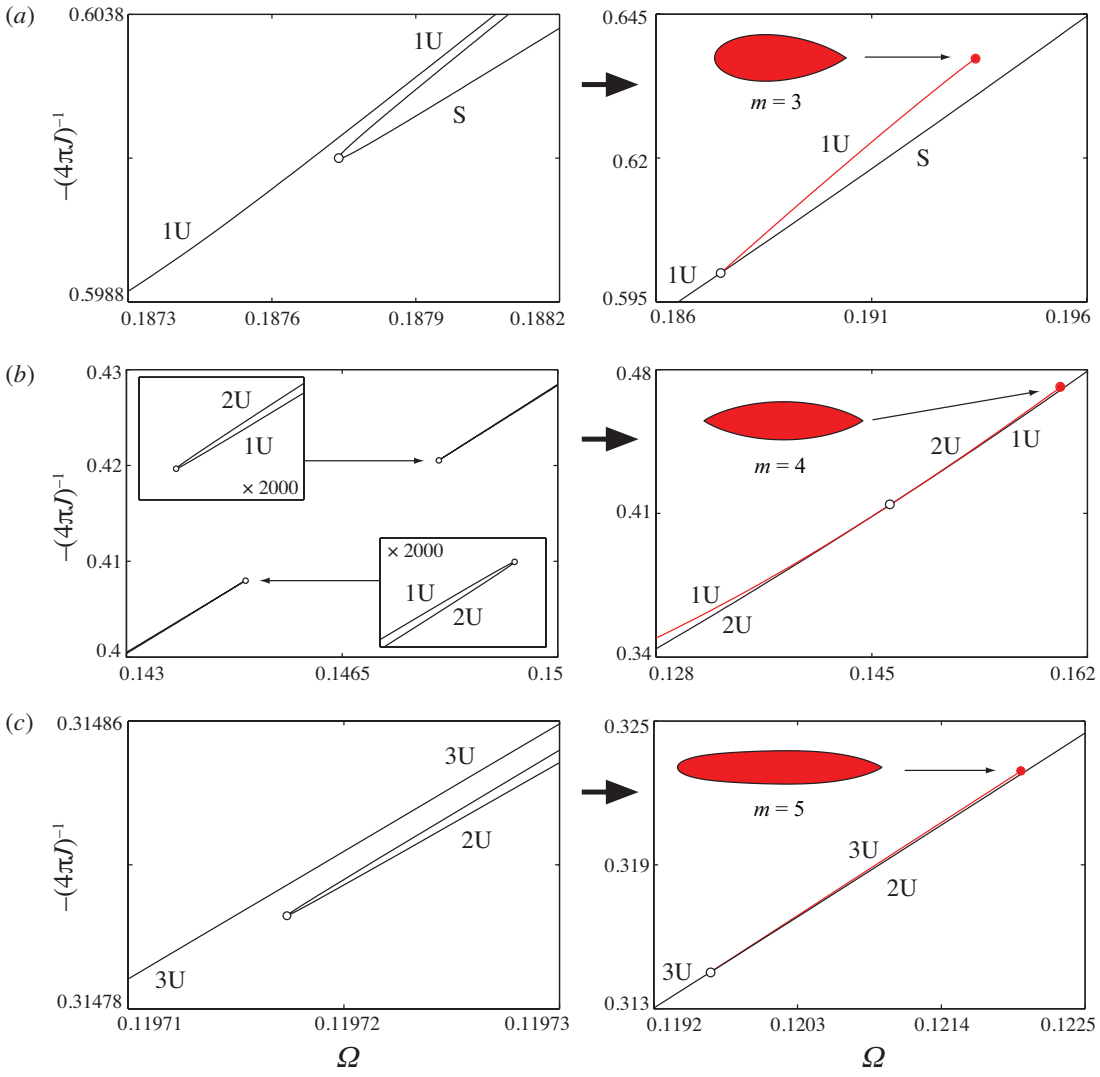

Figure 4.4: Construction of the IVI diagram for the first three bifurcations of the elliptical vortices. The left-hand column shows the branches that were computed after introducing the imperfection; on the right-hand side, the underlying bifurcated branch (computed by taking the imperfection to zero) is shown in red. From top to bottom, the bifurcations shown in (*a*), (*b*) and (*c*) are associated with perturbations having azimuthal wavenumber $m = 3, 4$ and 5, respectively. Open and filled circles denote changes of stability and limiting shapes, respectively.

tion. The second imperfect branch in figure 4.4*a* is computed by introducing the same imperfection to elliptical vortices further along the family (i.e. with lower Ω) and seeking steady states for progressively increasing Ω. By subse-

quently letting the strength of the source and sink approach zero, we recover the underlying bifurcated branch. This family is found to end with a limiting shape (shown in the right-hand part of figure 4.4*a*), which exhibits a 90° corner. By visual inspection of these non-elliptical shapes, we can establish that this bifurcation is associated with a perturbation with azimuthal wavenumber $m = 3$. The IVI diagram indicates that this family of solutions has one unstable mode.

The next bifurcation is investigated by introducing two point vortices, each having strength $\Gamma_{PV}/\Gamma = 10^{-4}$; more will be said on this choice of imperfection below. Restarting our search for equilibria past the $m = 3$ bifurcation, for decreasing Ω, we eventually encounter a new local minimum in J at $\Omega \doteq 0.1480637$, thus detecting a second loss of stability at an additional bifurcation (shown in the inset of figure 4.4*b*). Note that, in order to clearly see this minimum, we have had to magnify the plot by a factor of 2000! In a manner similar to the $m = 3$ case, this branch exhibits a turning point in Ω. However, in contrast to the $m = 3$ bifurcation, the adjacent branch now reveals a local maximum in J, after which the left-hand branch moves away from the right-hand one, instead of approaching it (second inset in figure 4.4*b*). Removing the imperfection, and computing the underlying family, indicates that these solutions connect to the elliptical vortices at a point of tangency in the velocity-impulse diagram, through what appears to be a transcritical bifurcation. For increasing Ω, the new bifurcated solution branch (shown in red) terminates with a shape resembling a cat's eye. With decreasing Ω, we are led to a state consisting of two identical vortices connected at a point (see the left-most shape in figure 4.5). This branch can be continued into a family of two identical co-rotating vortices (Cerretelli & Williamson, 2003*a*; Luzzatto-Fegiz & Williamson, 2011*c*). In this case, we find that this bifurcation is associated with modes with azimuthal wavenumber $m = 4$.

It should be pointed out that the use of a source/sink combination as an imperfection was also found to successfully break the $m = 4$ bifurcation into two branches. Although these two branches do not share any steady states, they are found to overlap at a point in the IVI diagram. While the resulting diagram is somewhat less clear for the purposes of illustration, stability properties can still be correctly inferred in a straightforward manner.

We employ again a source/sink combination for the next bifurcation. The imperfect steady states display a minimum at $\Omega \doteq 0.1197174$, leading to a further loss of stability (left-hand plot in figure 4.4*c*). The structure of this bifurcation is qualitatively similar to the $m = 3$ case. While the underlying solution branch also ends in a limiting shape with a 90° corner (right-hand plot in figure 4.4*c*), this bifurcation is found to be associated with an $m = 5$ perturbation.

For any bifurcations detected through the IVI diagram approach, the precise location Ω_{crit} of the change of stability is established by computing the steady state connecting two branches; a comparison with classical results is provided in the next section.

4.3.2 Stability from classical results

There is a large body of results regarding the stability of the elliptical vortices (see Mitchell & Rossi, 2008, for a recent review). Love (1893) obtained an expression for the eigenvalue σ associated with a perturbation of wavenumber m, as a function of the axis ratio λ:

$$\sigma^2 = -\frac{1}{4}\left\{\left[\frac{2m\lambda}{(1+\lambda)^2} - 1\right]^2 - \left[\frac{1-\lambda}{1+\lambda}\right]^{2m}\right\}, \tag{4.6}$$

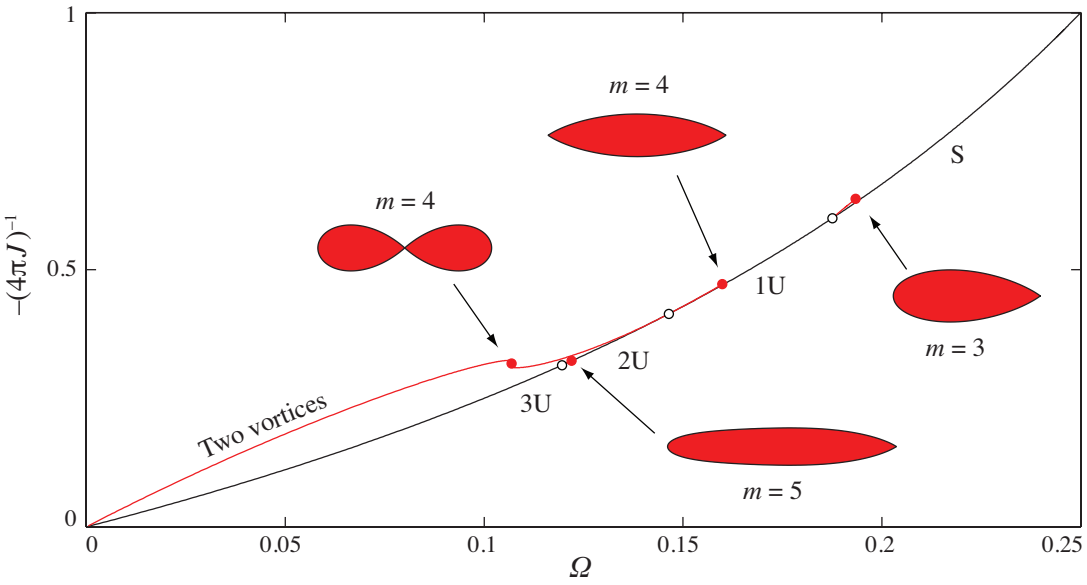

Figure 4.5: Overall view of the resulting IVI diagram, showing the first three branches bifurcating from the elliptical states.

where a real value of σ yields an instability. The values of Ω for each bifurcation m can then be calculated by setting $\sigma = 0$ in Eq. 4.6, and using the expression $\Omega = \lambda(\lambda+1)^{-2}$. We verify that, as one should expect, the locations of the changes of stability from our methodology match Love's prediction to at least seven significant figures. Indeed, since the changes of stability in our study are found by determining the intersection between the bifurcated and the basic solution branches, the precision in the stability boundaries is limited only by the numerical accuracy with which the steady states are computed.

Love's analysis formed the basis of part of the work of Kamm (1987), who computed the beginning of the bifurcated branches presented here; the $m = 4$ branch was later explored in its entirety by Cerretelli & Williamson (2003*a*), who approached the problem by initially considering two co-rotating vortices with lower Ω. Due to the large computational cost associated with previous numerical methods (Kamm, 1987), it appears that the $m = 3, 5$ families (including the

limiting shapes) had not been computed before.

It should be pointed out that the stability of all of these bifurcated branches was previously unknown. Furthermore, while attempting to apply the approach of Saffman & Szeto, involving a (J, E) plot, to determine stability, Kamm found that all of the new equilibria had the same energy and impulse as a member of the elliptical family (to numerical accuracy). The bifurcated branches were therefore indistinguishable from the elliptical family in a plot of E versus J, preventing Kamm from reaching any conclusions regarding stability. This appears to be a further problem that can be associated with the use of an impulse-energy plot, which should be considered in addition to the theoretical objections previously posed by Dritschel (1985). By contrast, the use of a velocity-impulse diagram does not appear to suffer from the same issues.

In spite of presenting a significant amount of fine-scale detail in the velocity-impulse plot, we must note that the bifurcations were easily detected with the imperfection approach presented here. As noted in § 4.2, the step change in the control parameter was automatically adjusted to preserve accuracy; we did not need to pose further restrictions to ensure that bifurcations were detected. Therefore an IVI diagram (coupled with a suitable numerical method) is found to be reliable in revealing bifurcations. Once a new branch is detected, the turning points can be carefully mapped by employing progressively smaller step sizes.

Finally, we should remark that, as a part of a separate work, the authors examine the $m = 4$ branch through a linear stability analysis (Luzzatto-Fegiz & Williamson, 2011*c*), finding accurate agreement with the results presented here.

4.4 Conclusions

In this paper, we successfully employ the "Imperfect-Velocity-Impulse" (IVI) diagram methodology to determine the stability of elliptical vortices, providing a detailed example of the application of this approach to a classical flow. The imperfection used to reveal bifurcations is constructed by placing either point vortices, or sources and sinks, at the stagnation points of the co-rotating flow; the steady states are then computed using a novel numerical approach capable of accurately resolving vortex shapes of lesser symmetry.

The first three bifurcations for the family of Kirchhoff elliptical vortices (corresponding to instabilities with azimuthal wavenumber $m = 3, 4$ and 5) are revealed; their detection appears to be insensitive to the numerical parameters employed. Inspection of the IVI diagram gives the stability properties for the elliptical vortices, as well as for the bifurcated families. Each non-elliptical branch is found to terminate with limiting shapes exhibiting one or more 90° corners.

While the locations of these changes of stability precisely match available results from linear analysis (Love, 1893), the stability of the non-elliptical shapes represents a new result. It also appears that the existence of limiting states for the $m = 3, 5$ branches had not been established before.

It should be pointed out that, in this study of the Kirchhoff elliptical vortices, all changes of stability are revealed by the use of imperfection theory. However, in general, one might expect to also find changes of stability occurring at extrema in impulse for the base flow.

In conclusion, we demonstrate that the new IVI-diagram approach outlined

here, which represents a rigorous implementation of Kelvin's argument, accurately and reliably detects changes of stability for the family of Kirchhoff elliptical vortices.

CHAPTER 5

RESONANT INSTABILITY IN TWO-DIMENSIONAL VORTEX ARRAYS

Published as

LUZZATTO-FEGIZ, P. & WILLIAMSON, C. H. K. (2010)

Proceedings of Royal Society A , in press.

We examine conditions for the development of an oscillatory instability in two-dimensional vortex arrays. By building on the theory of Krein signatures for Hamiltonian systems, and considering constraints due to impulse conservation, we show that a resonant instability (developing through coalescence of two eigenvalues) cannot occur for one or two vortices. We illustrate this deduction by examining available linear stability results for one or two vortices. Our work indicates that a resonant instability may, however, occur for three or more vortices. For these more complex flows, we propose a simple model, based on an elliptical vortex representation, to detect the onset of an oscillatory instability. We provide an example in support of our theory by examining three co-rotating vortices, for which we also perform a linear stability analysis. The stability boundary in our model is in good agreement with the full stability calculation. In addition, we show that eigenmodes associated with an overall rotation or an overall displacement of the vortices always have eigenvalues equal to zero and $\pm i\Omega$, respectively, where Ω is the angular velocity of the array. These results, for overall rotation and displacement modes, can also be used to immediately check the accuracy of a detailed stability calculation.

5.1 Introduction

The problem of determining the stability and dynamics of two-dimensional vortex configurations commonly arises across a wide range of disciplines, including geophysical flows (e.g. Turkington *et al.*, 2001), electron plasma columns (Kiwamoto *et al.*, 2007), and the study of quantum condensates (Keeling & Berloff, 2008). In all of these fields, the stability of coherent vortices is fundamental to the underlying dynamics. Unfortunately, performing a linear stability analysis is often a process substantially more laborious than computing the steady vortex flows. This is epitomized by the fact that the stability properties of several two-dimensional vortex flows have been the subject of protracted debates, in spite of their apparent simplicity. Prominent examples include co-rotating vortex pairs (Dritschel, 1995, and references therein), as well as Kármán streets of finite-area vortices (Meiron *et al.*, 1984, and several references therein). (More recently, similar debates have developed for ellipsoidal vortices in quasi-geostrophic flows; see Dritschel *et al.*, 2005).

For this reason, the development of a simple stability approach (circumventing the need for a complete linear analysis) would represent a particularly useful tool. Such an approach could be used in its own right to obtain basic stability information, or it could be employed in conjunction with more complex stability methods to provide a quick check of accuracy.

To discuss this in further detail, we need to point out that the instabilities experienced by a fluid flow may be subdivided into two qualitatively different categories. The first type is known as an *exchange of stability*, and is manifested by a perturbation that (to linear order) grows exponentially without propagat-

ing in space. An example of a fluid phenomenon associated with this instability is given by the merger of two co-rotating vortices, which has been the subject of extensive theoretical, experimental and numerical work in recent years (see Cerretelli & Williamson, 2003*b*; Meunier *et al.*, 2002, and references therein). The second type of instability is of *oscillatory* type, and develops through a resonance between two previously stable modes (as we discuss in detail further below; see Lamb & Roberts, 1998; MacKay, 1986). A classic example of resonance in a two-dimensional vortical flow is provided by the development of the Kelvin-Helmholtz instability, for an otherwise stably stratified fluid, as the velocity discontinuity ΔU is increased; two (previously stable) travelling modes interact to give rise to an instability that propagates while growing (Cairns, 1979; Craik, 1985). Recently, Luzzatto-Fegiz & Williamson (2010*b*,*c*) developed a simple methodology to detect *exchanges* of stability occurring along a family of steady flows, through the construction of "imperfect velocity-impulse" (IVI) diagrams. This recent work motivated us to develop a similar, simple diagnostic for predicting the occurrence of *oscillatory* instabilities in vortical flows.

In order to introduce the ideas that we propose to develop, let us first note that when investigating stability of vortex configurations, the focus is typically placed on inertial instabilities (see e.g. Eloy & Le Dizès, 2001). In the absence of solid boundaries or critical layers, it may therefore be possible to neglect viscous effects; one can then compute families of steady flows, without the need to introduce any external forcing. Furthermore, the lack of dissipation leads to a system that is time-reversible and Hamiltonian (see the reviews of Salmon, 1988; Morrison, 1998). This Hamiltonian, reversible structure is useful in categorizing the possible stability behaviour, as we discuss below.

When considering linear stability to a perturbation of the form $e^{\sigma t}$, one consequence of time reversibility is that all complex eigenvalues must appear in quadruplets $\pm(\sigma_R \pm i\sigma_I)$ (see Lamb & Roberts, 1998). Special cases are given by $\sigma = 0$, which may occur as a single eigenvalue, and by the purely real or purely imaginary cases ($\sigma_{1,2} = \pm\sigma_R$ or $\sigma_{1,2} = \pm i\sigma_I$), which can appear as pairs. If all of the eigenvalues are purely imaginary, the system is stable (e.g. Holm *et al.*, 1985).

For reversible flows, a different approach to investigating stability can be obtained by considering certain conserved quantities, which impose constraints on the possible dynamics. In essence, this method relies on finding a conserved quantity, say H (which may be the Hamiltonian), such that a stationary point of H (with respect to kinematically admissible perturbations) corresponds to an equilibrium flow. If one can prove that the equilibrium is a minimum or a maximum of H, then the system must be stable, since the growth of a perturbation would lead to a change in H, which is impossible. This argument forms the basis of several stability approaches, including Kelvin's variational argument (see Davidson, 1998, and references therein), as well as the method of Casimirs (Holm *et al.*, 1985).

Let us now suppose that we are interested in the stability properties of a family of equilibrium flows, which are organized according to a parameter λ. We further suppose that we have previously obtained detailed stability information for one specific steady solution within the family (say, $\lambda = \lambda_0$), and that we are interested in detecting any changes in stability that may take place as we traverse the solution series. If a stable flow initially corresponds to a maximum or minimum of H, a necessary condition for a change of stability is that, as we

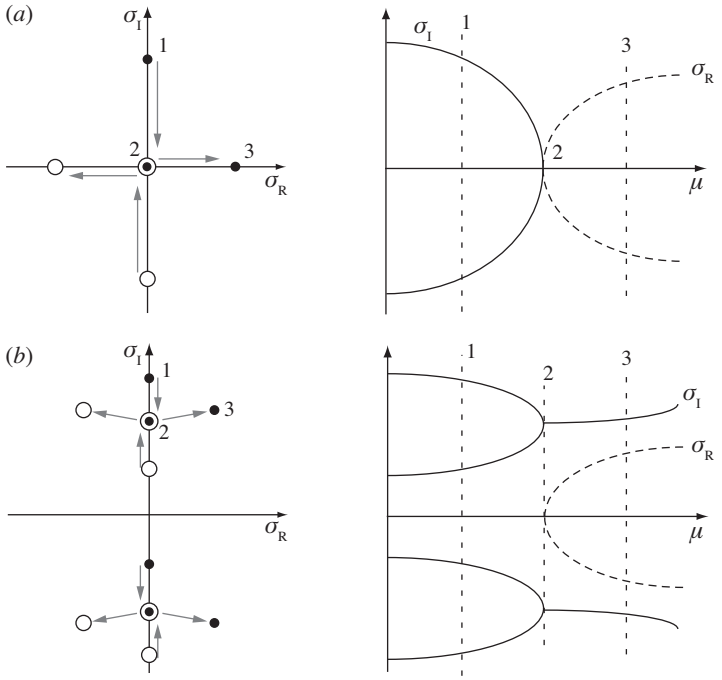

Figure 5.1: Possible eigenvalue behaviour for (*a*) an exchange of stability (giving rise to a non-propagating unstable eigenmode), and (*b*) a Hamiltonian Hopf bifurcation (leading to an oscillatory instability).

move along the family of solutions, the equilibrium must become a saddle of H. If a change of stability does occur, it must manifest itself as an *exchange of stability*: the imaginary eigenvalue pair $\sigma_{1,2} = \pm i\sigma_I$ goes through $\sigma_{1,2} = 0$, after which it becomes a purely real pair $\sigma_{1,2} = \pm\sigma_R$, as illustrated in figure 5.1(*a*) (see e.g. Lamb & Roberts, 1998). For $\sigma_{1,2} = 0$, a bifurcation to a new family of steady solutions may occur. For a family of steady flows, Luzzatto-Fegiz & Williamson (2010*b*) showed that the creation or destruction of a saddle of H can be immediately detected as a turning point in impulse in an IVI diagram, without the need for a more involved analysis.

However, for certain flows, the equilibrium at $\lambda = \lambda_0$ may already constitute a saddle of H, while still being stable; this allows for the development of an additional type of instability, as explained below. At a saddle of H, certain

eigenmodes will be associated with an increase in H, while others will drive a decrease in H. In dynamical systems theory, the sign of the change of H associated with a given eigenmode is named the *Krein signature* of the eigenmode (see Krein, 1950; Arnol'd & Avez, 1968; MacKay, 1986); its significance can be understood as follows.

At a maximum of H all eigenmodes must have negative signature. However, at a saddle, modes with positive and negative signatures coexist. Two otherwise stable modes with opposite signature may cooperate to give rise to an eigenmode that leaves H unchanged (and is therefore able to grow), thus enabling instability. This mechanism is sometime referred to as "Krein resonance" in the dynamical systems literature (MacKay, 1986; Morrison, 1998).

If we consider the evolution of the resonance in terms of the eigenvalue behaviour in the complex plane, we have that two purely imaginary eigenvalue pairs meet on the imaginary axis, after which they move parallel to the real axis, giving rise to an eigenvalue quadruplet (as illustrated in figure 5.1*b*). Since two (neutrally) stable oscillatory modes are destroyed, while an oscillatory instability develops, such a change of stability is also referred to as a *Hamiltonian Hopf bifurcation* or as a *reversible Hopf bifurcation*, by analogy to the Hopf bifurcation of dissipative systems (see Lamb & Roberts, 1998, and references therein).

The interpretation of resonant behaviour in terms of Krein signatures has found application in several contexts, including parallel, stratified flows (Cairns, 1979; Craik, 1985) and steep gravity waves (MacKay & Saffman, 1986). However, it appears that resonant instabilities on vortex flows have been almost exclusively studied through detailed eigenvalue calculations; a classic example is given by the elliptic instability of a single vortex in a weak strain field (see

the review of Kerswell, 2002). As a matter of fact, ideas from Krein's theory of Hamiltonian spectra have been introduced only relatively recently to the study of this flow (Fukumoto, 2003). To the best of our knowledge, the concept of eigenmode signatures has not been used before to study the stability of arrays of several vortices.

We now outline the approach taken in this paper. We suppose that, within a given family of steady flows, there exists a solution (at $\lambda = \lambda_0$) that is well approximated by a collection of uniform vortices, whose separation distances are large by comparison to their core sizes. For this solution, any eigenmodes (together with their signatures) may be readily found through asymptotic approaches. We then distinguish between two qualitatively different types of perturbations. The first type involves pure displacements of each of the vortices, which leave each core shape unchanged, as illustrated in figure 5.2(*a*). Modes of the second type are instead associated with a pure deformation of each core, but do not change the centroid location for any vortex in the configuration (as exemplified in figure 5.2*b*). In § 5.2, we begin by showing that, for well-separated vortices, pure displacement modes may have positive signature, while pure deformation modes always have negative signature. An important implication is that, in such a two-dimensional flow, an oscillatory instability must involve a pure displacement mode. In § 5.3, we argue that conservation of impulse constrains the behaviour of the eigenvalues for several pure displacement modes. In § 5.4, we make use of this conclusion to show that one or two vortices cannot exhibit a resonance in a two-dimensional flow. Our theory indicates that resonances are possible for three or more vortices. In § 5.5, after computing the mode signatures for three co-rotating vortices, we employ the ideas presented here to construct a simple model to approximately predict the onset of oscillatory insta-

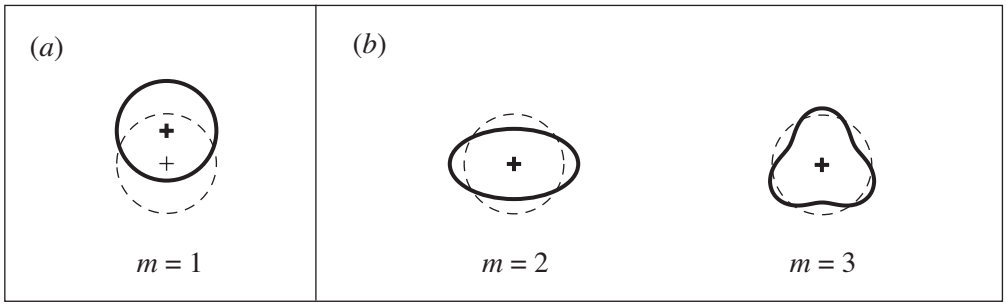

Figure 5.2: Schematic illustration of perturbations involving a displacement (*a*) or deformation (*b*) of the vortex cores. *m* denotes the azimuthal wavenumber of the perturbation. The dashed and continuous lines represent the unperturbed and perturbed configurations, respectively.

bility. In addition, we perform a linear stability analysis for three vortices, and compare these results with predictions from our model. Finally, as a point of interest, we present detailed stability properties for the three corotating vortices.

5.2 Finding mode signatures for well-separated vortices

In this section, we first review relevant concepts from variational fluid mechanics, and introduce the appropriate choice of H for vortical flows. As first pointed out by Lord Kelvin (then known as Sir William Thomson), a steady vortex flow realizes a stationary point of the energy, for given impulse (Thomson, 1876). This idea was later given analytical support by the well-known theorem of Arnol'd (1966) (see also Benjamin, 1976; Davidson, 1998). In mathematical terms, a steady vortex flow in two dimensions corresponds to a stationary point of the functional:

$$H = E - UP - VQ - \Omega J, \tag{5.1}$$

where E is the excess kinetic energy, (P, Q) is the linear impulse, and J is the angular impulse, given by (see e.g. Saffman, 1992):

$$E = \frac{1}{2}\int \omega\psi \,\mathrm{d}A, \tag{5.2}$$

$$(P, Q) = \int \omega(y, -x)\,\mathrm{d}A, \qquad J = -\frac{1}{2}\int \omega(x^2 + y^2)\,\mathrm{d}A, \tag{5.3}$$

where ω, ψ are the vorticity and streamfunction, related by $\nabla^2\psi = -\omega$. Since H involves a combination of conserved quantities, together with the fixed parameters U, V, Ω, we have that H is also a conserved quantity. Since the first variation of H vanishes about the equilibrium (that is, $\delta H = 0$), the second variation $\delta^2 H$ constrains the evolution of the system, as explained in § 5.1.

In order to define the signature of a specific eigenmode, we suppose that the flow may be represented through M independent variables, say, α_i (where $i = 1, ..., M$). First, we can write the second variation of H as (see e.g. Dritschel, 1985):

$$\delta^2 H = \sum_{i=1}^{M}\sum_{j=1}^{M} \delta\alpha_j \frac{\partial^2 H}{\partial\alpha_i \partial\alpha_j}\delta\alpha_i = \delta\boldsymbol{\alpha}^T \mathbf{H}_2 \delta\boldsymbol{\alpha}, \tag{5.4}$$

such that $\mathbf{H}_2$ is the Hessian of H. Next, in order to find the eigenmodes associated with the linear stability problem, note that the Hamiltonian structure implies that the equations of motion can be cast as (Salmon, 1988; Morrison, 1998):

$$\frac{\mathrm{d}\boldsymbol{\alpha}}{\mathrm{d}t} = \mathbf{A}\nabla_\alpha H, \tag{5.5}$$

where ∇_α is the gradient with respect to α, and $\mathbf{A}$ is an $M \times M$ matrix (known as the symplectic matrix). The linearized dynamics are then given by

$$\frac{\mathrm{d}(\delta\boldsymbol{\alpha})}{\mathrm{d}t} = \mathbf{A}\mathbf{H}_2\delta\boldsymbol{\alpha}, \tag{5.6}$$

where $\mathbf{A}\mathbf{H}_2$ is the Jacobian matrix of the linearized system.Writing the i^{th} eigen-

mode as $\delta\boldsymbol{\alpha}^{(i)} = \epsilon\Re\{\hat{\boldsymbol{\alpha}}^{(i)}\exp(\sigma^{(i)}t)\}$, where $\Re$ denotes the real part, we have:

$$\sigma^{(i)}\hat{\boldsymbol{\alpha}}^{(i)} = \mathbf{A}\mathbf{H}_2\hat{\boldsymbol{\alpha}}^{(i)}, \tag{5.7}$$

where $\sigma^{(i)}$ and $\hat{\boldsymbol{\alpha}}^{(i)}$ denote the eigenvalues and eigenvectors of $\mathbf{AH}_2$. The problem of determining signatures for the linear eigenmodes can therefore be stated as follows. For a given flow, we can first compute the Hessian $\mathbf{H}_2$ and the symplectic matrix $\mathbf{A}$. The eigenvectors of $\mathbf{AH}_2$ then yield the linear modes $\delta\boldsymbol{\alpha}^{(i)}$ ($i = 1, ..., M$), for which the signatures are found from the sign of:

$$\delta^2 H^{(i)} = (\delta\boldsymbol{\alpha}^{(i)})^T\mathbf{H}_2\delta\boldsymbol{\alpha}^{(i)}, \quad i = 1, ..., M. \tag{5.8}$$

In § (5.2.1), we employ these ideas to obtain an approach for computing the signatures of pure displacement modes.

5.2.1 Signature of pure displacement modes

In this section, we are interested in disturbances that involve displacements of N well-separated vortices; each vortex may be moved in a different direction by the perturbation. We therefore model this problem by studying a configuration of point vortices, for which the conserved quantities become (e.g. Aref, 1983):

$$E = -\frac{1}{4\pi}\sum_{\substack{k,l=1\\k\neq l}}^{N}\Gamma_k\Gamma_l\log[(x_k - x_l)^2 + (y_k - y_l)^2]^{1/2}, \tag{5.9}$$

$$(P, Q) = \sum_{k=1}^{N}\Gamma_k(y_k, -x_k), \qquad J = -\frac{1}{2}\sum_{k=1}^{N}\Gamma_k(x_k^2 + y_k^2), \tag{5.10}$$

where Γ_k is the circulation of the vortex located at (x_k, y_k). The Hamiltonian coordinates correspond to the vortex locations, giving

$$\boldsymbol{\alpha} = (x_1, x_2, \cdots, x_N, y_1, y_2, \cdots, y_N)^T, \tag{5.11}$$

such that the system has $2N$ coordinates. The matrix $\mathbf{H}_2$ can be written as

$$\mathbf{H}_2 = \mathbf{E}_2 - \Omega \mathbf{J}_2, \tag{5.12}$$

where $\mathbf{E}_2, \mathbf{J}_2$, are the Hessians of E, J. (Note that differentiating P and Q twice with respect to any pair of coordinates yields zero.) After defining $r_{ij}^2 = (x_i - x_j)^2 + (y_i - y_j)^2$, the second derivatives of E can be written as

$$\frac{\partial^2 E}{\partial x_i \partial x_j} = -\frac{\partial^2 E}{\partial y_i \partial y_j} = \begin{cases} \dfrac{\Gamma_i}{2\pi} \displaystyle\sum_{\substack{k=1 \\ k \neq i}}^{N} \Gamma_k \frac{(x_i - x_k)^2 - (y_i - y_k)^2}{r_{ik}^4}, & i = j \\ -\dfrac{\Gamma_i \Gamma_j}{2\pi} \dfrac{(x_i - x_j)^2 - (y_i - y_j)^2}{r_{ij}^4}, & i \neq j, \end{cases} \tag{5.13}$$

$$\frac{\partial^2 E}{\partial x_i \partial y_j} = \frac{\partial^2 E}{\partial x_j \partial y_i} = \begin{cases} \dfrac{\Gamma_i}{\pi} \displaystyle\sum_{\substack{k=1 \\ k \neq i}}^{N} \Gamma_k \frac{(x_i - x_k)(y_i - y_k)}{r_{ik}^4}, & i = j \\ -\dfrac{\Gamma_i \Gamma_j}{\pi} \dfrac{(x_i - x_j)(y_i - y_j)}{r_{ij}^4}, & i \neq j, \end{cases} \tag{5.14}$$

while for J we have:

$$\frac{\partial^2 J}{\partial x_i \partial x_j} = \frac{\partial^2 J}{\partial y_i \partial y_j} = \begin{cases} -\Gamma_i, & i = j \\ 0, & i \neq j. \end{cases} \tag{5.15}$$

The above relations, together with an expression for Ω (which, for a given equilibrium solution, is a known property) can thus be used to obtain $\mathbf{H}_2 = \mathbf{E}_2 - \Omega \mathbf{J}_2$.

Finally, to find the symplectic matrix $\mathbf{A}$, first note that the equations can be cast in Hamiltonian form as (see Aref, 1983; Newton, 2001):

$$\Gamma_i \frac{\mathrm{d}x_i}{\mathrm{d}t} = \frac{\partial H}{\partial y_i}, \qquad \Gamma_i \frac{\mathrm{d}y_i}{\mathrm{d}t} = -\frac{\partial H}{\partial x_i}, \tag{5.16}$$

such that the symplectic matrix $\mathbf{A}$ can be verified to be:

$$\mathbf{A} = \begin{pmatrix} \mathbf{O} & \mathbf{G} \\ -\mathbf{G} & \mathbf{O} \end{pmatrix}, \tag{5.17}$$

where $\mathbf{G}$ is an $N \times N$ diagonal matrix given by $G_{ii} = \Gamma_i^{-1}$, and $\mathbf{O}$ is the $N \times N$ zero matrix. Examples showing the application of the expressions above are given in sections 5.4 and 5.5.

5.2.2 Signature of pure deformation modes

To compute the signatures of the deformation modes, we prefer to adopt a different methodology, which involves generalizing a result of Fukumoto (2003) to an array of N well-separated vortices. For an isolated circular vortex of circulation Γ, Fukumoto (2003) computed explicitly the energy change associated with a perturbation of amplitude ϵ and azimuthal wavenumber m. In the present notation, he found:

$$\delta^2 E^{(m)} = -\frac{\Gamma^2}{4\pi}\Big(1 - \frac{1}{m}\Big)\epsilon^2, \quad m \geq 1. \tag{5.18}$$

A perturbation with azimuthal wavenumber $m = 1$ corresponds to a displacement mode, while $m \geq 2$ yields pure deformations, as illustrated earlier in figure 5.2. In what follows, we show that a generalization of Fukumoto's formula is possible, for the case of N vortices subject to pure deformations.

We begin by estimating $\delta^2 E$. By noting that $\nabla^2 \delta\psi = -\delta\omega$, and applying Green's theorem, we have:

$$\delta^2 E = \sum_{i=1}^{N} 2 \int_{A_i} \omega\, \delta^2\psi \, \mathrm{d}A \equiv \sum_{i=1}^{N} \delta^2 E_i, \tag{5.19}$$

where A_i denotes the region occupied by the i^{th} vortex, and $\delta^2\psi$ is is the second variation in ψ (evaluated at a point $\boldsymbol{x}$), due to perturbations that have been applied on all vortices. Let us decompose ψ into the individual contributions from

each vortex, such that we can write:

$$\begin{aligned}\delta^2 E_i &= 2\int_{A_i} \omega\, \delta^2\Big(\sum_{j=1}^{N} \psi_j\Big)\,\mathrm{d}A \\ &= 2\int_{A_i} \omega\left[\delta^2\psi_i + \delta^2\Big(\sum_{\substack{j=1\\ j\neq i}}^{N} \psi_j\Big)\right]\mathrm{d}A. \end{aligned} \tag{5.20}$$

In the above, ψ_j is obtained by considering the influence of the j^{th} vortex on the flow field through Biot-Savart's integral:

$$\psi_j(\boldsymbol{x}_j) = -\frac{1}{2\pi}\int_{A_j} \omega(\boldsymbol{x}_j')\log|\boldsymbol{x}_j - \boldsymbol{x}_j'|\,\mathrm{d}A', \tag{5.21}$$

where $\boldsymbol{x}_j$ denotes coordinates with origin at the centroid of the j^{th} vortex. For $|\boldsymbol{x}_j| \gg |\boldsymbol{x}_j'|$, noting that $\boldsymbol{x}_j' \sim a$ and $\boldsymbol{x}_j \sim L$, we have (see also Saffman, 1992):

$$\psi_j(\boldsymbol{x}_j) = -\frac{\Gamma_j}{2\pi}\log|\boldsymbol{x}_j| + \frac{(\boldsymbol{I}_j \wedge \boldsymbol{x}_j)\cdot\boldsymbol{k}}{2\pi|\boldsymbol{x}_j|^2} + O(\Gamma_j\frac{a^2}{L^2}), \tag{5.22}$$

where Γ_j, $\boldsymbol{I}_j = (P_j, Q_j, 0)$ are the circulation and impulse of the j^{th} vortex, and $\boldsymbol{k} = (0, 0, 1)$. Since the origin is at the centroid, $\boldsymbol{I}_j = \boldsymbol{0}$ by construction. Furthermore, under a perturbation of order ϵ to the shape of the j^{th} vortex, ψ_j expands as:

$$\psi_j = \psi_j^{(0)} + \delta\psi_j + \delta^2\psi_j + \ldots, \tag{5.23}$$

where $\psi_j^{(0)}$ is the streamfunction contribution from the unperturbed vortex, and $\delta\psi_j/\psi_j^{(0)} = O(\epsilon), \delta^2\psi_j/\psi_j^{(0)} = O(\epsilon^2)$, and so on. We now restrict our analysis to pure deformation modes, that is, $m \geq 2$. By definition, this type of perturbation leaves Γ_j and $\boldsymbol{I}_j$ unchanged. Therefore (5.22) yields:

$$\delta^2\psi_j = O(\Gamma_j\epsilon^2\frac{a^2}{L^2}), \quad \text{for} \quad |\boldsymbol{x}_j| \gg |\boldsymbol{x}_j'|. \tag{5.24}$$

Hence $\delta^2 E_i$ becomes, using the expression of Fukumoto (2003), and letting Γ denote the reference scale for the circulation of the vortices:

$$\begin{aligned}\delta^2 E_i &= 2\int_{A_i} \omega\,\delta^2\psi_i\,\mathrm{d}A + O(\Gamma^2\epsilon^2\frac{a^2}{L^2}) \\ &= -\frac{\Gamma_i^2}{4\pi}\Big(1 - \frac{1}{m}\Big)\epsilon^2 + O(\Gamma^2\epsilon^2\frac{a^2}{L^2}), \quad m \geq 2. \end{aligned} \tag{5.25}$$

This implies that the change in ψ due to perturbations on distant vortices makes a negligible contribution to the change of energy on a given vortex, such that each of the $\delta^2 E_i$ is found by simply considering the self-induced change in ψ.

Finally, we need to assess the contribution to $\delta^2 H$ from the second variation of the angular impulse. (As mentioned earlier, $\delta^2(P, Q) = (0, 0)$, since the centroid locations are unchanged by the perturbation.) Let us first write:

$$J = -\frac{1}{2}\sum_{i=1}^{N}\int_{A_i} \omega r^2 \,\mathrm{d}A \equiv \sum_{i=1}^{N} J_i, \tag{5.26}$$

where J_i is the impulse contribution from the i^{th} vortex, which we suppose has centroid at (X_i, Y_i). We expand r^2 as:

$$r^2 = L_i^2 + 2r_i(X_i \cos\theta_i + Y_i \sin\theta_i) + r_i^2, \tag{5.27}$$

where $L_i^2 = X_i^2 + Y_i^2$, and (θ_i, r_i) are local polar coordinates about (X_i, Y_i).

As before, we consider perturbations of the form $r_i = r_i^{(0)} + \delta r_i + \delta^2 r_i$, where $r_i^{(0)} = O(a), \delta r_i = O(a\epsilon), \ldots$. Substituting this into J_i, we obtain:

$$\begin{aligned} \delta^2 J_i &= -\int \omega \delta^2 r_i (X_i \cos\theta_i + Y_i \sin\theta_i)\,\mathrm{d}A - \frac{1}{2}\int \omega (2r^{(0)}\delta^2 r + (\delta r)^2)\,\mathrm{d}A \\ &= O(\Gamma_i L_i a \epsilon^2) + O(\Gamma_i a^2 \epsilon^2). \end{aligned} \tag{5.28}$$

The angular velocity Ω is of order $\sum_{i=1}^{N}\Gamma_i/L^2$ (as may be shown, for example, by considering an array of point vortices). Therefore, letting $\overline{\Gamma} = \sum_{i=1}^{N}\Gamma_i$:

$$|\Omega\,\delta^2 J| = O(\overline{\Gamma}^2 \frac{a}{L}\epsilon^2) \ll |\delta^2 E|, \tag{5.29}$$

so that $\Omega\,\delta^2 J$ is negligible. Incidentally, if the i^{th} vortex is placed at the location of the overall vorticity centroid, the corresponding $\Omega\,\delta^2 J_i = O(\overline{\Gamma}\Gamma_i \frac{a^2}{L^2}\epsilon^2)$ is even smaller, as may be expected on simple physical grounds.

Therefore, we finally obtain $\delta^2 H^{(m)}$, for N well-spaced uniform vortices:

$$\delta^2 H^{(m)} = -\frac{1}{4\pi}\Big(\sum_{i=1}^{N}\Gamma_i^2\Big)\Big(1-\frac{1}{m}\Big)\epsilon^2 + O(\overline{\Gamma}^2\frac{a}{L}\epsilon^2), \quad m \geq 2. \tag{5.30}$$

Therefore *all pure deformation modes have negative signature.* An important consequence of the analysis that we presented in this section is that, in a two-dimensional vortex configuration, deformation modes may not coalesce with each other to give oscillatory instability. Therefore *a resonance must involve at least one of the displacement modes* (which may have positive signatures).

5.3 Eigenvalue constraints for displacement modes

In this section, we employ simple physical considerations to argue that conservation of impulse prescribes the eigenvalues of certain displacement modes. In essence, we proceed by considering certain possible perturbations of the flow, and compare the evolution of the perturbed and unperturbed vortex configurations to extract information about the corresponding eigenvalues.

Let us begin by considering a perturbation involving an overall displacement of the configuration. As an example, let us examine a rotating configuration, whose centroid $\boldsymbol{x}_c$ is moved from $(0,0)$ to $(0,\delta y)$. After this displacement takes place, conservation of linear impulse preserves the new centroid, and the configuration will rotate at a rate Ω about the new location, as shown schematically in figure 5.3(a). Therefore, in a frame moving with the undisturbed configuration, the perturbation has the appearance of a (retrograde) mode, having constant amplitude and period $T = 2\pi\Omega^{-1}$ (as illustrated in figure 5.3b). We can conclude that *an overall displacement mode always has eigenvalue* $\pm i\Omega$. (For a translating configuration, an overall displacement perturbation will of course appear

stationary in a frame moving with the undisturbed vortices, thus yielding $\sigma = 0$, as expected).

We next consider a perturbation that involves an overall rotation of the configuration (by an angle $\delta\theta$, say; see the left-hand example shown later in figure 5.4 for an illustration). This mode leaves the centroid of the configuration unchanged, as shown in the figure. If the unperturbed configuration rotated at a rate Ω, the perturbed one will retain the same angular velocity, but will continue leading the motion of the undisturbed configuration by the angle $\delta\theta$. If we observe the flow in a frame of reference rotating with the undisturbed vortices, the perturbed configuration will appear stationary; this implies that the corresponding eigenvalue must be zero. Therefore *an overall rotation mode must be associated with a zero eigenvalue*.

Furthermore, we note that, if the undisturbed configuration originally translated, the perturbed one will now move along a straight path at an angle $\delta\theta$ from the original one. Therefore, the distance between the perturbed and unperturbed configurations will increase linearly in time. Since this corresponds to an algebraically growing instability, the associated eigenvalue must be zero also in this case.

To summarise, an overall displacement mode must have eigenvalue $\pm i\Omega$, while an overall rotation mode is associated with a zero eigenvalue. We should stress that this result does not rely on any approximation, and must therefore hold for any steady vortex flow.

Note that several investigators have previously commented on the properties of these eigenvalues, in the context of specific vortex flows. Havelock (1931)

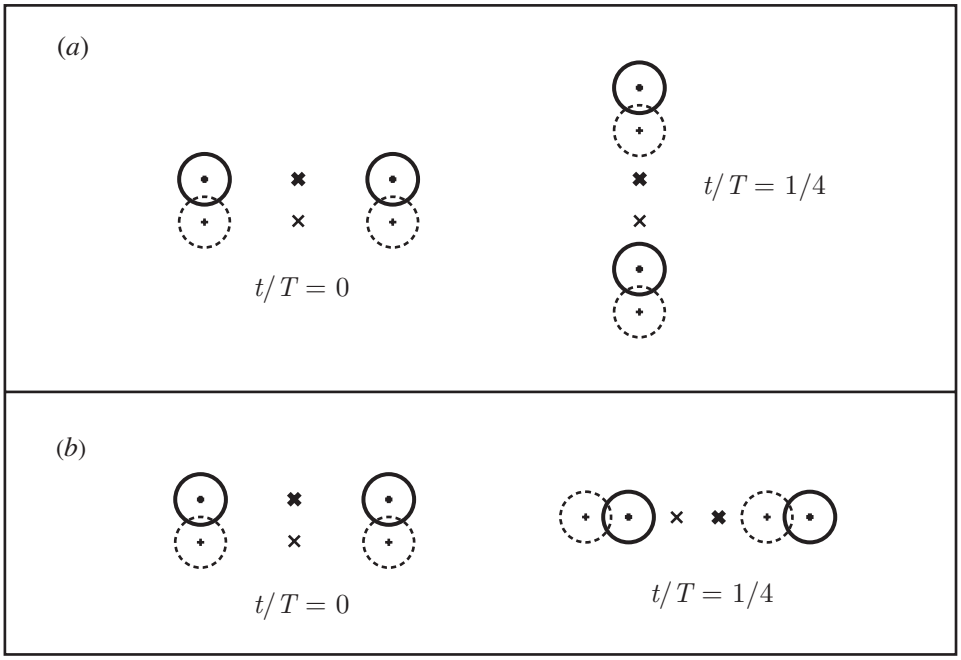

Figure 5.3: Perturbation involving an overall displacement of the configuration, schematically illustrated through the case of a co-rotating vortex pair. The evolution of the perturbation is shown for a quarter of the period of rotation; the dashed and continuous lines represent the unperturbed and perturbed configurations, respectively, in (*a*) a fixed reference frame, and (*b*) a frame of reference rotating with the undisturbed configuration.

obtained the same expressions for these two eigenvalues in the case of N equal-strength *point* vortices arranged in an equilateral polygon. Kamm (1987) and Dritschel (1985) also remarked that the overall rotation mode from their linear stability analyses appeared to have eigenvalue equal to zero; furthermore, Kamm (1987) observed that the magnitude of the overall-displacement eigenvalue that he computed numerically always seemed to match the value of the angular velocity of the configuration. However, in spite of the simplicity of the arguments used here, the fact that an overall displacement mode, for a general steady vortex vortex configuration, *must* have eigenvalue $\pm i\Omega$ does not seem to have appeared in the literature before.

Finally, it is important to address here the related (yet somewhat distinct) point that, when discretizing an Euler flow, one may expect the presence of a large number of zero-eigenvalue modes, which follow from the degeneracies inherent in the equations (as argued by Crowdy, 2002; Elcrat *et al.*, 2005). Specifically, these zero eigenvalues follow from the fact that if a particular vorticity distribution constitutes a steady solution, another flow obtained through a rotation or translation of the configuration also yields an equally valid solution. As a consequence, Crowdy (2002) found zero eigenvalues associated with *both* overall rotation and displacement modes. However, as already noted by Crowdy (2002), these zero eigenvalues should not be regarded as physically relevant to the actual dynamics. As a matter of fact, in our numerical work (which is presented in detail further below), we found that a zero-eigenvalue overall displacement mode appeared *in addition* to the mode with eigenvalue $\pm i\Omega$.

The constraints on the eigenvalues of pure displacement modes discussed above have two immediate applications. Firstly, one may use these results to quickly check the accuracy of a linear stability analysis. The second application involves the analysis of possible resonance scenarios, and is discussed in the next section.

5.4 Stability of two vortices

5.4.1 Signature of pure displacement modes for two vortices

We now illustrate a significant consequence of the theory described above, namely, that one or two vortices may not undergo a resonant instability in a

two-dimensional flow. The signatures of the pure displacement modes can be obtained by considering two point vortices with strengths Γ_1, Γ_2, separated by a distance $2L$. It is a classic exercise to show that the resulting flow is always an equilibrium configuration, with angular velocity

$$\Omega = \frac{\Gamma_1 + \Gamma_2}{8\pi L^2}. \tag{5.31}$$

Following the analysis in section 2 (5.2.1), we can compute the Hessians of E, J, and therefore $\mathbf{H}_2$. This is found to have eigenvalues and eigenvectors:

$$\begin{aligned}
\mu^{(1)} &= \frac{(\Gamma_1+\Gamma_2)^2}{8\pi L^2}, & \boldsymbol{v}^{(1)} &= \begin{pmatrix} \Gamma_1/\Gamma_2 & -1 & 0 & 0 \end{pmatrix}^T, \\
\mu^{(2)} &= \frac{\Gamma_1\Gamma_2}{4\pi L^2}, & \boldsymbol{v}^{(2)} &= \begin{pmatrix} \Gamma_1/\Gamma_2 & 1 & 0 & 0 \end{pmatrix}^T, \\
\mu^{(3)} &= \frac{\Gamma_1^2+\Gamma_2^2}{8\pi L^2}, & \boldsymbol{v}^{(3)} &= \begin{pmatrix} 0 & 0 & \Gamma_1/\Gamma_2 & 1 \end{pmatrix}^T, \\
\mu^{(4)} &= 0, & \boldsymbol{v}^{(4)} &= \begin{pmatrix} 0 & 0 & 1 & -\Gamma_1/\Gamma_2 \end{pmatrix}^T.
\end{aligned} \tag{5.32}$$

Notice that $\Gamma_1\Gamma_2 < 0$ implies $\mu^{(2)} < 0$, and the equilibrium is not a minimum of the energy any longer; however, we will see below that the configuration is still spectrally stable. We must also point out that $\mu^{(4)} \equiv 0$ is always associated with a pure rotation mode. This is to be expected, since the system is invariant under rotation; furthermore, we should note that this invariance requires that a pure rotation mode must yield $\delta^2 H = 0$, independently of the vorticity distribution considered. (Note, however, that the eigenmodes of $\mathbf{H}_2$ are in general different from the eigenmodes of the linear stability problem.)

After computing the symplectic matrix $\mathbf{A}$, the eigenvalues and eigenvectors of $\mathbf{AH}_2$ can be found as:

$$\begin{aligned}
\sigma^{(1,2)} &= \pm \mathrm{i}\frac{\Gamma_1+\Gamma_2}{8\pi L^2}, & \hat{\boldsymbol{\alpha}}^{(1,2)} &= \begin{pmatrix} \mp\mathrm{i} & \mp\mathrm{i} & 1 & 1 \end{pmatrix}^T, \\
\sigma^{(3,4)} &= 0, & \hat{\boldsymbol{\alpha}}^{(3,4)} &= \begin{pmatrix} 0 & 0 & 1 & -\Gamma_1/\Gamma_2 \end{pmatrix}^T,
\end{aligned} \tag{5.33}$$

where $\sigma^{(3)} = \sigma^{(4)}$ is a repeated eigenvalue. Note that $\sigma^{(1,2)} = \pm i\Omega$, as predicted by the argument in § 5.3. Hence $\delta H^{(i)} = (\delta\boldsymbol{\alpha}^{(i)})^T \mathbf{H}_2 \delta\boldsymbol{\alpha}^{(i)}$ gives

$$\delta^2 H^{(1,2)} = \frac{(\Gamma_1 + \Gamma_2)^2}{8\pi L^2}\epsilon^2 \geq 0, \qquad \delta^2 H^{(3,4)} = 0. \tag{5.34}$$

Therefore we find that, for two vortices, all displacement modes have nonnegative signatures. The overall displacement mode is the only eigenmode that may have positive signature; hence an oscillatory instability requires the interaction of the overall displacement mode with a deformation mode. One may expect instability to occur when these two modes have the same eigenvalue. However, since the eigenvalue of the overall displacement mode must be equal to $\pm i\Omega$, this eigenvalue cannot leave the imaginary axis, and may not produce a resonance. This implies that *an oscillatory instability cannot occur for two vortices.*

We can test this deduction by briefly reviewing existing stability results for one or two vortices. An isolated circular vortex is stable (in both a linear and nonlinear sense; see Thomson, 1880*b*; Dritschel, 1988*b*). Love (1893) showed analytically that an elliptical vortex becomes unstable exclusively through exchanges of stability. More recently, Dritschel (1995) studied numerically the stability of unequal-area, co-rotating and counter-rotating vortex pairs, without finding evidence of any resonances. Furthermore, Meunier *et al.* (2002) examined the linear stability of *nonuniform* co-rotating vortex pairs with different vorticity profiles, finding exchanges of stability but no resonances. In summary, to the best of our knowledge, all existing data supports the conclusion that one or two vortices will first become unstable through an exchange of stability.

5.5 Stability of three co-rotating vortices

Our theory indicates that an oscillatory instability is in principle possible for three co-rotating vortices. As a simple example, we consider three equal-area vortices, each having circulation Γ, arranged at the corners of a triangle.

Before beginning the analysis, we introduce the notation used to denote the different eigenmodes that are obtained from the linear stability problem. A given mode is associated with a deformation of azimuthal wavenumber m, which occurs simultaneously on all vortices, with a phase increment ϕ from one vortex to the next (moving in a counterclockwise sense). For N co-rotating vortices, the phase increment takes the form $\phi = 2\pi n/N$, where n ranges from 1 to N; a given eigenmode exhibits a fixed phase angle ϕ. We therefore can denote a mode with wavenumber m and phase increment $2\pi n/N$ as m_n. As an example, pure displacement modes labelled according to this approach (denoted as 1_1, 1_2 and 1_3) are shown in figure 5.4, for three vortices. Additionally, we may display information on a mode's signature by means of a superscript. Modes having positive, negative, or zero signature are therefore labelled as m_n^+, m_n^-, m_n^0, respectively, thereby building on notation introduced above (for example, m_n), or on the equally valid one used by Dritschel (1985) (for example, m/n).

5.5.1 Signatures of pure displacement modes for three vortices

For three point vortices, the angular velocity is (see e.g. Aref, 2009):

$$\Omega = \frac{\Gamma}{2\pi L^2}, \tag{5.35}$$

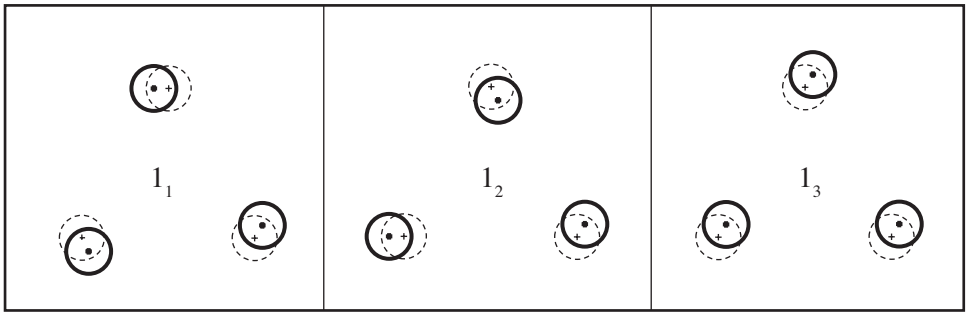

Figure 5.4: Schematic illustration of possible phase relations between disturbances on three vortices.

where, as before, L is the distance between each vortex and the vorticity centroid, and the eigenvalues and eigenvectors for the linear stability matrix $\mathbf{AH}_2$ are:

$$\begin{aligned}
\sigma^{(1,2)} &= 0, \qquad \hat{\boldsymbol{\alpha}}^{(1,2)} = \left(0 \quad 1 \quad -1 \quad -\tfrac{2}{\sqrt{3}} \quad \tfrac{1}{\sqrt{3}} \quad \tfrac{1}{\sqrt{3}}\right)^T, \\
\sigma^{(3,4)} &= \pm i\Omega, \qquad \hat{\boldsymbol{\alpha}}^{(3,4)} = \left(1 \quad \tfrac{-1\pm i\sqrt{3}}{2} \quad \tfrac{-1\mp i\sqrt{3}}{2} \quad \pm i \quad \tfrac{-\sqrt{3}\mp i}{2} \quad \tfrac{\sqrt{3}\mp i}{2}\right)^T, \\
\sigma^{(5,6)} &= \pm i\Omega, \qquad \hat{\boldsymbol{\alpha}}^{(5,6)} = \left(1 \quad 1 \quad 1 \quad \pm i \quad \pm i \quad \pm i\right)^T.
\end{aligned} \tag{5.36}$$

As for two vortices, we have the repeated eigenvalue $\sigma^{(1)} = \sigma^{(2)} = 0$ (This is of course consistent with the classical results of Havelock, 1931). Notice that these perturbations correspond, in the notation introduced above, to modes 1_1, 1_2, and 1_3, respectively (see figure 5.4 for an illustration). For three vortices, 1_1 and 1_3 are the overall rotation and overall displacement modes, respectively.

By using the same procedure as in § 5.4, we find the signatures from:

$$\delta^2 H^{(1,2)} = 0, \quad \delta^2 H^{(3,4)} = \frac{3\Gamma^2}{2\pi L^2}\epsilon^2 > 0, \quad \delta^2 H^{(5,6)} = \frac{3\Gamma^2}{2\pi L^2}\epsilon^2 > 0, \tag{5.37}$$

which leads us to denote the modes as $1_1^0, 1_2^+$, and 1_3^+. As for two vortices, the overall displacement and overall rotation eigenmodes have positive and zero signature, respectively. However, 1_2^+ now represents an *additional* positive-

signature eigenmode, which is free to cooperate with a negative-signature eigenmode to give rise to an oscillatory instability.

5.5.2 Elliptical model to predict the onset of oscillatory instability

Elliptical models of varying degrees of complexity have seen extensive development and use across several types of vortex flows (see Dritschel & Legras, 1991, and references therein). In this section, we employ the elliptical model to provide a simple predictive tool for the onset of oscillatory instability.

We parametrize the family of solutions through the separation distance between the vortices, which is quantified by the parameter r_1/r_2, as defined in figure 5.5(*b*). Our goal, therefore, is to predict the approximate value of r_1/r_2 for which resonance develops, without performing a linear stability analysis or computing the full numerical solutions.

The model can be outlined as follows. Firstly, we construct an approximate solution for this flow by representing each vortex as an ellipse (similarly to the work of Saffman & Szeto, 1980, for two vortices). Secondly, we employ the closed-form dispersion relation of Moore & Saffman (1971), for an elliptical vortex subject to strain and rotation, and plot *approximate* eigenvalues as a function of r_1/r_2. When the frequency curves for two opposite-signature eigenvalues intersect, we expect a Hamiltonian Hopf bifurcation to take place.

The construction of the elliptical steady solutions, for an array of three vortices, involves a conceptually straightforward extension of the two-vortex solu-

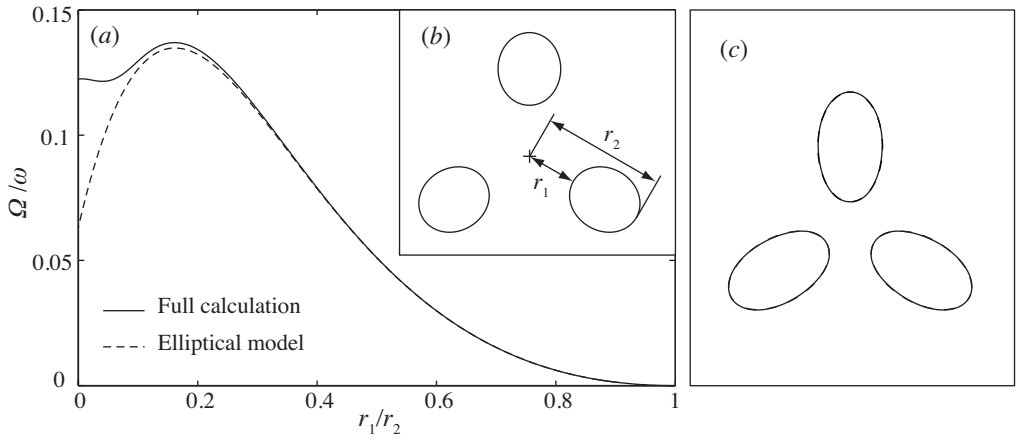

Figure 5.5: (*a*) Angular velocity for the elliptical model (dashed line) and the full solution (continuous line) for three identical co-rotating vortices. The parameter r_1/r_2 is defined in (*b*). Figure (*c*) compares vortex shapes from the elliptical model (shown by dashed contours) and from the full numerical solution (continuous contours), for $r_1/r_2 = 0.2$. The two contours are indistinguishable.

tions of Saffman & Szeto (1980), and is therefore not reported in detail here. The angular velocity Ω/ω that we obtain from the elliptical model is shown by the dashed line in figure 5.5(*a*), and will be compared to the full numerical solution in the next section.

After computing the ellipse axis ratio $\lambda = b/a$ and the angular velocity Ω/ω for each r_1/r_2, we obtain approximate eigenvalues as follows. For sufficiently large r_1/r_2, the dependence of the eigenvalues on the phase angle ϕ can be assumed to be weak. Hence we expect that the eigenvalues for, say, modes $1_1, 1_2, 1_3$ will be approximately the same. We therefore choose to approximate the eigenvalues using the dispersion relation for a single ellipse subject to strain and rotation, which was found by Moore & Saffman (1971) as:

$$\left(\frac{\sigma}{\omega}\right)^2 = -\frac{1}{4}\left\{\left[\left(1 - 2\frac{\Omega}{\omega}\right)\frac{2m\lambda}{1+\lambda^2} - 1\right]^2 - \left[\frac{1-\lambda}{1+\lambda}\right]^{2m}\right\}. \tag{5.38}$$

The eigenvalues obtained from the elliptical model are therefore labelled as $1^+_{\mathrm{E}}, 2^-_{\mathrm{E}}, 3^-_{\mathrm{E}}$..., and are plotted in figure 5.6(*a*). The accuracy of the resulting pre-

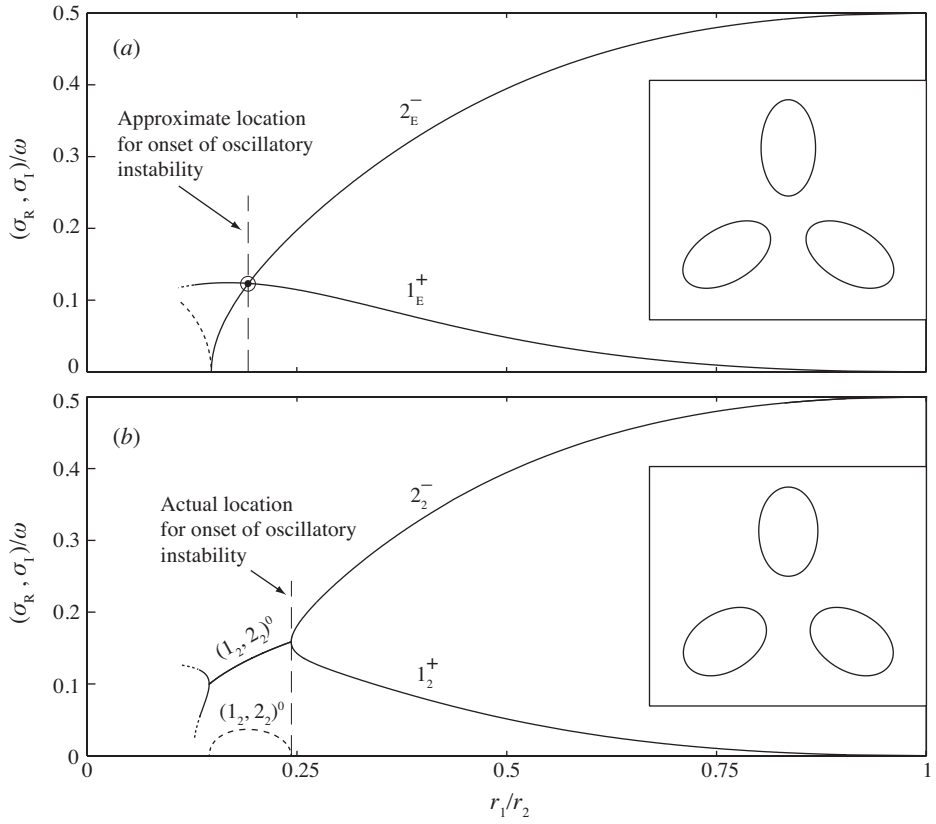

Figure 5.6: Selected eigenvalues for three co-rotating vortices, showing the prediction for the development of the first resonance from the elliptical model (*a*), together with results from an accurate linear stability analysis (*b*). The vortex shapes corresponding to the onset of instability are shown in the insets. Dashed and continuous lines denote real and imaginary parts, respectively.

diction of r_1/r_2 for the onset of resonance is discussed in the next section.

5.5.3 Stability of three vortices and comparison with elliptical model

In order to test the prediction from the elliptical model for three vortices, we computed numerically the steady states and performed a linear stability analysis. The numerical method that we used to compute the equilibrium flows

employs a novel discretization, together with Newton iteration, to accurately resolve vortices of arbitrary shape with an affordable computational cost. Once a steady solution is found, we evaluate the Jacobian associated with the linear stability problem, thus obtaining the eigenvalues and eigenvectors. Further details on the numerical method may be found in Luzzatto-Fegiz & Williamson (2011*a*). The vortex equilibria studied here were computed accurately to at least seven significant figures.

We begin by assessing the accuracy with which the elliptical model represents the vortex equilibria. To this end, we plot the angular velocity, as a function of r_1/r_2, for both the elliptical model and the full solution (see figure 5.5). Remarkably, the value of Ω from the elliptical model appears to be quite accurate down to $r_1/r_2 \approx 0.1$, where the error in Ω is still only about 2.3%. For smaller r_1/r_2, the accuracy of the elliptical model worsens rapidly.

We now discuss the elliptical model's ability to estimate the location of the oscillatory instability, as shown in figure 5.6(*a*). The eigenvalue curves for modes 1^+_{E} and 2^-_{E} intersect at $r_1/r_2 \doteq 0.1925$. We find that the actual eigenvalue plot for modes 1^+_2 and 2^-_2 (shown in figure 5.6*b*) does indeed exhibit a bubble of instability centred approximately at $r_1/r_2 \approx 0.19$. (The onset of the instability occurs at $r_1/r_2 \doteq 0.2432$). The vortex shapes corresponding to the onset of resonance are shown in the insets in figure 5.6. The elliptical model is therefore quite effective in predicting the onset of an oscillatory instability. Furthermore, we note that the effort required in constructing the elliptical model is small, especially if contrasted with the labor required to compute accurately the steady states, and to subsequently perform a linear stability analysis.

For completeness, we also report the full stability properties for the three

vortices, as obtained from our linear stability analysis. The eigenvalue plot (shown in figure 5.7) exhibits a very rich structure; we remark here on its main features.

As already noted above, the first instability (as r_1/r_2 is decreased) is associated with a resonance between modes 1_2^+ and 2_2^-. Shortly thereafter (at $r_1/r_2 \doteq 0.1823$), eigenmode 2_1^- undergoes an exchange of stability, turning into 2_1^0. For $r_1/r_2 \lesssim 0.1795$, 2_1^0 is the unstable mode with the largest growth rate.

The theory of eigenmode signatures presented here can be used to interpret the subsequent development of other resonances, as r_1/r_2 is reduced. For example, after the first instability "bubble", modes 1_2^+ and 2_2^- separate, leaving 1_2^+ free to interact with 3_2^-, leading to another resonance (as shown in figure 5.7).

Another remarkable fact from figure 5.7 is that the eigenvalue for mode 2_3^- touches $\sigma = 0$ at $r_1/r_2 \doteq 0.02185$, after which it *returns* to being purely imaginary (instead of becoming real and undergoing an exchange of stability, as one might expect). This is shown in detail in the close-up in figure 5.8. At slightly lower r_1/r_2, this eigenmode interacts with 2_2^- to yield another resonance (which, however, maintains a small growth rate). By the theory of Krein signatures discussed in § 1, we can therefore infer that 2_3^- must have changed its signature (becoming 2_3^+) when touching $\sigma = 0$.

This observation brings us to the point that, for vortices that are relatively close together, further resonances may *also* occur if a deformation acquires positive signature by going through $\sigma = 0$ without an exchange of stability. These resonances are, of course, not captured by the elliptical model discussed above.

Incidentally, when the eigenvalue for mode 2_3 touches zero, the family

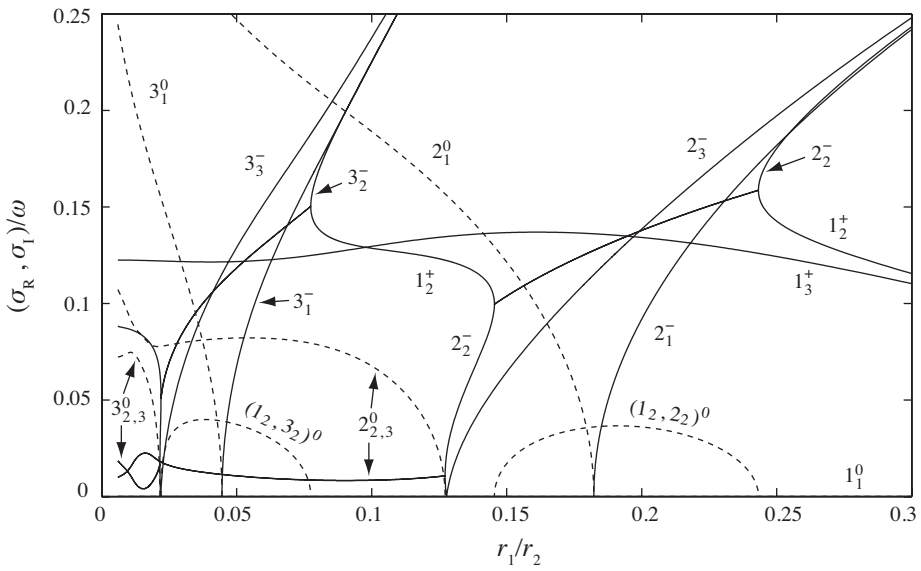

Figure 5.7: Eigenvalues for three corotating vortices.

of steady vortices studied here connects to a series of lower-symmetry flows through a transcritical bifurcation. Although these results are not shown here, we were able to resolve this bifurcation in detail using the IVI diagram approach discussed in Luzzatto-Fegiz & Williamson (2010*b*, 2011*b*).

Finally, it is essential to recognize that the properties of N corotating uniform vortices (including the $N = 3$ case) were first examined in the seminal study of Dritschel (1985). In this classic paper, Dritschel broke new ground by numerically computing both the shapes and the linear stability of the $N \geq 3$ vortices, revealing a very rich eigenvalue structure. However, we must address the fact that our linear stability results (shown in figure 5.7) present a number of differences from those computed by Dritschel (1985). For example, Dritschel observed that eigenvalue coalescence could occur only between modes with the same phase angle. However, in our results, we observe eigenvalue coalescence also between modes with different phase angles (but which have the same wavenumber m), such as 2_2^- and 2_3^+. In our data, the key factor in determining

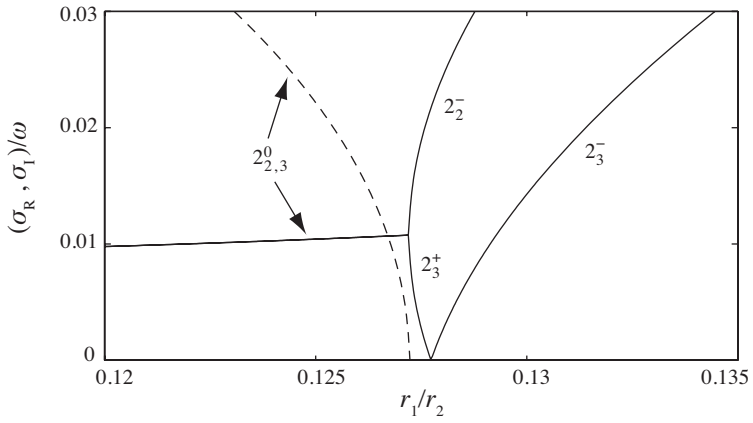

Figure 5.8: Close-up view of the second resonance occurring for three vortices.

allowable resonances seems to be the signature of the eigenmodes.

We can tentatively explain this and other differences with the work of Dritschel (1985) as follows. By the arguments presented in § 5.3, the eigenvalue for the overall displacement mode must be $\pm i\Omega$. We can use this as a consistency test for the stability results. Figure 5.9(*a*) shows the eigenvalue of the overall displacement mode (as a continuous line), together with selected values of Ω, adapted from figure 6 and table 1 of Dritschel (1985). While σ_I and Ω are close for larger r_1/r_2, they progressively diverge as r_1/r_2 is reduced and the vortices become more elongated, and thus are more expensive to compute accurately. Figure 5.9(*b*) shows σ_I and Ω for the calculations presented here; the two quantities are indistinguishable up to six significant figures.

5.6 Conclusions

In this paper, we build on concepts from the study of Hamiltonian dynamical systems, and develop a theory of resonant instability in two-dimensional

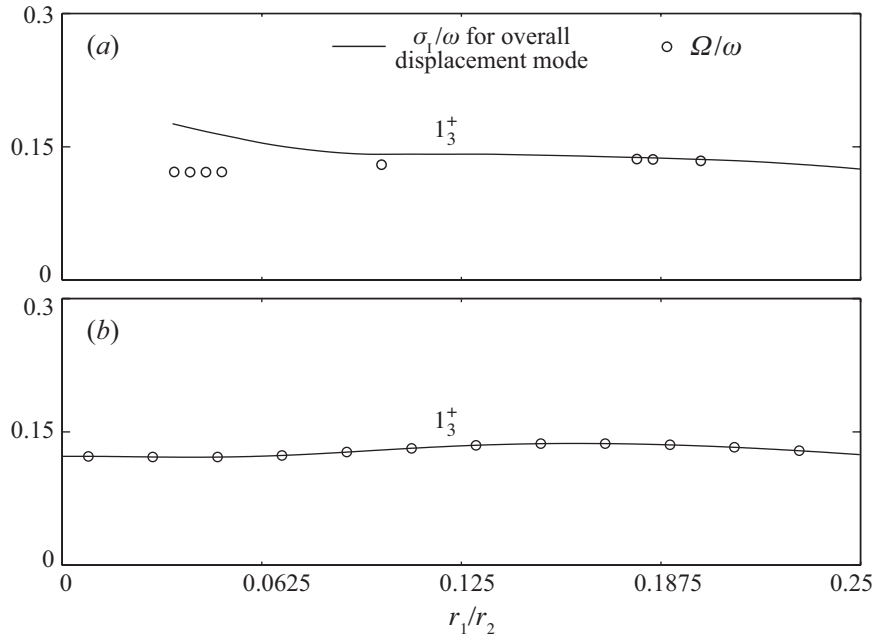

Figure 5.9: Imaginary part of the overall-displacement eigenvalue σ_I and of the angular velocity Ω of the configuration. (*a*): data from Dritschel (1985); (*b*): present results.

vortex configurations. We show that, for well-separated vortices, deformation modes always have negative signature, while displacement modes may have positive signature. A resonance requires the interaction of opposite-signature eigenmodes, and therefore must involve at least one displacement mode. By employing simple physical arguments, we show that the eigenmodes associated with an overall rotation and an overall displacement of the vortices must always have eigenvalues equal to zero and $\pm i\Omega$, respectively. Since, for one or two vortices, these are the only possible displacement modes, these constraints on the eigenvalues imply that a resonance cannot occur. All available stability data in the literature, for one or two vortices, supports this theoretical finding.

Our theory indicates that a resonant instability is possible for three or more vortices. For these more complex flows, we propose a simple elliptical model to

estimate the onset of resonance. We take, as an example, three co-rotating vortices, and compare the results from our model with those from a full eigenvalue calculation, finding good agreement.

We must be careful to point out that one further, *indirect* route to resonance exists, for small separation distances between the vortices. The eigenvalue of a deformation mode may go through zero and remain purely imaginary, while the eigenmode acquires *positive* signature. This perturbation may then interact with negative-signature deformation mode to give an oscillatory instability, as shown in the close-up of figure 5.8. The mechanism that allows such an indirect resonance deserves further study. Nevertheless, we can note that, as one progresses along an initially stable family of solutions, the eigenvalue of a negative-signature mode will necessarily cross the path of a positive-signature eigenvalue *before* being able to reach $\sigma = 0$ (this is immediately apparent, for example, by examining the path of the eigenvalues in figure 5.6*a*, as r_1/r_2 is reduced). This suggests that a direct resonance, when possible, will occur well before an indirect one, as one brings the vortices close together.

In summary, we find that the Krein signature theory presented here constitutes a valuable tool in studying resonant instabilities in two-dimensional vortex configurations. Further to this, our results can be used in combination with more involved stability approaches, to interpret, and compare with, detailed eigenvalue data.

CHAPTER 6

AN EFFICIENT AND GENERAL NUMERICAL METHOD TO COMPUTE STEADY UNIFORM VORTICES

Submitted to *Journal of Computational Physics.*

Steady uniform vortices are widely used to represent high Reynolds number flows, yet their efficient computation still presents some challenges. Existing Newton iteration methods become inefficient as the vortices develop fine-scale features; in addition, these methods cannot, in general, find solutions with specified Casimir invariants. On the other hand, available relaxation approaches are computationally inexpensive, but can fail to converge to a solution. In this paper, we overcome these limitations by introducing a new discretization, based on an inverse-velocity map, which radically increases the efficiency of Newton iteration methods. In addition, we introduce a procedure to prescribe Casimirs and remove the degeneracies in the steady vorticity equation, thus ensuring convergence for general vortex configurations. We illustrate our methodology by considering several unbounded flows involving one or two vortices. Our method enables the computation, for the first time, of steady vortices that do not exhibit any geometric symmetry. In addition, we discover that, as the limiting vortex state for each flow is approached, each family of solutions traces a clockwise spiral in a bifurcation plot consisting of a velocity-impulse diagram. By the recently introduced "IVI diagram" stability approach, each turn of this spiral is associated with a loss of stability for the steady flows. Such spiral structure is suggested to be a universal feature of steady, uniform-vorticity flows.

6.1 Introduction

The flow of an inviscid fluid is a topic of relevance across a vast number of applications, including dynamics of plasmas (Kiwamoto *et al.*, 2007), astrophysical and geophysical flows (Turkington *et al.*, 2001), and the dynamics of quantum condensates (Keeling & Berloff, 2008), to name a few. In all of these contexts, steady vortical solutions to the governing equations can play a particularly important role in characterizing the dynamics (Dritschel, 1985, 1995). Stable steady vortex flows are likely to be realized in practice (Dritschel, 1995), while unstable ones can act as attractors for the unsteady dynamics (Moffatt, 1985).

Perhaps surprisingly, computing steady solutions of the Euler equations can often prove far more involved than performing time-dependent simulations. This difficulty is due to the fact that each conservation law associated with Euler's equations gives rise to a corresponding degeneracy in the mathematical representation of the steady flow (see Saffman, 1992; Crowdy, 2002; Elcrat *et al.*, 2005, for a recent discussion and examples). More specifically, the Euler equations admit, beside the usual conserved quantities corresponding to mass, impulse, and energy, an additional set of invariants, known as *Casimirs* (Morrison, 1998). Comparing the stability of families of vortices with the same Casimirs can yield important information on the possible long-term evolution of the flow (Dritschel, 1995). Numerical methodologies (based on variational approaches) have so far been successful in computing *stable* vortices with prescribed Casimirs, in fixed reference frames (Vallis *et al.*, 1989). However, a particularly important class of solutions is given by flows that are steady when observed in a moving reference frame. Classic examples include the translating vortex pairs known as "modons" in geophysics (Kizner & Khvoles, 2004), the

rotating arrays observed in Bose-Einstein condensates (Keeling & Berloff, 2008), as well as gravity waves at fluid interfaces (Longuet-Higgins & Fox, 1978). A mathematical framework exists for studying equilibrium flows of this type, under the constraint that Casimirs must be prescribed (Shepherd, 1990). Nevertheless, to the best of our knowledge, a successful numerical method for computing general vortex flows with given Casimirs has not yet been developed (We point out here, however, the recent promising developments due to Morrison & Flierl, 2009).

A simple, widely used approximation involves representing the vorticity distribution through a collection of uniform-vorticity regions. This constitutes an implementation of the level-set method, which has seen extensive development for the study of unsteady fluid interfaces (Sethian, 2000; Zabusky *et al.*, 1979). In spite of the relative simplicity of this flow description, steady analytical solutions of this type remain rare (classical solutions are described in Saffman, 1992; major advances in this field have recently been made by Crowdy, 2002, 2010). In general, one must still resort to numerical methods in order to find new families of steady uniform vortices.

For uniform vortices, the Casimir invariants can be prescribed by fixing the area and vorticity inside each vortex. Solution families constructed in this manner present two numerically challenging features. Firstly, the vortex boundaries may eventually develop high-curvature regions, resulting in the formation of corners or cusps, which rapidly increase the computational cost (see Saffman & Tanveer, 1982; Overman, 1986; Crowdy, 2002). Secondly, the degeneracies associated with the steady vorticity equation make it difficult to ensure convergence, especially when considering flows with prescribed Casimirs, or when

examining lower-symmetry flows.

In this paper, we describe a numerical approach for uniform vortices that directly addresses these issues. We begin, in § 6.2, by providing a brief review of existing numerical approaches, and discuss their advantages and limitations. In § 6.3.1, we define a novel automatic discretization procedure, which can support efficient computation of vortices with high-curvature boundaries. Next, in § 6.3.2, we introduce a scheme to systematically remove the degeneracies in the governing equations, allowing lower-symmetry solutions to be computed efficiently and reliably by Newton iteration, as described in detail in § 6.3.3. The performance of the resulting numerical approach is assessed by computing elliptical vortices, and comparing results against the analytical solution of Kirchhoff (1876), in § 6.4. In addition, we perform detailed calculations for several families of steady vortices, for which we report detailed results in § 6.5 and 6.6.

6.2 A brief review of numerical approaches for computing uniform steady vortices

In this section, we provide a brief overview of existing numerical approaches for finding uniform steady vortices, illustrating their advantages and limitations. This review provides the background for the development of the methodology that we propose in the next section. From a physical standpoint, the key prerogative of a steady vortex configuration is that, as the group of vortices translate or rotate, their boundaries do not deform; this is equivalent to seeking vortices whose edges correspond to streamlines of the flow, as observed in the frame

of reference moving with the vortices. These two equivalent conditions can be formalized as:

$$\boldsymbol{u}_{\mathrm{mov}} \cdot \boldsymbol{n} = 0, \qquad \psi_{\mathrm{mov}} = C, \tag{6.1a, b}$$

on the vortex boundary, where $\boldsymbol{u}_{\mathrm{mov}}$ and ψ_{mov} are the velocity and streamfunction in the moving reference frame, $\boldsymbol{n}$ is the local normal vector, and C is an arbitrary constant. Depending on whether the reference frame translates or rotates, the velocity and streamfunction are:

$$\boldsymbol{u}_{\mathrm{mov}} = \boldsymbol{u} - (U, V), \quad \psi_{\mathrm{mov}} = \psi - Uy + Vx \tag{6.2a, b}$$

$$\boldsymbol{u}_{\mathrm{mov}} = \boldsymbol{u} + \Omega(y, -x), \quad \psi_{\mathrm{mov}} = \psi + \frac{\Omega}{4}(x^2 + y^2) \tag{6.3a, b}$$

One can solve either of the steady-state equations (6.1) as follows. Firstly, one starts with a guess for the shape of the vortex boundaries, and for the velocity of the moving frame ($\boldsymbol{U}$ or Ω). Using the guess for the vortex shapes, the resulting $\boldsymbol{u}$ or ψ is found using Biot-Savart's law of induction, which is obtained from the inversion of $\nabla^2\psi = -\omega$. Then (6.1) is solved by iteratively adjusting each of the boundary shapes.

The earliest numerical computations of vortex patch equilibria were performed by Deem & Zabusky (1978), who, in a seminal study, examined the m-fold radially symmetric flows that arise as bifurcations from a circular vortex. By exploiting the symmetry of the problem, they solved (6.1a) employing cylindrical polar coordinates $R(\theta)$ to describe the boundary for $0 \leq \theta \leq \pi/m$. The boundary $R(\theta)$ was then represented using a Fourier series, which was truncated after M terms. The no-through-flow condition was enforced at M collocation points (equispaced in θ), yielding a closed set of equations. Newton's method was used to obtain convergence to a new solution, thus giving a computational cost proportional to M^3. Through this methodology, Deem & Zabusky were

able to compute a substantial portion of each m-symmetric family of solutions. However, as the maximum curvature on the vortex boundary increased, their method became too expensive to accurately resolve these flows.

Saffman & Szeto (1980) employed a conceptually similar scheme while considering the properties of the symmetric, co-rotating vortex pair, where $R(\theta)$ was measured from the centroid of one of the vortices. In addition, in order to reduce the number of normal modes needed to represent the boundary, they introduced a *modified* variable $\tilde{\theta}$, defined such that $\theta = \tilde{\theta} + \alpha \sin\tilde{\theta}$; α is an arbitrary constant, chosen between 0 and 1. The expansion for $R(\theta)$ is then replaced with a series for $R(\tilde{\theta})$. A uniform spacing in $\tilde{\theta}$ automatically leads to a tighter node spacing near $\theta = 0, \pi$. These azimuthal locations can be arranged to correspond with the high-curvature regions on the boundary. Similar numerical discretizations were used by Saffman and co-workers to calculate counter-rotating vortex pairs (Saffman & Tanveer, 1982), as well as vortex rows (Saffman & Szeto, 1981; Saffman & Schatzman, 1981).

The main drawback associated with the introduction of this modified variable is that it relies on an *ad hoc* construction. As a matter of fact, one needs to know in advance the precise boundary location where the highest value of the curvature is expected to develop. Furthermore, there is no obvious way to define the value of the numerical parameter α, which instead needs to be manually adjusted through the calculation. These issues have so far prevented the implementation of numerical methods employing a modified variable, such as $\tilde{\theta}$, to general flows.

More recently, a different take on the use of Newton's method was proposed by Elcrat *et al.* (2005). This involves considering a given initial guess for the vor-

tex shapes, and representing the *correction* to the boundary through a Fourier series in the boundary arc-length, s. The resulting approach can offer good computational efficiency over a range of shapes that is significantly wider than methodologies based on the polar representation $R(\theta)$. Nevertheless, the computational cost does still rise rapidly as corners or cusps are approached, since there is no straightforward way to increase resolution only in regions of high curvature.

Another innovation introduced by Elcrat *et al.* (2005) is given by the fact that this study did not assume any symmetry, and sought vortices with arbitrary shape. In general, allowing for non-symmetric vortices leads to the development of zeros in the Jacobian matrix of the system, which may be understood as follows (see also Crowdy, 2002). If a particular vortex shape yields a solution, then a displacement, rotation, or rescaling of the same vortex configuration will also yield a steady flow, which is adjacent to the initial one in the solution space. This issue is illustrated in figure 6.1. While these neighbouring solutions are, of course, trivial, they do imply that technically the solution is not locally unique. Therefore a straightforward application of Newton's method fails to converge. For this reason, in Elcrat *et al.* (2005), a singular-value decomposition was used to project out these eigenvalues for the first few iterations of Newton's method, after which they returned to using the full Jacobian. It is important, however, to note that while this approach leads to a converged solution, unfortunately it does not allow one to prescribe Casimirs.

These methods based on Newton iteration can be contrasted with the approach proposed by Pierrehumbert (1980), who developed a relaxation method based on equation (6.1*b*). The boundary is represented using a set of nodes in

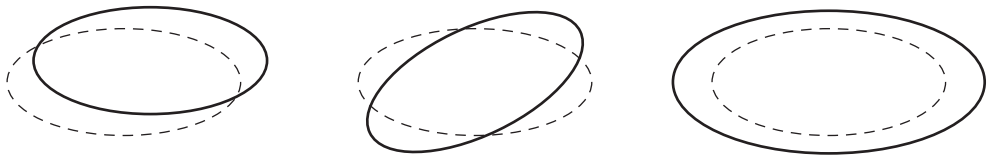

(*a*) (*b*) (*c*)

Figure 6.1: Schematic illustration of the source of zero eigenvalues in the Jacobian, for numerical methods employing Newton iteration. If a given vortex shape (shown by the dashed ellipse) constitutes a steady flow, then there will be neighboring solutions that are obtained by either (*a*) translation, (*b*) rotation, and (*c*) scaling of the original solution. These trivial, neighboring solutions must be removed to ensure convergence.

a suitable coordinate system; for example, let us consider cylindrical polar coordinates (r, θ), with corresponding velocities (u_r, u_θ). Suppose that the vortex configuration rotates at velocity Ω, and that the *exact* boundary shape is given by $R^*(\theta)$. We may then decompose a guess for the solution as $R(\theta) = R^*(\theta) + \Delta R(\theta)$, where ΔR is essentially the deviation from an equilibrium shape. Then, at any one node location (say, $\theta = \theta_i$), we can Taylor expand $\psi_{\rm mov}$ as:

$$\begin{aligned} \psi_{\rm mov}(R^* + \Delta R) &= C + \frac{\partial \psi_{\rm mov}}{\partial r}\,\Delta R + ... \\ &= C + (\Omega R - u_\theta)\,\Delta R + ..., \end{aligned} \tag{6.4}$$

where Ω and C are found by requiring that R remains unchanged at two locations on the boundary (say, θ_1, θ_2). Then, at each iterate, the correction to the shape is found by inverting (6.4) to get $\Delta R \simeq (\psi_{\rm mov} - C)/(\Omega R - u_\theta)$. Note that $R(\theta_1)/R(\theta_2)$ is effectively the control parameter in the continuation procedure.

Since the correction is evaluated locally, the computational cost scales with the square of the number of nodes employed to represent the boundary; hence this method is significantly more efficient than any approach employing Newton iteration. Furthermore, nodes can be easily concentrated in regions of high

curvature according to a suitable discretization scheme (see e.g. Dritschel, 1988*a*, 1989, 1995). As a consequence, this numerical method has been used successfully to compute a variety of flows, including co-rotating and counter-rotating vortex pairs (Pierrehumbert, 1980; Dritschel, 1985, 1995), shear layers (Pierrehumbert & Widnall, 1981), and configurations of up to eight co-rotating vortices (Dritschel, 1985).

It should also be pointed out that care must be taken when trying to use Pierrehumbert's relaxation method to compute limiting shapes, since at corners or cusps the streamfunction will not be an analytic function, and hence a simple Taylor expansion will yield erroneous results, as first pointed out by Saffman & Tanveer (1982). Overman (1986) analyzed in detail possible scenarios involving corner or cusp formation on uniform vortices. Wu *et al.* (1984) constructed a more reliable relaxation method for vortex shape calculation by employing the no-through flow condition (6.1*a*) instead of (6.1*b*). They used their method to accurately compute limiting states for several flows, including pairs of equal-area vortices, as well as the radially symmetric vortices first studied by Deem & Zabusky (1978). (We should note that relaxation methods employing a two-dimensional mesh have also been developed; these are not discussed here. See e.g. Elcrat *et al.*, 2000; Cerretelli & Williamson, 2003*a*; Gallizio *et al.*, 2010)

In spite of their remarkable efficiency, all of these relaxation methods remain subject to several limitations. Firstly, differently from methods based on Newton iteration, convergence to a solution is, in general, not always ensured (see e.g. Saffman & Schatzman, 1981; Dritschel, 1985, 1995). Furthermore, the method requires one to define an explicit geometric parametrization (in the example above, $R(\theta_1)/R(\theta_2)$), which must change *monotonically* along the family of

solutions. While such a parametrization may be easily guessed for certain flows (see Dritschel, 1985), in general a valid parametrization will not be known *a priori*. Indeed, Dritschel (1995) reports that, for the case of two opposite-signed vortices, finding a geometric parametrization that captured most of the solutions required a substantial amount of trial and error.

The second limitation associated with these relaxation methods is that it is not possible, in general, to compute nonsymmetric solutions. This issue stems from the fact that fixing only two points on a general vortex shape is not sufficient to uniquely define the solution (this is illustrated in figure 6.2, with reference to an elliptical vortex). For a single vortex, it seems that one must either prescribe two symmetry planes, as shown in the figure, or specify a radial *m*-fold symmetry (of the type employed by Wu *et al.*, 1984). To the best of our knowledge, so far there are no relaxation methods that can compute vortices without *any* symmetry plane.

To summarize, presently one can choose between two main families of methods to compute steady uniform vortices. The first option is given by Newton iteration methods, which are guaranteed to converge and therefore can, in principle, compute shapes without symmetry (provided the zeros in the Jacobian are dealt with appropriately). However, all implementations of these methods so far require *ad hoc* treatments when dealing with high-curvature boundaries. The second family of available approaches is given by relaxation methods, which are more efficient, but are limited by the necessity of an explicit geometric parametrization, and by the need to prescribe a sufficient number of geometric symmetries in the flow.

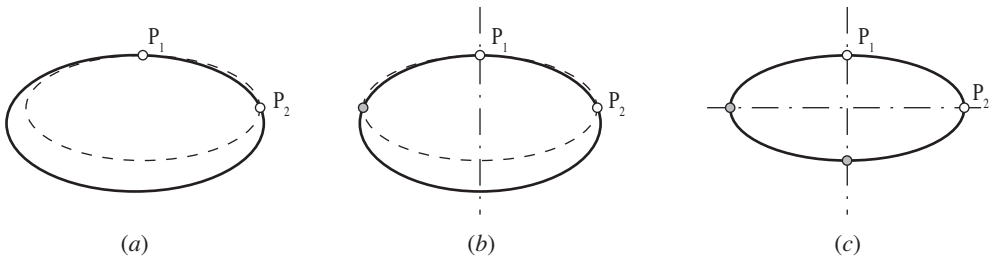

Figure 6.2: Illustration explaining the need to prescribe geometric symmetries, when using a relaxation method. The solution procedure requires fixing two points on the boundary. However, this condition alone does not uniquely specify the solution, as shown in (*a*); another elliptical shape can of course be drawn through the same two points. For an ellipse, the problem persists also if one symmetry plane is prescribed, as shown in (*b*). Fixing *two* symmetry planes resolves the issue (*c*).

6.3 A general and efficient method for computing uniform vortices

6.3.1 Boundary discretization through the inverse velocity mapping

For simplicity, let us begin by considering an approximate discretized solution given by a single vortex, rotating with angular velocity Ω. We suppose that we have an initial guess for the boundary shape, which is represented by a set of N nodes, corresponding to cartesian coordinates (X_n, Y_n) (with $n = 1, 2, ..., N$). We then seek a correction $(\Delta X_n, \Delta Y_n)$ such that $(X_n + \Delta X_n, Y_n + \Delta Y_n)$ will represent a solution to the discretized problem.

We introduce a parametrization $\tilde{s}$ (precisely defined further below), which increases monotonically along the vortex boundary, such that the boundary lo-

cations can be written as $(X_n, Y_n) = [X(\tilde{s}_n), Y(\tilde{s}_n)]$. Then (setting aside the node index n, for clarity) one can consider corrections normal to the boundary, written as:

$$[\Delta X(\tilde{s}), \Delta Y(\tilde{s})] = \gamma(\tilde{s})\, \boldsymbol{n}(\tilde{s}), \tag{6.5}$$

where $\boldsymbol{n}(\tilde{s})$ is the local unit normal vector, and $\gamma(\tilde{s})$ is a scalar. This quantity, in turn, is represented using a series of M basis functions:

$$\gamma(\tilde{s}) = \sum_{m=1}^{M} \alpha_m \phi_m(\tilde{s}), \tag{6.6}$$

where each of the α_m represents a constant coefficient, for a given steady vortex. Therefore, we can already observe that finding a steady vortex solution amounts essentially to computing the coefficients α_m, for a given value of Ω. The basis functions are chosen as sines and cosines:

$$\phi_m(\tilde{s}) = \frac{1}{\sqrt{\pi}} \left\{ \frac{1}{\sqrt{2}}, \cos\tilde{s}, \cos 2\tilde{s}, ..., \cos \bar{M}\tilde{s}, \sin\tilde{s}, \sin 2\tilde{s}, ..., \sin \bar{M}\tilde{s} \right\}, \tag{6.7}$$

with $\bar{M} = (M-1)/2$, and where, without loss of generality, $\tilde{s}$ has been defined such that $0 \leq \tilde{s} \leq 2\pi$.

At this stage, we can point out that the boundary discretization presented so far reverts to the one used by Elcrat *et al.* (2005), provided that we set $\tilde{s} = s$, where s is the arc-length along the vortex boundary. As found in Elcrat *et al.* (2005), as high-curvature regions develop on the boundary, this choice gives slow convergence in the series of coefficients α_m. In order to increase the rate of convergence in the series, different definitions for $\tilde{s}$ may be introduced. One could, in principle, employ a methodology based on the local curvature of the boundary to compute $\tilde{s}$. This would require differentiating twice the boundary variables X, Y with respect to the arc-length s; unfortunately, this can cause $\tilde{s}$ to be strongly affected by small errors in the initial guess for the vortex shape.

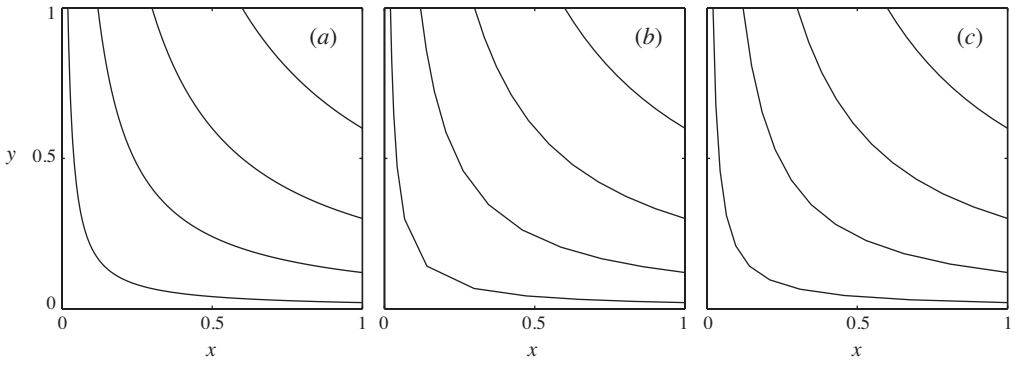

Figure 6.3: Schematic example for the discretization of selected streamlines near a corner flow. (*a*) shows the streamlines for the flow $(u, v) = \epsilon(x, -y)$, for (x, y) between 0 and 1. In the next two plots, these streamlines are discretized using 15 nodes each, using (*b*) uniform spacing in arc-length s, and (*c*) uniform spacing in the modified variable $\tilde{s}$, which is obtained from the inverse-velocity mapping.

Therefore, here we choose to employ a simpler and more reliable approach, which is constructed as follows.

We start from the physical observation that a corner (or cusp) in the vortex boundary must be associated with a stagnation point of the flow, when observed in a reference frame that is moving with the vortex shape. This, of course, is true for any streamline in a fluid flow (and not just for the boundary of a steady vortex). As a schematic example, let us consider here the pure strain flow $\boldsymbol{u}_{\text{mov}} = \varepsilon(x, -y)$; selected streamlines for the region $0 < (x, y) < 1$ are plotted in figure 6.3(*a*). We discretize each of these streamlines with $N = 15$ points. In figure 6.3(*b*), we show the result obtained by collocating the nodes using a uniform spacing in arc-length s along each streamline. It can be seen that, as we choose streamlines that pass closer to the stagnation point at the origin, the resolution becomes progressively less adequate.

To overcome this issue, we propose here to exploit the fact that the velocity

magnitude, $|\boldsymbol{u}_{\text{mov}}|$, approaches zero as we near the stagnation point. This suggests the use of a re-scaled arc-length, given by the following simple mapping, based on the inverse of the velocity:

$$\tilde{s}(s) = A \int_0^s \frac{\mathrm{d}s'}{|\boldsymbol{u}_{\text{mov}}(s')|}, \tag{6.8}$$

where A is a constant, chosen so that $\tilde{s}$ runs from 0 to 2π. If we compute $\tilde{s}$ and re-discretize the streamlines uniformly according to this variable, we obtain the nodes shown in figure 6.3(c). For a given number of points, the inverse-velocity transform for $\tilde{s}(s)$ produces a more accurate discretization, as can be immediately observed from the figure. (A quantitative comparison of the performance of the two discretizations is provided further below.) In the vortex calculations presented below, (6.8) is integrated using cubic spline interpolation, together with two-point Gaussian quadrature.

The use of the inverse-velocity mapping (here referred to as IVM, for short) for discretization has two main advantages. Firstly, the velocity is a quantity that is typically already available, in a vortex patch calculation; therefore the additional computational cost associated with finding $\tilde{s}$ is small. Secondly, it can be noted that the velocity on the edge of the vortex is obtained from an integral, which effectively acts to smooth out any spurious oscillations in the initial guess for the boundary representation. This helps ensure that the resulting numerical approach is robust.

It can be noted that (6.8) yields a quantity that is proportional to the travel time of a particle, from a location $s' = 0$ to $s' = s$. Dritschel exploited this viewpoint, in the context of formulating a linear stability analysis, to show that a travel-time parametrization can be used to dramatically increase the rate of convergence of the series expansion for the eigenmodes (Dritschel, 1990, 1995).

To the best of our knowledge, however, an expression of the type (6.8) has not been used before to discretize and compute steady vortices.

By making explicit all dependencies, the steady flow condition can now be written as:

$$\boldsymbol{u}_{\text{mov}}(\boldsymbol{\alpha}; \Omega; \tilde{s}) \cdot \boldsymbol{n}(\boldsymbol{\alpha}; \tilde{s}) = 0, \quad 0 \leq \tilde{s} \leq 2\pi, \tag{6.9}$$

where $\boldsymbol{n}$ is obtained by using cubic-spline differentiation of the boundary with respect to $\tilde{s}$, while $\boldsymbol{u}_{\text{mov}}$ is found from (Dritschel, 1986):

$$\boldsymbol{u}(\boldsymbol{x}) = \frac{\omega}{2\pi} \oint \frac{\boldsymbol{x} - \boldsymbol{X}}{|\boldsymbol{x} - \boldsymbol{X}|^2} (\boldsymbol{x} - \boldsymbol{X}) \cdot \frac{\mathrm{d}\boldsymbol{X}}{\mathrm{d}\tilde{s}} \, \mathrm{d}\tilde{s}. \tag{6.10}$$

In the above, the values of $\mathrm{d}\boldsymbol{X}/\mathrm{d}\tilde{s}$ can be obtained through the same spline differentiation operation that gave $\boldsymbol{n}$. Since the discretization is uniform in $\tilde{s}$, we can integrate (6.10) by the trapezium rule while retaining formal infinite-order accuracy, provided care is taken in handling the removable singularity at $\boldsymbol{x} = \boldsymbol{X}$.

Finally, we need to discretize (6.9). One could naively attempt a straightforward Galerkin approach:

$$\oint [\boldsymbol{u}_{\text{mov}}(\boldsymbol{\alpha}; \Omega; \tilde{s}) \cdot \boldsymbol{n}(\boldsymbol{\alpha}; \tilde{s})] \, \phi_m(\tilde{s}) \, \mathrm{d}\tilde{s} = 0, \quad m = 1, \ldots M. \tag{6.11}$$

However, as explained in the next section, (6.11) leads to a degenerate set of equations. The problem of removing these degeneracies is the subject of the next section.

6.3.2 Removing trivial Jacobian eigenmodes

Unfortunately, as discussed in § 6.2, discretizing the no through-flow condition (6.9) leads to a set of equations that is, in general, *not* linearly independent.

As explained earlier, this interdependence manifests itself through the presence of several zero eigenvalues of the Jacobian matrix, each of which is associated with a trivial change in the solution. In this section, we explain our approach to removing these zero eigenvalues.

In order to introduce the essential idea, let us consider a single vortex, which occupies a region D in the flow. Let us now consider again the trivial perturbations illustrated earlier in figure 6.1. The zero eigenvalues associated with a displacement of the vortex can be removed, in principle, by explicitly prescribing the location of the centroid of area:

$$x_c = A^{-1} \iint_D x \, \mathrm{d}x \, \mathrm{d}y = 0, \tag{6.12}$$

$$y_c = A^{-1} \iint_D y \, \mathrm{d}x \, \mathrm{d}y = 0 \tag{6.13}$$

Similarly, we propose to remove the zero eigenvalue associated with a rescaling of the vortex shape, by requiring that the area A of the vortex is equal to a specific value, say, A_0:

$$A - A_0 = \iint_D \mathrm{d}x \, \mathrm{d}y - A_0 = 0. \tag{6.14}$$

Finally, to remove the zero eigenvalue associated with a rotation of the solution, we prescribe the cross-product of inertia of the vortex shape, as this will fix the orientation of the steady flow:

$$I_{xy} = \iint_D xy \, \mathrm{d}x \, \mathrm{d}y = 0. \tag{6.15}$$

We are now faced with the problem of introducing these additional four constraints into the solution. One could naively attempt to achieve this by discarding four of the M equations in (6.11), and replacing them with the constraints above. This is easily implemented in practice; however, we find that while the

Newton iteration typically converges, the resulting answer is not an accurate solution of the no-through-flow equation (6.9).

In this work, we propose to remove the degeneracies by introducing to vortex flows a somewhat subtler approach, which was first suggested, in the context of the study of irrotational gravity waves, by Chen & Saffman (1980). To the best of our knowledge, the methodology described here has not been developed before for calculating steady vortices.

To introduce the essential ideas, let us first note the no-through-flow condition, paired with the constraints (6.12)-(6.15), is isomorphic to the simpler-looking problem:

$$\begin{aligned} F(\alpha; \Omega; \tilde{s}) &= 0 \\ G(\alpha) &= 0, \end{aligned} \tag{6.16}$$

where, once again, α is the solution, Ω plays the role of the control parameter and $\tilde{s}$ is a space coordinate, running, say, from 0 to 2π. Suppose that (6.16) has a locally unique solution. Further to this, let us also suppose that the constrained equation

$$H(\alpha; \Omega; \tilde{s}) = F(\alpha; \Omega; \tilde{s}) + G(\alpha)\,\tau(\tilde{s}) = 0, \tag{6.17}$$

where $\tau(\tilde{s})$ is a nontrivial function of $\tilde{s}$, also has a locally unique solution. (In practice, with a given F, G, τ, this hypothesis can be checked directly by computing the Jacobian of (6.17)).

Next, suppose that, with a given Ω, we find a particular solution of (6.16) (given say, by $\alpha = \alpha^*$). This must, of course, also be a solution of the constrained problem (6.17). Since (6.17) has a locally unique solution, we can then use α^* as a starting point for finding more solutions of (6.17), as we change Ω in small increments. However, since both the constrained and unconstrained problems

have a locally unique solution, all of the values of α found by continuing the solution of (6.17) must *also* solve (6.16). Therefore, provided we initialize our continuation scheme with a steady flow, an equation of the form (6.17) can be used to accurately compute new steady flows, for other values of the angular velocity Ω.

For a uniform vortex, we therefore introduce the following modified no-through-flow equation:

$$\begin{aligned} H(\boldsymbol{\alpha};\Omega;\tilde{s}) &= \boldsymbol{u}_{\text{mov}}(\boldsymbol{\alpha};\Omega;\tilde{s})\cdot\boldsymbol{n}(\boldsymbol{\alpha};\tilde{s}) + w_1\,\tau_1(\tilde{s})\,x_c(\boldsymbol{\alpha}) + w_2\,\tau_2(\tilde{s})\,y_c(\boldsymbol{\alpha}) \\ &\quad + w_3\,\tau_3(\tilde{s})\,[A(\boldsymbol{\alpha}) - A_0] + w_4\,\tau_4(\tilde{s})\,I_{xy}(\boldsymbol{\alpha}) \\ &\equiv \boldsymbol{u}_{\text{mov}}(\boldsymbol{\alpha};\Omega;\tilde{s})\cdot\boldsymbol{n}(\boldsymbol{\alpha};\tilde{s}) + \sum_{i=1}^{4} w_i\,G_i(\boldsymbol{\alpha})\,\tau_i(\tilde{s}) = 0, \end{aligned} \tag{6.18}$$

where the w_i's represent constant weight factors, which can be chosen to ensure that the Jacobian is well-conditioned. Finally, (6.18) is discretized using a Galerkin approach, as explained before:

$$f_m(\boldsymbol{\alpha};\Omega) \equiv \oint H(\boldsymbol{\alpha};\Omega;\tilde{s})\,\phi_m(\tilde{s})\,\mathrm{d}\tilde{s} = 0, \quad m = 1, ..., M, \tag{6.19}$$

where, once, again, the integral is computed using the trapezium rule. In the rest of this paper, we use $\tau_i = (i+1)[\tilde{s}/(2\pi)]^i$, and set all of the $w_i = 10^2$. Note that it is easy to generalize this methodology to a configuration of several vortices, provided the area of each vortex region is specified.

6.3.3 Details of the predictor-corrector scheme

For completeness, we briefly report here the details of the predictor-corrector scheme used to continue steady vortex solutions. Let us begin by supposing

that we have a steady flow, given by the vortex shape $\boldsymbol{X}^*$ and by the angular velocity Ω^*, and that we wish to compute a neighboring solution, for a slightly different Ω.

We begin by using the velocity on the boundary to compute $\tilde{s}$ for $\boldsymbol{X}^*$, and re-discretize the boundary uniformly in $\tilde{s}$. To ensure that we can handle any turning points that may arise in Ω, we define the extended solution vector $\boldsymbol{\alpha}_e = (\boldsymbol{\alpha}^{\mathrm{T}}\, \Omega)^{\mathrm{T}}$, and introduce the pseudo-arclength ℓ in the solution space as the new continuation parameter (this quantity is defined in detail further below). Let us denote the solution at the i^{th} iterate as $\boldsymbol{\alpha}_e^{(i)}$. The initial guess for a new solution, at a specified distance $\Delta\ell$ from the previous one in the solution space, is given by:

$$\boldsymbol{\alpha}_e^{(0)} = \begin{pmatrix} \mathbf{0} \\ \Omega^* \end{pmatrix} + \Delta\ell\, \boldsymbol{t}^* \tag{6.20}$$

where $\boldsymbol{t}^*$ represents the unit vector tangent to the solution curve, evaluated at the last steady solution. It can be shown that $\boldsymbol{t}^*$ is given by (Deuflhard, 2006):

$$\boldsymbol{t}^* = \ker\left[\mathbf{J}^*, \left(\frac{\partial \boldsymbol{f}}{\partial \Omega}\right)^*\right]. \tag{6.21}$$

where ker(**A**) denotes the kernel of **A**, and **J** is the Jacobian matrix (defined such that $J_{mn} = \partial f_m / \partial \alpha_n$).

Once the guess $\boldsymbol{\alpha}_e^{(0)}$ has been computed, a new solution is obtained using a Newton corrector. To this end, the vector $\boldsymbol{f}$ is extended through the introduction of the equation:

$$\Delta\ell^{(i)} - \Delta\ell = 0, \tag{6.22}$$

where, at the i^{th} iterate, $\Delta\ell^{(i)}$ is found from

$$\Delta\ell^{(i)} = \boldsymbol{t}^* \cdot \left[\boldsymbol{\alpha}_e^{(i)} - \begin{pmatrix} \mathbf{0} \\ \Omega^* \end{pmatrix}\right], \tag{6.23}$$

such that $\Delta\ell$ is, in essence, the distance between solutions, measured along $\boldsymbol{t}^*$. Therefore, the extended Jacobian (which has size $(M+1)\times(M+1)$) is:

$$\mathbf{J}_e^{(i)} = \begin{bmatrix} \mathbf{J}^{(i)} \left(\dfrac{\partial \boldsymbol{f}}{\partial \Omega}\right)^{(i)} \\ (\boldsymbol{t}^*)^{\mathrm{T}} \end{bmatrix}, \tag{6.24}$$

and the solution at the next iterate is given by the standard Newton iteration formula $\boldsymbol{\alpha}_e^{(i+1)} = \boldsymbol{\alpha}_e^{(i)} - (\mathbf{J}_e^{(i)})^{-1} \boldsymbol{f}_e^{(i)}$, until $\|\boldsymbol{\alpha}_e^{(i+1)} - \boldsymbol{\alpha}_e^{(i)}\|$ is smaller than a pre-determined tolerance (in the results presented below, typically 10^{-12}). Once a converged solution is obtained, the magnitude of the highest-order terms in the vector $\boldsymbol{\alpha}$ are checked to be smaller than a prescribed tolerance. If this is found not to be true, the calculation is restarted with either a larger number of normal modes M, or a smaller step $\Delta\ell$ in the solution space. Since the correction $\boldsymbol{\alpha}$ is computed with reference to a previously found solution, we found it to be practically advantageous to limit the allowable computational cost of each iterate by prescribing a maximum number of normal modes (say, $M_{\max}$) to be used in the calculation. Once M reaches $M_{\max}$, accuracy is preserved by decreasing the step $\Delta\ell$ in the solution space. As for any other spectral methods, once a solution branch is computed, its accuracy can be verified by re-calculating selected steady flows using a different value of M.

6.4 Comparison between IVM and uniform arc-length discretization

In this section, we test our numerical method by computing steady elliptical vortices, and comparing our results with the classical analytical solution of

Kirchhoff (see Kirchhoff, 1876; Saffman, 1992). In the interest of clarity, we take advantage of the fact that the family of elliptical vortices does not display any turning points in Ω, and dispense with the pseudo arc-length ℓ. We therefore directly use Ω as the control parameter in this section, and employ the (non-extended) Jacobian $\mathbf{J}$ for iteration. In order to provide a measure of the increase in computational efficiency due to the inverse-velocity mapping, we also perform calculations using a uniform discretization in arc-length (that is, by setting $\tilde{s} = s$ in our numerical procedure), and report the corresponding results.

The elliptical vortex family starts with a circular vortex, and terminates with a vortex sheet as the axis ratio $\lambda \equiv b/a \to 0$. It is, of course, not reasonable to expect that any general numerical method would be able to accurately resolve the vortex shape in this limit. Nevertheless, this family of solutions provides a stringent test of performance for any numerical procedure.

To perform a numerical test, we first select a value of the vortex axis ratio λ (such that $0 < \lambda < 1$), and a number of normal modes M. The area of the vortex is set to $A_0 = \pi$. We then use Kirchhoff's analytical solution to calculate the corresponding angular velocity (given by $\Omega^* = \lambda(\lambda + 1)^{-2}$), together with the vortex shape and fluid velocity on the boundary. The vortex shape is discretized uniformly in $\tilde{s}$ (or s, as appropriate) using $N = 4M + 1$ points.

Once the exact solution with angular velocity Ω^* has been discretized, we select a step $\Delta\Omega > 0$, and use the discretized exact solution as the initial guess for computing a vortex with angular velocity $\Omega = \Omega^* - \Delta\Omega$, which is found by Newton iteration. Note that the use of a minus sign in the preceding expression implies that we are looking for a vortex that is *more* eccentric than the original one. We stop the iteration after the magnitudes of both $\boldsymbol{f}$ and $(\mathbf{J}^{-1}\boldsymbol{f})$ fall below

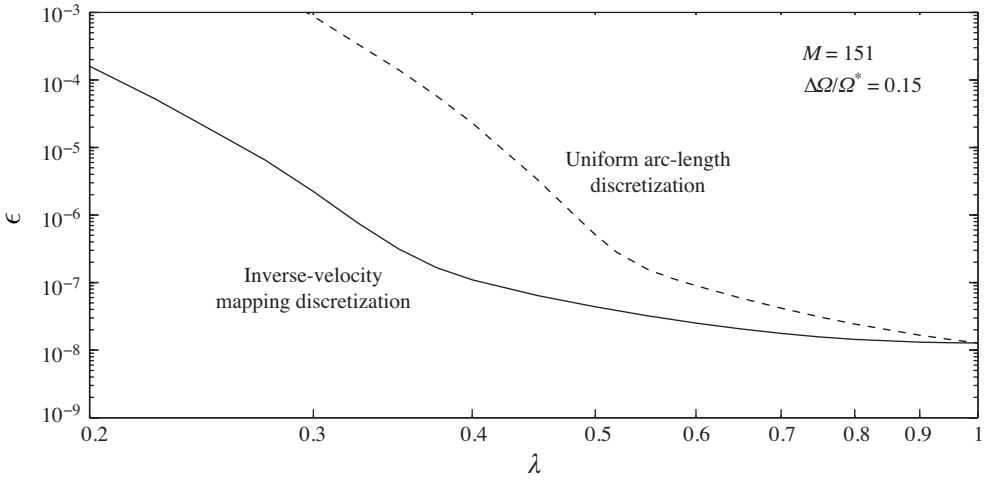

Figure 6.4: Shape error ϵ, for calculations starting with elliptical vortices of axis ratio λ and angular velocity Ω^*. For simplicity, in these tests, the step in the solution space is taken as $\Delta\Omega = 0.15 \times \Omega^*$; the number of normal modes is $M = 151$.

10^{-10}.

In order to provide a numerical measure of the accuracy in the numerical solution, we record the error in the vortex shape as follows. We compare the numerical solution against the analytical results for an elliptical vortex having the same angular velocity (that is, $\Omega^* - \Delta\Omega$), and define the error ϵ as:

$$\epsilon = A_0^{-3/2} \left(\oint \eta^2(s)\, \mathrm{d}s \right)^{1/2} \tag{6.25}$$

where $\eta(s)$ is the distance between the numerical and analytical boundaries, measured along a line normal to the analytical contour.

We begin our tests by setting $M = 151$, $\Delta\Omega = 0.15 \times \Omega^*$, and calculating the resulting error ϵ for various λ. We run the same calculations for both the inverse-velocity mapping (IVM) and the uniform arc-length discretizations; the results are shown in figure 6.4. For all $\lambda < 1$, the IVM discretization provides greater accuracy; the improvement becomes more pronounced for more eccentric vor-

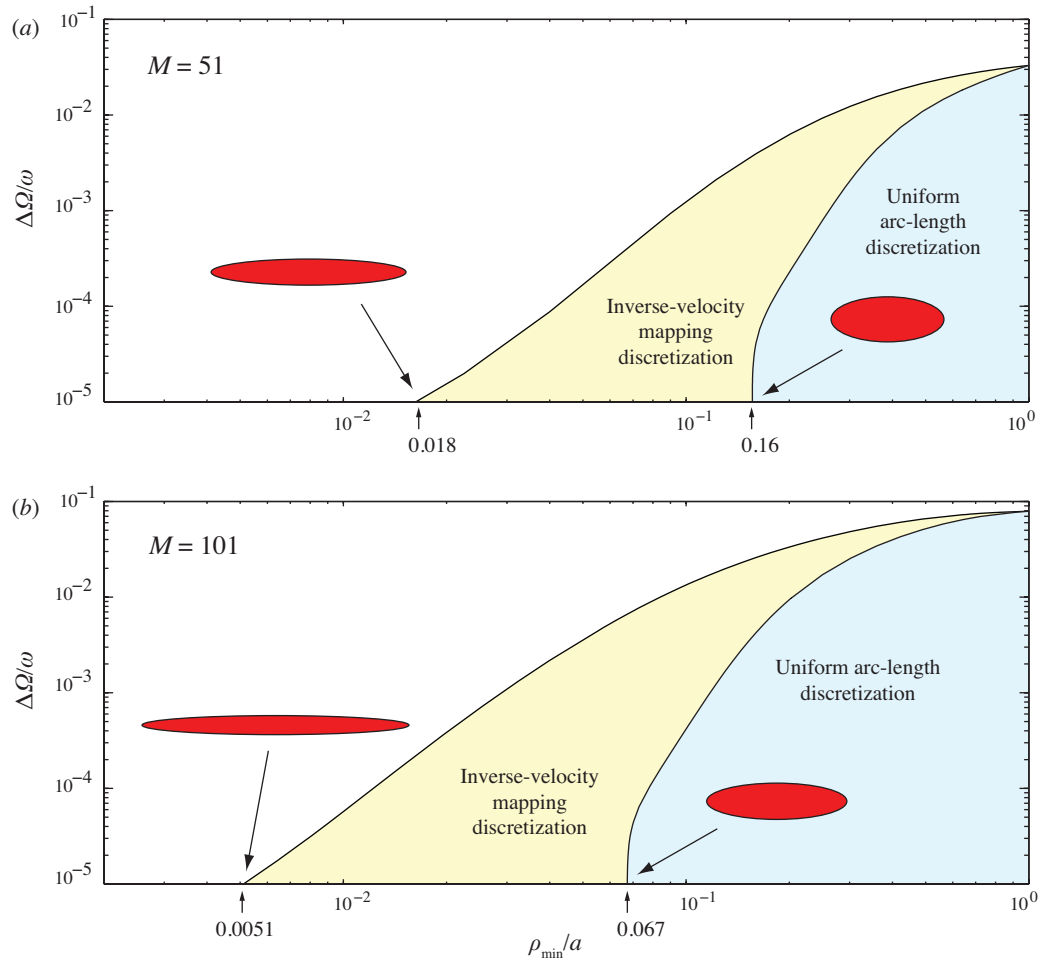

Figure 6.5: Plots of control-parameter step $\Delta\Omega/\omega$ versus the minimum radius of curvature $\rho_{\min}/a$, for the family of elliptical vortices. The shape error is set to $\epsilon = 10^{-6}$. (*a*) shows results for $M = 51$, and (*b*) with $M = 101$.

tices. For example, at $\lambda = 0.3$, the error associated with the uniform arc-length discretization is 8.8×10^{-4}, while the corresponding value for the IVM discretization is 2.2×10^{-6} (that is, almost three orders of magnitude smaller).

In order to formulate a more valuable comparison between the two discretizations, we note that, in practice, one is interested in the number of normal modes and in the step size required to obtain a certain accuracy in the numerical solution. For this reason, it is interesting to start by *prescribing* the value of the

error ϵ. For a given initial axis ratio λ, we can then examine the combinations of $\Delta\Omega$ and M that realize sufficiently accurate solutions. Furthermore, in practice, it can also be desirable to prescribe the value of M to be used, as this gives control over the computational cost for each iteration. Therefore we choose to characterize the performance of the numerical procedure by computing $\Delta\Omega$ as a function of λ, for fixed ϵ and M.

Before examining these results, we also note that a key measure of performance, for fluid flow problems, is given by the ratio between the smallest and largest scales that can be accurately resolved. For an elliptical vortex, the largest scale is given by the major axis a, while the shortest scale corresponds to the smallest value of the radius of curvature of the boundary (say, $\rho_{\min}$). By using the definition of the radius of curvature ρ for a parametric curve (Kreyszig, 1991), it can be shown that, for an ellipse with axis ratio λ, one has simply:

$$\frac{\rho_{\min}}{a} = \lambda^2. \tag{6.26}$$

We therefore plot the values of $\Delta\Omega$ that we find versus $\rho_{\min}/a$.

We performed tests with $\epsilon = 10^{-6}$ and $M = 51, 101$; for each λ, the value of $\Delta\Omega$ that gives the required ϵ was found using a bisection scheme. Figure 6.5 shows results for calculations using the inverse-velocity mapping (IVM), as well as with uniform discretization in boundary arc-length. In essence, these plots define operating "envelopes", inside of which the accuracy requirement $\epsilon < 10^{-6}$ is satisfied. Note that a logarithmic scale is used for both $\Delta\Omega$ and $\rho_{\min}/a$. For both discretizations, we initialize our calculations with a circular vortex, for which $\rho_{\min}/a = 1$, and eventually stop the calculation when $\Delta\Omega$ becomes smaller than 10^{-5}.

Using $M = 51$, the calculations employing a uniform arc-length discretiza-

tion meet this threshold at $\rho_{\min}/a \doteq 0.16$ (corresponding to $\lambda \doteq 0.4$, as shown in the figure). By contrast, the IVM discretization meets the same threshold in $\Delta\Omega$ at a value of $\rho_{\min}/a$ that is almost one order of magnitude smaller ($\rho_{\min}/a \doteq 0.018$, corresponding to $\lambda \doteq 0.13$). With $M = 151$, the difference in performance between the two discretizations increases, as the $\Delta\Omega = 10^{-5}$ threshold is met by the two sets of calculations at $\rho_{\min}/a \doteq 0.067$ and 0.0051, respectively; for this value of M and $\Delta\Omega$, the improvement in the range of scales resolved is over one order of magnitude.

As pointed out earlier, the elliptical vortex is an exceptionally demanding test case. As we shall see in the examples below, it is of course possible to obtain a much greater range of scale separations by appropriately increasing the number of normal modes M; indeed, we reach $\rho_{\min} \sim 10^{-7}$ in the calculations presented in the next section.

6.5 Computing families of lower-symmetry vortices

In this section, we examine two classical vortex flows, and employ our algorithm to compute lower-symmetry solution branches, which are obtained through bifurcations from well-known solution families.

Firstly, let us frame the analysis presented here in the context of the recently proposed "imperfect velocity-impulse" (IVI) diagram stability approach (Luzzatto-Fegiz & Williamson, 2010*b*). This methodology provides a formal link between the occurrence of turning points in impulse J (in a plot of J versus Ω) and the occurrence of exchanges of stability for the flow of interest. This framework also allows one to find new families of solutions, which bifurcate from the

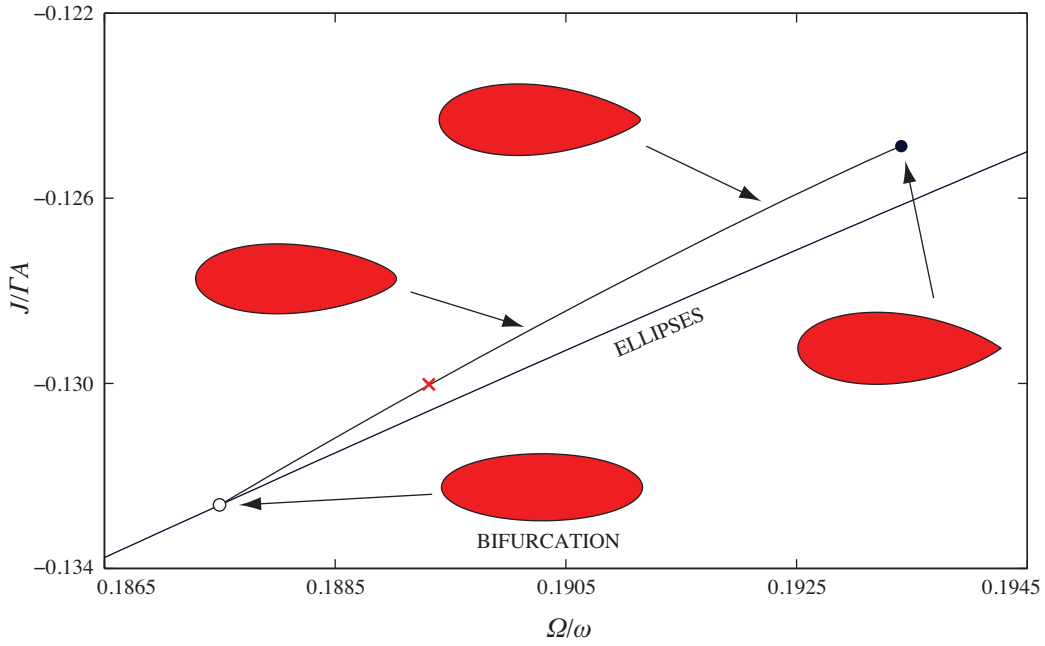

Figure 6.6: The first branch of solutions bifurcating from the elliptical vortices, computed with $M = 151$. The red × symbol denotes the last solution that could be obtained using the uniform arc-length discretization, by employing the same M and the same level of accuracy.

original series of flows, without the need to perform a linear stability analysis (see Luzzatto-Fegiz & Williamson, 2010*b*,*c*). In the spirit of these works, here we also choose to employ velocity-impulse diagrams to display the families of solutions that we compute using our numerical approach. The angular impulse J of a vortex configuration is found from the integral (Saffman, 1992):

$$J = -\frac{1}{2}\iint \omega(x^2 + y^2)\,\mathrm{d}x\,\mathrm{d}y. \tag{6.27}$$

For a collection of uniform vortices, it is straightforward to transform (6.27) to a contour integral in $\tilde{s}$, which can be accurately evaluated by the trapezium rule. All of the results presented in the paper were obtained using a laptop computer with a 2.26 GHz processor, which is an indication of the modest computational power required to implement the numerical method.

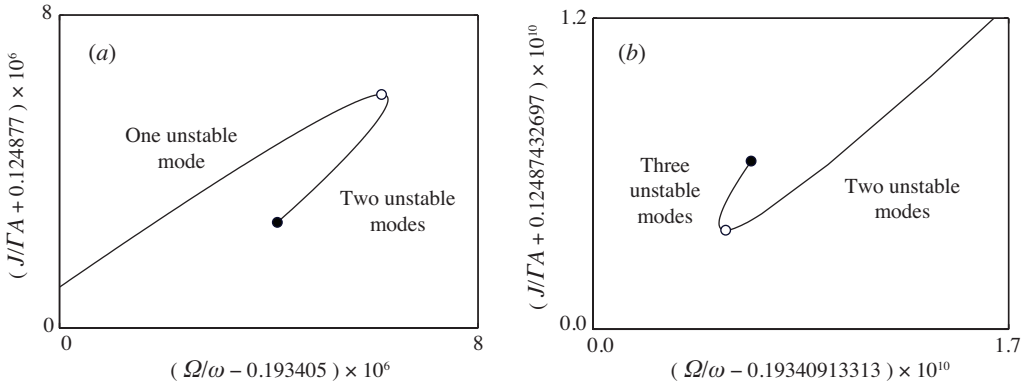

Figure 6.7: Close-up views of the velocity-impulse diagram near the limiting vortex state, for the first bifurcated branch from the elliptical family.

6.5.1 Vortices with one symmetry plane: the $m = 3$ bifurcation from the Kirchhoff ellipses

As an initial example, we consider the first bifurcation that arises from the family of elliptical vortices, as the ellipticity is progressively increased. This bifurcation arises at an axis ratio $\lambda = 1/3$, and is associated with a mode with azimuthal wavenumber $m = 3$ (as implied by the linear stability analysis of Love, 1893). The beginning of this bifurcated solution branch was computed by Kamm (1987), who used a numerical conformal mapping approach. As the vortex developed a region of greater curvature, numerical cost prevented him from progressing further along this solution branch.

We begin our calculations at a bifurcated solution near the original family of ellipses. The initial guess is obtained using the imperfection approach described in detail in Luzzatto-Fegiz & Williamson (2010*c*). We use $M = 151$ normal modes and let the procedure automatically adjust $\Delta\ell$ to ensure that the highest-order terms in the Fourier series are smaller than 10^{-7}. The result is shown in fig-

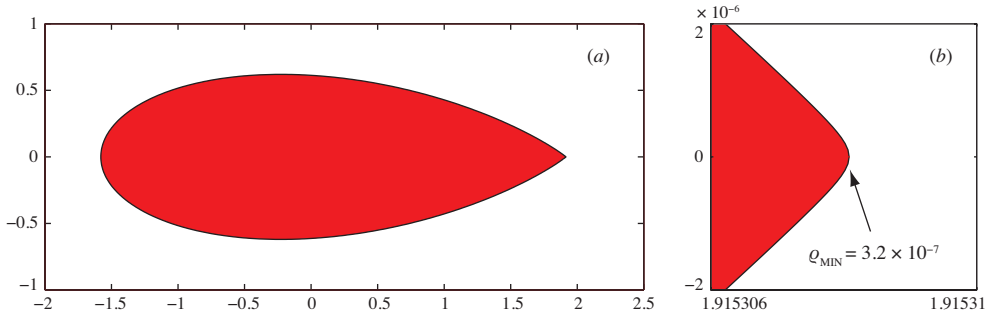

Figure 6.8: The limiting vortex state for the first bifurcated branch from the elliptical vortex. (*a*) shows the overall shape. (*b*) shows a close-up of the high-curvature region.

ure 6.6, where we also show selected vortex shapes, for illustration. All of the velocity-impulse plots shown in this paper were prepared using straight lines, joining points at which equilibria were computed. The angular velocity of the configuration is normalized by the vorticity ω, while the impulse is made nondimensional by using the circulation Γ and the area A of the vortex. For reference, we also computed this branch using the uniform arc-length discretization, while keeping the same M, as well as the same accuracy requirement; the farthest location that this procedure was able to reach is marked by a red cross ($\times$) in the figure. We find that the vortex progressively develops a region of particularly high curvature, where the boundary approaches the shape of a 90° corner. In the velocity-impulse diagram of figure 6.6 the location of this limiting vortex state is shown by a solid circle.

As we follow the solution branch, starting from the bifurcation from the elliptical vortices, we discover a turning point in impulse at $(\Omega/\omega, J/\Gamma A) \doteq (0.19341116, -0.12487103)$, as shown in the close-up in figure 6.7(*a*). The IVI-diagram stability approach implies that this turning point in impulse is linked to an exchange of stability; more specifically, this corresponds to a *further* loss

of stability (that is, beside the already unstable $m = 3$ eigenmode). Progressing slightly further along the solution family, we find a turning point in velocity (just to the right of the open circle in the figure), at normalized values of velocity and impulse of (0.19341128, –0.12487116); this is also visible in the figure. In this region of the velocity-impulse plot, vortex shapes exhibit a minimum radius of curvature of $O(10^{-3})$. Since the area of the ellipse is set to π, for this flow the value of the curvature also directly provides a quantitative measure of the separation of scales resolved in the calculation. The neighbourhood of these turning points, in the velocity-impulse diagram, was resolved using a finer step in the solution space, $\Delta\ell \approx 10^{-4}$.

At this stage, the high curvature exhibited by the boundary would suggest that these solutions are very close to the limiting shape. One might therefore expect that the solution curve would lead more or less directly to the limiting state, giving rise to a curve that is monotonic in both Ω and J in the velocity-impulse plot. As we progressed further along the solution family, however, we were surprised to discover a *further* sequence of turning points in J and Ω, as shown in the close-up in figure 6.7(*b*). Note that the axes span a range of 1.7×10^{-10} in Ω/ω, and of 1.2×10^{-10} in $J/(A\Gamma)$. This figure therefore corresponds to a 10^4 magnification from figure 6.7(*a*), and to an approximately 10^8 magnification from the original plot of figure 6.6! The data in this figure was computed using $M = 701$ and $5 \times 10^{-8} < \Delta\ell < 10^{-6}$. Once again, we note that the IVI approach implies that this turning point in impulse is associated with an additional loss of stability.

The last steady vortex that we computed on this solution branch is shown in figure 6.8. The close-up in figure 6.8(*b*) shows the region of highest curva-

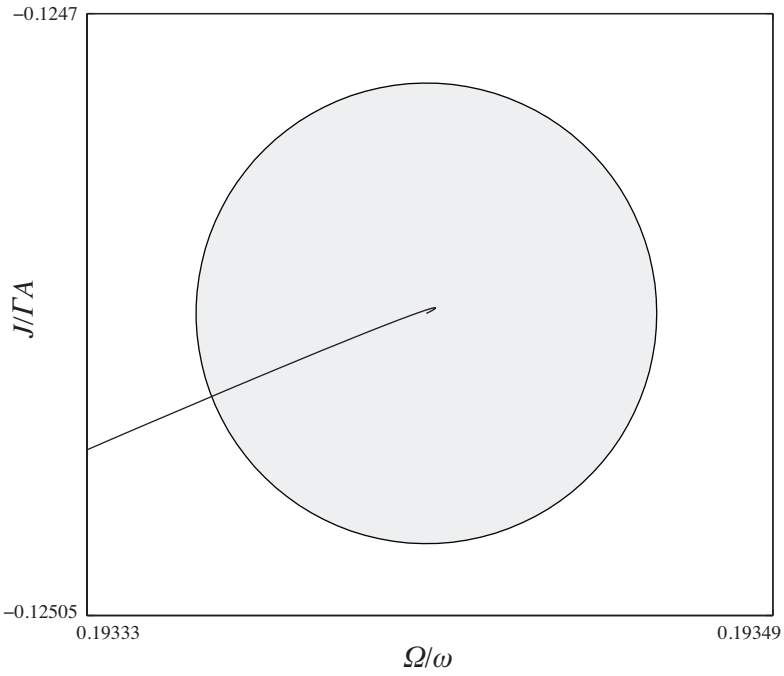

Figure 6.9: Close-up of the solid black circle in figure 6.6. The circle has been made transparent; the first set of turning points (seen in detail earlier in figure 6.7) is visible near the centre.

ture, magnified by a factor of approximately 10^6. The smallest radius of curvature is $\rho_{\min} = 3.2 \times 10^{-7}$. Since the length-scale of the overall vortex patch is $O(1)$, this means that the ratio between largest and smallest resolved scales is $O(10^7)$. The vortex shown in the figure is not, technically, the limiting shape (as the minimum radius of curvature is not zero); however, inspection of figure 6.7 suggests that the non-dimensional velocity and impulse are within 10^{-11} of the corresponding values for the actual limiting flow. From a numerical standpoint, therefore, the distinction between the vortex computed here (shown in figure 6.8) and the limiting shape can be argued to be insignificant.

In concluding this section, we illustrate the difference in scales between elements of the velocity-impulse diagram (this scale difference is evident in figure 6.6, and in the close-up of figure 6.7*a*). The solid circle that marks the the

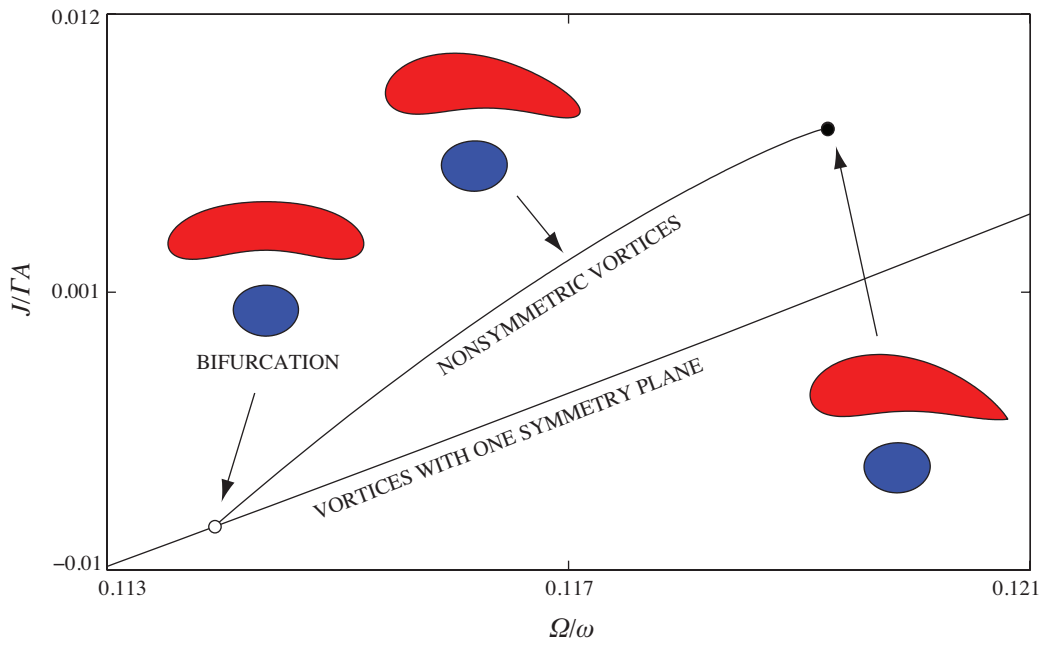

Figure 6.10: Velocity-impulse diagram for the nonsymmetric vortex pairs.

limiting shape in figure 6.6 has been enlarged to fill the whole of figure 6.9. With this magnification, we see the first turn of the spiral as the almost indistinguishable 'hook' at the centre of figure 6.9!

6.5.2 Vortices without any symmetry planes: bifurcation from the unequal-strength vortex pairs

We next consider another, slightly more complex flow. This is given by two vortices of opposite sign, unit vorticity magnitude, and unequal area. Since the overall circulation is non-zero, these vortex configurations also rotate about a fixed point. For this example, we set $A_1 = \pi$ and $A_2 = 0.3\pi$, such that the vorticity, area and circulation for nondimensionalizing the results are $\omega = 1$, $A = A_1 + A_2 = 1.3\pi$, and $\Gamma = \Gamma_1 + \Gamma_2 = 0.7\pi$. By starting with two vortices

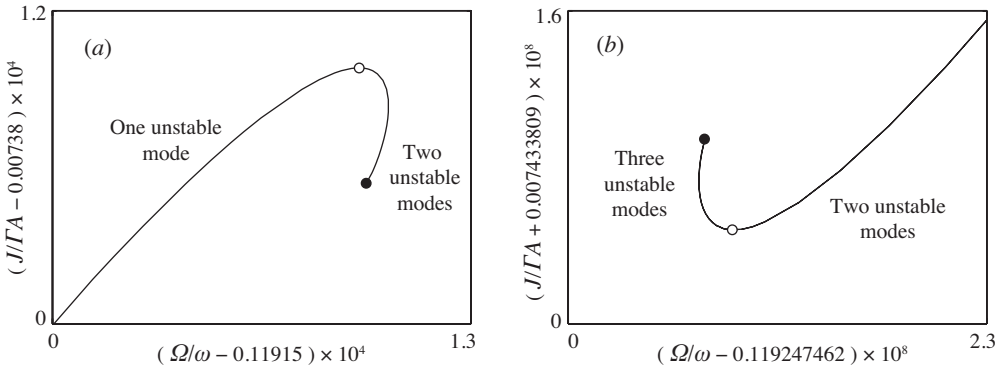

Figure 6.11: Close-up views of the velocity-impulse diagram near the limiting vortex state, for the nonsymmetric vortex pair.

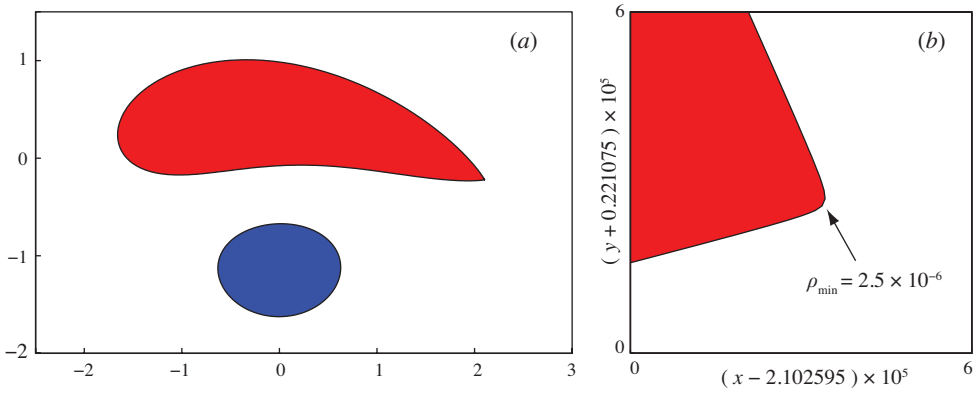

Figure 6.12: The limiting vortex state for the nonsymmetric, opposite-signed vortex pair. (*a*) shows the overall shape. (*b*) shows a close-up of the high-curvature region.

separated by a large distance, and progressively bringing them closer, one obtains a family of flows that are symmetric about a plane bisecting both vortices. These vortex pair solutions, having one symmetry plane, were first computed by Dritschel (1995). In a recent work, we employed our imperfection approach, together with the numerical method described here, to search for bifurcations from these families of solutions, and discovered a new family of steady, nonsymmetric vortices (Luzzatto-Fegiz & Williamson, 2010*b*). To the best of our knowledge, uniform-vortex solutions that lack any geometric symmetry, in an

unbounded flow, had never been computed before. In what follows, we examine in detail the properties of this new solution family.

Figure 6.10 shows an overall view of this branch of nonsymmetric solutions in a velocity-impulse diagram; a selection of vortex shapes are also shown. The numerical parameters employed for this flow follow closely those employed to compute the example in the previous section. We encounter a pair of turning points in normalized impulse and velocity, as shown in figure 6.11(*a*). According to the theory in Luzzatto-Fegiz & Williamson (2010*b*), this turning point in J corresponds to the addition of an unstable mode. As we continue along the solution curve, we find a second set of turning points in impulse and velocity. This second pair of turning points develop on a scale approximately 10^4 times smaller than for the previous pair, and are shown in figure 6.11(*b*); these results closely resemble those from the previous section. The last vortex state that we computed is shown in figure 6.12; this solution was obtained using $M_1 = 601, M_2 = 401$.

6.6 Velocity-impulse spirals

In § 6.5 we examined two families of steady flows; we found that both of these examples exhibit series of turning points in impulse and velocity, as each limiting state is approached. The velocity-impulse plots thus take the shape of a spiral, with the peculiar feature that the second turn of the spiral takes place on a scale approximately 10^4 times smaller than the first turn. We did not attempt to compute further turns.

We employed the numerical procedure described here to compute a wide

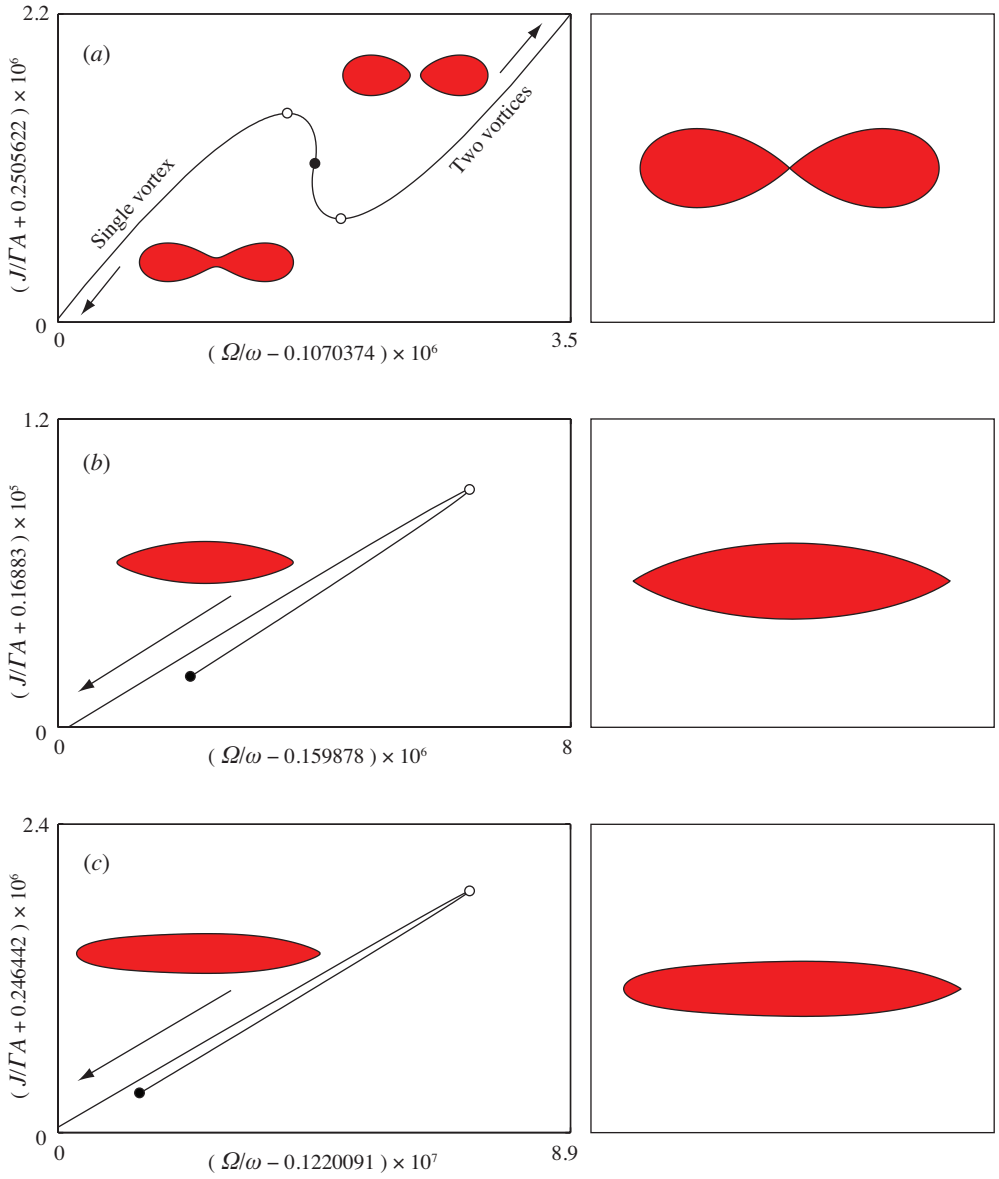

Figure 6.13: (*a*) and (*b*) show the velocity-impulse plots near the two limiting states for the family of solutions that departs from the elliptical family at a transcritical bifurcation associated with azimuthal wavenumber $m = 4$. (*c*) shows the branch for $m = 5$. The right-hand panels show the corresponding limiting shapes.

range of flows; these include other single-vortex solutions, corotating and counterrotating vortex pairs, vortex rows, finite-area Kármán streets, and arrays of N equal-area vortices. In all of the flows that we examine, we find velocity-

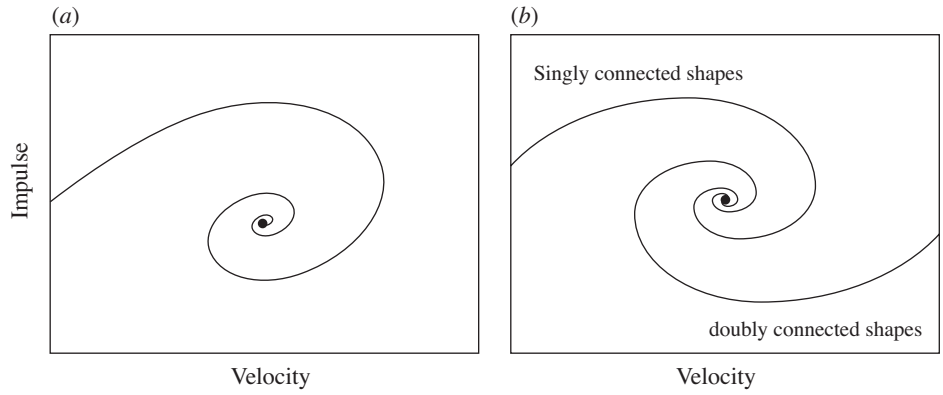

Figure 6.14: Highly schematic diagram to illustrate the qualitative structure of the velocity-impulse plot near a limiting vortex state. (*a*) "single-spiral" pattern observed for the majority of solutions. (*b*) "double-spiral" found for the "dumbbell" shaped vortices arising from the $m = 4$ bifurcation, which share their limiting state with the family of co-rotating, equal-area vortex pairs, leading to a double-spiral structure. For clarity, the open circles marking exchanges of stability at turning points in impulse are not shown.

impulse spirals developing near the corresponding limiting states.

Figure 6.13 shows the first set of turning points for a few of these examples; we show the families of solutions arising from the next two bifurcations on the family of elliptical vortices. For this flow, an overall view of the solution branches can be found in Luzzatto-Fegiz & Williamson (2010*c*). In this paper, we focus on the the the first turn each spiral, using a magnification factor of about 10^5 with respect to figure 5 in Luzzatto-Fegiz & Williamson (2010*c*).

The bifurcation associated with azimuthal wavenumber $m = 4$ is a transcritical one (Kamm, 1987), and therefore leads to two distinct limiting states, which are shown in figure 6.13(*a*),(*b*). The first flow (displayed in *a*) leads to a limiting state given by two vortices that are connected at a point. This constitutes the limiting vortex state also for a family of equal-area, corotating vortices (Dritschel, 1995; Cerretelli & Williamson, 2003*a*); the two-vortex solutions that

we computed are also shown in the figure. Our calculations reveal that, in the neighborhood of this limiting state, a distinctive double-spiral structure takes place. Figure 6.13(*b*) shows the other end of the $m = 4$ solution branch, where the vortices take a "cat's eye" shape, while figure 6.13(*c*) shows the $m = 5$ solutions. To try to better appreciate the patterns in these plots, we show in figure 6.14 highly schematic versions of these velocity-impulse diagrams. Figure 6.14(*a*) shows the single-spiral pattern observed for the majority of solutions, including the $m = 3, 5$ single-vortex families, the portion of the $m = 4$ single-vortex family involving "cat's eye" shapes, and the vortex pair solutions of § 6.5.2. By contrast, (*b*) shows the "double-spiral" structure found for the "dumbbell" shaped vortices (which arise from the $m = 4$ bifurcation). These vortices share their limiting state with the family of co-rotating, equal-area vortex pairs.

These results are intriguing, as they suggest that *any* flow involving uniform vortices may give rise to a series of turning points, as the solutions approach their limiting state. This situation may be analogous, to an extent, to the behavior exhibited by steep gravity waves in an irrotational fluid. For this flow, Longuet-Higgins & Fox (1978) developed an asymptotic theory, valid for near-limiting waves, showing that the velocity and impulse undergo a countable infinity of turning points, as the limiting wave shape (exhibiting a 120° corner) is approached. The results presented in this paper suggest that a similar result may hold for uniform-vorticity flows. Furthermore, according to the IVI diagram stability theory (Luzzatto-Fegiz & Williamson, 2010*b*), the existence of a countable infinity of turning points in impulse would immediately imply the development of a corresponding infinite number of exchanges of stability, as one traverses the solution family.

6.7 Conclusions

In this paper, we overcome previous limitations that have affected numerical methods for computing uniform vortices. We solve for each vortex boundary through a spectral representation in terms of a *modified* arc-length variable, $\tilde{s}$, which is constructed through an inverse-velocity mapping (IVM). In addition, we introduce a methodology to remove all degeneracies in the steady vorticity equation, and to find solutions with prescribed Casimir invariants. As a result, our numerical approach can efficiently and accurately resolve uniform vortices of arbitrary shape.

We tested our numerical method against the analytical family of elliptical vortices due to Kirchhoff. Furthermore, we compared the performance of the IVM discretization with calculations using an uniform-arc-length discretization. For a given error ϵ in the computed shape and prescribed number of normal modes M, we calculate the admissible step in the solution space between neighboring steady flows. For any elliptical vortex, the IVM discretization enables one to take a larger step along the solution branch. Furthermore, for a given computational effort, our numerical method can resolve vortices with significantly finer features without losing accuracy.

We illustrate the method in detail by considering two examples. The first flow is given by the first family of solutions that bifurcates from the well-known Kirchhoff ellipses. Using the IVM discretization, we are able to explore this solution branch in its entirety for the first time. As an additional example, we compute in detail a novel family of solutions, involving nonsymmetric, opposite-signed vortex pairs. To the best of our knowledge, this is the first time that a

steady configuration of uniform vortices lacking any symmetry has been found, in an unbounded flow.

For both of these solutions, the vortex boundaries eventually develop high-curvature regions (which approach 90°). We continue our calculations along these solution families until the scale separation achieved, in the vortex boundary, is of order 10^7. To the best of our knowledge, this is the first time that a numerical method based on Newton iteration has been able to compute steady vortices with this level of resolution.

For both of the examples just described, we obtain what appears to be a clockwise spiral in a velocity-impulse diagram, as we approach the limiting vortex shape. We have found similar spirals for all uniform-vorticity flows that we computed; we report here three more more examples, arising through other bifurcations from the family of elliptical vortices. Our results suggest that velocity-impulse spirals may be a universal feature of families of vortex flows. All of these spirals wind clockwise in a velocity-impulse diagram; by the IVI diagram stability approach, each turn in the spiral is therefore associated with an additional loss of of stability, as the limiting flow is approached.

Finally, we point out that the numerical method presented here can also be used to compute linear stability properties, for families of steady solutions. In order to find the eigenvalues of a previously obtained equilibrium flow, it is sufficient to evaluate the Jacobian *without* the constraints used to remove the degeneracies (this approach was used in Luzzatto-Fegiz & Williamson, 2010*a*, to construct eigenvalue plots). It is worthwhile noting, however, that computing accurate eigenvalues typically requires a level of resolution significantly greater than the one that would be needed to just compute the steady flows (see Saffman

& Schatzman, 1982*b*; Dritschel, 1985; Elcrat *et al.*, 2005). For this reason, the stability boundaries from an IVI diagram are more robust than those from an eigenvalue calculation, and can be obtained with lower computational effort. If a detailed linear stability analysis is required, one can perform a quantitative check on the eigenvalues using the recent results described in Luzzatto-Fegiz & Williamson (2010*a*).

In summary, the numerical methodology described here enables one to efficiently compute uniform vortices of arbitrary shape. Remarkably, there are several families of fundamental vortex flows whose bifurcation structure and stability has yet to be fully studied. Well-known examples include vortex pairs, multipolar vortices, and finite-area vortex streets, to name a few. We intend to examine in detail several of these steady flows in future work.

CHAPTER 7

A DERIVATION OF KELVIN'S ARGUMENT, LEADING TO EXTENSIONS FOR COMPRESSIBLE, BAROTROPIC AND BAROCLINIC FLOWS

Submitted to *Journal of Fluid Mechanics*

In 1876, Lord Kelvin stated an energy-based argument for establishing equilibrium and stability in circulation-preserving flows. Kelvin published this argument without proof; the mathematical framework for his ideas is traditionally attributed to Benjamin (1976). In the present paper, we develop a simple conceptual basis for Kelvin's ideas, with the objective of providing a first-principle derivation for Kelvin's argument. We present a brief historical overview of the subject, and discuss several works that have so far been largely overlooked in the vortex dynamics literature. We next provide a derivation of Kelvin's argument from the fundamental principle of virtual work. For a homogeneous fluid, the virtual work is shown to correspond to the energy expended against vortex forces, yielding effectively a principle of *virtual vortex work*. We exploit the frame-independent nature of the principle to show that formulating the analysis in a moving reference frame leads to the condition that the impulse must be prescribed, as originally specified by Kelvin. Our derivation enables us to formulate generalizations to more complex flows. By replacing the requirement that circulation is preserved with a condition that is more widely applicable, namely that the perturbation be dynamically admissible, we are able to extend Kelvin's argument to compressible, barotropic *and* baroclinic flows.

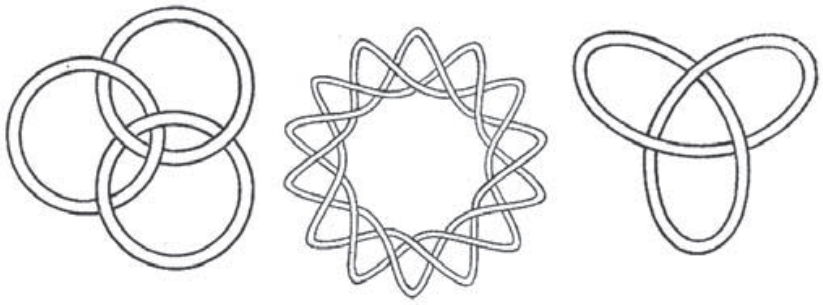

Figure 7.1: Possible patterns considered by Lord Kelvin in the exploration of the theory of vortex atoms. A simple approach to establish stability was essential for determining which of these configurations would be viable candidates to represent specific elements.

7.1 Introduction

Over a century ago, Lord Kelvin (then known as Sir William Thomson) proposed an energy-based argument for defining equilibrium and stability in an inviscid, uniform-density fluid. According to Thomson (1876), a steady flow would correspond to a stationary point of the energy, under perturbations that preserve the fluid vorticity and impulse. Thomson was particularly interested in considering flows that appear in equilibrium when observed in a reference frame that is moving with constant velocity. A typical example is given by a vortex ring, which (in an inviscid fluid) may advance steadily without deforming, and will thus appear stationary in a reference frame translating at the ring's velocity. At the time, Thomson (1867) was a strong proponent of the theory of vortex atoms. According to this idea, each element would correspond to a different arrangement of vortex filaments; examples of the vortex structures that he proposed are shown in figure 7.1. Thomson was interested in a simple criterion for determining which patterns would be stable, and could thus form possible candidates for actual atoms.

Motivated by this viewpoint, Thomson (1876) formulated the following argument for stability. If the energy is conserved, and the equilibrium point corresponds to a maximum or minimum of the energy, any change bringing the fluid system away from the equilibrium point would require a change of the energy, which is impossible (as illustrated schematically in figure 7.2*a*, *b*). Hence the equilibrium must be stable. On the other hand, if the steady flow corresponds to a saddle point, the system can depart from the equilibrium point while retaining constant energy, and may thus be unstable (figure 7.2*c*).

Puzzlingly, Thomson (1876) stated the ideas above, which amount essentially to a variational principle for fluid equilibrium and stability, without proof. The first analytical confirmation of Thomson's ideas (for a two-dimensional flow) is instead traditionally attributed to Brooke Benjamin (1976), a century after Thomson's first publication on the subject. Since then, Kelvin's argument for determining steady flows has been applied in a wide variety of fluid problems. Examples include determining criteria for optimal vortex ring formation in biological propulsion (Gharib *et al.*, 1998; Dabiri, 2009), deriving accurate expressions for the translational velocity of a vortex ring (Fukumoto & Moffatt, 2008), and investigating the stability of families of steady flows (see Luzzatto-Fegiz & Williamson, 2010*b*, and references therein).

However, a number of outstanding questions still surround Kelvin's argument. Firstly, the path that took Thomson to his 1876 statement remains unknown. Perhaps for this reason, Kelvin's argument is often referred to as Kelvin's *principle* in the vortex dynamics literature (see Dabiri, 2009, and references therein). This characterization carries with it the implication that these ideas of Kelvin constitute a fundamental entity in mechanics, and that the argu-

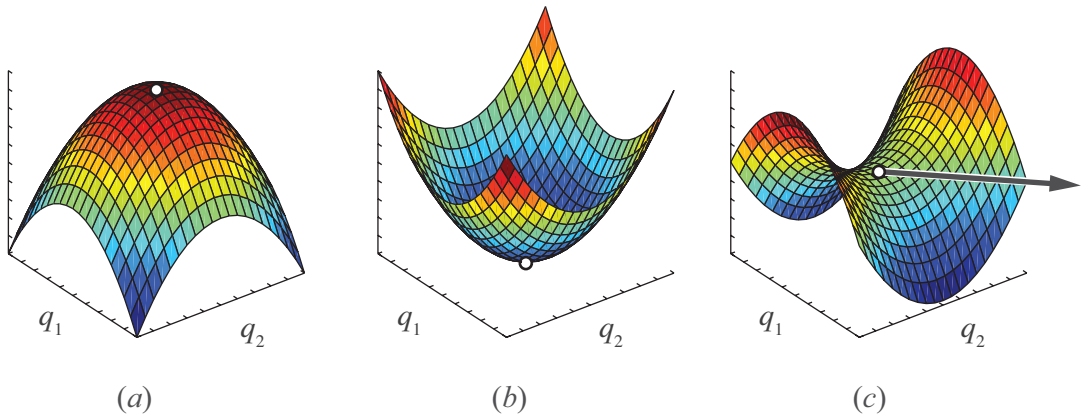

Figure 7.2: Schematic illustration of the relation between the second variation of a conserved quantity, such as the energy, and the stability of an equilibrium, shown here for a solution space $\boldsymbol{q} = (q_1, q_2)^{\mathrm{T}}$. If the equilibrium represents a maximum (*a*) or a minimum (*b*) of the energy, moving away from the equilibrium point would require a change of energy, which is impossible. Hence equilibria (*a*) and (*b*) must be stable. On the other hand, if the solution is associated with a saddle of the energy (as shown in *c*), instability is possible.

ment may not be derived from a simpler physical idea.

A closely related issue involves the possibility of generalizing Kelvin's argument to determine steadiness and stability of nonhomogeneous or compressible flows, for which further complications arise. One expects that the potential energy of the fluid will now play a role, and will need to be introduced in addition to the kinetic energy considered by Benjamin (1976). Furthermore, for nonbarotropic fluids (such as, for example, stratified, incompressible flow), circulation is *not* conserved, even in the inviscid case. This leads to the failure of the key condition proposed by Thomson (1876) and employed by Benjamin (1976), and therefore prevents the extension of Kelvin's ideas to a wide range of flows of practical importance. We suggest here that a derivation of Kelvin's argument from a simple physical idea naturally leads to a resolution of these issues.

We begin, in the following section, by offering a concise historical overview of the developments associated with Kelvin's argument. We then show how, in fact, Kelvin's argument can be derived from the principle of virtual work. Our derivation allows us to formulate generalizations of Kelvin's argument with little conceptual effort, as we explain below.

7.2 Kelvin's argument: a brief historical perspective

In this section, we summarize the main steps in the development of Kelvin's argument. (We must note here the excellent bibliography compiled by Meleshko & Aref, 2007, which proved invaluable while researching 19^{th} century developments in vortex dynamics.)

The earliest reference to the existence of a link between extrema in energy and steady flows appears to be due to James Clerk Maxwell, who explored the idea in an unpublished work (Maxwell, 1855*b*), and in a letter sent to William Thomson (Maxwell, 1855*a*). In these two manuscripts, Maxwell derives, by considering the perturbations of the vorticity field, a stability criterion based on the profile of a vorticity distribution. An energy principle is mentioned briefly, without proof or justification. Unfortunately, we do not know how Thomson responded to Maxwell's letter.

Over a decade and a half later, Thomson (1870), in a letter to George Gabriel Stokes, proposed that one may consider stability of flows that appear steady, if observed in a moving reference frame. Thomson and Stokes' correspondence on the subject culminated in Thomson's 1875 lecture at the Royal Society of Edinburgh, titled *Vortex Statics*. Thomson's address appeared in printed form

the following year (Thomson, 1876); in this work, he states the now famous principle:

> If, with vorticity and "impulse" given, the kinetic energy is a maximum or a minimum, it is obvious that the motion is not only steady, but stable. If, with same conditions, the energy is a maximum-minimum, the motion is clearly steady, but it may be either unstable or stable.

Note that, differently from Maxwell (1855*a*), Thomson stipulates that vorticity (as well as impulse) must be prescribed; as we shall discuss in the next section, this is essential to ensure that accurate stability predictions are obtained.

In a subsequent article, Thomson (1878) briefly outlines a variational argument for point vortices, involving an energy proportional to $\log(D_1 D_2 D_3 ...)$, where each D denotes the distance between two vortices. Thomson does not discuss the physical basis for this argument, or its generalization to continuous vorticity distributions. During approximately the same period of time, Kirchhoff (1876) published a Hamiltonian formulation for the *dynamics* of point vortices in his *Vorlesungen der Physik* (see Saffman, 1992, for a modern treatment). Beginning in the first half of the 20^{th} century, much work was invested in relating Hamilton's principle to Euler's equations. A summary of the literature on this fascinating subject is beyond the scope of the present paper; one may refer to the reviews by Salmon (1988) and Morrison (1998).

Returning to variational arguments for equilibrium flows, a key step forward was made by Arnol'd (1966), who showed that, for the three-dimensional

steady flow of a homogenous fluid, the kinetic energy is stationary under circulation-preserving perturbations. While Arnol'd appears to have been unaware of Thomson's work, he effectively confirmed Kelvin's argument for steady flow in a *fixed* reference frame.

Roberts (1972), inspired by the possibility of constructing a Hamiltonian framework for the study of the flow of liquid helium, developed a variational approach for determining the translational velocity of a vortex ring. Roberts assumed a homogeneous, axisymmetric fluid flow, with given vorticity *and* impulse. Remarkably, it seems that Roberts had no exposure to the works of Thomson and Arnol'd. A few years later, Brooke Benjamin (1976), unaware of Roberts' paper, built on the theorem of Arnol'd (1966) to develop a variational principle for axisymmetric flows with fixed impulse, thus obtaining the same result as Roberts (1972).

Roberts' paper seems to have been largely overlooked in the vortex dynamics literature. This may be due to the fact that Roberts (1972) presented his analysis in the context of obtaining an expression for the translational velocity of vortex rings, without pointing out the broader implications of his result. The lack of recognition of Roberts' work is exemplified in a subsequent paper on vortex rings (Fraenkel & Berger, 1974), where one finds: "Kelvin's variational principle for steady vortex flows [...] is merely stated in physical terms and its analytical basis is obscure." The *Annual Review* paper of Saffman & Baker (1979) on vortex interactions also does not mention this work of Roberts.

It should also be noted that an explanation in terms of a simple physical idea remained elusive. For example, Saffman & Baker (1979) point out that Kelvin's arguments "are physical and rather obscure". They go on to note: "Brooke Ben-

jamin (1976) gives similar arguments in a mathematical framework."

A few years later, Lynden-Bell & Katz (1981) extended the analysis of Arnol'd (1966) to compressible, barotropic fluids. Lynden-Bell & Katz (1981) focused on astrophysical flows; their work does not seem to have reached the vortex dynamics literature.

The following decade saw the beginning of a protracted debate on the practical application of Kelvin's argument for determining stability of families of steady flows (see Saffman & Szeto, 1980; Dritschel, 1985, 1995, and references therein). Recently, Luzzatto-Fegiz & Williamson (2010*b*) introduced a stability approach, based on "imperfect velocity-impulse" (IVI) diagrams, which represents a rigorous and practical implementation of Kelvin's argument. Following this development, it is interesting to ask whether Kelvin's argument may be extended to a wider range of flows, whose stability may then be determined through the "IVI diagram" technique.

7.3 Deriving Kelvin's argument from the principle of virtual work

7.3.1 Incompressible, homogeneous flow in three dimensions

We propose to derive Kelvin's argument from the fundamental principle of virtual work. The principle is based on the physical observation that, in a mechanical system, a component of the externally impressed forces may be opposed by constraints that limit the possible motion of the system. (A classic example

is given by a bead constrained to move along a rigid wire.) Therefore, for a system to be in equilibrium, one needs the overall impressed force $\boldsymbol{F}$ in the direction of the kinematically admissible (virtual) displacements $\delta\boldsymbol{\ell}$ to vanish, that is $\delta W = \boldsymbol{F} \cdot \delta\boldsymbol{\ell} = 0$, where δW is defined as the virtual work (Goldstein, 1950). This principle naturally describes the equilibrium of a system from a particle-based viewpoint, and is therefore typically associated with a Lagrangian view of mechanics (Serrin, 1959). However, here we focus on flow equilibria for which fluid properties do not change in time, at any fixed point in space, and we must therefore take an Eulerian viewpoint.

In what follows, we shall first prove that the vanishing of the virtual work, in a moving reference frame, corresponds to a vortical flow that is steady in the moving frame. We next show that the vanishing of the virtual work also corresponds to an extremum of the fluid energy, for a given impulse.

We begin by considering the work done on an infinitesimal control volume $\mathrm{d}V$ (which is fixed in space), as fluid is pushed through it by means of a displacement $\delta\boldsymbol{\ell}(\boldsymbol{x})$, which is incompressible and vanishes on the fluid boundary. Let us first examine a fixed reference frame, for which we write the external force $\boldsymbol{f}$ that must be *applied* in order to balance fluid forces (see Batchelor, 1967):

$$\boldsymbol{f} = \nabla \cdot (\rho \boldsymbol{u}\boldsymbol{u}) + \nabla p. \tag{7.1}$$

By exploiting the fact that the fluid has uniform density (say, $\rho = 1$), and making use of the identity $\boldsymbol{u} \cdot \nabla \boldsymbol{u} = -\boldsymbol{u} \times \boldsymbol{\omega} + \frac{1}{2}\nabla|\boldsymbol{u}|^2$, we have $\boldsymbol{f} = -\boldsymbol{u} \times \boldsymbol{\omega} + \nabla h$, where $h = p + \frac{1}{2}|\boldsymbol{u}|^2$. We can therefore write the virtual work as:

$$\delta W = \int \boldsymbol{f} \cdot \delta\boldsymbol{\ell} \, \mathrm{d}V \tag{7.2}$$

$$= -\int (\boldsymbol{u} \times \boldsymbol{\omega}) \cdot \delta\boldsymbol{\ell} \, \mathrm{d}V + \int h \, \delta\boldsymbol{\ell} \cdot \boldsymbol{n} \, \mathrm{d}S. \tag{7.3}$$

where the surface integral vanishes, since $\delta\boldsymbol{\ell} = \mathbf{0}$ on the boundary. In the study of vortex dynamics, the term $\boldsymbol{u}\times\boldsymbol{\omega}$ is typically referred to as the *vortex force*. Thus the volume integral represents the work done against vortex forces, through the displacement $\delta\boldsymbol{\ell}$. Hence, for a homogeneous fluid, we obtain that the principle of virtual work becomes effectively a principle of *virtual vortex work*.

Since the variation is taken by employing a kinematically possible displacement, we need $\nabla\cdot\delta\boldsymbol{\ell} = 0$, such that $\delta\boldsymbol{\ell} = \nabla\times\delta\boldsymbol{a}$, where $\delta\boldsymbol{a}$ is arbitrary. Integration by parts gives:

$$\delta W = \int [\nabla\times(\boldsymbol{u}\times\boldsymbol{\omega})]\cdot\delta\boldsymbol{a}\,\mathrm{d}V - \int (\boldsymbol{u}\times\boldsymbol{\omega})\cdot(\boldsymbol{n}\times\delta\boldsymbol{a})\,\mathrm{d}S, \tag{7.4}$$

where the surface integral vanishes, provided $\boldsymbol{\omega}$ decays sufficiently rapidly with distance. Hence requiring $\delta W = 0$ for any kinematically possible displacements yields

$$\nabla\times(\boldsymbol{u}\times\boldsymbol{\omega}) = -\boldsymbol{u}\cdot\nabla\boldsymbol{\omega} + \boldsymbol{\omega}\cdot\nabla\boldsymbol{u} = \mathbf{0}, \tag{7.5}$$

which can be recognized as the steady vorticity equation for flow in three dimensions. Of course, the work δW performed on the system must correspond to an energy gain δE. Hence a stationary point of the energy corresponds to a balance between forces acting on each infinitesimal control volume in the fluid.

Let us now consider the virtual work (say, $\delta W'$) for flow in a reference frame that is translating with constant speed $\boldsymbol{U}$. While there are no apparent forces due to frame accelerations, the momentum flux term in (7.1) is changed by substituting $\boldsymbol{u}$ with $\boldsymbol{u}' = \boldsymbol{u} - \boldsymbol{U}$, where $\boldsymbol{u}'$ is the velocity in the moving frame. Then $\boldsymbol{f}' = -(\boldsymbol{u}-\boldsymbol{U})\times\boldsymbol{\omega} + \nabla h'$, where $h' = p + \frac{1}{2}|\boldsymbol{u}'|^2$, and, by steps similar to those in (7.2)-(7.5) we obtain, with $\delta W' = 0$:

$$\nabla\times[(\boldsymbol{u}-\boldsymbol{U})\times\boldsymbol{\omega}] = -(\boldsymbol{u}-\boldsymbol{U})\cdot\nabla\boldsymbol{\omega} + \boldsymbol{\omega}\cdot\nabla\boldsymbol{u} = \mathbf{0}, \tag{7.6}$$

which is the steady vorticity equation in the moving frame. Hence the vanishing of the virtual work, in a translating reference frame, corresponds to a steadily moving vortex equilibrium.

Next, in order to show that requiring $\delta W' = 0$ corresponds to seeking an extremum of the energy, for given fluid impulse, let us write $\delta W'$ as:

$$\delta W' = -\int (\boldsymbol{u} \times \boldsymbol{\omega}) \cdot \delta \boldsymbol{\ell} \, \mathrm{d}V - \boldsymbol{U} \cdot \int \delta \boldsymbol{\ell} \times \boldsymbol{\omega} \, \mathrm{d}V. \tag{7.7}$$

The first integral is just the virtual vortex work in the fixed reference frame, $\delta W = \delta E$. The integral of $\delta \boldsymbol{\ell} \times \boldsymbol{\omega}$ can be understood to be the variation of the linear impulse (see e.g. Fukumoto & Moffatt, 2008). Hence the above becomes:

$$\delta W' = \delta W - \boldsymbol{U} \cdot \delta \boldsymbol{I}. \tag{7.8}$$

Standard techniques from variational calculus then imply that setting $\delta W' = 0$ corresponds to seeking $\delta W = 0$, with prescribed $\boldsymbol{I}$, while $\boldsymbol{U}$ plays the role of a Lagrange multiplier. Hence the vanishing of the virtual work, in a steadily translating frame, is equivalent to a stationary point of the energy, for given linear impulse.

The same derivation can be repeated for a steadily rotating frame; we show the essential steps below. Besides introducing $\boldsymbol{u}' = \boldsymbol{u} - \boldsymbol{\Omega} \times \boldsymbol{x}$, we need to also include apparent forces due to Coriolis and centrifugal accelerations. Then the force $\boldsymbol{f}'$ is (see Batchelor, 1967):

$$\boldsymbol{f}' = \nabla \cdot (\rho \boldsymbol{u}' \boldsymbol{u}') + \nabla p + 2\rho \, \boldsymbol{\Omega} \times \boldsymbol{u}' - \frac{1}{2} \rho \nabla |\boldsymbol{\Omega} \times \boldsymbol{x}|^2. \tag{7.9}$$

For a fluid with unit density, this simplifies to $\boldsymbol{f}' = -(\boldsymbol{u} - \boldsymbol{\Omega} \times \boldsymbol{x}) \times \boldsymbol{\omega} + \nabla h'$, with $h' = p + \frac{1}{2}|\boldsymbol{u}'|^2 - \frac{1}{2}|\boldsymbol{\Omega} \times \boldsymbol{x}|^2$. Substituting this into $\delta W' = \int \boldsymbol{f}' \cdot \delta \boldsymbol{\ell} \, \mathrm{d}V = 0$ gives the steady vorticity equation, in the rotating frame:

$$\nabla \times [(\boldsymbol{u} - \boldsymbol{\Omega} \times \boldsymbol{x}) \times \boldsymbol{\omega}] = -(\boldsymbol{u} - \boldsymbol{\Omega} \times \boldsymbol{x}) \cdot \nabla \boldsymbol{\omega} + \boldsymbol{\omega} \cdot \nabla (\boldsymbol{u} - \boldsymbol{\Omega} \times \boldsymbol{x}) = \boldsymbol{0}. \tag{7.10}$$

Next, to prove that the vanishing of $\delta W'$ implies a stationary point of the energy, for given angular impulse, write:

$$\begin{aligned}\delta W' &= -\int (\boldsymbol{u}\times\boldsymbol{\omega})\cdot\delta\boldsymbol{\ell}\,\mathrm{d}V + \int [(\boldsymbol{\Omega}\times\boldsymbol{x})\times\boldsymbol{\omega}]\cdot\delta\boldsymbol{\ell}\,\mathrm{d}V + \int h'\delta\boldsymbol{\ell}\cdot\boldsymbol{n}\,\mathrm{d}S \\ &= \delta W - \boldsymbol{\Omega}\cdot\int \boldsymbol{x}\times(\delta\boldsymbol{\ell}\times\boldsymbol{\omega})\,\mathrm{d}V, \end{aligned} \tag{7.11}$$

where the last integral can be shown to correspond to the variation of the angular impulse $\boldsymbol{J} = -\frac{1}{2}\int \rho\,\boldsymbol{\omega}|\boldsymbol{x}|^2\mathrm{d}V$, yielding:

$$\delta W' = \delta W - \boldsymbol{\Omega}\cdot\delta\boldsymbol{J}, \tag{7.12}$$

and we therefore have that the vanishing of the virtual work, in a steadily rotating frame, implies a stationary point of the energy, with given angular impulse.

Based on the above analysis, for both translating and rotating flows, we have shown that Kelvin's argument may be derived directly from the principle of virtual work.

7.3.2 Compressible, barotropic or baroclinic flow

Let us first focus on deriving the equations for steady motion from the principle of virtual work. In the context of compressible or stratified flows, a further advantage of considering the virtual work δW, instead of the energy variation δE, is that it is not necessary to account separately for changes in kinetic and potential energy. Instead, the main difference from the homogeneous case is that $\delta\boldsymbol{\ell}$ is arbitrary. Therefore the equilibrium condition is simply $\boldsymbol{f}' = \boldsymbol{0}$! For flow in a translating frame, we can write:

$$\nabla\cdot(\rho\boldsymbol{u}')\,\boldsymbol{u}' + \rho(\boldsymbol{u}'\cdot\nabla\boldsymbol{u}' + \rho^{-1}\nabla p) = \boldsymbol{0}, \tag{7.13}$$

which is just the steady momentum equation, in the moving frame, that is:

$$\frac{\partial(\rho \boldsymbol{u}')}{\partial t'} = \frac{\partial \rho}{\partial t'}\boldsymbol{u}' + \rho \frac{\partial \boldsymbol{u}'}{\partial t'} = \boldsymbol{0}, \tag{7.14}$$

where $\partial/\partial t' = \partial/\partial t + \boldsymbol{U} \cdot \nabla$ is the time derivative in the moving frame. As it is customary, we choose to define a steady flow as having density and velocity fields that do not change in time, such that $\partial \rho/\partial t' = 0$ as well as $\partial \boldsymbol{u}'/\partial t' = \boldsymbol{0}$. Hence we find that a steady flow satisfies $\delta W' = 0$, but the vanishing of the virtual work (or, equivalently, a stationary point of the energy) is *not* sufficient to yield a steady flow. This conclusion has important implications; for example, a solution procedure that seeks iteratively energy extrema (such as the one developed by Vallis *et al.*, 1989) may fail to converge to a steady solution, while instead leading to a flow with no net fluid force at each point.

We should note here that our finding is in apparent disagreement with the barotropic flow results of Lynden-Bell & Katz (1981), who instead found that a stationary point of the energy would always correspond to a steady flow. The reason for this discrepancy will be explained below. It may be noted here that (7.14) was obtained without making use of the isovortical condition, and must therefore hold also for a baroclinic flow.

We now would like to show explicitly that $\delta W' = \delta W - \boldsymbol{U} \cdot \delta \boldsymbol{I}$ in a compressible flow. Let us start by writing $\delta W'$ as:

$$\begin{aligned} \delta W' &= \int [\nabla \cdot (\rho \boldsymbol{u}\boldsymbol{u}) + \nabla p] \cdot \delta \boldsymbol{\ell} \, \mathrm{d}V \\ &- \boldsymbol{U} \cdot \left\{ \int \rho [\delta \boldsymbol{\ell} \times \boldsymbol{\omega} - \nabla(\boldsymbol{u} \cdot \delta \boldsymbol{\ell}) + (\delta \boldsymbol{\ell} \cdot \nabla)\boldsymbol{u}] \, \mathrm{d}V + \int \delta \boldsymbol{\ell} \, \nabla \cdot (\rho \boldsymbol{u}') \, \mathrm{d}V \right\} \end{aligned} \tag{7.15}$$

The first integral is the virtual work (or energy variation) in the fixed frame, while the last integral vanishes if the density field is steady ($\partial \rho/\partial t' = -\nabla \cdot (\rho \boldsymbol{u}') = 0$). It remains to show that the second integral is $\delta \boldsymbol{I}$. Let us recall the definition

of the impulse, for a nonhomogeneous flow in D dimensions (see Eames, 2008, and references therein):

$$\boldsymbol{I} = (D-1)^{-1} \int \boldsymbol{x} \times [\nabla \times (\rho \boldsymbol{u})] \, \mathrm{d}V, \tag{7.16}$$

such that, in order to find $\delta \boldsymbol{I}$, we need to first evaluate $\delta(\rho \boldsymbol{u}) = \delta\rho \, \boldsymbol{u} + \rho \, \delta \boldsymbol{u}$, where $\delta\rho$ and $\delta \boldsymbol{u}$ are the changes in density and velocity at a fixed point in space. Mass conservation in a compressible flow implies $\delta\rho = -\nabla \cdot (\rho \, \delta \boldsymbol{\ell})$ (see e.g. Lynden-Bell & Katz, 1981). The expression for $\delta \boldsymbol{u}$ follows from a somewhat subtle analysis. For a homogeneous or barotropic fluid, $\delta \boldsymbol{u}$ is traditionally found from the *isovortical* condition (Arnol'd, 1966). This stipulates that the circulation around any contour in the fluid is conserved by the variation. Equivalently, one can say that $\boldsymbol{\omega}$ is advected by $\delta \boldsymbol{\ell}$, yielding (see Moffatt, 1986):

$$\delta \boldsymbol{\omega} = \nabla \times (\delta \boldsymbol{\ell} \times \boldsymbol{\omega}) \quad \Rightarrow \quad \delta \boldsymbol{u} = \delta \boldsymbol{\ell} \times \boldsymbol{\omega} + \nabla \alpha. \tag{7.17}$$

In homogeneous flow, $\nabla\alpha$ is fixed by $\nabla \cdot \delta \boldsymbol{u} = 0$; however, for barotropic flow, $\nabla\alpha$ is considered to be arbitrary (Lynden-Bell & Katz, 1981).

For baroclinic flow, the isovortical condition does not apply, since circulation is not conserved. To the best of our knowledge, this has prevented the extension of Kelvin's argument to baroclinic fluids. However, from the virtual work standpoint, there is nothing special about baroclinic flows. This motivates us to seek $\delta \boldsymbol{u}$ directly from Euler's equation; in other words, we replace an isovortical perturbation with one that is *dynamically admissible*. Through the procedure shown in detail further below, in § 7.4, we obtain:

$$\delta \boldsymbol{u} = \delta \boldsymbol{\ell} \times \boldsymbol{\omega} - \nabla(\boldsymbol{u} \cdot \delta \boldsymbol{\ell}) - \rho^{-1} \nabla P, \tag{7.18}$$

where P is an impulsive pressure, which is negligible in compressible flow, as explained in § 7.4. In any case, P does not contribute to the virtual work, as

shown below. We should point out that, for a barotropic flow, any dynamically admissible $\delta\boldsymbol{u}$ is also isovortical. However, the converse is not true; indeed, (7.17) and (7.18) show that any $\delta\boldsymbol{u}$ with $\alpha \neq \boldsymbol{u}\cdot\delta\boldsymbol{\ell}$ does not represent the evolution of the flow under the displacement $\delta\boldsymbol{\ell}$. In other words, assuming α to be arbitrary does not yield the correct dynamics. Furthermore, if α is replaced with $\boldsymbol{u}\cdot\delta\boldsymbol{\ell}$ in the barotropic flow analysis of Lynden-Bell & Katz (1981), one obtains the steady momentum equation (7.13), in agreement with the result presented here.

Finally, returning to the impulse variation, we find:

$$\begin{aligned}\delta\boldsymbol{I} &= (D-1)^{-1}\int \boldsymbol{x}\times\left\{\nabla\times[\rho\delta\boldsymbol{\ell}\times\boldsymbol{\omega}-\rho\nabla(\boldsymbol{u}\cdot\delta\boldsymbol{\ell})-\nabla\cdot(\rho\delta\boldsymbol{\ell})-\nabla\times\nabla P]\right\}\mathrm{d}V\\ &= \int\rho[\delta\boldsymbol{\ell}\times\boldsymbol{\omega}-\nabla(\boldsymbol{u}\cdot\delta\boldsymbol{\ell})+(\delta\boldsymbol{\ell}\cdot\nabla)\boldsymbol{u}]\,\mathrm{d}V, \qquad (7.19)\end{aligned}$$

where $\nabla\times\nabla P\equiv\boldsymbol{0}$, and we have employed the identity (Saffman, 1992)):

$$\int\boldsymbol{x}\times(\nabla\times\boldsymbol{b})\,\mathrm{d}V=\int[\boldsymbol{n}(\boldsymbol{b}\cdot\boldsymbol{x})-\boldsymbol{b}(\boldsymbol{x}\cdot\boldsymbol{n})]\,\mathrm{d}S+(D-1)\int\boldsymbol{b}\,\mathrm{d}V. \qquad (7.20)$$

We therefore have shown that $\delta W' = \delta W - \boldsymbol{U}\cdot\delta\boldsymbol{I}$ for a general compressible flow. The analysis for a rotating reference frame can be developed by following steps similar to the ones shown above (yielding $\delta W' = \delta W - \boldsymbol{\Omega}\cdot\delta\boldsymbol{J}$ for a general compressible flow), and is therefore not reported here.

7.4 The dynamically admissible velocity variation $\delta\boldsymbol{u}$

We consider flows which are not necessarily developing about a steady state, and compare the dynamics associated with the "unperturbed" motion (that is, in the absence of the variation) to those corresponding to the "perturbed" motion. The variation is enacted through a velocity field $\boldsymbol{v}(\boldsymbol{x})$, which is active for

$0 < t < \delta t$, such that, to linear order, the resulting displacement field is $\delta\boldsymbol{\ell} = \boldsymbol{v}\,\delta t$ (as also prescribed in Moffatt, 1986). The time interval δt is assumed to be small enough for the change in the underlying variables to be small, by comparison to the change in the perturbation variables.

Consider Stokes' form of Euler's equation:

$$\frac{\partial \boldsymbol{u}}{\partial t} = \boldsymbol{u} \times \boldsymbol{\omega} - \frac{1}{2}\nabla|\boldsymbol{u}|^2 - \rho^{-1}\nabla p. \tag{7.21}$$

We expand each quantity into an unperturbed and a perturbed component as:

$$\begin{aligned} \boldsymbol{u}(\boldsymbol{x},t) &= \boldsymbol{u}_u(\boldsymbol{x},t) + \boldsymbol{u}_p(\boldsymbol{x},t) + \boldsymbol{v}(\boldsymbol{x}) \\ p(\boldsymbol{x},t) &= p_u(\boldsymbol{x},t) + p_p(\boldsymbol{x},t) \\ \rho(\boldsymbol{x},t) &= \rho_u(\boldsymbol{x},t) + \rho_p(\boldsymbol{x},t) \end{aligned} \tag{7.22}$$

Then define $\delta\boldsymbol{u}$ as the change in the velocity field that *persists* at $t = \delta t$, immediately after $\boldsymbol{v}$ has been turned off, and which is given by $\delta\boldsymbol{u} = \int_0^{\delta t} (\partial \boldsymbol{u}_p/\partial t)\,\mathrm{d}t$. Substituting the expansions for each variable into Euler's equation, removing the "unperturbed" component (since the unperturbed motion independently satisfies Euler's equation), gives:

$$\frac{\partial \boldsymbol{u}_p}{\partial t} = \boldsymbol{v} \times \boldsymbol{\omega}_u + \boldsymbol{u}_u \times \boldsymbol{\omega}_p - \nabla(\boldsymbol{u}\cdot\boldsymbol{v}) - \rho_u^{-1}\nabla p_p + \rho_u^{-2}\rho_p \nabla p_u + O(t), \tag{7.23}$$

where we have assumed $|\boldsymbol{u}_p| \ll |\boldsymbol{v}|$ in the right-hand side, and $\boldsymbol{v}$ has been taken as irrotational. Note that if $\boldsymbol{u}_p = O(t)$, we have $|\boldsymbol{u}_u \times \boldsymbol{\omega}_p| \ll |\boldsymbol{v} \times \boldsymbol{\omega}_u|$. The term in ρ_p can also be shown to be negligible, since continuity implies $\rho_p(t) = -\nabla\cdot(\rho_u \boldsymbol{v})t + O(t^2) = O(t)$. We therefore integrate the remaining terms to get $\delta\boldsymbol{u}$:

$$\delta\boldsymbol{u} = \int_0^{\delta t} \frac{\partial \boldsymbol{u}_p}{\partial t}\mathrm{d}t = \delta\boldsymbol{\ell} \times \boldsymbol{\omega}_u - \nabla(\boldsymbol{u}_u \cdot \delta\boldsymbol{\ell}) - \rho_u^{-1}\nabla \int_0^{\delta t} p_p\,\mathrm{d}t + O(\delta t^2), \tag{7.24}$$

Then we obtain, dropping the subscripts from the underlying quantities, and defining the impulsive pressure $P = \int_0^{\delta t} p_p\,\mathrm{d}t$:

$$\delta\boldsymbol{u} = \delta\boldsymbol{\ell} \times \boldsymbol{\omega} - \nabla(\boldsymbol{u}\cdot\delta\boldsymbol{\ell}) - \rho^{-1}\nabla P, \tag{7.25}$$

a result which holds for both barotropic and baroclinic flow. In incompressible flow, P is determined by $\nabla\cdot\delta\boldsymbol{u} = 0$. On the other hand, if the flow is compressible, $p = f(\rho, T)$ can be written as a function of density and temperature; then it can be shown that $p_p = O(t)$, such that $P = O(\delta t^2)$ is negligible in (7.25).

7.5 Concluding remarks

In summary, we derive Kelvin's argument from the fundamental principle of virtual work. To the best of our knowledge, this is the first analysis which links Kelvin's statement to a simple physical idea. The principle of virtual work implies that a stationary point of the energy corresponds to the presence of a force balance at all fixed points in the fluid, under kinematically admissible displacements. Since, for a homogenous fluid, the only forces that can perform work are vortex ones, we are led to a principle of virtual vortex work for three-dimensional homogeneous flows.

For compressible flows, we replace the notion of an isovortical variation with that of a dynamically admissible perturbation. When combined with the virtual work approach, this allows us to generalize Kelvin's argument to both barotropic and baroclinic flows.

The work presented here is expected to be useful in formulating stability approaches. For example, in a conservative system, the second variation $\delta^2 W$ of the work performed on the system may be used to establish bounds on the growth of the perturbation. We are particularly interested in coupling the results presented here with the imperfect-velocity-impulse (IVI) diagram stability approach recently introduced to the study of vortical flows in Luzzatto-Fegiz &

Williamson (2010*b*,*c*). We look forward to presenting examples of the application of this stability technique, for nonhomogeneous flows, in a future contribution.

APPENDIX A

PAPERS DERIVING FROM THIS WORK

A.1 Peer-reviewed publications

LUZZATTO-FEGIZ, P. & WILLIAMSON, C.H.K. A derivation of Kelvin's argument, leading to extensions for compressible, barotropic and baroclinic flows. Submitted to *Journal of Fluid Mechanics*.

LUZZATTO-FEGIZ, P. & WILLIAMSON, C.H.K. An accurate and efficient method for computing uniform vortices. Submitted to *Journal of Computational Physics*.

LUZZATTO-FEGIZ, P. & WILLIAMSON, C.H.K. Stability of steady flows and new fluid equilibria from Imperfect Velocity-Impulse diagrams. Submitted to *Journal of Fluid Mechanics*.

LUZZATTO-FEGIZ, P. & WILLIAMSON, C.H.K. 2010 Resonant instability in two-dimensional vortex arrays. *Proceedings of the Royal Society A*. In press.

LUZZATTO-FEGIZ, P. & WILLIAMSON, C.H.K. 2010 Stability of conservative flows and new steady-fluid solutions from bifurcation diagrams exploiting a variational argument. *Physical Review Letters*, **104**, 044504.

LUZZATTO-FEGIZ, P. & WILLIAMSON, C.H.K. 2010 Stability of elliptical vortices from Imperfect Velocity-Impulse diagrams. *Theoretical and Computational Fluid Dynamics* **24**, 181188.

LUZZATTO-FEGIZ, P. & WILLIAMSON, C.H.K. 2009 Stability of steady vortices and new equilibrium flows from Imperfect-Velocity-Impulse diagrams. *Advances in Turbulence XII* (Ed. B. Eckhardt), **132**, 305-308.

Papers in preparation: (work forming the basis of these papers is complete)

LUZZATTO-FEGIZ, P. & WILLIAMSON, C.H.K. The structure and stability of uniform and distributed opposite-signed vortex pairs. To be submitted to *Journal of Fluid Mechanics.*

LUZZATTO-FEGIZ, P. & WILLIAMSON, C.H.K. Stability and evolution of uniform vortices related to vortex merger. To be submitted to *Journal of Fluid Mechanics.*

LUZZATTO-FEGIZ, P. & WILLIAMSON, C.H.K. Structure and stability of the finite-area Kármán vortex street. To be submitted to *Physics of Fluids.*

A.2 Conference presentations

LUZZATTO-FEGIZ, P. & WILLIAMSON, C.H.K. 2010 An accurate and efficient method to compute steady uniform vortices. *Bulletin of the American Physical Society*, **55**, GN6.

LUZZATTO-FEGIZ, P. & WILLIAMSON, C.H.K. 2010 Stability of steady vortices and new equilibrium flows from Imperfect-Velocity-Impulse diagrams. 8^{th} *Euromech Fluid Mechanics Conference,* 13-16 September, Bad Reichenhall, Germany.

LUZZATTO-FEGIZ, P. & WILLIAMSON, C.H.K. 2010 Determining the structure and stability of steady wake flows using IVI-diagrams. 6^{th} *IUTAM Symposium on Bluff Body Wakes and Vortex-Induced Vibration,* 22-25 June, Capri, Italy.

LUZZATTO-FEGIZ, P. & WILLIAMSON, C.H.K. 2009 Deriving Kelvin's argument through the principle of virtual vortex work. *Bulletin of the American Physical Society*, **54**, BT1.

LUZZATTO-FEGIZ, P. & WILLIAMSON, C.H.K. 2009 Stability of steady vortices and new equilibrium flows from Imperfect-Velocity-Impulse diagrams. 12^{th} *Euromech Turbulence Conference,* 7-10 September, Marburg, Germany.

LUZZATTO-FEGIZ, P. & WILLIAMSON, C.H.K. 2008 Determining the stability of steady inviscid flows through Imperfect Velocity-Impulse diagrams. *Bulletin of the American Physical Society*, **53**, AU5.

LUZZATTO-FEGIZ, P. & WILLIAMSON, C.H.K. 2008 Stability of steady inviscid flows from preferred bifurcation diagrams. *IUTAM Symposium: 150 Years of Vortex Dynamics*, 12-16 October, Copenhagen and Lyngby, Denmark.

WILLIAMSON, C.H.K. & LUZZATTO-FEGIZ, P. 2008 Stability of classical flows and new vortical solutions from preferred bifurcation diagrams. *IUTAM Symposium: 150 Years of Vortex Dynamics*, 12-16 October, Copenhagen and Lyngby, Denmark.

LUZZATTO-FEGIZ, P. & WILLIAMSON, C.H.K. 2007 The stability and evolution of a family of $M = 2$ uniform vortices. *Bulletin of the American Physical Society*, **52**, ER8.

LUZZATTO-FEGIZ, P. & WILLIAMSON, C.H.K. 2007 The stability and evolution of a family of $M = 2$ uniform vortices. *SCAT Workshop: Vortices and vortex sheets: theories, numerics and applications*, 4-10 June, Porquerolles, France.

LUZZATTO-FEGIZ, P. & WILLIAMSON, C.H.K. 2006 Stability of a family of uniform vortices related to vortex configurations before merging. *Bulletin of the American Physical Society*, **51**, GI3.

LUZZATTO-FEGIZ, P. & WILLIAMSON, C.H.K. 2005 Equilibrium solutions of the Euler equations related to m = 3 symmetric vortex merger. *Bulletin of the American Physical Society*, **50**, NG5.

BIBLIOGRAPHY

AREF, H. 1983 Integrable, chaotic, and turbulent vortex motion in two-dimensional flows. *Ann. Rev. Fluid Mech.* **15**, 345–389.

AREF, H. 2009 Stability of relative equilibria of three vortices. *Phys. Fluids* **21**, 094101.

ARNOL'D, V. I. 1965 Conditions for nonlinear stability of stationary plane curvilinear flows of an ideal fluid. *Dokl. Akad. Nauk. SSSR* **162**, 773–777.

ARNOL'D, V. I. 1966 Sur un principe variationnel pour les écoulements stationnaires des liquides parfaits et ses applications aux problèmes de stabilité nonlinéaires. *J. Méc.* **5**, 29–43.

ARNOL'D, V. I. 1984 *Catastrophe theory*. Springer.

ARNOL'D, V. I. & AVEZ, A. 1968 *Ergodic problems of classical mechanics*. Benjamin.

BAGHERI, S., HENNINGSON, D. S., HOEPFFNER, J. & SCHMID, P. J. 2009 Input-output analysis and control design applied to a linear model of spatially developing flows. *Appl. Mech. Rev.* **62** (2), 020803.

BATCHELOR, G. K. 1967 *An Introduction to Fluid Dynamics*. Cambridge University Press.

BENJAMIN, T. B. 1976 The alliance of practical and analytical insights into the nonlinear problems of fluid mechanics. In *Applications of Methods of Functional Analysis to Problems in Mechanics*, pp. 8–29. Springer.

BERLOFF, N. G. & ROBERTS, P. H. 2004 Motions in a Bose condensate: X. New results on the stability of axisymmetric solitary waves of the Gross-Pitaevskii equation. *J. Phys. A: Math. Gen.* **37**, 11333–11351.

BURBEA, J. & LANDAU, M. 1982 The kelvin waves in vortex dynamics and their stability. *J. Comp. Phys.* **45**, 127–156.

CAIRNS, R. A. 1979 The role of negative energy waves in some instabilities of parallel flows. *J. Fluid Mech.* **92**, 1–14.

CASADEMUNT, J. & JASNOW, D. 1991 Defect dynamics in viscous fingering. *Phys. Rev. Lett.* **67**, 3677–3680.

CERRETELLI, C. & WILLIAMSON, C. H. K. 2003*a* A new family of uniform vortices related to vortex configurations before merging. *J. Fluid Mech.* **493**, 219–229.

CERRETELLI, C. & WILLIAMSON, C. H. K. 2003*b* The physical mechanism for vortex merging. *J. Fluid Mech.* **475**, 41–77.

CHANDRASEKHAR, S. 1969 *Ellipsoidal figures of equilibrium*. Yale University Press.

CHAPLYGIN, S. A. 1903 One case of vortex motion in fluid. *Trans. Phys. Sect. Imperial Moscow Soc. Friends of Natural Sciences* **11**, 11–14.

CHAVANIS, P. H. 2002 Phase transitions in self-gravitating systems: Self-gravitating fermions and hard-sphere models. *Phys. Rev. E* **65**, 056123.

CHAVANIS, P. H. & SOMMERIA, J. 1996 Classification of self-organized vortices in two-dimensional turbulence: the case of a bounded domain. *J. Fluid Mech.* **314**, 267–297.

CHAVANIS, P. H. & SOMMERIA, J. 1998 Classification of robust isolated vortices in two-dimensional hydrodynamics. *J. Fluid Mech.* **356**, 259–296.

CHEN, B. & SAFFMAN, P. G. 1980 Numerical evidence for the existence of new types of gravity waves of permanent form on deep water. *Stud. Appl. Math.* **62**, 1–21.

CHEN, Y.-J. & STEEN, P. H. 1996 Suppression of the capillary instability in the Rayleigh-Taylor slot problem. *Phys. Fluids* **8**, 97–102.

COTTET, G. H. & KOUMOUTSAKOS, P. D. 2000 *Vortex Methods: Theory and Applications*. Cambridge University Press.

CRAIK, A. D. D. 1985 *Wave interactions and fluid flows*. Cambridge University Press.

CROWDY, D. G. 2002 Exact solutions for rotating vortex arrays with finite-area cores. *J. Fluid Mech.* **469**, 209–235.

CROWDY, D. G. 2010 A new calculus for two-dimensional vortex dynamics. *Theo. Comp. Fluid Dyn.* **24**, 9–24.

DABIRI, J. O. 2009 Optimal vortex formation as a unifying principle in biological propulsion. *Ann. Rev. Fluid Mech.* **41**, 17–33.

DAVIDSON, P.A. 1998 On the application of the Kelvin-Arnol'd energy principle to the stability of forced two-dimensional inviscid flows. *J. Fluid Mech.* **356**, 221–257.

DEEM, G. S. & ZABUSKY, N. J. 1978 Vortex waves: stationary "V States", interactions, recurrence, and breaking. *Phys. Rev. Lett.* **40**, 859–862.

DELBENDE, I. & ROSSI, M. 2009 The dynamics of a viscous vortex dipole. *Phys. Fluids* **21**, 073605.

DERRICK, G. H. 1964 Comments on nonlinear wave equations as models for elementary particles. *J. Math. Phys.* **5**, 1252–1254.

DEUFLHARD, P. 2006 *Newton Methods for Nonlinear Problems – Affine Invariance and Adaptive Algorithms*. Springer.

DRAZIN, P. G. & REID, W. H. 1981 *Hydrodynamic stability*. Cambridge University Press.

DRITSCHEL, D. G. 1985 The stability and energetics of corotating uniform vortices. *J. Fluid Mech.* **157**, 95–134.

DRITSCHEL, D. G. 1986 The nonlinear evolution of rotating configurations of uniform vorticity. *J. Fluid Mech.* **171**, 157–182.

DRITSCHEL, D. G. 1988*a* Contour surgery: A topological reconnection scheme for extended integrations using contour dynamics. *J. Comp. Phys.* **77**, 240–266.

DRITSCHEL, D. G. 1988*b* Nonlinear stability bounds for inviscid, two-dimensional, parallel or circular flows with monotonic vorticity, and the analogous three-dimensional quasi-geostrophic flows. *J. Fluid Mech.* **191**, 575–581.

DRITSCHEL, D. G. 1988*c* Nonlinear stability bounds for inviscid, two-dimensional, parallel or circular flows with monotonic vorticity, and the analogous three-dimensional quasi-geostrophic flows. *J. Fluid Mech.* **191**, 575–581.

DRITSCHEL, D. G. 1989 Contour dynamics and contour surgery. *Comp. Phys. Rep.* **10**, 78–146.

DRITSCHEL, D. G. 1990 The stability of elliptical vortices in an external straining flow. *J. Fluid Mech.* **210**, 223–261.

DRITSCHEL, D. G. 1995 A general theory for two-dimensional vortex interactions. *J. Fluid Mech.* **293**, 269–303.

DRITSCHEL, D. G. & LEGRAS, B. 1991 The elliptical model of two-dimensional vortex dynamics. II: Disturbance equations. *Phys. Fluids A* **3**, 855–869.

DRITSCHEL, D. G., SCOTT, R. K. & J. N, REINAUD 2005 The stability of quasi-geostrophic ellipsoidal vortices. *J. Fluid Mech.* **536**, 401–421.

DRITSCHEL, D. G., SCOTT, R. K., MACASKILL, C., GOTTWALD, G. A. & TRAN, C. V. 2008 Unifying scaling theory for vortex dynamics in two-dimensional turbulence. *Phys. Rev. Lett.* **101**, 094501.

DURAISAMY, K. & LELE, S. K. 2008 Evolution of isolated turbulent trailing vortices. *Phys. Fluids* **20**, 035102.

EAMES, I. 2008 Disappearing bodies and ghost vortices. *Phil. Trans. R. Soc. A* **366**, 2219–2232.

EHRENSTEIN, U. & LE DIZÈS, S. 2005 Relationship between corotating vortex-pair equilibria and a single vortex in an external deformation field. *Phys. Fluids* **17**, 074103.

EHRENSTEIN, U. & ROSSI, M. 1999 Equilibria of corotating nonuniform vortices. *Phys. Fluids* **11**, 3416–3425.

ELCRAT, A., FORNBERG, B., HORN, M. & MILLER, K. 2000 Some steady vortex ows past a circular cylinder. *J. Fluid Mech.* **409**, 13–27.

ELCRAT, A., FORNBERG, B. & MILLER, K. 2005 Stability of vortices in equilibrium with a cylinder. *J. Fluid Mech.* **544**, 53–68.

ELOY, C. & LE DIZÈS, S. 2001 Stability of the Rankine vortex in a multipolar strain field. *Phys. Fluids* **13**, 660–676.

EYDELAND, A. & TURKINGTON, B. 1988 A computational method of solving free-boundary problems in vortex dynamics. *J. Comp. Phys.* **78**, 194–214.

FRAENKEL, L. E. & BERGER, M. S. 1974 A global theory of steady vortex rings in an ideal fluid. *Acta Math.* **132**, 13–51.

FUKUMOTO, Y. 2003 The three-dimensional instability of a strained vortex tube revisited. *J. Fluid Mech.* **493**, 287–318.

FUKUMOTO, Y. & MOFFATT, H. K. 2008 Kinematic variational principle for motion of vortex rings. *Physica D* **237**, 2210–2217.

GALLIZIO, F., IOLLO, A., PROTAS, B. & ZANNETTI, L. 2010 On continuation of inviscid vortex patches. *Physica D* **239**, 190–201.

J. H. G. M. VAN GEFFEN, G. J. F. VAN HEIJST 1998 Viscous evolution of 2D dipolar vortices. *Fluid Dyn. Res* **22**, 191–213.

GHARIB, M., RAMBOD, E. & SHARIFF, K. 1998 A universal time scale for vortex ring formation. *J. Fluid Mech.* **360**, 121–140.

GOLDSTEIN, H. 1950 *Classical Mechanics*. Addison-Wesley.

GOLUBITSKY, M. & SCHAEFFER, D. G. 1985 *Singularities and groups in bifurcation theory*. Springer.

GRANT, M. A. 1973 The singularity at the crest of a finite amplitude progressive Stokes wave. *J. Fluid Mech.* **59**, 257–262.

GUCKENHEIMER, J. & HOLMES, P. 1985 *Nonlinear oscillations, dynamical systems, and bifurcations of vector fields*. Springer.

HAVELOCK, H. 1931 The stability of motion of rectilinear vortices in ring formation. *Phil. Mag.* **11**, 617–633.

VAN HEIJST, G. J. F. & CLERCX, H. J. H. 2008 Laboratory modeling of geophysical vortices. *Ann. Rev. Fluid Mech.* **41**, 143–164.

HELMOLTZ, H. 1858 Über Integrale der hydrodynamischen Gleichungen, welche den Wirbelbewegungen entsprechen. *J. Reine Angew. Math.* **55**, 25–55, English trans.: *Phil. Mag.* **33**:485–511.

HOLM, D.D., MARSDEN, J. E., RATIU, T. & WEINSTEIN, A. 1985 Nonlinear stability of fluid and plasma equilibria. *Phys. Rep.* **123**, 1–116.

JIMÉNEZ, J. 1987 On the linear stability of the inviscid Kármán vortex street. *J. Fluid Mech.* **178**, 177–194.

JONES, C. A., PUTTERMAN, S. J. & ROBERTS, P. H. 1986 Motions in a Bose condensate: V. Stability of solitary wave solutions of non-linear schrödinger equations in two and three dimensions. *J. Phys. A* **19**, 2991–3011.

JONES, C. A. & ROBERTS, P. H. 1982 Motions in a Bose condensate: IV. Axisymmetric solitary waves. *J. Phys. A* **15**, 2599–2619.

KAMM, J. R. 1987 Shape and stability of two-dimensional uniform vorticity regions. PhD thesis, California Institute of Technology, Pasadena.

KATZ, J. 1978 On the number of unstable modes of an equilibrium. *Mon. Not. R. Astr. Soc.* **183**, 765–769.

KEELING, J. & BERLOFF, N. G. 2008 Spontaneous rotating vortex lattices in a pumped decaying condensate. *Phys. Rev. Lett* **100**, 250401.

KERSWELL, R. 2002 Elliptical instability. *Annu. Rev. Fluid Mech.* **34**, 83–113.

KIDA, S. 1982 Stabilizing effects of finite core on Kármán vortex street. *J. Fluid Mech.* **122**, 487–504.

KIRCHHOFF, G. 1876 *Vorlesungen über mathematische Physik: Mechanik*. Teubner, Leipzig.

KIWAMOTO, Y., HASHIZUME, N., SOGA, Y., AOKI, J. & KAWAI, Y. 2007 Formation and relaxation of two-dimensional vortex crystals in a magnetized pure-electron plasma. *Phys. Rev. Lett* **99**, 115002.

KIZNER, Z. & KHVOLES, R. 2004 Two variations on the theme of Lamb-Chaplygin: Supersmooth dipole and rotating multipoles. *Regul. Chaotic Dyn.* **9**, 509–518.

KREIN, M. G. 1950 A generalization of several investigations of A. M. Liapunov on linear differential equations with periodic coefficients. *Dokl. Akad. Nauk. SSSR* **73**, 445–448.

KREYSZIG, E. 1991 *Differential geometry*. Dover.

LAMB, H. 1932 *Hydrodynamics*. Cambridge University Press.

LAMB, J. & ROBERTS, J. A. G. 1998 Time-reversal symmetry in dynamical systems: A survey. *Physica D* **112**, 1–39.

LANCZOS, C. 1986 *The variational principles of mechanics*. Dover.

LEGRAS, B. & DRITSCHEL, D. G. 1993 Comparison of the contour surgery and pseudo-spectral methods. *J. Comp. Phys.* **104**, 287–302.

LONGUET-HIGGINS, M. S. 1978*a* The instabilities of gravity waves of finite amplitude in deep water. I. Superharmonics. *Proc. R. Soc. Lond. A* **360**, 471–488.

LONGUET-HIGGINS, M. S. 1978*b* The instabilities of gravity waves of finite amplitude in deep water. II. Subharmonics. *Proc. R. Soc. Lond. A* **360**, 489–505.

LONGUET-HIGGINS, M. S. 1984*a* New integral relations for gravity waves of finite amplitude. *J. Fluid Mech.* **149**, 205–215.

LONGUET-HIGGINS, M. S. 1984*b* On the stability of steep gravity waves. *Proc. R. Soc. Lond. A* **396**, 269–280.

LONGUET-HIGGINS, M. S. 1985 Bifurcation in gravity waves. *J. Fluid Mech.* **161**, 467–475.

LONGUET-HIGGINS, M. S. 1986 Bifurcation and instability in gravity waves. *Proc. R. Soc. Lond. A*. **403**, 167–187.

LONGUET-HIGGINS, M. S. & FOX, M. J. H. 1978 Theory of the almost-highest wave. Part 2. Matching and analytic extension. *J. Fluid Mech.* **85**, 769–786.

LOVE, A. E. H. 1893 On the stability of certain vortex motions. *Proc. London Math. Soc.* **25**, 18–42.

LUZZATTO-FEGIZ, P. & WILLIAMSON, C. H. K. 2010*a* Resonant instability in two-dimensional vortex arrays. *Proc. Roy. Soc. A*. In press.

LUZZATTO-FEGIZ, P. & WILLIAMSON, C. H. K. 2010*b* Stability of conservative flows and new steady fluid solutions from bifurcation diagrams exploiting a variational argument. *Phys. Rev. Lett.* **104**, 044504.

LUZZATTO-FEGIZ, P. & WILLIAMSON, C. H. K. 2010*c* Stability of elliptical vortices from “Imperfect-Velocity-Impulse” diagrams. *Theo. Comp. Fluid Dyn.* **24**, 181–188.

LUZZATTO-FEGIZ, P. & WILLIAMSON, C. H. K. 2011*a* An accurate and efficient method for computing uniform vortices. *J. Comp. Phys.* Submitted.

LUZZATTO-FEGIZ, P. & WILLIAMSON, C. H. K. 2011*b* Determining the stability of steady inviscid flows through "Imperfect-Velocity-Impulse" diagrams. *J. Fluid Mech.* Submitted.

LUZZATTO-FEGIZ, P. & WILLIAMSON, C. H. K. 2011*c* On the stability of a family of steady vortices related to merger. *J. Fluid Mech.* In preparation.

LYNDEN-BELL, D. 1965 On the evolution of frictionless ellipsoids. *Astrophys. J.* **142**, 1648–1649.

LYNDEN-BELL, D. & KATZ, J. 1981 Isocirculational flows and their Lagrangian and energy principles. *Proc. R. Soc. Lond. A* **378**, 179–205.

LYTTLETON, R. A. 1953 *The Stability of rotating liquid masses*. Cambridge University Press.

MACKAY, R. S. 1986 Stability of equilibria of Hamiltonian systems. In *Nonlinear phenomena and chaos* (ed. S. Sarkar), pp. 254–270. Adam Hilger, Bristol.

MACKAY, R. S. & SAFFMAN, P. G. 1986 Stability of water waves. *Proc. R. Soc. Lond. A* **406**, 115–125.

MADDOCKS, J. H. 1987 Stability and folds. *Arch. Rat. Mech. Anal.* **99**, 301–328.

MAXWELL, J. C. 1855*a* Letter to William Thomson. In *The Scientific Letters and Papers of James Clerk Maxwell* (ed. P. M. Harman), , vol. 1, pp. 309–313. Cambridge University Press (1990).

MAXWELL, J. C. 1855*b* Manuscript on the steady motion of an incompressible fluid. In *The Scientific Letters and Papers of James Clerk Maxwell* (ed. P. M. Harman), , vol. 1, pp. 295–299. Cambridge University Press (1990).

MCDONALD, R. 1999 The motion of geophysical vortices. *Phil. Trans. R. Soc. Lond. A* **357**, 3427–3444.

MEACHAM, S. P. 1992 Quasigeostrophic, ellipsoidal vortices in stratified fluid. *Dyn. Atmos. Oceans* **16**, 189–223.

MEIRON, D. I., SAFFMAN, P. G. & SCHATZMAN, J. C. 1984 The linear two-dimensional stability of inviscid vortex streets of finite-cored vortices. *J. Fluid Mech.* **147**, 187–212.

MELESHKO, V. V. & AREF, H. 2007 A bibliography of vortex dynamics 1858-1956. *Adv. Appl. Mech* **41**, 197–292.

MELESHKO, V. V. & VAN HEIJST, G. J. F. 1994 On Chaplygin's investigations of two-dimensional vortex structures in an inviscid fluid. *J. Fluid Mech.* **272**, 157–182.

MEUNIER, P., EHRENSTEIN, U., LEWEKE, T. & ROSSI, M. 2002 A merging criterion for two-dimensional co-rotating vortices. *Phys. Fluids* **14**, 2757–2766.

MITCHELL, T. B. & ROSSI, L. F. 2008 The evolution of Kirchhoff elliptic vortices. *Phys. Fluids* **20**, 054103.

MIYAZAKI, T., UENO, K. & SHIMONISHI, T. 1999 Quasigeostrophic tilted spheroidal vortices. *J. Phys. Soc. Japan* **68**, 2592–2601.

MOFFATT, H. K. 1985 Magnetostatic equilibria and analogous Euler flows of arbitrarily complex topology. Part 1. Fundamentals. *J. Fluid Mech.* **159**, 359–378.

MOFFATT, H. K. 1986 Magnetostatic equilibria and analogous Euler flows of arbitrarily complex topology. Part 2. Stability considerations. *J. Fluid Mech.* **166**, 359–378.

MOORE, D. W. & SAFFMAN, P. G. 1971 Structure of a line vortex in an imposed strain. In *Aircraft wake turbulence* (ed. Olsen, Goldburg & Rogers), pp. 339–354. Plenum.

MORRISON, P. J. 1998 Hamiltonian description of the ideal fluid. *Rev. Mod. Phys.* **70** (2), 467–521.

MORRISON, P. J. & FLIERL, G. R. 2009 Computing vortex states with Dirac constraints. *Bull. Am. Phys. Soc.* **54**, ET 8.

NEWTON, P. K. 2001 *The N-vortex problem*. Springer.

NIELSEN, A. H. & RASMUSSEN, J. J. 1997 Formation and temporal evolution of the Lamb-dipole. *Phys. Fluids* **9**, 982–991.

NORBURY, J. 1973 A family of steady vortex rings. *J. Fluid Mech.* **57**, 417–431.

OVERMAN, E. A. 1986 Steady-state solutions of the euler equations in two dimensions II. Local analysis of limiting V-states. *SIAM J. Appl. Math.* **46**, 765–800.

PIERREHUMBERT, R. T. 1980 A family of steady, translating vortex pairs with distributed vorticity. *J. Fluid Mech.* **99**, 129–144.

PIERREHUMBERT, R. T. & WIDNALL, S. E. 1981 The structure of organized vortices in a free shear layer. *J. Fluid Mech.* **102**, 301–313.

POINCARÉ, H. 1885 Sur l'équilibre d'une masse fluide animée d'un mouvement de rotation. *Acta Math.* **7**, 259–380.

POSTON, T. & STEWART, I. 1978 *Catastrophe theory*. Dover.

PULLIN, D. 1992 Contour dynamics methods. *Annu. Rev. Fluid Mech.* **24**, 89–115.

ROBERTS, P. H. 1972 A Hamiltonian theory for weakly interacting vortices. *Mathematika* **19**, 169–179.

SAFFMAN, P. G. 1985 The superharmonic instability of finite-amplitude water waves. *J. Fluid Mech.* **159**, 169–174.

SAFFMAN, P. G. 1988 The stability of vortex arrays to two- and three-dimensional disturbances. *Fluid Dyn. Res.* **3**, 13–21.

SAFFMAN, P. G. 1992 *Vortex Dynamics*. Cambridge University Press.

SAFFMAN, P. G. & BAKER, G. R. 1979 Vortex interactions. *Ann. Rev. Fluid Mech.* **11**, 95–122.

SAFFMAN, P. G. & SCHATZMAN, J. C. 1981 Properties of vortex street of finite vortices. *SIAM J. Sci. Stat. Comput.* **2**, 285–295.

SAFFMAN, P. G. & SCHATZMAN, J. C. 1982*a* An inviscid model for the vortex-street wake. *J. Fluid Mech.* **122**, 467–486.

SAFFMAN, P. G. & SCHATZMAN, J. C. 1982*b* Stability of a vortex street of finite vortices. *J. Fluid Mech.* **117**, 171–186.

SAFFMAN, P. G. & SZETO, R. 1980 Equilibrium shapes of a pair of equal uniform vortices. *Phys. Fluids* **23**, 2339–2342.

SAFFMAN, P. G. & SZETO, R. 1981 Structure of a linear array of uniform vortices. *Stud. Appl. Math.* **65**, 223–248.

SAFFMAN, P. G. & TANVEER, S. 1982 The touching pair of equal and opposite uniform vortices. *Phys. Fluids* **25**, 1929–1930.

SALMON, R. 1988 Hamiltonian fluid mechanics. *Ann. Rev. Fluid Mech.* **20**, 225–256.

SATIJN, M. P., VAN BUREN, M. G., CLERCX, H. J. H. & VAN HEIJST, G. J. F. 2004 Vortex models based on similarity solutions of the two-dimensional diffusion equation. *Phys. Fluids* **16**, 3997–4011.

SCHMID, P. & HENNINGSON, D. S. 2001 *Stability and transition in shear flows*. Springer.

SERRIN, J. 1959 Mathematical principles of classical fluid mechanics. In *Handbuch der Physik*, , vol. VIII-1, pp. 125–263. Springer-Verlag.

SETHIAN, J. A. 2000 *Level set methods and fast marching methods*. Cambridge University Press.

SHEPHERD, T. G. 1990 A general method for finding extremal states of Hamiltonian dynamical systems, with applications to perfect fluids. *J. Fluid Mech.* **213**, 573–587.

SIPP, D., JACQUIN, L. & COSSU, C. 2000 Self-adaptation and viscous selection in concentrated two-dimensional vortex dipoles. *Phys. Fluids* **12**, 245–248.

STOKES, G. G. 1879 Letter to William Thomson. In *The correspondence between Sir George Gabriel Stokes and Sir William Thomson, Baron Kelvin of Largs* (ed. D. B. Wilson), , vol. 2, pp. 470–471. Cambridge University Press (1990).

STUART, J. T. 1967 On finite amplitude oscillations in laminar mixing layers. *J. Fluid Mech.* **29**, 417–440.

TANAKA, M. 1983 The stability of steep gravity waves. *J. Phys. Soc. Japan* **52**, 3047–3055.

TANAKA, M. 1985 The stability of steep gravity waves. Part 2. *J. Fluid Mech.* **156**, 281–289.

THOM, R. 1972 *Stabilité structurelle et morphogénèse*. Benjamin.

THOMPSON, J. M. T. 1975 Experiments in catastrophe. *Nature* **254**, 392–395.

THOMPSON, J. M. T. 1979 Stability predictions through a succession of folds. *Phil. Trans. R. Soc. Lond. A* **292**, 1–23.

THOMPSON, J. M. T. & HUNT, G. W. 1973 *A general theory of elastic stability*. John Wiley and Sons.

THOMSON, W. 1867 Vortex atoms. *Proc. R. Soc. Edinb.* **6**, 94–105, reprinted in: *Phil. Mag.* **33**, 15–24 (1867).

THOMSON, W. 1870 Letter to George Gabriel Stokes. In *The correspondence between Sir George Gabriel Stokes and Sir William Thomson, Baron Kelvin of Largs* (ed. D. B. Wilson), , vol. 2, pp. 375–379. Cambridge University Press (1990).

THOMSON, W. 1875 Vortex statics. *Math. Phys. Pap.* **IV**, 115–128.

THOMSON, W. 1876 Vortex statics. *Proc. R. Soc. Edinb.* **9**, 59–73, also: *Phil. Mag.* (1880) **10**, 97–109.

THOMSON, W. 1878 Floating magnets. *Nature* **18**, 13–14.

THOMSON, W. 1880*a* On maximum and minimum energy in vortex motion. *Nature* **22**, 618–620.

THOMSON, W. 1880*b* Vibrations of a columnar vortex. *Proc. Roy. Soc. Edinb.* **10**, 443–450, also *Phil. Mag.* 1880, **10**, 155–168.

THOMSON, W. 1880*c* Vibrations of a columnar vortex. *Mathematical and physical papers* **IV**, 152–165.

TURKINGTON, B., MAJDA, A., HAVEN, K. & DIBATTISTA, M. 2001 Statistical equilibrium predictions of jets and spots on Jupiter. *Proc. Nat. Acad. Sci.* **98**, 12346–12350.

VALLIS, G.K., CARNEVALE, G.F. & YOUNG, W. 1989 Extremal energy properties and construction of stable solutions of the Euler equations. *J. Fluid Mech.* **207**, 133–152.

VAN DE FLIERT, B. W. 1995 Planar relative equilibrium vortices with free boundaries. *Nonlinearity* **8**, 963–981.

VON KÁRMÁN, T. 1912 über den Mechanismus des Widerstands, den ein bewegter Korper in einer Flüssigkeit erfährt. *Gött. Nachr. Math. Phys. Kl.* **13**, 547–556.

WAITE, M. L. & SMOLARKIEWICZ, P. K. 2008 Instability and breakdown of a vertical vortex pair in a strongly stratified fluid. *J. Fluid Mech.* **606**, 239–273.

WHITNEY, H. 1955 Singularities of mappings of Euclidean spaces. Mappings of the plane into the plane. *Ann. Math* **2**, 374–470.

WU, H. M., OVERMAN, E. A. & ZABUSKY, N. J. 1984 Steady-state solutions of the Euler equations in two dimensions: Rotating and translating V-states with limiting cases. I. Numerical algorithms and results. *J. Comp. Phys.* **53**, 42–71.

ZABUSKY, N. J., HUGHES, M. H. & ROBERTS, K. V. 1979 Contour dynamics for the euler equations in two dimensions. *J. Comp. Phys.* **30**, 96–106.

ZAKHAROV, V. E. 1968 Stability of periodic waves of finite amplitudes on the surface of a deep fluid. *Zh. Prokl. Mekh. Tekh. Fiz.* **9**, 86–94.